NASA Contractor Report 180852

Improved Numerical Methods for Turbulent Viscous Recirculating Flows

A. Turan and J.P. VanDoormaal
Avco Research Laboratory, Inc.
Everett, Massachusetts

July 1988

Prepared for
Lewis Research Center
Under Contract NAS3-24351

National Aeronautics and
Space Administration

TABLE OF CONTENTS

FOREWORD

The work reported in this program was performed jointly with Avco Research Laboratory/TEXTRON and Advanced Scientific Computing Ltd. Special acknowledgement is given to the contributions made by the following:

P.F. Galpin

B.R. Hutchinson

G.D. Raithby

M.J. Raw

1.0 SUMMARY

The Hybrid-Upwind finite volume discretization schemes adopted in numerical combustor codes for routine use is plagued with excessive numerical diffusion errors, which generally preclude accurate quantitative calculations. In addition, the overall solution algorithm as well as the resulting discrete algebraic equations require excessive computational resources for a solution on grids of practical significance, either due to the inadequacy of the coupling approximations introduced or the unacceptably slow convergence characteristics of the solvers used. The National Aeronautics and Space Administration, under the HOt Section Technology program, sponsored efforts to identify and evaluate quantitatively potentially attractive schemes that promise improved discretization accuracy, while yielding stable and physically meaningful solutions. Also considered in this program were various means of enhancing convergence thus reducing the computational costs associated with a solution, especially for three-dimensional applications. This report describes the details of one such study.

The desirable attributes of optimum discretization schemes and convergence enhancement techniques adopted in this study for initial qualitative assessment, concern issues of accuracy, stability (robustness), efficiency, storage requirements and ease of implementation in a three-dimensional code structured in TEACH methodology. The initial evaluation of more than ten potential techniques considered was primarily based on examination of accuracy and linear stability of the resulting difference equations via evaluation of the properties of the coefficient matrix, Taylor series analysis and existing heuristic stability analyses for iterative solvers commonly used in segregated solution procedures, as well as criteria for implementational details. This effort was aided by information available in the literature, prior experience, qualitative/quantitative assessment derived from a deep appreciation of both the schemes and requirements of practical engineering computations. In addition a Technical Advisory Committee with a broad base of in depth experience contributed significantly.

Upon completion of this initial evaluation, four of the most promising techniques were incorporated in a variant of 2D-TEACH code for further quantitative evaluation. The particular schemes selected address issues of both discretization accuracy and convergence enhancement and include:

i) Second order upwind differencing scheme
ii) Variants of skewed upstream differencing schemes
iii) Variants of compact implicit method
iv) Strongly implicit procedure accelerated by:
    a) Conjugate gradient algorithm
    b) Block correction technique
    c) Additive correction multigrid algorithm

Several two dimensional test problems, for which analytical or "exact" numerical solutions exist or can be generated with relative ease, were adopted to quantitatively evaluate the performance of the selected techniques regarding issues of accuracy, stability and nature of solutions, and the associated computational cost. The test problems included general scalar transport and various flow problems (both laminar and turbulent) and were specifically designed to evaluate the sensitivity of the above techniques in response to convection, diffusion and source terms of a general conservation equation, as well as the nature of the coupling approximations introduced in the particular incompressible flow solver. Such two-dimensional exercises identified the variants of skewed upstream differencing schemes, coupled with the strongly implicit procedure accelerated by the additive correction multigrid algorithm as deserving further evaluation in three dimensions. The selection criteria were based on the practical concerns of best accuracy on coarse grids, robustness and stability and efficiency. Subsequently, these schemes were incorporated in a variant of 3D-TEACH code and were further evaluated regarding issues of accuracy and convergence enhancement characteristics in modelling of a jet in cross flow.

This study has clearly demonstrated that appropriate solution techniques for incompressible, turbulent, viscous, recirculating flows in current use benefit substantially from the introduction of the convergence enhancement techniques adopted here (up to 40 percent). Furthermore, the various improved discretization schemes considered, specifically variants of skewed upstream differencing schemes with physical advection correction, usually provide a

significant improvement in accuracy relative to Hybrid differencing. The CPU times to obtain a solution using these improved schemes are larger than Hybrid for a given grid but, compared on the basis of equal accuracy, CPU improvements ranging from a factor of 2 to a factor greater than 50 can be realized via their use. However, as the results of this study are based on a limited and carefully selected set of problems, the performance of such schemes should be examined on a wider range of problems and as such this study has presented only a phase of progress in the complex, but steadily evolving subject concerned with the development of improved discretization techniques and effective solution algorithms. A number of questions have been generated as a result of this study and it is expected that answers to these questions will lead to further improvements in accuracy and computational efficiency.

Finally, it is noted that the enhanced solution and discretization schemes considered represent but a portion of new technology that would be optimally utilized if freed of the constraints improved by TEACH, which is structured to suit different methods with different priorities.

2.0 INTRODUCTION

2.1 BACKGROUND

The trend in aircraft gas turbines continues to maintain or increase engine life while improving performance by going to higher operating temperatures and pressures. This imposes increasingly stringent requirements on combustor designs. Heat release per unit volume becomes higher, the uniformity of combustor exit temperature becomes more critical and the liner environment is more hostile.

Hot section components such as the combustor liner and turbine airfoils account for a major portion of engine maintenance costs. A predominant failure mode for current combustor designs is creep/low cycle fatigue interaction which leads to cracking. Critical liner loads are caused by cyclically imposed thermal gradients. These gradients are generated by the local radiative and convective heat fluxes within the combustor.

The uniformity of the combustor exit temperature profile is very important to cycle and turbine design. The structural design of a turbine is a very complex process. Stress limits are a function of overall engine operating conditions, material characteristics, geometry and local temperatures. Therefore, spatial variations in the temperature profile entering the turbine will produce local regions of high temperature which usually determines this limiting design condition. The turbine generally will be designed to withstand this local high temperature at all locations, if the profile is known (either through analysis or previous development testing). Since the rest of the turbine is exposed to lower temperatures, the engine will be forced to operate at an average temperature which is lower than it would withstand if the profile were more uniform. In effect, the material is stressed to the limit of its capabilities only in the region of local high temperature. The reduction in average cycle temperature leads to a corresponding reduction in overall engine performance. In addition, local high temperature regions can lead to premature failure when they have not been identified during development. For these reasons a comprehensive combustor model, which can accurately predict performance and flow field characteristics, is particularly valuable to engine designers.

Gas turbine combustion involves extremely complex physio-chemical processes, including three-dimensional two-phase flow dynamics, turbulent mixing, fuel evaporation, radiative and convective heat transfer, and chemical kinetics. Conceptually, distinct zones can be identified within a convectional combustor. These characteristic regions are dominated by one or more of these processes. In the primary zone, evaporation and mixing rates are comparatively high, and flame stabilization is achieved by recirculation of partially burned products. In the secondary and dilution zones, partially converted products are allowed to react further, and additional air is added to reduce the final gas temperature to a level and pattern acceptable to the turbine.

An effective combustor aerothermal model has to treat each of the individual processes, as well as their nonlinear interdependencies, in a cost effective manner. The end goal is to develop a design and analysis tool which is significantly less expensive to employ than actual testing of alternative hardware designs. It must be capable of determining the effects of geometry, fuel flow, and inlet airflow conditions on the following global design parameters:

i) Combustion efficiency
ii) Total pressure loss
iii) Exit temperature distribution
iv) Ignition, stability, and relight
v) Pollutant levels
vi) Thermal loading at the walls
vii) Characteristic times

Currently available, three-dimensional, fully elliptic combustor models frequently employ numerical algorithms and discretization procedures derived from the original work performed at Imperial College as embodied in the TEACH family of codes.[1] Specifically, these solution methodologies, coupled with appropriate physical models to describe the various physical and chemical processes, generally employ a segregated method and a staggered computational grid to solve the algebraic transport equations, derived from the parent differential equations using a finite volume method. The usual formulation is intended for fully incompressible or subsonic flows. Segregated methods solve the algebraic equations for each variable separately.

According to the finite volume procedure, fluxes by convection and diffusion are required at control volume faces. The diffusive fluxes are obtained by assuming a linear variation of variable between nodes. In the original discretization scheme, now commonly used for routine engineering computations notwithstanding its inherent low accuracy, the value of a convected variable was approximated by a Hybrid scheme that combines Central and Upwind differencing.

TEACH/derivative methods have proven to be robust, and the results obtained for a given mesh are generally user independent if convergence is achieved. The number of iterations to reach convergence is small for coarse meshes but escalates quickly as the mesh is refined. The solutions of momentum equations in each cycle are inexpensive compared to the solution of a Poisson-like equation for pressure; improving solution economy, therefore, requires reduction in the cost of the pressure equation.

The Hybrid approximation of convected quantities that results in a robust method, introduces significant numerical error into the solution. One of the manifestations of the error is that sharply varying features of the flow are smeared in the solution.

The need to alleviate the above shortcomings related specifically to computational and algorithm dependent aspects of comprehensive numerical combustor models in current use, were clearly identified (re-iterated) along with improvements required in physical models for various phenomena during Phase I of the Aerothermal Modelling Program sponsored by NASA[2,3,4]. The three participants performed independent assessments of the state of the art regarding numerical simulations for combustor performance and concluded that current models can only qualitatively predict the complex aerodynamic flow field in combustors. Quantitative characterization of combustor flow fields was shown to require a significant reduction in the numerical diffusion levels introduced by the current convective differencing practices incorporated in such models. Furthermore, especially for three-dimensional applications, the computational cost associated with obtaining converged solutions was found to be prohibitive, thus a clear need to perform economical computations using improved solution methodologies was identified. Improvements in the physical modelling areas related to the description of; fuel spray distribution, details of multi-phase flow, chemical kinetics, radiation, heat transfer, etc.

were structured to follow the development of an accurate, cost effective, aerodynamic model.

Another problem identified during Phase I was a deficiency in test data from well defined and documented benchmark experiments which could be conveniently used to verify the overall code and its constituent models.

The smearing of sharply varying features of flow (fronts) associated with the numerical diffusion of low order convective differencing schemes can, in principle, be overcome by the use of several alternate practices. The simplest to implement amongst such potential techniques concerns the use of mesh refinement. However, for three-dimensional applications especially, the greatly increased number of grid points and therefore iterations required to reach an accurate converged solution, make the cost of this approach prohibitive. NASA has therefore, evaluated other practices using alternative differencing schemes, less susceptible to numerical diffusion, under a separate program.[5] The evaluation included Quadratic Upstream Interpolation for Convective Kinematics (QUICK) and variants of accurate Skewed Upwind Differencing Schemes (SUDS) appropriately blended with less accurate, but stable Upwind differencing. These approaches improve accuracy at the expense of a significant increase in the number of iterations required for a converged solution. Therefore, two alternative solution algorithms primarily designed to enhance convergence, SIMPLER and the Pressure Implicit Split Operator (PISO),[6] were also evaluated. The general conclusion of this study was that no single scheme emerged displaying superior performance for all flow situations.

2.2 OBJECTIVES AND APPROACH

The overall objective of the present study is to investigate methods of improving the accuracy and efficiency of numerical techniques used to predict incompressible, turbulent, viscous, recirculating fluid flows. However, accuracy issues related to improved modelling of turbulence are not explicitly considered; emphasis is solely on reducing the discretization error and solution cost via improved solution algorithms and differencing schemes. Furthermore, in this effort accuracy is emphasized over cost when the requirements to reduce numerical diffusion and solution cost are incompatible.

The approach adopted here to accomplish the above stated objectives was a structured effort to identify from the literature and/or other sources over ten potentially promising techniques to be subsequently assessed for discretization accuracy, solution stability and overall algorithm cost effectiveness. Included in the selection were convergence enhancement techniques to improve the cost effectiveness of the solution algorithm, as well as those including more accurate discretization schemes. The initial assessment was primarily based on examination of the accuracy and linear stability of the resulting difference equations via evaluation of the properties of the coefficient matrix, Taylor series analyses and existing heuristic stability analyses for iterative solvers of segregated solution algorithms adopted here. Cost effectiveness was judged on the combined outcome of the foregoing assessment.

This quantitative/qualitative initial evaluation yielded the four most promising techniques compatible with the objectives, which were subsequently incorporated in a variant of 2D-TEACH code for further quantitative evaluation. The stability, accuracy and cost effectiveness of these techniques were then examined by computing a number of scalar transport as well as various laminar and turbulent flow test cases. These test cases, for which analytical or "exact" numerical solutions exist or can be generated with relative case, display predominant features encountered in gas turbine combustors, i.e., the delicate local balance between the influences of convection, diffusion and sources of a general transport equation.

Such two-dimensional exercises identified the appropriate techniques to improve solution accuracy and overall cost effectiveness in three-dimensional applications via convergence enhancement and accurate discretization. These techniques were then incorporated in a variant of 3D-TEACH code and subsequently their performances were assessed in a test case of modelling a row of jets in a cross flow by comparison with experimental data and prior computations.

2.3 ORGANIZATION

In Section 3 a brief discussion is provided to examine the computational details of the solution algorithms in current use for the class of flow problems considered in this study. Sections 4 and 5 present a detailed account of the schemes. In addition, details of the particular assessment procedure

adopted, regarding issues of solution cost effectiveness by consideration primarily of accuracy and stability (discretization as well as iterative solvers) aspects, prior to quantitatively evaluating the schemes in a variant of 2D-TEACH code, is examined. Section 6 provides detailed derivations of the selected schemes, while Section 7 describes the results of the corresponding computations obtained for two-dimensional test cases. A similar discussion is presented in Section 8 for three-dimensional applications. Finally, in Section 9 concluding remarks are given and recommendations for future work are outlined.

3.0 OVERVIEW OF THE COMPUTATIONAL DETAILS OF THE SOLUTION ALGORITHMS FOR FLOW PROBLEMS

3.1 INTRODUCTION

The majority of heat transfer and fluid flow problems of engineering interest are analytically intractable. Approximate solutions of varying degrees of sophistication are currently obtained via numerical methods. Combustion research, in particular, is presently benefitting from the enormous potential, versatility and reliability offered by these numerical procedures. As combustor developments move into the widely varying, challenging, dynamic field of innovative and conventional power generation including gas turbine engines, the designer's task can be greatly aided by prior prediction via a mathematical model. Furthermore, the current interest in fuel efficient, low maintenance, clean engines has brought forward the neccessary to gain refined insight into the innumerous problems. The cut-and-try design methods of the past which cannot answer the above questions in a satisfactory detailed manner are being guided, if not replaced, by the superior predicting capabilities of the present approaches.

A common approach adopted by the above numerical predictive techniques for analysis of viscous recirculating flows, such as those arising in gas turbines, involves the formation and solution of discrete algebraic equations that represent the conservation of mass momentum and other relevant variables. Various techniques ranging from simple Taylor series expansion to finite volume and finite element methods are currently used to affect such a transformation that systematically reduces the governing partial differential equations to an algebraic set. In the finite volume technique, adopted as the primary scheme in this study, the algebraic set is generated by integration of the governing partial differential equation over spatial dimensions spanned by discrete (finite) control volumes.

For each control volume of the relevant variable there exists an algebraic equation to be solved. Assembly of such nodal equations with due account for nonlinearity and intervariable coupling yields the equation set

that is solved iteratively upon specification of necessary initial and boundary conditions. As the algebraic nodal equations consistently approximate the partial differential equations (valid for control volumes of infinitesimal size) over finite spatial dimensions, increased numerical accuracy in the finite volume solution is usually achieved through mesh refinement. However, for a given problem domain, decreasing the control volume sizes increases the number of control volumes, thus increasing the size of the discrete equation set to be solved and hence presenting a greater computational task. The practical limitations of mesh refinement are severe; prohibitive demands may be placed on computing resources before a grid independent solution is attained. This problem is particularly acute for many three-dimensional fluid flow and heat transfer problems.

The need for greater computing economy in predictive techniques has opened up two basic avenues of research. The first involves the development of more efficient solution methods designed to reduce the computational resources required to affect the solution of the algebraic equations resulting from the finite volume method or otherwise. The second involves the development of more accurate discretization schemes, aimed at reducing the number of control volumes (nodes) needed to achieve a given accuracy in the finite volume solution. Closely tied with this issue are considerations regarding false diffusion or spurious spatial conditions. Effectively dealing with the above problems of solution accuracy and efficiency forms the main themes of this study and such efforts should contribute to reducing both computing time and storage requirements for engineering predictions. The latter is essential if the scope of tractable three-dimensional problems is to be expanded.

In the following sections are presented the basic building blocks appropriate for the development of such techniques

3.2 THE MATHEMATICAL PROBLEM

The conservation laws governing heat transfer, fluid flow and other related processes are generally expressed in terms of integro/differential equations derived via continuum or microscopic considerations. The identification of all the relevant phenomena that can be described by a representative equation of a common form is the first step toward constructing a general solution

procedure. Specification of two additional algebraic relations completely defines the mathematical problem. The first of these describes the thermodynamic and transport properties of the fluid, e.g., the equation of state relating local values of density, pressure and temperature. In the latter category are the boundary conditions that uniquely specify the problem. These usually take the form of either specification of the value of the dependent variable at the boundary, or the value of the associated flux or a combination of the two.

3.2.1 General Conservation Equations

The differential transport equations listed below apply equally to both laminar and turbulent flows (the latter referring to instantaneous description of the flow). In Cartesian tensor notation, the equations for mass, momentum, energy and species conservation are:

Conservation of Mass

$$\frac{\partial \rho}{\partial t} + \frac{\partial}{\partial x_j}(\rho u_j) = 0 \tag{3.1}$$

Conservation of Momentum

$$\frac{\partial}{\partial t}(\rho u_i) + \frac{\partial}{\partial x_j}(\rho u_i u_j - \tau_{i,j}) - S_{u_i} + \frac{\partial p}{\partial x_i} = 0 \tag{3.2}$$

Conservation of Energy

$$\frac{\partial}{\partial t}(\rho h) + \frac{\partial}{\partial x_j}(\rho u_j h - J_{h,j}) - S_h = 0 \tag{3.3}$$

Conservation of Chemical Species

$$\frac{\partial}{\partial t}(\rho m_i) + \frac{\partial}{\partial x_j}(\rho u_j m_i - J_{m_i,j}) - S_{m_i} = 0 \tag{3.4}$$

In the above the x_j are the three Cartesian coordinates, the u_j are the three components of the velocity vector; p is the pressure; ρ is density. S_u, S_h and S_{mi} are volumetric rates of body forces, energy generation

and chemical species generation respectively. h denotes the specific stagnation enthalpy defined by:

$$h = c_{P,j}\, m_j T + \frac{1}{2} u_i^2 \tag{3.5}$$

where $c_{P,j}$ is constant pressure specific heat capacity, m_i is mass fraction of chemical species i, T is temperature. In equation (3.2) $\tau_{i,j}$ is the stress tensor with components defined in a general form by:

$$\tau_{i,j} = -\mu \left(\frac{\partial u_i}{\partial x_j} + \frac{\partial u_j}{\partial x_i} - \frac{2}{3} \frac{\partial u_k}{\partial x_k} \delta_{i,j} \right) \tag{3.6}$$

$\delta_{i,j}$ = Kronecker delta

μ is laminar viscosity. In the energy and species equations the $J_{h,j}$ and $J_{m_i,j}$ terms refer to diffusion fluxes and can be written as, if expressed by Fourier's and Fick's law of diffusion:

$$J_{h,j} = \frac{\mu}{\sigma_h} \frac{\partial h}{\partial x_j} \tag{3.7}$$

$$J_{m_i,j} = \frac{\mu}{\sigma_{m_i}} \frac{\partial m_i}{\partial x_j} \tag{3.8}$$

where σ_h and σ_{m_i} are respectively the Prandtl and Schmidt numbers.

3.2.2 Modelled Form of the Conservation Equations

For the description of turbulent flows the above instantaneous conservation equations are transformed into ensemble-averaged equations by an averaging operator that assumes rapid and random fluctuations about an ensemble-averaged value. The ensemble-averaged equations are similar to those for the instantaneous equations except for the appearance of the additional terms containing correlations of fluctuating components, Reynolds stresses, turbulent diffusion fluxes, etc. In order that these equations form a closed set, these additional terms must be related to known or easily calculated quantities.

Following the generally adopted practice of Launder and Spalding,[7] the additional terms are modelled as diffusion processes in order to make the ensemble-averaged equations compatible with those for laminar flow, i.e., the additional terms are expressed in terms of gradients of average quantities as:

$$-\overline{\rho u_i' u_j'} = \mu_t\left(\frac{\partial \bar{u}_i}{\partial x_j} + \frac{\partial \bar{u}_j}{\partial x_i}\right) - \frac{2}{3} k \delta_{i,j} \tag{3.9}$$

$$-\overline{\rho u_j' h'} = \frac{\mu_t}{\sigma_{h,t}} \frac{\partial \bar{h}}{\partial x_j} \tag{3.10}$$

$$-\overline{\rho u_j' m_i'} = \frac{\mu_t}{\sigma_{m_i,t}} \frac{\partial \bar{m}_i}{\partial x_j} \tag{3.11}$$

where k is the turbulent kinetic energy ($= \overline{u_i' u_i'}/2$); μ_t is a turbulent viscosity; the superscript ' stands for fluctuating quantities; $\bar{u}$, $\bar{h}$ and m represent ensemble-averaged values of velocity, stagnation enthalpy and mass fraction of the chemical species respectively; $\sigma_{h,t}$ and $\sigma_{m_i,t}$ are turbulent Prandtl and Schmidt numbers respectively and are usually assigned constant values determined by experiments.

Finally, the modelled forms of the ensemble-averaged conservation equations are given as, dropping the bars over time-averaged quantities:

$$\frac{\partial}{\partial t}(\rho) + \frac{\partial}{\partial x_j}(\rho u_j) - S_p = 0 \tag{3.12}$$

$$\frac{\partial}{\partial t}(\rho u_i) + \frac{\partial}{\partial x_j}\left(\rho u_j u_i - (\mu + \mu_t)\frac{\partial u_i}{\partial x_j}\right) - S_{u_i} = 0 \tag{3.13}$$

$$\frac{\partial}{\partial t}(\rho h) + \frac{\partial}{\partial x_j}\left(\rho u_j h - \left(\frac{\mu}{\sigma_h} + \frac{\mu_t}{\sigma_{h,t}}\right)\frac{\partial h}{\partial x_j}\right) - S_h = 0 \tag{3.14}$$

$$\frac{\partial}{\partial t}(\rho m_i) + \frac{\partial}{\partial x_j}\left(\rho u_j m_i - \left(\frac{\mu}{\sigma_{m_i}} + \frac{\mu_t}{\sigma_{m_i,t}}\right)\frac{\partial m_i}{\partial x_j}\right) - S_{m_i} = 0 \qquad (3.15)$$

where S_p, S_{u_i}, S_h and S_{m_i} comprise terms arising from sources of non-uniformities in fluid properties.

To close the solution of the above equation set, spatial and temporal evolution of μ_t has to be described. This is generally achieved by developing two transport equations for the turbulent kinetic energy, k, and its dissipation rate ε, $= (\mu/\rho)\,\overline{\partial u_i'/\partial x_j)^2}$, an approach moderate in complexity, but sufficient for most engineering flows (8). The ensemble-averaged equation for k and ε are given by:

Turbulent Kinetic Energy Equation

$$\frac{\partial}{\partial t}(\rho k) + \frac{\partial}{\partial x_j}\left(\rho u_j k - \frac{\mu_t}{\sigma_k}\frac{\partial k}{\partial x_j}\right) - S_k - G + \rho\,\varepsilon = 0 \qquad (3.16)$$

Dissipation Rate Equation

$$\frac{\partial}{\partial t}(\rho \varepsilon) + \frac{\partial}{\partial x_j}\left(\rho u_j \varepsilon - \frac{\mu_t}{\sigma_\varepsilon}\frac{\partial \varepsilon}{\partial x_j}\right) - S_\varepsilon - (C_1 G - C_2 \rho \varepsilon)\,\varepsilon/k = 0 \qquad (3.17)$$

where C_1, C_2, σ_k and σ_ε are empherical constants [8] and S_k and S_ε are additional source terms.

From dimensional analysis, the relation between μ_t and these two variables is given as:

$$\mu_t = \rho\, C_\mu k^2/\varepsilon \qquad (3.18)$$

C_μ is generally a constant.

3.3 ALGEBRAIC REPRESENTATION OF CONSERVATION EQUATIONS

Review of the above differential transport equations (3.12) to (3.17) reveals that they are similar in structure and all the dependent variables are

conserved, intensive properties. If a typical representative variable is denoted by ϕ, the general differential equation

$$\frac{\partial}{\partial t}(\rho\phi) + \frac{\partial}{\partial x_j}(\rho u_j \phi - \Gamma_\phi \frac{\partial \phi}{\partial x_j}) - S_\phi = 0 \qquad (3.19)$$

where the expressions for Γ_ϕ and S_ϕ can be deduced from the parent equations, forms the central theme of discretization studies. The four terms in the above equation describe successively unsteady, convection, diffusion and generation/dissipation effects. (In fact all terms not explicitly accounted for in the first three terms are included in the "catch-all source" term.)

3.3.1 Domain Discretization

In the following sections the finite volume technique is adopted as the primary means of transforming the differential transport equation into a consistent algebraic set. Furthermore, the discussion will be restricted to two-dimensional, steady, incompressible form of the equations, where the density approaches a constant value. Thus, the temporal derivative of density in mass conservation vanishes with corresponding modifications in the remaining equations.

Generation of the nodal algebraic relations proceeds by discretizing the calculation domain in some fashion. To prevent the occurences of decoupled pressure solutions and spatial oscillations of the velocity solution that can arise in the incompressible limit,[1] the staggered grid, figure (3.1) first used by Harlow and Welch,[9] is utilized. Recently there have been approaches that use co-located storage for variables and overcome the pressure decoupling problem in alternate ways;[10] however, their use so far has been limited. The calculation domain is divided uniformly into non-overlapping and contiguous control volumes over which mass, energy and species conservation are to apply. Locating the pressure, temperature and other scalar variables in the center of these control volumes, the staggered velocity nodes are located at the faces of the scalar (e.g. continuity) control volume. The control volumes for momentum conservation are arranged so that pressure nodes lie on the faces of their respective momentum conservation volumes.

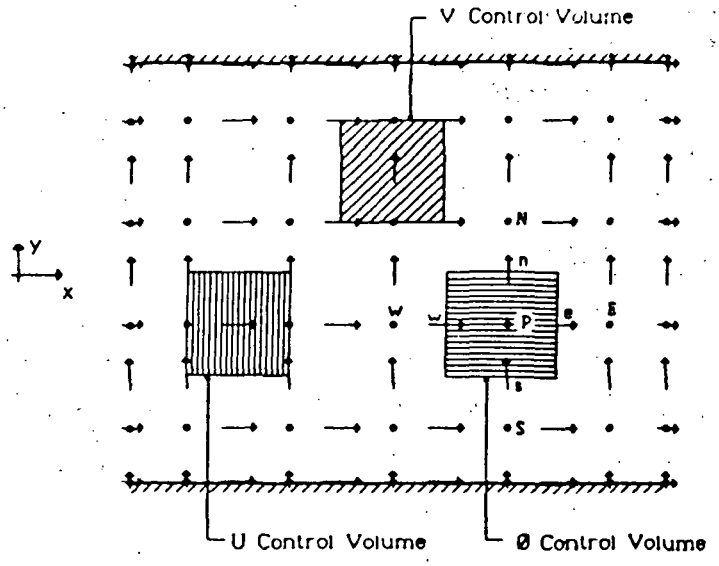

Figure 3.1 Grid Structure Showing Variable Locations

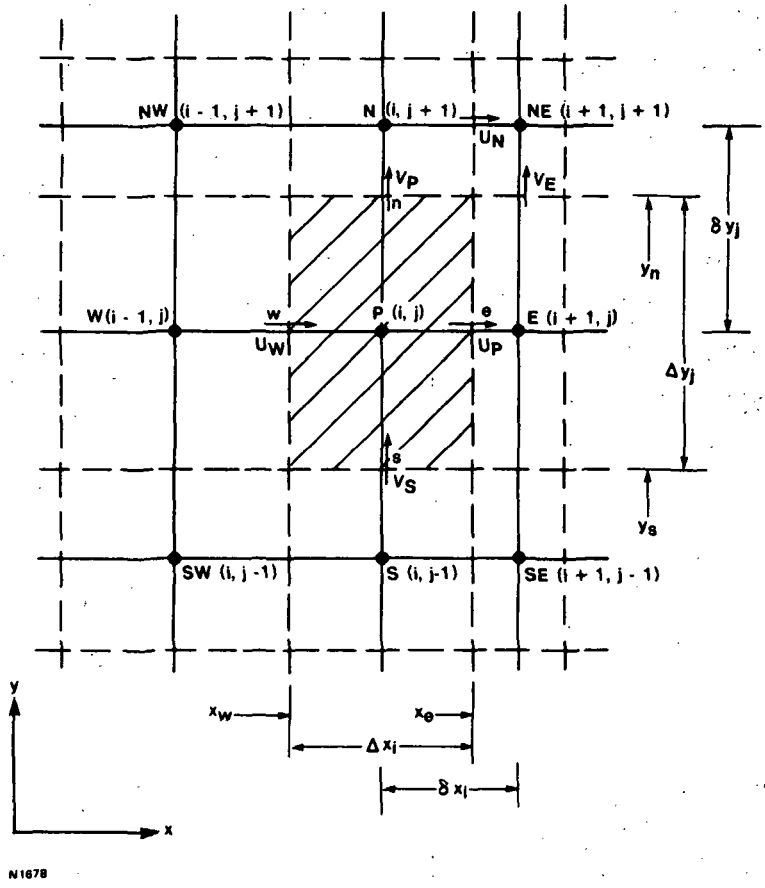

Figure 3.2 Illustration of Grid, Finite Volumes and Notation for a Typical Finite Volume

The notation used to denote relative control volume locations is illustrated in figure (3.2). The subscripts E, W, N and S denote quantities associated with control volumes to the right, left, above and below of an arbitrary location in the domain denoted by a subscript P. The P nodes of x and y components of velocity are associated with the pressure nodes directly to the left and below P.

3.3.2 Discretization of Differential Equations

The differential equation is formally integrated over individual finite volumes, and the resulting volume integrals are transformed to their surface counterparts where possible. The remaining integrals are subsequently approximated by algebraic expressions. In this process, the surface integrals are initially subdivided into piecewise segments, associated with specific grid points, in a symmetrical fashion. The resulting integrals are then approximated with the aid of the mean value theroem. Finally, the approximated piecewise surface integrals are transformed into algebraic expressions connecting the given grid point values. This transformation may be done in various ways, e.g. profile assumptions, finite differencing or local analytic solutions etc. It should be stressed here that in all cases particular attention must be paid to satisfying certain constraints discussed in Section (3.3.3). Finally, the discretised equation is assembled as the approximated integral equation.

To clarify the above approach and to develop adequate appreciation for the subtleties of the advanced discretization schemes discussed in Section 5, the following example illustrates the application of the technique for two-dimensional transport of a scalar. This model equation plays a central role in the development and evaluation of improved discretization schemes.

Equation (3.19) for a general scalar in Cartesian coordinates is expressed as:

$$\frac{\partial}{\partial x}(\rho u \phi) + \frac{\partial}{\partial y}(\rho v \phi) = \frac{\partial}{\partial x}\left(\Gamma_\phi \frac{\partial \phi}{\partial x}\right) + \frac{\partial}{\partial y}\left(\Gamma_\phi \frac{\partial \phi}{\partial y}\right) + S_\phi$$

where u and v are time averaged components of the velocity in the x and y directions, Γ_ϕ is the appropriate diffusive exchange coefficient and S_ϕ is the corresponding source term. Integrating the above equation over the control volume of dimensions Δx and Δy, figure (3.2).

$$\int_{\Delta x}\int_{\Delta y}\left\{\frac{\partial}{\partial x}(\rho u\phi) + \frac{\partial}{\partial y}(\rho v\phi)\right\} dydx = \int_{\Delta x}\int_{\Delta y}\left\{\frac{\partial}{\partial x}\left(\Gamma_\phi \frac{\partial \phi}{\partial x}\right)+\frac{\partial}{\partial y}\left(\Gamma_\phi \frac{\partial \phi}{\partial y}\right)+S_\phi\right\} dxdy \tag{3.20}$$

the following form is obtained upon application of the Gauss' theorem:

$$\int_{\Delta y}\left\{[\rho u\phi]_e - [\rho u\phi]_w\right\} dy + \int_{\Delta x}\left\{[\rho v\phi]_n - [\rho v\phi]_s\right\} dx$$

$$= \int_{\Delta y}\left\{\left[\Gamma_\phi \frac{\partial \phi}{\partial x}\right]_e - \left[\Gamma_\phi \frac{\partial \phi}{\partial x}\right]_w\right\} dy + \int_{\Delta x}\left\{\left[\Gamma_\phi \frac{\partial \phi}{\partial y}\right]_n - \left[\Gamma_\phi \frac{\partial \phi}{\partial y}\right]+S_\phi\right\}\Delta x\Delta y \tag{3.21}$$

where S_ϕ is assumed to be constant over the control volume and the subscripts e, w, n and s represent evaluations along the corresponding control volume faces.

To derive algebraic representations of the balance given by equation (3.21), evaluations of the convective and diffusive fluxes, expressed in terms of the nodal values of ø, are required along each of the four control volume faces in the manner described below.

Diffusive Fluxes

The diffusive flux across the e face, e.g. J_e^D, is evaluated as follows:

$$J_e^D = \int_{\Delta y}\left[\Gamma_\phi \frac{\partial \phi}{\partial x}\right]_e dy \simeq \Gamma_\phi \frac{\phi_E - \phi_P}{\Delta x} \tag{3.22}$$

Implicit in the above expression are the following assumptions regarding variable profiles along the e face:

i) Γ_ϕ is constant

ii) $\partial\phi/\partial x$ varies at most linearly along the face

iii) $\partial\phi/\partial x$ can be represented by $(\phi_E-\phi_P)/\Delta x$

Similar relations can be derived for the diffusive fluxes across each of the other faces.

Convective Fluxes

For the convective fluxes an approach similar to that adopted for the diffusive fluxes can be used. In general, this approach will lead to any number of discretization schemes including the five point-operator discretization schemes, such as Central differencing and Hybrid differencing[11] or the nine point discretization schemes such as the Skewed Upwind differencing scheme of Raithby.[12] In general, these schemes result in discretizations which suffer from false diffusion or spurious spatial oscillations. In both instances, these errors can be shown to arise from an inadequate evaluation of convective fluxes across the control volume faces.

3.3.3 Discussion on the Discretization and Solution Schemes

As there exist a myriad of arbitrary ways to reduce the differential transport equations to their corresponding algebraic sets, some guidelines have to be followed to arrive at rational choices. First, a consistent discretization scheme should reproduce the exact differential solution in the limit of an infinite number of grid points. Section (4.2) discusses the properties likely to be displayed by exact solutions. A practical appreciation of the above leads to the notion of the behavior of solution accuracy with modest grid refinement achievable, especially for three-dimensional problems. A closely related issue regarding order of accuracy is to avoid the false diffusion of first order accurate schemes or the instability of conventional second order accurate differencing for convection.

Thus, some descriptive attributes of an "ideal" discretization scheme might be stated as follows:

i) Generality and ease of application.

A discretization scheme should be capable of treating many simultaneous and strongly coupled phenomena in practical configurations of engineering geometry, i.e., a wide range of flow regimes in the presence of turbulence, heat and mass transfer, chemical reactions in arbitrary geometries. Furthermore, ease of application is also an important consideration. Generally speaking, the more complex the scheme, the more troublesome the imposition of boundary conditions.

ii) Accuracy and Economy

Minimization of solution error and computational cost are increasingly assuming significance as the primary motivation for the development and assessment of improved discretization and solution schemes. Taylor Series Expansion error analysis favored heavily in the past in the delineation of order of accuracy, has important restrictions on its validity in certain circumstances. However, one of the advantages still offered by such analyses is an indication regarding the nature of the error, i.e. dispersive (unbounded) or diffusive (dissipative). It also indicates the likely rate of reduction of approximation error with mesh spacing as the latter, in principle, becomes vanishingly small.

Currently other techniques including comparison with analytical solutions of idealized model problems are being used to guide the construction of discretization schemes. This is notwithstanding the fact that such model problems cannot embody all the pertinent characteristics of practical flow problems for which these schemes are being developed.

Economy of solution for schemes specifically refers to the relative cost of obtaining solutions of specified accuracy to a given problem by different schemes. This is generally influenced by: the accuracy of the schemes; the number of arithmetic operations required in coefficient assembly; and the type of solution algorithms which the discretized equations admit.

iii) Transparency and Reliability

As the discretized algebraic equations are the finite volume (or otherwise) analogs of the parent differential transport equations, the solution behavior displayed by them should reflect the fundamental transport physics embodied in the latter, regardless of the solution variables. This is discussed further in Section (4.2). Furthermore, appreciation of the simplifying assumptions and approximations embodied by discretization schemes should help to understand and monitor their behavior.

3.4 GENERAL SOLUTION METHODOLOGIES FOR INCOMPRESSIBLE FLOW PROBLEMS

The conservation equations of mass, momentum, energy and species presented in Section (3.2.2), equations (3.12) to (3.15), are both nonlinear and coupled. After suitably discretizing them to generate the corresponding algebraic set, it is convenient to linearize them to fully utilize the advantages

offered by the well developed techniques for the solution of linear algebraic equations. Iteration is then required to account for the nonlinearities.

Generally, there are two classes of methods used to solve the linearized algebraic equations for pressure and velocity for incompressible flows; direct methods[13] and iterative methods.[14] Direct methods are usually not used because of the excessive computational resources that are needed. However, because of the implicit nature of pressure and the pressure ~ velocity coupling the development of iterative methods can be difficult.

3.4.1 Linearization of Mass and Momentum Conservation

For two-dimensional incompressible flows where the density is a constant, the conservation of x and y momentum yield finite volume equations of the following form for u_p and v_p respectively, figure (3.1).

$$a_P^u u_P = \sum_{NP} a_{NP}^u u_{NP} + b_P^u - \Delta y(p_E - p_P) \tag{3.23}$$

$$a_P^v v_P = \sum_{NP} a_{NP}^v v_{NP} + b_P^v - \Delta x(p_N - p_P) \tag{3.24}$$

In equations (3.23) and (3.24) the summations may imply a five point or nine point computational molecule depending on the discretization scheme. From these discrete momentum equations it is seen that pressure differences appear as separate source terms. These pressure differences arise from the integration of the pressure gradient volumetric source strengths in the partial differential momentum equations. They are distinguished from the remaining source terms b_P^u and b_P^v in order to make explicit the coupling between pressure and velocity. The b_P^u and b_P^v terms may contain transient and body force effects.

The conservation of mass for the p_p control volume is expressed by:

$$\rho\Delta y(u_p - u_w) + \rho\Delta x(v_p - v_s) = 0 \tag{3.25}$$

where a constant fluid density ρ has been assumed.

A primitive variable solution procedure must arrive at u,v and p fields which satisfy equations (3.23), (3.24) and (3.25) for every u_p, v_p and p_p control volume (respectively) in the solution domain.

From Section (6.1) it is easy to appreciate that the x-momentum coefficients (a_p^u and a_{NP}^u) and the y momentum coefficients (a_p^v and a_{NP}^v) must depend strongly on the mass fluxes at the faces of the respective velocity control volumes. To illustrate how these mass fluxes are estimated, consider the mass flux through the west face of the u_p control volume in figure (3.2).

$$\dot{m}_w^u = \rho\Delta y\left(\frac{u_p + u_W}{2}\right) \tag{3.26}$$

Similarly, the mass flux through the south face of the v_p control volume in figure (3.2) is approximated by:

$$\dot{m}_s^v = \rho\Delta x\left(\frac{v_p + v_S}{2}\right) \tag{3.27}$$

Mesh uniformity has been assumed in equations (3.26) and (3.27) in that the velocities at these faces are estimated as the arithmetic mean of the nodal velocities on either side of the faces. The mass flux through the north face of the u_p control volume is comprised of two velocities, each occupying half of the face:

$$\dot{m}_n^u = \rho\frac{\Delta x}{2} v_p + \rho\frac{\Delta x}{2} v_E \tag{3.28}$$

Similarly for the east face of the v_p control volume:

$$\dot{m}_e^v = \rho\frac{\Delta y}{2} u_p + \rho\frac{\Delta y}{2} u_N \tag{3.29}$$

From these examples it is clear how the mass flux at any face of a velocity control volume may be calculated.

Since the momentum coefficients in (3.23) and (3.24) depend on mass fluxes, such as (3.26) through (3.29), which themselves depend on the unknown velocity field, it is evident that equations (3.23) through (3.25) constitute a nonlinear equation set. The linearization of equations (3.23) and (3.24) is accomplished by simply basing the momentum coefficients on mass fluxes that are calculated from best available velocity fields. Once velocity and pressure fields are obtained which comply with equations (3.23), (3.24) and (3.25), they become the best available field for the next coefficient iteration. The coefficient iteration is terminated when the velocity and pressure fields converge.

3.4.2 Solution of the Unreduced System of Equations

Linearized equations (3.23) through (3.25) can be expressed in the corresponding matrix form as:

$$[A^u]\ \{u\} + [C_p^u]\ \{p\} = \{b^u\} \tag{3.30}$$

$$[A^v]\ \{v\} + [C_p^v]\ \{p\} = \{b^v\} \tag{3.31}$$

$$[M^u]\ \{u\} + [M^v]\ \{v\} = \{0\} \tag{3.32}$$

or equivalently,

$$[A^x]\ \{X\} = \{b^x\} \tag{3.33}$$

where

$$A^x = \begin{bmatrix} A^u & 0 & C_p^u \\ 0 & A^v & C_p^v \\ M^u & M^v & 0 \end{bmatrix}$$

$$X = \begin{Bmatrix} u \\ v \\ p \end{Bmatrix}$$

$$b^x = \begin{Bmatrix} b^u \\ b^v \\ 0 \end{Bmatrix}$$

The solution of equation (3.33) can be obtained directly by inversion of $[A^x]$, by Gaussian elimination or their variants. However, the computational effort and storage requirements of these methods often are prohibitive. The computational effort requirements are further increased by having to solve (3.33) for each coefficient iteration.

To reduce the computational resources needed to solve equation (3.33) iterative solution methods are often considered. However, examination of $[A^x]$ reveals that there are entries along the principal diagonal which are zero. These zero entries, which arise because pressure does not appear in the equation representing mass conservation, makes the development of iterative methods particularly difficult. Iterative methods must ensure that the implicit influence of pressure on velocity through momentum conservation is accounted for appropriately. Iterative methods based on equivalent set of reduced equations overcome this difficulty.

3.4.3 Solution via a Generalized Segregated Approach

Using the Direct Simultaneous Variable Solution[13] a sound basis can be established for the development of a generalized segregated approach. The velocities appearing in equations (3.30) through (3.32) can be expressed in terms of the pressure by multiplying equations (3.30) and (3.31) by $[A^u]^{-1}$ and $[A^v]^{-1}$ respectively.

$$u = [A^u]^{-1} b^u - [D_p^u] p \tag{3.34}$$

$$v = [A^v]^{-1} b^v - [D_p^v] p \tag{3.35}$$

where

$$[D_p^u] = [A^u]^{-1}[C_p^u]$$

$$[D_p^v] = [A^v]^{-1}[C_p^v]$$

and where $[D_p^v]$ and $[D_p^v]$ represent the influence of all pressures in the calculation domain on the u and v velocities respectively. Substituting for the velocities from equations (3.34) and (3.35) into (3.32) there results:

$$[A^p]\ \{p\} = \{b^p\} \tag{3.36}$$

where

$$[A^p] = -[M^u]\,[D_p^u] - [M^v]\,[D_p^v]$$

$$\{b^p\} = -[M^u]\,[A^u]^{-1}\,\{b^u\} - [M^v]\,[A^v]^{-1}\,\{b^v\}$$

Such an approach still requires excessive storage and effort (in general, less than those for the unreduced system discussed in the previous section) to invert and store $[A^p]$, $[D_p^u]$, $[D_p^v]$ etc. Van Doormaal[14] through a detailed study regarding the nature of $[D_p^u]$ matrix established how the mechanisms of convection and diffusion can spread the influence of pressure throughout the complication domain and analyzed the implications of adopting localized approximations (a feature that is prevalent in most segregated approachs) for it. Denoting by $[\bar{D}_p^u]$ and $[\bar{D}_p^v]$ the approximate evaluations of $[D_p^u]$ and $[D_p^v]$, a generalized segregated approach that employs iteration for these approximations is now formulated. Taking the value of pressure at the k'th segrated iteration to be $\{p^*\}$, the estimate of pressure, the corresponding $\{u^*\}$ and $\{v^*\}$ velocities which satisfy equations (3.30) and (3.30) are given by:

$$\{u^*\} = [A^u]^{-1}\,\{b^u\} - [D_p^u]\,\{p^*\} \tag{3.37}$$

$$\{v^*\} = [A^v]^{-1}\{b^v\} - [D_p^v]\,\{p^*\}' \tag{3.38}$$

Because $\{p^*\}$ is not correct, then $\{u^*\}$ and $\{v^*\}$ are not correct. To obtain improved estimates of velocity given by $\{\bar{u}\}$ and $\{\bar{v}\}$, it is necessary to subtract out the effect of $\{p^*\}$ on $\{u^*\}$ and $\{v^*\}$ and add in the effect of an improved pressure estimate given by $\{\bar{p}\}$. This can be accomplished in an approximate way by subtracting $-[\bar{D}_p^u]\,\{p^*\}$ from and adding $-[\bar{D}_p^u]\,\{\bar{p}\}$ to equation (3.37), and subtracting $-[\bar{D}_p^v]\,\{p^*\}$ from and adding $-[D_p^v]\,\{\bar{p}\}$ to equation (3.38). As a result;

$$\{\bar{u}\} = \{\hat{u}\} - [\bar{D}_p^u]\,\{\bar{p}\} \tag{3.39}$$

$$\{\bar{v}\} = \{\hat{v}\} - [\bar{D}_p^v]\,\{\bar{p}\} \tag{3.40}$$

where

$$\left\{\hat{u}\right\} = \left\{u^*\right\} + \left[\bar{D}_p^u\right] \left\{p^*\right\}$$

$$\left\{\hat{v}\right\} = \left\{v^*\right\} + \left[\bar{D}_p^v\right] \left\{p^*\right\}$$

Requiring that the velocities $\left\{\bar{u}\right\}$ and $\left\{\bar{v}\right\}$ satisfy mass conservation

$$\left[M^u\right] \left\{\bar{u}\right\} + \left[M^v\right] \left\{\bar{v}\right\} = \left\{0\right\} \tag{3.41}$$

and substituting for velocities from equations (3.30) and (3.40) the following equation for pressure results,

$$\left[\bar{A}_p\right] \left\{\bar{p}\right\} = \left\{\bar{b}^{\bar{p}}\right\} \tag{3.42}$$

where

$$\left[\bar{A}_p\right] = - \left[M^u\right] \left[\bar{D}_p^u\right] - \left[M^v\right] \left[\bar{D}_p^v\right]$$

$$\left[\bar{b}^{\bar{p}}\right] = - \left[M^u\right] \left\{\hat{u}\right\} - \left[M^v\right] \left\{\hat{v}\right\}$$

The success of the generalized segregated approach described by equations (3.37) to (3.42) depends on how accurately $[D_p^u]$ and $[D_p^v]$ are approximated and how readily $[\bar{D}_p^u]$ and $[\bar{D}_p^v]$ are evaluated and the solution for pressure is determined. To ensure that the solution for pressure is easily found it is convenient to relate each of the velocities in terms of nodal values of pressure and velocity (cf. equations 3.23 and 3.24).

$$\bar{u}_p = \hat{u}_p - \bar{d}^u \left(\bar{p}_E - \bar{p}_p\right) \tag{3.43}$$

$$\bar{v}_p = \hat{v}_p - \bar{d}^v \left(\bar{p}_N - \bar{p}_p\right) \tag{3.44}$$

where

$$\hat{u}_p = u_p^* + \bar{d}^u (p_E^* - p_P^*)$$

$$\hat{v}_p = v_p^* + \bar{d}^v (p_N^* - p_P^*)$$

and where for SIMPLE,[1] e.g.

$$\bar{d}^u = \Delta y / a_p^u$$

$$\bar{d}^v = \Delta x / a_p^v$$

Substituting for the velocities from equations (3.43) and (3.44) into (3.25) the equation for pressure is given by, figure (3.2):

$$a_P^{\bar{p}} \bar{p}_P = \sum_{NP} (a^{\bar{p}} p)_{NP} + b^{\bar{p}} \tag{3.45}$$

where

$$a_P^{\bar{p}} = \sum_{NP} a_{NP}^{\bar{p}}$$

$$a_E^{\bar{p}} = \rho \Delta y \, \bar{d}_p^u$$

$$a_W^{\bar{p}} = \rho \Delta y \, \bar{d}_W^u$$

$$a_N^{\bar{p}} = \rho \Delta x \, \bar{d}_p^v$$

$$a_S^{\bar{p}} = \rho \Delta x \, \bar{d}_S^v$$

$$\bar{b^p} = - \rho \Delta y \hat{u}_p + \rho \Delta y \hat{u}_W - \rho \Delta x \hat{v}_p + \rho \Delta x \hat{v}_S$$

4.0 ASSESSMENT OF IMPROVED DISCRETIZATION SCHEMES AND SOLUTION ALGORITHMS FOR GENERAL (INCOMPRESSIBLE) FLOW PROBLEMS

4.1 INTRODUCTION

Recently substantial progress has been made in the development numerical procedures for the solution of differential equations governing fluid flow, heat and mass transfer for engineering applications. However, there remain, in practice, certain deficiencies in these methods that need to be resolved before they can be used reliably and efficiently.

Prediction of complex turbulent flow structures including separated zones using "conventional" discretization and solution schemes runs into serious accuracy issues, as such schemes display appreciable deterioration in accuracy due to misalignment of the flow and computational mesh. Most practical schemes in current use artificially dissipate steep gradients due to limited spatial resolution capabilities. The resulting effect, in some cases, may completely overshadow real effects such as physical diffusion due to turbulence.

Alternative schemes specifically designed to alleviate such dissipative errors succeed only partially, as the solution is usually plagued with improperly bounded, non-physical oscillations. Associated with such behavior are problems of numerical instability due to unfavorable conditioning of the coefficient matrix.

The discretization errors of diffusive schemes can, in principle, be alleviated through mesh refinement. However, such an approach is not always feasible nor effective, as the solution cost and resources can become prohibitive especially for three-dimensional problem. What is required is a stable scheme that yields bounded solutions while minimizing the influence of diffusive errors. Rational construction of such schemes through careful analysis of the properties of exact solutions for the differential transport equations is one concern of this Section.

The numerical solution of incompressible flow problems is further complicated due to nonlinearities and couplings inherent in the corresponding differential transport equations, thus considerable computing resources are

required to obtain solutions to the algebraic equation set derived from an appropriate discretization scheme. If a segregated (SIMPLE-like)[15] approach is adopted to solve these algebraic equations, then, in many instances, a major portion of the computational cost is associated with the solution of the equation for pressure (or its correction). Minimization of the computational costs associated with solving the linear pressure equation, as well as a descriptive structure analysis of general segregated methods are also discussed in this Section.

4.2 CHARACTERISTICS OF ACCURATE DISCRETIZATION SCHEMES

Some guidelines regarding the attributes of an "ideal" discretization scheme can be formulated on the requirement of consistency between the differential and discretized equations. However, before such a task is undertaken, the pertinent characteristics likely to be displayed by the exact solutions of the differential equation are reviewed.

Properties of Exact Solution[16]

i) Conservation

For any region D with surface S the volume integral of the differential equation (3.19) is expressed using vector notation as:

$$\oint_S \left\{ \rho \vec{u} \phi - \Gamma_\phi \text{grad } \phi \right\} \vec{n} \, dS - \int_D S_\phi \, dD = 0 \qquad (4.1)$$

where $\vec{n}$ is the unit normal surface vector (positive outward)

ii) Boundedness

It is straightforward to appreciate the significance of the Maximum principle for the simple case of source free conservation equations. These solutions cannot display positive maximum or negative minimum inside the region D., i.e., the solution must be bounded in D by its extreme values on S

$$\min (\phi_S) \leq \phi \leq \max (\phi_S) \qquad (4.2)$$

Similar bounds can be derived for more general cases of different boundary conditions and/or finite source effects.

iii) Levelness

If the differential equation contains only derivatives of the dependent variable ϕ, then the functions ϕ and $\phi + C$ (C is an arbitrary constant) both satisfy the differential equation.

iv) Transportive

In the regions of flow where convection dominates, the solution is strongly influenced by upstream conditions. The directional behavior of flow is generally associated with the existence of domain of dependence notion with each mesh point.

Guidelines for the Construction of Discretization Schemes

The nodal algebraic equation is an integral approximation to the differential equation and hence should preserve all the important properties of the latter as described above. Such constraints generally furnish specific requirements to be satisfied in the construction of discretization schemes.

By adopting a "suitable" approximation scheme for the convection terms of equation (3.21), the resulting nodal algebraic equation is symbolically represented by:

$$\phi_P = \frac{1}{a_P} \sum_{NP} a_{NP}\phi_{NP} + b_P \qquad (4.3)$$

In the above (using the conventional notation) the subscript NP refers to the neighbours of P. The quantity a_P is the coefficient for ϕ_P and a_{NP} is the coefficient for ϕ_{NP} (i.e., a_E for ϕ_E, a_W for ϕ_W, etc.). Term b_P denotes the source term for the control volume P that may contain physical source or sink and/or a transient storage term for unsteady problems. The quantities a_{NP}/a_P are generally referred to as influence coefficients and should ideally all be non-negative to satisfy the boundedness requirement of exact solutions.[17] The existence of negative influence coefficients anywhere in the finite volume equations is commonly referred to as the negative coefficient problem. The appearance of negative coefficients in sufficient numbers and magnitudes in the finite volume equation set may violate the smoothness of solutions by generating non-physical overshoots and/or undershoots and also lead to difficulties in iteratively solving the algebraic set. Closely associated with the latter issue is the mathematical

notion of diagonal dominance. The matrix of influence coefficients is diagonally dominant if, for every node P:

$$\sum_{NP} \left| \frac{a_{NP}}{a_P} \right| \leq 1 \qquad (4.4)$$

with strict inequality holding for at least one node. Clearly negative influence coefficients violate this rule. For a constant set of coefficients, matrix theory guarantees convergence to a ø solution provided the matrix of influence coefficients is diagonally dominant. It is important, however to make two points regarding diagonal dominance. First diagonal dominance is not a necessary condition for convergence. Second, the matrix of influence coefficients often is not constant in practice since the coefficients change as other coupled solution variables change in the progress of the iterative solution; the linearization process, whereby the influence coefficient matrix is updated, is another potential source of instability in the overall solution scheme.

An additional property of significance for equation (4.3) is that of adidivity expressed by:

$$a_P = \sum_{NP} a_{NP} + \underbrace{\frac{\rho \Delta x \Delta y}{\Delta t}}_{\text{unsteady term}} \qquad (4.5)$$

This condition is assured provided the convecting mass fluxes used to establish equation (4.3) obey continuity for control volume P. This property is important, since it permits a linear function of ø also to obey the finite volume equations, levelness property of exact solutions.

Regarding the conservation property of exact solutions, the algebraic equation set should satisfy the integral conservation relation (4.1) both locally and globally. To meet the additional global conservation, flux continuity in the discretized equation at cell boundaries must be assured. Only under such circumstances will interface fluxes at adjoining volume cancel in pairs, leaving the exterior surface integral to be balanced by interval sources/sinks.

The transportive property of exact solutions requires, in the limit of strong convection, the solution of the algebraic nodal equation to display the pertinent "directional" sensitivity, i.e., nodal values lying outside the domain of dependence/influence of a particular node should not feature in the discretization. Failure to comply with this requirement can give rise to the negative coefficient problem described above and hence, from the boundedness principle, unrealistic solutions may result.

A practical primary qualifier of a discretization scheme is its accuracy. For problems of interest in this study, a pragmatic interpretation of accuracy refers to obtaining solutions uncorrupted by numerical diffusion using practical grid sizes and covering a range of solution variables, notably arbitrary inclination of flow to grid and arbitrary values of Peclet number. The issues of conservation and boundedness are closely tied to the overall question of the accuracy of a given discretization scheme, for which however it is much more difficult to derive, in general, a priori criteria or measures. As discussed in Section (3.3.3) earlier analyses of accuracy comprising mainly Taylor Series Expansions have recently been shown[18] to have serious limitations and shortcomings. A practical measure of accuracy freely adopted in this study relates to the rate of convergence of a discretization scheme. Such a criterion displays quantitively the sensitivity of the numerical solution to grid refinement in asymptotically approaching the analytical solution for model problems.[19]

Analysis of additional characteristics including generality and ease of application as well as economy and efficient are also important considerations in the development and assessment of discretization schemes. A concise summary outlining the attributes of desired discretization schemes is provided in Section (4.4).

4.3 COMPUTATIONAL DETAILS OF THE IMPROVED SOLUTION SCHEMES FOR INCOMPRESSIBLE FLOWS

Majority of the incompressible flow solution algorithms in current use adopt a particular form of the Generalized Segregated Approach, Section (3.4.3), to deal with the pressure ~ velocity coupling problem, although recently there have appeared algorithms designed to solve the relevant equation set directly.[20,24] The following discussion will thus focus on the structure of segregated approaches including implementation and operational details.

The $[D_p^u]$ matrix in Section (3.4.3) was shown to represent the influence of pressures on velocities and was later approximated by $[\bar{D}_p^u]$ to affect an easy solution for the pressure. However, this simple form $[\bar{D}_p^u]$ where each velocity is linearly related to the local pressure difference, introduced primarily to minimize computational requirements, has two major shortcomings.

For high Reynolds number flows of concern in this study, using minimal or no under-relaxation for the solution that implies large effective time steps for a time marching scheme,[22] pressure differences far upstream of a velocity can significantly influence the velocity, thus a relation between the velocity and only the local pressure difference is not likely to be appropriate. The implication is that the use of any segregated method which simplifies the evaluation of $[\bar{D}_p^u]$ by relating each velocity to only the local pressure difference for solving convection dominated steady flows, necessarily implies considerable under-relaxation for the variables.

The second shortcoming of this simple form of $[\bar{D}_p^u]$ is that, without taking special care, the convergence of the segregated method could degrade significantly with grid refinement. To illustrate this, consider using a segregated method that adopts the simple form of $[\bar{D}_p^u]$ for a high Reynolds number problem using two grids, one with relatively few control volumes, another with a large number of control volumes. Suppose that on the coarse grid a value for E, defined as a multiple of the maximum of explicit time step,[15] is chosen such that the simple form of $[\bar{D}_p^u]$ was appropriate. (Discussion here refers to time integration of equations to reach steady state, although relaxation and time integration approaches can be related by a simple relationship that exists between E and the more conventional under-relaxation parameter used in study). Then on the fine grid choose E so that the effective time step is the same as that for the coarse grid. Now, because the effective time steps are the same for both grids, the spatial distribution of the normalized influence of pressure differences for both grids will also be similar. Therefore, on the coarse grid where the E was chosen to that the simple form $[\bar{D}_p^u]$ would be appropriate, the majority of pressure difference influence would arise in the distance given by the coarse grid spatial step size. However, on the fine grid, the same distance is covered by a number of fine grid spatial steps. As a result, on the fine grid the velocity may be influenced by more than one fine grid pressure difference and the

simple form of $[D_p^u]$ will not be appropriate. Only by reducing the value of E (or the under-relaxation parameter) will the simple form of $[D_p^u]$ be appropriate for the fine grid. But in the process of reducing the value of E (or the effective time step) the number of coefficient iterations (or time steps) required to achieve convergence (or steady state) is increased and, subsequently, the rate of convergence is reduced. To increase the implicitness of the pressure ~ velocity coupling of segregated approaches, improved pressure algorithms notably SIMPLER,[1] PISO,[6] SIMPLEC[15] and others[14] have been proposed and will be used freely throughout this study.

To provide a background for appreciation of some of the techniques considered in this study, it is also appropriate to discuss the solution of the pressure equation of the SIMPLE algorithm,[1] equation (3.45).

The solution of the pressure equation is a major component of the segregated approach and can represent a significant portion of the total cost of solving a flow problem. It is therefore a high priority to solve for pressure in an efficient manner. As discussed previously, the use of direct solution methods tends to be unattractive due to large storage requirements and computer effort. Extremely fast Poisson solvers are available[20] but these are not applicable to the pressure equation. Furthermore, the coefficients of the pressure equation change each coefficient iteration so that sparse matrix solvers that are applicable require a new decomposition at each iteration. Iterative methods such as Successive Over-relaxation and line by line methods using the Tri-Diagonal Matrix Algorithm,[25] Stone's Strongly Implicit Procedure[26] and the Modified Strongly Implicit Methods of Schneider and Zedan[27] are better suited to this application. Finally, because for incompressible flows, the pressure is determined by solving a symmetric positive definite matrix equation, equation (3.42), the Chebyshev and Conjugate Gradient techniques[25] may be used to accelerate the convergence of many of the methods listed above.

With the use of iterative solution methods for the solution of the pressure equation, termination of the iterative procedure becomes an important consideration. If iteration of the pressure equation is terminated before sufficient convergence is achieved, mass conservation is poorly satisfied by the corrected velocities. Since it is usual for only one iteration of the segregated method to be performed, these corrected velocities are then used to calculate new coefficients of the linearized algebraic equations. Propagating

the error in this fashion can result in divergence or slow convergence of the coefficient iteration. On the other hand, it is uneconomical and wasteful to solve the pressure equation to a tight convergence at each segregated iteration.

Let $\|r^p\|^l$ represent a measure of the residual of the pressure equation after each l iterations of the iterative method used to solve the pressure equation. One measure of the residuals is given by the Euclidean norm where:

$$r^p{}^l = \left[\sum_{AV}(a_P^p \bar{p}_p{}^l - \sum_{NP}(a^p \bar{p})_{NP}^l - b^p)^2\right]^{1/2} \tag{4.6}$$

and where $\sum_{AV}$ is the summation of all interior volumes. An alternative measure is provided by the sum of the absolute values of the control volume residuals.

$$\left\| r^p \right\|^l = \sum_{AV} a_P^p \bar{p}_p{}^l - \sum_{NP}(a^p \bar{p})_{NP}^l - b^p \tag{4.7}$$

A convenient method of terminating the pressure iteration is given by:

$$\left\| r^p \right\|^l \leq \gamma^p \left\| r^p \right\|^0 \tag{4.8}$$

where the 0 superscript on $\|r^p\|$ is used to denote the initial measure of the residual for l = 0. Equation (4.8) guarantees that iteration has reduced the residual of the pressure equation to at least the fraction γ^p and can be used for most problems with optimal values of the residual reduction factor γ^p typically ranging from 0.25 to 0.05. This avoids costly trials to determine a suitable value of the convergence criterion. Additionally, the number of iterations on the pressure equation for each coefficient iteration is roughly the same.[19]

4.4 SELECTION OF THE ASSESSMENT CRITERIA AND METHODOLOGY

The desired characteristics of a discretization scheme in terms of preserving the basic properties of the exact solutions (i.e. conservation, boundedness, levelness and transportive) as related to issues of accuracy and stability of solutions have been discussed in detail in Sections (3.3.3) and (4.2). This Section will expound on those ideas and introduce additional auxilliary criteria such that a comprehensive list of attributes is developed to critically evaluate the schemes considered in this study.

It was established in Section (3.3.3) that a priori assessment of accuracy of a scheme in a complex turbulent flow environment of the kind considered in this study was extremely difficult. This was shown to be primarily due to the inadequacy of the error analysis provided Taylor Series Expansion for the relatively coarse grids used (especially for three dimensions) as well as the limited guide offered by comparison with model solutions. However, such methods could be effectively used to economically identify schemes of maximum potential. Also when evaluating the performances of selected schemes in accurately predicting the engineering details of turbulent flow, means have to be provided to delineate the uncertainties and error introduced by the turbulence model.

Stability of the iterative solvers, used primarily to minimize computational costs associated with a solution, were also shown to be strongly influenced by the condition of the matrix of influence coefficients. The impact of such restrictive requirements can, in principle, be alleviated or lessened by solvers that are more transparent to the details of the discretization scheme (stable). However, development and assessment of such solvers to cover a wide range of condition numbers, as variables continually change in the course of the iterative solution, is a very demanding undertaking.

The specific definition of economy or alternatively cost effectiveness of solutions, as adopted in this study, pertains to the relative costs of obtaining solutions of specified accuracy to a given problem by different schemes. The cost will generally be a complex function of the accuracy of the schemes, the nature and the number of computer operations required in coefficient generation and assembly, the type of solution algorithms which the discretized equations admit, and the details of the computer architecture used

for solutions. Economic considerations generally yield quantitative criteria to identify and dispense with discretization schemes that are only marginally more accurate but require substantially larger computational resources for a solution.

Closely associated with the above notion of computational economy are considerations related to variable storage requirements. Although significant advances have recently been made in extending the storage capability of current machines and the trend is likely to continue in the future, providing adequate storage to solve practical engineering problems, especially in three dimensions, still remains a major problem even for non-reacting flows. Considering the enormous additional complexity introduced by reaction, to obtain sufficiently resolved solutions for the two-phase, turbulent, reacting, radiating flow in arbitrary combustor configurations places prohibitive demands on the storage available. Thus, in spite of the extended finite difference computational molecule (hence storage) implied by more accurate discretization schemes, their use might still be preferred over schemes of lower accuracy as the grids required may be relatively coarse.

Finally, some additional requirements of a more practical nature are adopted by the present study to arrive at rational choices for the schemes considered. These pertain to implementation and application details and specifically refer to compatibility with the present codes and the inherent complexity. As the present study was structured to develop improved discretization schemes and solution algorithms for use with TEACH-type methodologies, it is important that the use of proposed schemes be compatible with the constraints implied therein. In addition, generally speaking, the more complex the scheme, the more difficult is the implementation and application and hence possibility of errors, especially in imposing boundary conditions in a finite duration program.

The following list, based on the above discussion, summarizes the desired attributes that potentially viable techniques should possess to merit further consideration:.

i) Accuracy

ii) Stability

iii) Expected efficiency

iv) Variable storage requirements

v) Expected computing times

vi) Ease with which the techniques can be incorporated into existing 3-D codes for computing turbulent, recirculating flows.

It is clear from the above list that strict satisfaction of all the items considered is exceedingly difficult, if not impossible. Thus, invariably judicious compromises have to be introduced. It can be argued that the most significant requirements regarding discretization schemes considered are that, they are conservative and bounded, as these characteristics generally enhance accuracy. Also a bounded scheme yields a well-conditioned coefficient matrix which is diagonally dominant, irrespective of the magnitude of the Peclet number and the angle of inclination between the flow and the mesh. Such desirable attributes are strictly realized for certain simple five-point schemes like Hybrid or Upwind differencing schemes utilizing a finite volume formulation. However, for the majority of the schemes with extended computational stencils considered in this study, issues of conservation and boundedness cannot be established a priori and qualitative/quantitative guidelines have to be established to examine their expected behavior. In the present effort, for this purpose a judicious combination of quantitative/qualitative assessment practices have been employed. These include accuracy and linear stability of the resulting difference equations via evaluation of the properties of the coefficient matrix, Taylor series analyses and existing heuristic stability analyses for iterative solvers commonly used in segregated solution procedures like TEACH. These analyses, performed primarily for model problems with known analytical or "exact" numerical solutions, yield further qualitative information regarding solution cost effectiveness, complexity and variable storage requirements. In addition assessment can be made of the inherent accuracy and stability characteristics of the schemes considered. Naturally, if a consistent finite volume discretization framework is employed in the above test problems, conservation is strictly ensured locally, as well as globally and the specification of boundary conditions arises naturally.

The above model problems incorporate highly idealized flows in the presence of a dominant influence (convection, diffusion, source). However, for practical performance evaluations such problems have to be replaced by more realistic flow cases to examine the interdependency and delicate balance

displayed by coupled, nonlinear flow equations. Invariably, identification and effective treatment of accuracy issues in practical engineering computations is a much more difficult but deserving undertaking and should utilize effectively the results obtained from individual model problems.

4.5 CLOSURE

This Section has reviewed in some detail the relevant characteristics of accurate discretization schemes as well as the computational details of improved solution algorithms for incompressible flows. Practical criteria to guide the identification and assessment of select techniques were established. These will be used readily in the next Section to provide a unified qualitative/quantitative basis to discuss the pertinent details of the schemes considered and hence examine their suitability for further quantitative evaluation.

5.0 DESCRIPTION AND PRELIMINARY ASSESSMENT OF CANDIDATE SCHEMES

5.1 IMPROVED DISCRETIZATION AND RELATED TECHNIQUES

The following potential schemes were identified and qualitatively assessed to provide improved (more accurate) predictions of isothermal, incompressible, turbulent, recirculating flowfields:

i) Second Order Upwind Differencing Scheme
ii) Advanced Skewed Upstream Differencing Schemes
iii) Higher Order Schemes including Various Compact Implicit Differencing Schemes
iv) Explicit Dissipation Schemes
v) Improved Flux Blending Schemes
vi) Variational Discretization Schemes including Finite Elements
vii) Spectral Methods
viii) Lagrangian Methods
ix) Adaptive Gridding and Modified Equation Analysis

The following sections briefly describe these techniques with references to original works and comment on their relevancy, strengths and shortcomings relative to the application of interest. The assessment criteria developed in the previous Section will be referred to frequently to identify potential techniques for subsequent quantitative evaluation in a two-dimensional code.

Although the structure, application and other attributes of the considered schemes vary widely, a careful scrutiny of the relevant literature reveals considerable success in meeting the primary concern of accuracy for most schemes in problems of interest. Hence, this preliminary assessment will emphasize issues of accuracy and stability leaving the less significant criteria of economy, compatability, etc. as practical constraints in the selection of the final four schemes.

5.1.1 Second Order Upwind Differencing Scheme (SOU)

This scheme is going to be discussed in detail in Section (6.2), however, some of its relevant characteristics will be outlined below for completeness.

Second order upwind Differencing Scheme (SOU) combines, in general, the desirable monotonic character of upwind schemes with second order accuracy for certain grid distributions. The scheme was first introduced by Atias, et al[28] in model problems including the square cavity problem and the impinging jet flow. The convergence and stability characteristics of the scheme were subsequently studied by Gupta and Manohar[29] for the linearized one-dimensional vorticity transport problem. During Phase I Aerothermal Modelling effort sponsored by the Nasa Lewis Research Center, it was further studied by General Electric[2] in a variety of model problems.

The stability analysis of the scheme, via a one-dimensional scalar transport problem, reveals that the characteristic difference equation exhibits a monotonic behavior with no spatial instability for uniform sign of convecting velocity. However, the case of the velocity changing sign across a finite volume cell, characteristics of recirculation boundaries, warrants further investigation.

The scheme can be shown to be second order accurate only on a smoothly varying grid using an error analysis provided a Taylor Series Expansion, Section (6.2). However, owing to the introduction of an extraneous boundary condition in the solution of the model difference equation (three solutions vs two required by the differential form) care needs to be exercised in the proximity of the boundaries for uniform application throughout the domain. In fact, it is claimed by Gupta and Manohar[29] that the overall accuracy of the scheme is severely affected by the inconsistencies introduced in boundary condition specification.

5.1.2 Advanced Skewed Upstream Differencing Schemes

These are going to be discussed in detail in Section (6.3), however a brief description is provided here for introduction.

The original Skewed Upstream Differencing (SUDS) of Raithby,[12] although non-diffusive, was for some applications, plagued by problems of unbounded solutions. Furthermore, potential iterative solution difficulties were evident, as the resulting coefficient matrix was not diagonally dominant owing to the possibility of main model coefficients becoming negative, e.g. a_W in equation (3.23). A practical means of overcoming the boundedness and related issues was later introduced by Syed, et al[5] who, blending SUDS with a less accurate but bounded scheme (e.g. Hybrid differencing) in varying

ratios, was able to obtain improved solutions. However, the particular form of the adopted blending strategy is not strictly path independent, thus possibility of non-unique solutions exist.

Recent works by Huget[30] and Raw[10] using similar implementations of the Physical Advection Correction (PAC) concept within the framework of SUDS, have overcome most of the original objections to the scheme as well as providing a sound formulation to replace/augment the blending strategy. Two variants of advanced SUDS are considered:

i) Linear Profile Skewed Upstream Differencing Scheme (LP-SUDS): admits minor oscillations in the solution, but consequently yields most accurate results (uniformerly second order) of any SUDS scheme for a variety of problems.

ii) Mass Weighted Skewed Upstream Differencing Scheme (MW-SUDS): a positive definite skew scheme that produces stable, bounded solutions which are significantly more accurate than those Hybrid differencing.

As with SOU, these schemes can be formulated conveniently, in a manner to satisfy most of the assessment criteria.

5.1.3 Higher Order Schemes Including Various Compact Implicit Differencing Schemes

These will be discussed in detail in Section (6.4), however the following serves as a brief introduction.

Use of higher order schemes (fourth and up) in atmospheric and oceanographic applications has been advocated primarily by Kreiss.[31] Order in this context strictly refers to classical error analysis provided by a Taylor Series Expansion, Section (3.3.3).

The advantages of fourth order schemes over second order schemes are most aptly demonstrated for the test problem of the one-dimensional wave (hyperbolic) equation. Using centered second order differencing and a widely available fourth order approximation to the advection term, Orszag[32] examined the structure of local errors in the difference scheme and concluded that the fourth order scheme requires roughly a factor 2 less resolution to achieve a 5 percent maximum error, than does the second order scheme. Furthermore, the fourth order scheme also localizes the error near the singularity better. The second and fourth order schemes used in this and other studies are due to Arakawa.[33] They possess extremely desirable properties

in identically conserving vorticity, enstrophy (half the vorticity squared) and kinetic energy. Due to these characteristics, they are especially well suited to study hydrodynamic stability problems. Since they conserve enstrophy they are not subject to the nonlinear instability of Phillips[34] which arises from aliasing errors.[18]

Among the objections raised towards the use of higher order differencing schemes in complex flow field simulations, one notes, in general, issues related to cell Reynolds number restrictions (boundedness and transportive characteristics), cost and the nature of the solution algorithms. For example, the conventional fourth order differencing for the first order advection term involves five points in the formulation. This practice generally suffers from the usual problems associated with the degradation of numerical accuracy at the boundaries (an excessive number of image points have to be used for a uniformly valid application of the technique). Furthermore, the solution of the algebraic differencing equations is accomplished by more involved steps than the application of the simple Tri-Diagonal Matrix Algorithm, Section (6.4.4).

There is a certain class of higher order schemes which have been shown to resolve some of the deficiencies associated with the conventional schemes. These are generally referred to as Operator Compact Implicit (OCI) schemes. Related techniques including Hermitian differencing, Pade' approximations, spline collection techniques of Rubin and Khosla[35] can essentially be developed in the same spirit as OCI schemes. However, experience with these is relatively limited. Thus the following discussion will concentrate on OCI schemes.

Classical OCI schemes are designed to produce a relationship between the unknown solution ϕ and the <u>entire differential operator</u> $L(\phi)$ on three adjacent points using a general finite difference approach. If the resulting scheme is formally fourth order accurate, then the method is known as OCI. Note that the formal fourth order accuracy is the highest that can be obtained by such derived methods, unlike the spline collection schemes of Rubin and Khosla.[35]

Experience with such schemes using model and practical problems, has revealed serious issues of stability and boundedness as well as degradation in accuracy with grid non-uniformity and implementation of non-physical boundary conditions, Ciment.[36] To overcome such undersirable attributes Berger, et al[37] recently derived a further class of OCI schemes. These consider the OCI coefficients obtained from the Taylor series approach as

asymptotic series in the mesh size. The resulting scheme contains nine free parameters. Using six of these parameters it is possible to obtain formally a fourth order method with no cell Reynolds number limitation. Moreover, the tri-diagonal system of equations is diagonally dominant. The fourth order accuracy is normally achieved by incorporating an appropriate exponential character into the coefficients. However, the cost issues involved in the iterative computation of such exponentials need to be examined critically, Section (6.4.3).

5.1.4 Explicit Dissipation Schemes

The idea of artificial dissipation is credited to Von Neumann and Richtmeyer[38] in connection with shock capturing calculations. This concept is very commonly used with time marching, compressible, Lax-Wendroff and/or other implicit schemes to attenuate high frequency oscillations associated with shocked flows. The essence of the method lies in introducing an artificial dissipation term into the difference equations (not the differential equation) such that the added term is of order higher than the truncation error of the difference scheme provided by a Taylor Series Expansion. The dissipation so introduced, however, does not represent any loss of energy or other conserved quantities; the kinetic energy that is removed from high frequency oscillations is left in the system as internal energy of the fluid.

Most explicit dissipation schemes utilize pressure as the relevant sensor to activate the dissipation term (appropriate for shocked flows), MacCormack.[39] For uniform pressure (or slowly varying pressure, characteristics of the flows considered here) other variables have to be considered to serve the same purpose. Advantages of explicit dissipation schemes are the strict local control of the boundedness and stability of solutions provided by an inherently dispersive but accurate scheme (Central differencing), as well as the simplicity of the corresponding formulation. Moreover, such schemes have seen an extended development and application period in the prediction of mostly compressible external flows using time marching techniques by Jameson,[40] Beam and Warming,[41] MacCormack,[42] etc. However, the somewhat non-unique nature of the implementation for various problems, as well as the influence of the added terms on the solution, in conjunction with the implicit dissipation provided higher order upwind schemes are only now beginning to be analyzed for time dependent implicit schemes, Pulliam.[43]

The time dependent Beam and Warming algorithm[41] which requires a fourth order damping term when spatial Central differencing is used, was recently adopted by Kwak, et al[44] to obtain numerical solutions for incompressible Navier Stokes equations in a generalized system. These authors used the artificial compressibility technique of Chorin[45] to perform a time integration of the equations in primitive form. The formulation of the artificial dissipation term was based on a fourth derivative of the form (x-direction):

$$S_j = -\alpha/8\ (\Delta x^4)\ \left(\frac{\partial^4 \phi}{\partial x^4}\right)_j = -\alpha/8\ (\phi_{j+2} - 4\phi_{j+1} + 6\phi_j - 4\phi_{j-1} + \phi_{j-2}) \tag{5.1}$$

where α is an adjusted constant, ϕ is a conserved variable, j is the particular grid node. A similar expression is used in the y-direction.

An important point regarding time dependent methods must be further elaborated. Convergence to steady state can be characterized (based on the theory of characteristics) as a physical process of acoustic and entropy waves clearing from the computational domain. A spatial smoothing procedure can then be viewed to cause dual effects; dissipation of transient acoustic/entropy waves and dissipation of high frequency oscillations introduced by the differencing schemes (oscillations are real solutions of difference equations).[18] Artificial dissipation introduced into difference equations as a term of higher order than the truncation error of the scheme is unlikely to influence the true solution of the differential equation (either transient or steady state). This means that enhancement of damping transient acoustic/entropy waves would require a dissipation term which is either of the same or lower order than the truncation error. The converged solution, however, could be in serious error in such cases. Based on this argument it is readily seen that the dissipation term must be designed to achieve stability of the difference scheme (e.g. Central) by filtering growth of the high frequency oscillations.

It is relevant at this point to discuss the general nature of a dissipation term that could be used in relaxation algorithms (steady state discretization of equations) for modelling of incompressible, turbulent, recirculating flows.

A steady state matrix equation of the form (cf. equation (3.33)):

$$A(\phi) = b \tag{5.2}$$

is replaced by an equation of the form:

$$A(\phi) - D(\phi) = b \tag{5.3}$$

where A denotes the spatial discretization operator for the variable ϕ, defined by a Central or an equivalent scheme, b the source and D the dissipative operator. D is assumed to be fourth order accurate with a form given for two dimensions as:

$$D(\phi) = D_x(\phi) + D_y(\phi) \tag{5.4}$$

where

$$D_x(\phi) = d_{i+1/2,j} - d_{i-1/2,j}$$

$$D_y(\phi) = d_{i,j+1/2} - d_{i,j-1/2}$$

and

$$d_{i+1/2,\ j} = - K_{i+1/2,j}\ \Delta_{i+1/2,j}\ \phi$$

In the above i and j denote grid indices and $K_{i+1/2,\ j}$ is generally a constant for model problems derived from a stability analysis of the linear difference equations. For complex flows however, no rigorous stability analysis exists and the spatial variation of K due to non-homogeneous, non-linear flow processes has to be specified iteratively. $\Delta_{i+1/2}$ is a suitable difference operator that renders the smoothing term fourth order accurate, i.e.,

$$\Delta_{i+1/2,\ j}\phi = (\phi_{i+2,j} - 3\phi_{i+1,j} - 3\phi_{i,j} - \phi_{i-1,j}) \tag{5.5}$$

The formulation outlined above is by no means unique, however it introduces dissipation for the conserved variable in a consistent manner and has been implemented successfully by Jameson,[40] Kwak[44] and Beam and Warming[41] for damping spurious oscillations in rapidly varying regions. Care has to be exercised in treating the continuity equation to maintain proper accuracy using such techniques.

5.1.5 Improved Flux Blending Schemes

The objections associated with the semi-heuristic formulation and application of explicit smoothing terms in the difference equations can, in principle, be alleviated by schemes that add and subtract dissipation based on the local behavior of the solution. A scheme with some of these characteristics was first proposed by Boris and Book[46] and later generalized by Zalesak[47] for a more general class of problems. The basic idea incorporated in such schemes is to construct the net flux at a point as a weighted average of the flux computed by a low and high order scheme. The weighting is introduced in a manner that ensures maximum use of the higher order scheme while producing tolerable or no oscillations. The resulting procedure is commonly referred to as a flux correction scheme.

The nature and elimination of dispersive post-shock oscillations in a shock capturing scheme have been the subject of intensive research effort since the early attempts by Von Neumann and Richtmeyer.[38] There have been numerous formulations with various levels of success to implicitly or explicitly filter out the oscillations encountered, e.g., upwinding, artificial damping, flux correction and more recently flux vector splitting.[48] Under NASA sponsorship some of these concepts have been evaluated for flow problems similar to the ones considered here, by Syed, et al.[5] These authors effectively used a weighted mean flux blending scheme incorporating first order Upwind and SUDS schemes, to obtain bounded solutions of comparable accuracy to those yielded by SUDS alone. The nature of the shortcomings associated with the use of such blending procedures is discussed in Section (5.3).

Notwithstanding some of the unresolved problems and implementational difficulties, a similar flux blending strategy could be developed to exploit the high accuracy provided by an appropriate fourth order differencing scheme, e.g. OCI. Using such an approach it is also conceivable that some of the

obvious shortcomings of the particular blending formulation (source influence, path dependency, etc) could be alleviated. In addition, flux blending provides a further basis for rationally constraining the artificial dissipation coefficient of the previous section to obtain bounded, stable solutions to equation (5.2).

5.1.6 Variational Discretization Schemes Including Finite Elements

The cell Reynolds number problem of the classical finite difference methods leading to boundedness and stability problems could, in principle, be relaxed by Galerkin based methods, or more generally speaking, by methods founded on a variational principle that minimizes some error norms. Techniques employing Galerkin or other related procedures preserve certain important integral constraints, e.g. total kinetic energy. A conserved quadratic integral of energy is necessary for stable integration of the equations of motion by prohibiting unbounded nonlinear instabilities which often arise with finite differences.

In the literature, variational techniques, including finite elements, are presented as an alternative approach for reducing the relevant differential equations to an algebraic set (finite volume, finite differencing, etc), and hence do not strictly constitute distinct discretization methods. However, they are reviewed here briefly for completeness. Furthermore, recently their use in becoming more frequent in similar problems of interest in this study and they encompass a semi-mature field rich in concepts and applications and hence can be exploited, Raw.[10]

Variational methods, in particular finite element method, seek an approximate solution to the differential equation over finite subregions or "elements" in terms of a piecewise-continuous local interpolation formula (trial or shape functions), by controlling the error in some average sense through a variational principle or Galerkin procedures of weighting. The shape function is defined over an element, with elements joined together to cover the entire domain. For flow problems Galerkin procedures are generally used.

The finite elements may be of orbitrary shape, although commonly triangular or quadrilateral elements are based. The solution ϕ is approximated over each element by:

$$\phi = \sum_i N_i \phi_i \tag{5.6}$$

where $\sum_i$ denotes summation over all the grid points within the element of interest and the N_i are the shape functions, defined piecewise element by element. They are usually polynominals of low degree. The polynominal coefficients are determined by the requirement of continuity of ϕ, but not necessarily of its derivatives, between the elements. Thus if the differential equation describing the problem is represented by:

$$L(\phi) = 0 \tag{5.7}$$

then using the weighted residual method in which the weighting function is equal to the shape function, the Galerkin representation for the problem is given by:

$$\int_R N_J L \left(\sum_i N_i \phi_i\right) dR = 0 \tag{5.8}$$

where R is the domain. By choosing a succession of weighting functions, a system of algebraic discretized equations can be obtained.

It can be shown that the conventional Galerkin finite element method for convection-diffusion problems experiences similar difficulties as the dispersive finite volume/difference techniques, Gresho and Lee.[49] Thus, means have to be introduced to bound the solution using practices similar to the techniques considered here. To overcome such problems, several upwind type finite element methods including the Streamline Upwind Scheme[50] (similar in concept to SUDS) have been proposed. The difficulties associated with such formulations, either in terms of unbounded solutions or excessive diffusion, are similar in nature to finite volume/difference methods. However, recently Raw[10] developed a co-located control volume based finite element procedure. The approach taken by the author introduces a rational basis for approximating the convected variable at the control volume face and provides the basic concepts involved in the development of advanced SUDS, Section (5.1.2). Raw relates the interface variables to the nodal variables

via an algebraic approximation of their respective differential equation applied at the control volume surface. This causes, for flow problems, the appearance of pressure in the continuity equation in a form that removes the need for "reduced order pressure interpolation", typical of most finite element methods. In addition, a discrete convection operator is developed that does not produce non-physical spatial oscillations and does not suffer from false diffusion.

There is a further very desirable attribute of finite elements for flow problems in the flexibility and generality provided by various element shapes. Such elements might also be moved appropriately to track interfaces and fronts for improved resolution.

5.1.7 Spectral Methods

Spectral methods are based on representing the solution to a problem as a truncated series of smooth functions of the independent variables. Whereas finite element methods, discussed above, are based on expansions in local basis functions, spectral methods base expansions in global functions. Spectral methods are the extension of the standard technique of separation of variables to the solution of arbitrarily complicated problems.

Spectral methods involve the approximation of the flow using appropriate combinations of Fourier series, Chebyshev polynomial series, Legendre polynominal series, etc.[51] While these methods do guarantee infinite order rates of convergence to smooth flows, they appear at first to be excessively complicated compared to more conventional low order difference methods. However, with the introduction of transform methods and spectral iterative methods, they can be applied and used effectively to adequately resolve complicated flow physics in arbitrary geometries. Spectral methods offer the significant advantage over other (lower-order) methods in that they automatically achieve high order accuracy at rigid no slip boundaries.

The underlying concept behind the transform methods, introduced to deal with the nonlinearities present in the equations, Gottlieb and Orszag[51] and Gottlieb, Hussaini and Orszag[52] uses spectral representations only to obtain accurate evaluations of derivatives and to impose the boundary conditions accurately. All the complicated nonlinear physics is evaluated locally in physical space, so that flow physics of any desired degree of complexity may be accommodated.

The extension of spectral methods to complicated geometries was investigated using two key ideas by Orszag[53] and Gottlieb, et al:[51] the spectral iteration technique and spectral element patching. These will be described briefly.

Spectral approximations to general boundary value problems lead to full NxN matrix equations for the N expansion coefficient a_n. It would seem that the solution of these equations requires O (N^3) arithmetic operations, while storage of the matrix requires O (N^2) memory locations. Since typical problems involve $N \sim 10^6$, the direct solution (or even the direct formulation) of such problems is clearly unworkable presently. The spectral iteration technique circumvents this problem by allowing the solution of the full matrix problems using just the storage and computational work required by low order finite difference methods. The underlying idea is to approximate the spectral operators that must be inverted by suitable sparse matrix operators and devise an iteration scheme (in a deferred corrector sense) that leads to machine accurate solutions in only a few iterations.

Consider the solution of a general linear differential equation $L\phi = b$. Let an N term spectral approximation to this problem be given by:

$$L_{sp}\phi_N = b_N \tag{5.9}$$

where b_N is a suitable N term approximation to b. Equation (5.9) is generally a full NxN matrix.

Suppose it is possible to construct an approximation L_{ap} to the spectral operator L_{sp} that has the following properties.

i) L_{ap} has a sparse matrix representation so that it can be represented using only O(N) storage locations.

ii) L_{ap} is efficiently invertible in the sense that the equation

$$L_{ap}\phi_N = b_N \tag{5.10}$$

is soluble as efficiently as a first order finite difference approximation to the problem.

iii) L_{ap} approximates L_{sp} in the sense that,

$$0 < m \leq \left\| L_{ap}^{-1} L_{sp} \right\| \leq M < \infty \tag{5.11}$$

for suitable constants m, M as $N \to \infty$. Roughly speaking equation (5.11) requires that the eigenvalues of $L_{ap}^{-1} L_{sp}$ be bounded from above and below as $N \to \infty$. Examples regarding the necessary bounds and other convergence considerations for some model problems is provided by Orszag.(53)

In this manner the solution of (5.9) can be accomplished using order N storage locations with the number of arithmetic operations of the order of N log N and the number of operations required to solve the above equation by a first order finite difference method. The important conclusion is that spectral methods for general problems, in arbitrary geometries, can be implemented efficiently with operational costs and storage not much larger than that of the simplest finite difference approximation (e.g. first order Upwind) to the problem with the same number of degrees of freedom. Since spectral methods require many fewer degrees of freedom to achieve a given accuracy than required by finite difference approximations, important computational efficiencies can result. Nearly equivalently, spectral methods achieve much higher accuracy for a given number of degrees of freedom.

The second key concept involved in application of spectral methods in complex geometries refers to patching together complicated domains out of simpler ones by using moderate sized "global spectral elements". Because of the nice boundary properties of spectral methods, little accuracy is lost by patching together these spectral elements. However, the patching scheme does give essentially complete geometric flexibility, especially where the global elements are isoparametrically mapped curved elements. The resulting spectral patching/spectral element methods combine the efficiency and flexibility of finite difference/finite element methods with the accuracy of spectral methods.

Application of spectral techniques in problems involving non-smooth solutions using certain eigenfunction expansions, may result in undesirable Gibbs' oscillations in the vicinity of the discontinuity. However, such problems are conveniently treated by either patching the solution at discontinuties or pre and post filtering the solution.

5.1.8 Lagrangian Methods

Although pure Lagrangian methods are not strictly viewed as distinct discretization techniques, they possess a very appealing feature in that the numerical formulation does not include the convective derivative, the major source of difficulty in Eulerian calculations. Thus, Lagrangian calculations

are able to treat high Reynolds number flows for long times relative to their Eulerian counterparts and can effectively treat interfaces, free surfaces and moving boundaries. However, the methods do suffer from severe drawbacks in practical calculations. The foremost problem occurs in multi-dimensional calculations when the convection of the grid with the flow leads to large grid deformations and a corresponding decrease in numerical accuracy. Regridding and remapping techniques introduce severe numerical diffusion into the problem just as if a simpler Eulerian calculation were performed initially. Schemes incorporating Lagrangian and Eulerian features into a composite calculation algorithm, e.g. ALE[54] suffer degradation as any relocation of the grid necessarily re-introduces numerical diffusion through the smoothing provided by interpolation.

A second problem arises because a high order of accuracy, particularly of spatial derivative terms, is difficult to achieve in Lagrangian calculations. When the computational grid moves, uniform spacing is not generally possible. To construct high order derivatives in a time varying non-uniform mesh is difficult and first order algorithms are hard to avoid. One problem of maintaining monotonicity, is replaced by another; the introduction of first order aspects into the calculation.

Lagrangian calculations in multi dimensions are very complicated and can be much more expensive per grid point than Eulerian computations. Another problem is that inexpensive direct solution algorithms of elliptic equations cannot be applied. Finally, adaptive gridding[55] is just as important in Lagrangian simulations for front resolution as it is in Eulerian calculations, and is more difficult to implement.

5.1.9 Adaptive Gridding and Modified Equation Analysis

Techniques considered in this Section contribute only indirectly in obtaining improved resolution and other desirable aspects of solutions.

In general calculation procedures a priori spatial information concerning significant gradients of dependent variables is usually not available, thus the practical grids used reveal wasteful practices and the inability to satisfactorily resolve regions of interest.

Adaptive gridding provides a means of overcoming the above problems via grids generated dynamically as the solution develops. The basic concepts have been successfully used in boundary layer computations for years, to capture the

spatial and temporal details in a sound and economical way. For flame propagation in a solid, Dwyer and Sanders[56] used the scheme in a very effective manner to generate adequately resolved, economical solutions. Recently a sound mathematical basis was formulated for general application by Brackbill, et al[57] incorporating grid smoothness and skewness, together with resulting cell volumes in a functional to be minimized.

The adaptive gridding technique coupled with an accurate numerical technique offers an indirect means of resolving the cell Reynolds number (boundedness) problem of current prediction techniques. The solution continually updates the grid either explicitly or implicitly clustering mesh points in high gradient regions to satisfy the critical Reynolds number criterion. A potentially viable way of achieving sufficient grid resolution is through the use of nonlinear modified equation analysis.[58] Apart from establishing a sound basis for generating adaptive grids, the modified equation approach also yields insight into the local behavior of the numerical scheme by providing the relative magnitude of the truncation errors to the original terms of the differential system.

The modified equation is derived by expanding in a Taylor series the difference equations of a particular numerical scheme. While the modified equation contains an infinite number of terms with increasing powers of spatial mesh intervals, it does represent the system of original differential equations solved by the differencing scheme. It is not possible however, to investigate the complete modified equation. For dissipative differencing, most of the information regarding nonlinear truncation errors is contained in the leading few terms. Therefore it is sufficient to investigate the truncated modified equation. The important point is that the modified equation gives the exact nonlinear truncation errors for the complete system of differential equations being solved numerically.

Since the higher order terms in the modified equation do not appear in the original differential equations, contributions from these term lead to inaccuracies when compared to an analytic solution of the original differential equation. The removal or cancellation of these terms results in a higher order integration scheme. In fact, an essentially third order scheme results by removing only the dominant second order terms. The improved accuracy is achieved with no change to the differencing scheme and with very little extra computational work.

Devising an automatic mesh clustering scheme is accomplished via the local truncation error levels provided by the modified equation analysis and the choice of a suitable smoothing filter. Here special care has to be exercised in resolving the stiffness introduced into the governing equation through the grid refinement procedure. However, the impressive grid reduction achievable, especially in three dimensions (one or two orders of magnitude), for adequate resolution, lends support for developing such schemes.

5.2 IMPROVED SOLUTION ALGORITHMS FOR ENHANCING CONVERGENCE AND EFFICIENCY OF METHODS FOR INCOMPRESSIBLE FLOWS

Currently most incompressible flow solution algorithms adopt a particular form of a general segregated solution procedure discussed in detail in Section (3.4.3), SIMPLE, SIMPLER, PISO, SIMPLEC, SIMPLEX, etc. Central to all the above approaches is the generation of one or more Poisson-type pressure/correction equations that constrain the flow to satisfy the vanishing of the mass divergence. As remarked in Section (4.3), the algebraic solution of such equations accounts for a significant portion of the total cost of solving the flow problem, hence efficient and economical solvers have to be devised. These are presented briefly in the following discussion, prior to their detailed development in Section (6.5).

Considerations regarding the structure of the discretized pressure/correction equation (3.45) (symmetric, with properties similar to those for a diffusion process) permits the grouping of various solvers as base solvers and acceleration techniques. These are:

i) Approximate Factorization Techniques as base solvers.

These include, but are not limited to, Incomplete Choleski Algorithm and Stone's Strongly Implicit Procedure

ii) Conjugate Gradient Acceleration

iii) Block Correction Acceleration

iv) Multilevel Multigrid Acceleration Schemes

Finally, coupled numerical schemes are considered briefly for completeness. These are much different in philosophy, structure and implementational details than a general segregated solution procedure.

5.2.1 Approximate Factorization Techniques

A commonly adopted technique for solving linearized algebraic equation sets such as (3.45) in multi dimensions is repeated application of an Alternating Direction Line Gauss-Seidel solver. However, uncertain convergence rates associated with the use of such solvers in certain problems with strongly anisotropic coefficients, mixed boundary conditions, etc necessitate development and application of more implicit solvers. A particular class of such methods are conveniently based on approximate factorization techniques. For instance, Incomplete Choleski (IC) is a suitable approximation to the conventional Choleski Decomposition.[59] In IC, the Choleski Decomposition matrices are approximated by some simple sparse diagonal matrices whose coefficients are determined from constraints imposed by the product of the approximate decomposition matrices. In fact, the constraints are such that the product of the approximate decomposition matrices must be identical to the product of the Choleski Decomposition matrices for every non-zero entry of the latter product. Naturally, the product of the approximate decomposition also contains non-zero entries where none should appear.

Stone's Strongly Implicit Procedure (SIP) is an alternative approximate factorization technique. However, in SIP an attempt is made to partially cancel the effect of the spurious non-zero entries of the product of the approximate decompositions. A parameter, α, is introduced to control the degree of partial cancellation. In fact, when the value of α is set to zero, i.e. no cancellation, it can be shown that SIP and IC become algebraically equivalent.[59]

Although as base solvers both IC and SIP have often been shown to be attractive relative to other iterative solvers, their rate of convergence is still unacceptably slow in many cases. To enhance their rate of convergence, a number of acceleration techniques are available.

5.2.2 Conjugate Gradient Acceleration

Due to the symmetry of the linear set of equations for pressure, the generalized Conjugate Gradient Method (CG) of Concus and Golub[60] could be used effectively for their solution. Employing this acceleration technique in conjunction with IC (or equivalently, SIP with no partial cancellation), the resulting method becomes a finite (direct) method, with each iteration determining an additional orthogonal basis vector of the solution such that a pre-

defined norm of the error is reduced. Unfortunately, due to the asymmetries introduced, the Concus and Golub variant of CG acceleration is not appropriate for accelerating SIP with partial cancellation.

5.2.3 Block Correction Acceleration

The Block Correction acceleration (BC) is applicable to both IC and SIP methods. Based on the procedure of Settari and Aziz[64] and as discussed in some detail by Hutchinson and Raithby,[62] BC technique adjusts the solution in blocks, normally along rows or columns of the computational domain, by an additive constant such that the residuals in each block sum to zero. A particular mode of application of BC could apply it independently along both rows and columns with one IC or SIP iteration employed between each row and column BC. Specifically such a sequence is given by:

i) the application of BC to ensure that the residuals in each column sum to zero,

ii) an application of one IC or SIP iteration,

iii) the application of BC to ensure that the residuals in each row sum to zero, and

iv) the application of one IC or SIP iteration.

In steps i) and iii) given above, the Tri-Diagonal Matrix Algorithm can be used to solve the BC equations.

5.2.4 Multilevel Multigrid Acceleration

In algorithms incorporating "explicit" schemes like the line Gauss Seidel or Successive Line Over-relaxation for the solution of the algebraic equations, the high frequency error modes are reduced very effectively. However, the attenuation of the low frequency components is very poor. The Multilevel Multigrid technique attempts to resolve this dilemma by employing a sequence of grids ranging from fine to very coarse to eliminate the different error modes. As such, it can be viewed as a routine for reducing or smoothing out the error modes in a particular frequency band on a given grid structure.

For relaxation type solutions, the error vector at any phase of the iteration cycle is expressable as a discrete Fourier transform. If a small number of iterations are subsequently carried out using a fine grid, the high frequency modes of the error are much reduced, although the low frequency end of the spectrum remains largely unaffected. If recourse is then made to a

coarser grid, say with half the number of grid points, due to the resolution capabilities of the grid, the solution will only reduce error modes of correspondingly lower frequencies. This cascade-like process is continued down to the coarsest grid until the complete error spectrum has been covered. There exist various applied versions of the above ideas collectively referred to as classical multigrid methods, by Brandt.[63] The following discussion will emphasize the details of an alternative multigrid strategy based on BC ideas and successfully used by Hutchinson and Raithby,[62] the Additive Correction Multigrid (ACM).

In the ACM, coarser grids (contiguous blocks) are formed from 2x2 configurations of fine grid nodes, (two-dimensional), hence the solution of the coarse mesh equations and subsequent correction for the fine mesh solution yields a residual field that sums to zero over each block. In addition to prescribing the method used to evaluate coefficients on the coarser meshes, the ACM method also prescribes the manner in which residuals are transferred to the coarser grids, how coarse grid corrections are applied to the fine grid solution as well as how boundary conditions are treated. It is also worthy to note that ACM is equally applicable to symmetric and non-symmetric systems of linear equations and is not restricted to fine grids with $2^m x 2^n$ points in the two coordinate directions.

A particular application of the above methodology reproduces the classical "flexible cycle" multigrid algorithm of Brandt[63] with one difference. Instead of iterating on the fine grid until convergence becomes slow, only one fine grid iteration is performed before initiating the solution on the coarser mesh. Employing IC/SIP on each of the meshes (ranging from the finest to the coarsest, a 2x2 mesh in two dimensions), the single iteration residual reduction rate for each of the meshes except the finest and coarsest may conveniently be chosen to be 0.5. Regarding the specific details of terminating the smoothing procedure, iteration on all but the finest and coarsest mesh is considered sufficiently converged when the l_2-norm of the residuals is less than 25 percent of the l_2-norm of the residuals when they are last obtained from the next finer mesh. Finally, iteration on the 2x2 mesh is taken to be converged when the l_2-norm of the residuals is reduced to 0.01 percent.

5.2.5 Coupled Numerical Schemes

Conceptually, the elliptic influence and interequation coupling in a computational domain can be properly accounted for by discretizing all the governing equations at every grid point and then simultaneously solving them using coupled iterative solvers.[20] For three-dimensional applications especially, such solution procedures require computational resources that are beyond the capabilities of current machines. Another approach deserving study is to use parabolic solutions with "best possible" elliptic corrections (with appropriate treatment of the continuity equation). SIMPLE/derivative algorithms belong to this class of solutions. These methods, however, require the use of variable under-relaxation parameters to obtain a converged solution. As methods progress in complexity to account for elliptic influence, the need for a lower under-relaxation parameter decreases. SIMPLER thus requires a lower under-relaxation parameter than SIMPLE.[64] Another example of such an approach is reported by Caretto et al,[65] where the authors adopted the SIVA (Simultaneous Variable Adjustment) procedure. This is basically a point iteration method which properly couples the continuity and momentum equations (to satisfy mass conservation better) and obtains all dependent variables simultaneously. The resultant scheme, although more expensive due to the adopted point iteration procedure, did not require any under-relaxation, while for the same problem SIMPLE was unstable requiring under-relaxation.

An analogous observation was reported by Srivastava et al[66] in their study of viscous shock layer equations. Viscous shock layer equations are parabolic in nature with ellipticity introduced through the unknown shock shape.[67] In their study it was found that any attempt to solve the equations using parabolic procedures (with corrections on the shock shape analogous to pressure corrections) required problem dependent under-relaxation. To alleviate the need for practices using ad-hoc specification of under-relaxation parameter, a solution scheme was devised that couples the two relevant first order equations and solves them simultaneously using either a box or a staggered scheme.

All the above observations for the model problem are relevant in consideration of the structure of SIMPLE/derivative algorithms. Therefore, a procedure that treats fully elliptic difference equations by approximate parabolic methods merits further consideration in the present study.

The concept of coupling, and simultaneous solution for the two first order partial differential equations of continuity and radial momentum, of relevance in the study of viscous shock layer structure, is demonstrated next by considering the inviscid perturbation equations of compressible flow, i.e.,

$$A \frac{\partial u}{\partial x} + \frac{\partial v}{\partial y} = 0 \tag{5.12}$$

$$\frac{\partial u}{\partial y} - \frac{\partial v}{\partial x} = 0 \tag{5.13}$$

where $A = (1-M^2)$ and M denotes the Mach number. Solution method depends on the sign of A; the equations are hyperbolic for $M>1$, while for $M<1$ or $M=0$, the equations are elliptic.

Considering elliptic equations, the above equations can be coupled using Keller's box scheme[68] extended by applying the difference equation in two sweeps; x and y directions. Using Central differencing scheme, equations (5.12) and(5.13) applied at (j-1/2,k+1/2) and (j-1/2,k-1/2), where j and k denote grid locations in the x and y directions respectively, will contain variables at (j,k), (j,k+1), (j,k-1), (j-1,k) and (j-1,k+1). However, these equations can be readily manipulated to obtain tri-diagonal forms for the x and y sweeps in the following manner:

Applying the box scheme at (j-1/2, k-1/2) for equations (5.12) and at (5.13)

$$\frac{A_{j-1/2,k-1/2}}{2\Delta x} (u_{j,k}-u_{j-1,k} + u_{j,k-1}-u_{j-1,k-1}) \tag{5.14}$$

$$+ \frac{1}{2\Delta y} (v_{j,k} + v_{j-1,k}-v_{j,k-1}-v_{j-1,k-1}) = 0$$

$$\frac{1}{2\Delta x} (v_{j,k} - v_{j-1,k} + v_{j,k-1}-v_{j-1,k-1}) - \frac{1}{2\Delta y} (u_{j,k} + u_{j-1,k}-u_{j,k-1}-u_{j-1,k-1}) = 0 \tag{5.15}$$

where Δx and Δy denote grid dimensions in x and y, equations (5.14) and (5.15) can be combined to yield:

$$A_1 u_{j,k} + B_1 u_{j-1,k} + C_1 v_{j,k} = D_1 \tag{5.16}$$

where D_1 contains variables at (k-1).

Similarly equations written at (j+1/2,k-1/2) yield:

$$A_2 u_{j+1,k} + B_2 u_{j,k} + C_2 v_{j,k} = D_2 \qquad (5.17)$$

where D_2 again contains variables at (k-1). Equations (5.16) and (5.17) can now be manipulated to obtain a tri-diagonal form to readily yield x-direction solutions for $u_{j,k}$ and $v_{j,k}$ for a given k-line. y-direction sweeps to determine $u_{j,k}$ and $v_{j,k}$ for a given j-line are accomplished in a similar manner.

The above inviscid approach, although formulated using the box scheme, can be extended to incorporate any discretization procedure by a suitable elimination scheme. The key lies in realizing that an elliptic formulation can be alternatively viewed as two parabolic formulations in two coordinate directions, cf. SIMPLE/SIMPLER algorithms.

Treatment of the diffusion terms, present in general flow equations could be handled in a manner suggested by Keller for a box scheme, or in any heuristic manner for any discretization scheme as long as the coupled nature of solutions for continuity and momentum are preserved. Furthermore, incorporation of viscous terms tends to stabilize the solution procedure and does not contribute significantly to solution difficulties.

5.3 PRELIMINARY EVALUATION OF CANDIDATE TECHNIQUES

Due to the widely ranging nature of the techniques discussed above, regarding issues of applicability, implementation and required computational resources, a vigorous quantitative evaluation procedure is difficult to device. In this regard the expertise associated with a Technical Advisory Committee specifically established for this program, as well as a critical assessment of information available in the literature was utilized fully to arrive at rational choices. The Technical Advisory Committee included individuals active in the field of computational fluid dynamics with the members:

- Dr. S. A. Orszag
- Dr. S. G. Rubin
- Dr. R. T. Davis
- Dr. C. J. Knight
- Dr. B. N. Srivastava

A close scrutiny of the candidate schemes considered, reveals a wide disparity in relevant critical merits and shortcomings. Such issues pertain to in/applicability (within the framework of TEACH methodology), extensive further development and implementation, only marginal development over the current algorithm capabilities, resources allocated to the present study. Even though such issues were given only minor consideration in the foregoing discussion that emphasized primarily accuracy, stability and convergence enhancement, the impact they have on a finite effort has to be critically assessed. The following discussion will thus provide mostly a qualitative justification for the choices adopted in the study.

Use of explicitly damped schemes that incorporate a fourth order dissipation term in the transport equation and achieving higher order accuracy via deferred correction techniques employing lower and higher order (unbounded) difference operators, can be mathematically shown to proceed on identical paths, i.e., second order accuracy can be recovered using first order Upwind differencing for the convective derivative, if a correction term evaluated at a previous iteration is included in the discretized equations to give at convergence a Centred approximation. However, the artificial viscosity introduced in explicitly damped schemes has to be fine tuned to be selectively effective in regions where it is required. Such a practice strictly introduces issues of non-uniqueness and/or need for a priori knowledge of the solution. Furthermore, a rational basis for appreciating the physical nature of the incorporated terms, in a manner similar to the Physical Advection Correction (PAC) of the Skewed Upwind Differencing Schemes, (SUDS) is lacking. Even though for simple model problems the impact of damping terms can be clearly identified, for the complex viscous, recirculating flows of interest here, the determination of the "optimum" dissipation coefficient and the related issues of convergence and stability is usually determined in an ad-hoc manner.

Flux blending schemes, that attempt to optimally combine the bounded, but albeit smeared, solutions of a lower order scheme with that of an unbounded, but more accurate higher order scheme suffer from similar problems. There have been utilized in the past, various formulations operating on different solution variables in a tailor-made manner. Recently, two formulations blending first order Upwinding with SUDS have been assessed by Syed, et al[5] who concluded that the final solution might not be path

independent. In fact, it has been suggested that different initial values of the adopted blending factor may produce different converged solutions, where convergence is measured by the level of residual source error. Even though various arbitrary practices can be utilized to reduce or eliminate the resulting solution uniqueness, a scheme that incorporates the correct physical influence in the the determination of blending factors is preferable and should alleviate the reported solution difficulties.

Introduction of variational discretization techniques in complex, reacting flow field predictions (in the same vein as the established finite element analysis of structural mechanics) is fairly recent and has not enjoyed comparable development and analysis as the corresponding finite volume/difference methods. Even though the two formulations (finite volume/difference vs finite element) can, in principle, be shown to be identical, and finite element techniques afford greater flexibility in the treatment of complex geometries, practical issues of implementation, familiarity, maturity, etc. rule out their being considered as serious candidates. In addition, there exist comparable problems of convective differencing and the reduced pressure interpolation to circumvent the checker-board effect of incompressible flows in most formulations.

Spectral methods enjoy enormous popularity in transition/stability predictions and their use is becoming widespread in a variety of applications. However, for practical combustor computations dominated by high Reynolds number effects and various coupled physical processes, their routine use requires extensive further development and computational resources. Lagrangian methods were already found unsuitable for the problems of interest here, due to unresolved issues of rezoning and consequent numerical diffusion, implementation in three dimensions, etc.

Finally, adaptive gridding (and the related modified equation analysis), in spite of the intense current activity and interest therein, has not achieved adequate maturity to consider its use in reacting three-dimensional flow situations and thus remain a research topic. Furthermore, for coupled, nonlinear equations, e.g., full Navier Stokes, modified equation analysis becomes extremely unwieldy and cumbersome.

Concerning the use of coupled numerical scheme/solution algorithms to substantially enhance convergence, a critical assessment as well as discussions with S.V. Vanka of Argonne Labs revealed serious potential draw-

backs associated with their use in the light of the criteria of Section (4.4). In essence, these approaches are very much different in philosophy, structure and implementational details than a general segregated solution procedure, and thus require substantial departures from the methodology incorporated in TEACH. Furthermore, potential problems are anticipated in three-dimensional applications due to required computational resources. These and other related considerations (time and resource commitments for their development being outside the scope of the present study) helped exclude them from further consideration.

5.4 SELECTION OF FOUR SCHEMES FOR FURTHER QUANTITATIVE EVALUATION

Based on the above qualitative assessment, as well as considerations regarding relevant additional information available in the literature and prior experience, the following four most promising techniques were identified as deserving further quantitative evaluation:

i) Second order upwind differencing scheme
ii) Variants of skewed upstream differencing scheme
iii) Variants of compact implicit method
iv) Strongly implicit procedure accelerated by:
    a) Conjugate gradient algorithm
    b) Block correction technique
    c) Additive correction multigrid algorithm

It will be seen that the particular schemes selected address issues of both discretization accuracy and convergence enhancement in a well-balanced manner. Detailed formulation emphasizing issues of accuracy, stability and convergence together with implementational details, including computational requirements for the above schemes are provided in the next section. The results of the two-dimensional evaluation exercises is presented in Section 7.

6.0 DERIVATION OF THE SELECTED SCHEMES FOR TWO-DIMENSIONAL EVALUATION

6.1 FINITE VOLUME DISCRETIZATION AND SOLUTION OF THE CONSERVATION EQUATIONS FOR A SCALAR, MOMENTUM AND MASS

A general steady transport equation governing the conservation of a typical scalar, momentum and mass can be expressed for both laminar and (time-averaged) turbulent flows as, equation (3.19):

$$\frac{\partial}{\partial x}(\rho u \phi) + \frac{1}{r^{\delta}}\frac{\partial}{\partial r}(r^{\delta}\rho v \phi) = \frac{\partial}{\partial x}(\Gamma_{\phi}\frac{\partial \phi}{\partial x}) + \frac{1}{r^{\delta}}\frac{\partial}{\partial r}(\Gamma_{\phi} r^{\delta}\frac{\partial \phi}{\partial \phi}) + S_{\phi} \quad (6.1)$$

where δ=0 for two-dimensional (planar) flow and δ=1 for axisymmetric flow. The variable ϕ represents any one of the dependent variables (e.g., the velocity components u, v, w, species i, turbulent kinetic energy and dissipitation). The exchange coefficient, Γ_{ϕ}, represents the sum of both laminar and turbulent contributions and is interpreted as effective viscosity for u, v, w, the effective diffusivity for species, etc. S_{ϕ} denotes a generalized source term. Table (6.1) presents the particular forms of S_{ϕ} adopted for various variables.

Using the techniques and practices developed in Sections (3.3.1) to (3.3.3), equation (6.1) is integrated over a finite control volume appropriate for each variable ϕ, figures (3.1) and (3.2), to yield the following conservation expression:

$$(J_{nf} - J_{sf} + J_{ef} - J_{wf}) - \int_{y_s}^{y_n}\int_{x_w}^{x_e} S_{\phi}\, dxdy \quad (6.2)$$

TABLE 6.1 TYPICAL SORUCE TERMS FOR RELEVANT VARIABLES

Variable ø	Source Term $S_ø$
u*	$\frac{\partial}{\partial x}(\mu_e \frac{\partial u}{\partial x}) + \frac{1}{r}\frac{\partial}{\partial r}(r\mu_e \frac{\partial v}{\partial x}) - \frac{\partial p}{\partial x}$
v	$\frac{\partial}{\partial x}(\mu_e \frac{\partial u}{\partial y}) + \frac{1}{r}\frac{\partial}{\partial r}(r\mu_e \frac{\partial v}{\partial r}) + 2\mu_e v \frac{\partial}{\partial r}(\frac{1}{r}) + \frac{\rho w^2}{r} - \frac{\partial p}{\partial r}$
rw	$-\frac{2}{r}\frac{\partial}{\partial r}(\mu_e rw)$
k**	$\mu_e G - \rho\varepsilon$
ε	$\frac{\varepsilon}{k}(c_1 \mu_e G - C_2\rho\varepsilon)$
f(mixture fraction)	0
m_{fu}*** (mass fraction of unburned fuel)	Either $S_{fu} = S_{fu,1} = -F\rho^2 m_{fu} m_{ox}\sqrt{T} \exp(-E/RT)$ or $S_{fu} = [\![S_{fu,1}, S_{fu,2}]\!]$ where $S_{fu,2} = C_R m_{fu} \rho\varepsilon/k$
h	0 (except when radiation is present)

* μ_e denotes effective viscosity

** G is given by:

$$G = \left\{ \sum_{i=1}^{2} \sum_{j=1}^{2} \left(\frac{\partial u_i}{\partial x_j} + \frac{\partial u_j}{\partial x_i}\right) \frac{\partial u_i}{\partial x_j} \right\} + 2\left(\frac{w}{r}\right)^2 + \left[r\frac{\partial}{\partial x}\left(\frac{w}{r}\right)\right]^2 + \left[r\frac{\partial}{\partial r}\left(\frac{w}{r}\right)\right]^2$$

*** It is supposed that the rate of combustion of fuel per limit volume is governed by the Arrhenius-type relation $\dot{m}_{fu}=S_{fu,1}$ where F is a pre-exponential factor and E is the activation energy. $[\![A,B]\!]$ denotes the minimum of absolute values of arguments.

Adoption of Cartesian geometry for ease of highlighting the significant aspects of the formulation is implied in equation (6.2) and throughout most of this Section. In equation (6.2) each J_{if} denotes the total local transport of ø across the i boundary of the finite volume by convection and diffusion, while the last term signifies transport due to source generation/dissipation. By taking the east boundary as an example, J_{ef} is expressed as:

$$J_{ef} = C_{ef} + D_{ef} \tag{6.3}$$

where

$$C_{ef} = \int_{y_s}^{y_n} (\rho u \phi)_e \, dy \quad \text{and} \quad D_{ef} = -\int_{y_s}^{y_n} (\Gamma_\phi \frac{\partial \phi}{\partial x})_e \, dy \tag{6.4}$$

To approximate equation (6.2) for each finite volume by an algebraic equation requires specific assumptions about the variations of ø in the integrals of equation (6.4) between the selected grid points in space. Making use of the mean value theorem, that implies either constant or linearly varying fluxes along each cell boundary, allows the integrals to be replaced by:

$$\begin{aligned} C_{ef} &= C_e \phi_e \quad , \quad C_e = \Delta y_j (\rho u)_e \\ D_{ef} &= - d_e (\partial \phi / \partial x)_e \, \delta x_i \, , \quad d_e = \Gamma_{\phi e} \, \Delta y_j / \delta x_i \end{aligned} \tag{6.5}$$

where subscript e denotes the values of the associated quantities at the cell interface. The subsequent step of expressing ϕ_e and $\partial\phi/\partial x)_e$ in terms of nodal values is crucial in that it influences boundedness, stability and other characteristics of resulting solutions and will be taken up in most of this Section.

Introducing suitable approximations for ϕ_e and $\partial\phi/\partial x)_e$ as well as the last term in equation (6.2), and subsequent linearization of momentum equations yield the final algebraic representation of mass and momentum conservation as:

$$m_e^u u_p + m_w^u u_W + m_n^v v_p + m_s^v v_S = 0 \tag{6.6}$$

$$a_p^u u_p = \sum_{NP} a_{NP}^u u_{NP} - C^u (p_E - p_p) + b^u \tag{6.7}$$

$$a_p^v v_p = \sum_{NP} a_{NP}^v v_{NP} - C^v (p_N - p_p) + b^v \tag{6.8}$$

where $\sum_{NP}$ denotes influences of neighboring nodes. The various variables in equations (6.6) to (6.8) have their usual definitions given in Section 3. The absence of the dependent variable pressure in the mass conservation equation requires that special numerical techniques be used to solve equations (6.6) to (6.8), and many of these techniques are devised such that an equation for pres- sure results. To minimize the computational requirements associated with the formation and solution of the pressure equation, a segregated approach is often adopted, Section (3.4.3). In the segregated approach (e.g. SIMPLE) an attempt to minimize computational requirements is made by introducing approxi- mations to the momentum equations so that each nodal velocity is expressed in terms of a local pressure difference:

$$\bar{u}_p = \hat{u}_p - \bar{d}^u (p_E - p_p) \tag{6.9}$$

$$\bar{v}_p = \hat{v}_p - \bar{d}^v (p_N - p_p) \tag{6.10}$$

Substituting for the velocities in the algebraic representation of mass conservation, equation (6.6), a pressure equation of the following form results:

$$a_P^p p_p = \sum_{NP} a_{NP}^p p_{NP} + b^p \tag{6.11}$$

With equation (6.11) providing an equation for each nodal pressure, the re- sulting set of linear algebraic equations for the conservation of mass, momentum and relevant scalars can be conveniently solved.

6.1.1 Calculation and Discussion of the Interface Fluxes

To provide a clear understanding of the significant aspects of discretization schemes in a unified approach, the following discussion will initially be developed in the context of the one-dimensional analog of equation (6.1) and hence (6.2). Furthermore, where appropriate, reference will be made to the specific details of the particular schemes presented in Section 5 to establish a unified framework for assessment.

Equations (6.1) and (6.2) in one dimension become:

$$\frac{d}{dx}(\rho u \phi) = \frac{d}{dx}\left(\Gamma_\phi \frac{d\phi}{dx}\right) + S_\phi \tag{6.12}$$

$$J_{ef} - J_{wf} - \int_{x_w}^{x_e} S_\phi dx = \left(\rho u \phi - \Gamma_\phi \frac{d\phi}{dx}\right)_e - \left(\rho u \phi - \Gamma_\phi \frac{d\phi}{dx}\right)_w - S_\phi \Delta V \tag{6.13}$$

where ΔV is the volume of the control volume. In equation (6.13) the interface derivative of ϕ is conveniently approximated by employing the usual centred finite difference approximation characteristic of diffusion processes. The representation of interface values of ϕ, however, is not as straightforward and the approach used distinguishes one discretization scheme from another.

The discussion of various discretization schemes adopted in this study begins by considering the Upwind Differencing Scheme (UDS) for $u>0$ (a quantitative baseline), where the east face value of ϕ is taken as the upwind nodal value of ϕ, i.e.,

$$\phi_e \simeq \phi_P \tag{6.14}$$

The advantage of this approach is the simplicity and robustness of the resulting scheme. Also in the absence of any significant diffusive or source effects, the accuracy of this approach for one-dimensional flows is quite acceptable. However, in the presence of diffusion or source effects, UDS is only first order accurate and hence significant errors can arise. Therefore it is necessary to improve the accuracy of equation (6.14). Recognizing that equation (6.14) is the first term of a Taylor Series representation of ϕ_e, the accuracy of equation (6.14) can be improved by including additional terms of the series. For instance,

$$\phi_e \simeq \phi_P + \frac{\delta x_i}{2} \left(\frac{d\phi}{dx}\right)_e \tag{6.15}$$

where δx_i is the distance between nodes E and P. Now if an adequate evaluation of $(d\phi/dx)_e$ can be found, the evaluation of ϕ_e would be second order. An obvious choice is the centred finite difference representation about e given by:

$$\left(\frac{d\phi}{dx_e}\right) \simeq \frac{\phi_E - \phi_P}{\delta x_i} \tag{6.16}$$

Combining equations (6.15) and (6.16) and substituting for ϕ_e as well as ϕ_w into equation (6.13), it can be shown that the resulting discretization scheme is Central Difference Scheme (CDS). With this perspective CDS can be viewed as UDS with the upwind representation of ϕ corrected by a centred difference representation of the spatial derivative. The disadvantage of CDS is the non-physical negative dependence of ϕ_p on the node downwind of ϕ_p, which is referred to as negative influence and which can result in non-physical oscillatory solutions.

Naturally, there are alternatives to equation (6.16). One is to evaluate the derivative using an upwind finite difference representation,

$$\left(\frac{d\phi}{dx}\right)_e \simeq \frac{\phi_P - \phi_W}{\delta x_{i-1}} \tag{6.17}$$

Combining equations (6.15) and (6.17) and substituting into equation (6.13) the result is the Second Order Upwind (SOU) scheme. The advantage of SOU is that, unlike CDS, negative downwind influences do not arise. Equations (6.16) and (6.17) do not provide the only means of evaluating the derivative in equation (6.15). In fact, a complete family of schemes result from taking the following linear combination of upwind, centred and downward finite difference representations for $(d\phi/dx)_e$.

$$\left(\frac{d\phi}{dx}\right)_e \simeq a\left(\frac{\phi_P-\phi_W}{\delta x_{i-1}}\right) + b\left(\frac{\phi_E-\phi_P}{\delta x_i}\right) + c\left(\frac{\phi_{EE}-\phi_E}{\delta x_{i+1}}\right) \qquad (6.18)$$

where a+b+c=1. The family of schemes described by equation (6.18) includes CDS and SOU as well as the QUICK Scheme of Leonard.[69] The advantage of equation (6.18) is that by appropriate choices of a,b and c, it is possible to control the distribution of influence. Unfortunately, there appears to be no combination of values of a,b and c which ensures that the resulting numerical solutions do not exhibit spurious overshoots and undershoots.[70] Therefore an alternative approach of evaluating $(d\phi/dx)_e$ is considered.

The evaluation of $(d\phi/dx)_e$ given by equation (6.18) is equivalent to assuming the variation or profile of ϕ between the nodal values of ϕ surrounding the east face of the control volume. As a result, these schemes are referred to as profile schemes. An alternative approach is based on physical arguments. As mentioned previously, for one-dimensional flows the upwind evaluation of ϕ_e given by equation (6.14) is appropriate in the absence of diffusion or sources. Therefore, the correction applied in equation (6.15) can be interpreted as the correction necessary to account for the influences of diffusion and sources. This physical interpretation can be arrived at by first considering the non-conservative form of equation (6.12),

$$\rho u \frac{d\phi}{dx} = \frac{d}{dx}\left(\Gamma_\phi \frac{d\phi}{dx}\right) + S_\phi \qquad (6.19a)$$

or rearranging,

$$\frac{d\phi}{dx} = \frac{1}{\rho u}\left[\frac{d}{dx}\left(\Gamma_\phi \frac{d\phi}{dx}\right) + S_\phi\right] \qquad (6.19b)$$

Substituting for $d\phi/dx$ in equation (6.15)

$$\phi_e \simeq \phi_p + \frac{\partial x_i}{2\rho u}\left[\frac{d}{dx}\left(\Gamma_\phi \frac{d\phi}{dx}\right) + S_\phi\right]_e \qquad (6.20)$$

Clearly in equation (6.20) ϕ_e is given by ϕ_p and any changes in ϕ that arise between the P node point and the east face due to diffusion and source term influences. Consequently, the resulting scheme is referred to as UDS with correction for diffusion and source term influences.

To complete the description of the physical correction, the evaluation of diffusion and source term influences must be provided. There are a number of possible methods available. A convenient choice is to base the evaluation of the corrections on the evaluations already made in the control volume, equation (6.13). For instance, based on upwind control volumes, the correction terms of equation (6.20) are given by:

$$\frac{\delta x_i}{2\rho u}\left[\frac{d}{dx}\left(\Gamma_\phi \frac{d\phi}{dx}\right) + S_\phi\right] \simeq \frac{\delta x_i}{2\rho u}\left\{\left(\Gamma_\phi \frac{d\phi}{dx}\right)_e - \left(\Gamma_\phi \frac{d\phi}{dx}\right)_w + S_e \Delta V\right\} \quad (6.21)$$

The correction terms can also be based on downwind control volume values, as well as a linear combination of upwind and downwind control volumes.

The physically based correction of the upwind estimate described above uses an explicit evaluation of the correction terms. That is, the corrections are expressed only in terms of the nodal values of ϕ. A more implicit approach is taken in Operator Compact Implicit Methods (OCI), Section (6.4), where the corrections are expressed implicitly in terms of operators and nodal values of ϕ which are both determined as part of the solution. The result is an exponential scheme which accounts for convective and diffusive effects and an implicit correction to account for source term influences.

In summary, for one-dimensional flows, the SOU scheme, UDS with diffusion and source term influences, and the OCI Scheme can all be expressed as an Upwind difference scheme with correction to account for the variation in ϕ. The SOU scheme bases the correction on profile assumptions, while the OCI and UDS with diffusion and source term influences employ corrections reflecting the effects of diffusion and sources.

The implications of the above one-dimensional analysis can be easily extended to cover two-dimensional formulations. Approximations of interface values can again be accomplished by Upwind differencing. However, for multi-dimensional flows use of UDS is accompanied with severe false diffusion, i.e., solutions display excessive amounts of smearing.

To eliminate false diffusion, a correction to the upwind estimate, as in equation (6.15), is required. The correction can be determined from profile assumptions, as provided by equation (6.18), or a physical correction which, for two-dimensional flows, must account for the effects of diffusion and

source terms as well as a component of convection in one of the two coordinate directions. For instance, the correction at the east face of a control volume is given by:

$$\left(\frac{\partial \phi}{\partial x}\right)_e = \left[\frac{1}{\rho u}\left\{-\rho v \frac{\partial \phi}{\partial y} + \frac{\partial}{\partial x}\left(\Gamma_\phi \frac{\partial \phi}{\partial x}\right) + \frac{\partial}{\partial y}\left(\Gamma_\phi \frac{\partial \phi}{\partial y}\right) + S_\phi\right\}\right]_e \quad (6.22)$$

For multi-dimensional flows OCI also requires correction, through the appropriate definition of operators, for the effects of the additional components of convection and diffusion.

The advantage of the profile or physical corrections as described above for two dimensions is that they are relatively straightforward to implement. However, such implementations may also be subject to relatively large overshoots and undershoots, especially when flows are at a large angle to the grid. The primary reason these overshoots undershoots arise is because the corrections for the additional component of convection, based on either profile assumptions or physical arguments, introduce non-physical negative influence coefficients.

An alternative is to use Skewed Upstream Differencing Schemes[12] (SUDS). In SUDS, the two convective terms of equation (6.1) are replaced by a single streamline derivative term:

$$\frac{\partial}{\partial x}(\rho u \phi) + \frac{\partial}{\partial y}(\rho v \phi) = \rho V \frac{\partial \phi}{\partial s} \quad (6.23)$$

where $V = \sqrt{u^2+v^2}$ and s is the streamline coordinate. Upwinding along the streamline, the convective terms at the east face of a control volume are then given by:

$$\rho V \frac{\partial \phi}{\partial s} \simeq \rho \frac{V}{L}(\phi_e - \phi_u) \quad (6.24)$$

where ϕ_u is the skewed upwind value of ϕ and L is the distance between the locations where ϕ_e and ϕ_u are defined, figure (6.1). The correction of SUDS can then be expressed as:

$$\phi_e \simeq \phi_u + L \left(\frac{\partial \phi}{\partial s}\right)_e \tag{6.25}$$

where $(\partial\phi/\partial s)_e$ represents the correction required to account for diffusion and source terms and is given by:

$$\left(\frac{\partial \phi}{\partial s}\right)_e \simeq \left[\frac{1}{\rho V}\left\{\frac{\partial}{\partial x}\left(\Gamma_\phi \frac{\partial \phi}{\partial x}\right) + \frac{\partial}{\partial y}\left(\Gamma_\phi \frac{\partial \phi}{\partial y}\right) + S_\phi\right\}\right]_e \tag{6.26}$$

Note that the correction to SUDS given in equation (6.26) does not include a correction for any component of convection. All components of convection are included in the Skewed Upstream differencing.

In summary, for multi-dimensional flows, SOU, SUDS and OCI schemes all adopt an upwind representation of convection. Conventional implementations of OCI and SOU employ upwinding along coordinate directions, while SUDS upwind along streamlines. Furthermore, each of the schemes require correction of Upwind differencing. In SOU corrections are determined from profile assumptions. In both SUDS and OCI corrections are more physically based with corrections in SUDS including diffusion and source effects, and corrections in OCI including effects for diffusion, sources and components of convection.

With this background it is appropriate to consider the details of the schemes.

6.2 SECOND ORDER UPWIND DIFFERENCING SCHEMES

6.2.1 Derivation and Characteristics of Finite Difference Equations

As discussed above, SOU schemes attempt to improve the convective accuracy of UDS by the inclusion of additional terms in the Taylor Series Expansion for the interface value. The scheme will be developed initially in one dimension to study its accuracy, stability and convergence characteristics. Assuming a profile for ϕ_e in the form given by (uniform convective velocity and grid), figure (6.1),

$$\phi_e \simeq \begin{cases} \phi_P + \dfrac{\phi_P - \phi_W}{2} & u > 0 \\ \phi_E + \dfrac{\phi_{EE} - \phi_E}{2} & u < 0 \end{cases} \tag{6.27}$$

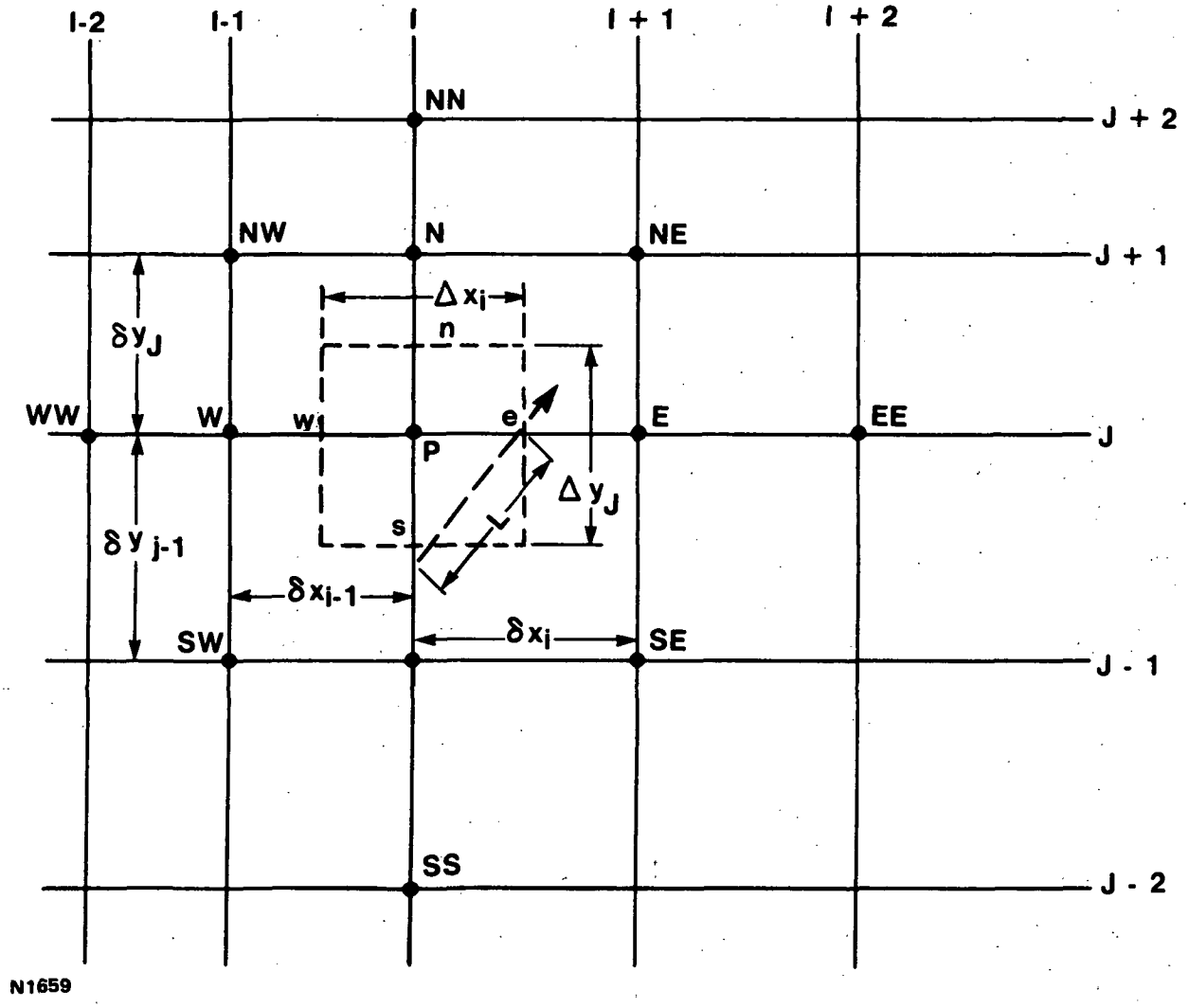

Figure 6.1 Control Volume Details for SUDS (Positive Velocity at East Face) and SOU

and similarly for ϕ_w, the net convective flux balance is expressed as:

$$u \frac{d\phi}{dx} \simeq \frac{u}{\delta x} \left(\frac{3}{2} \phi_P - 2\phi_W + \frac{1}{2} \phi_{WW}\right) \quad u > 0$$
$$\frac{u}{\delta x} \left(-\frac{3}{2} \phi_P + 2\phi_E - \frac{1}{2} \phi_{EE}\right) \quad u < 0 \tag{6.28}$$

Substituting for the convective derivative in equation (6.19a) with no sources and incorporating the usual approximation for the diffusive fluxes yields a difference equation for ϕ_p. The stability and monotonicity aspects of the difference equation are conveniently analyzed as follows (u>o): The discretized form of equation (6.19a) is:

$$\frac{1}{h} \left(\frac{3}{2} \phi_i - 2\phi_{i-1} + \frac{1}{2} \phi_{i-2}\right) - \frac{1}{P} \left(\frac{\phi_{i+1} - 2\phi_i + \phi_{i-1}}{h^2}\right) = 0 \qquad i = 2,\ldots n \tag{6.29}$$

In the above i denotes the particular node and P signifies the ratio u/Γ_ϕ. In addition to (6.29), the analysis requires the usual boundary conditions,

$$\phi_0 = 1 \qquad \phi_{n+1} = 0 \tag{6.30}$$

and the first order upwind formula to be applied at i=1 to yield ϕ_1, i.e.,

$$\frac{\phi_1 - \phi_0}{\delta x} - \frac{1}{P\delta x^2} (\phi_2 - 2\phi_1 + \phi_0) = 0$$

Denoting $P\delta x$ by Pe, the grid Peclet number, and $\phi_i - \phi_{i-1}$ by α_i, then equation (6.29) becomes:

$$Pe\ (3\alpha_i - \alpha_{i-1}) - 2\ (\alpha_{i+1} - \alpha_i) = 0 \qquad i=2, \ldots .n \tag{6.31}$$

The boundary condition on α_i is given by (6.30) as:

$$\alpha_2 = (1 + Pe)\alpha_1 \tag{6.32}$$

Rearranging equation (6.31) yields

$$2\,\alpha_{i+1} - (2 + 3\,Pe)\,\alpha_i + Pe\alpha_{i-1} = 0$$

a three term, linear recurrence relation with constant coefficients. Thus there exist constants A,B, λ_1, λ_2 such that

$$\alpha_\mu = A\lambda_1^\mu + B\,\lambda_2^\mu \qquad \mu = 1, \ldots.n+1$$

where λ_1 and λ_2 satisfy

$$2\,\lambda^2 - (2 + 3Pe)\,\lambda + Pe = 0 \tag{6.33}$$

i.e.,

$$\lambda_{1,2} = 1/2 \left\{ 1 + \frac{3}{2} Pe \pm \sqrt{1 + Pe + 9Pe^2/4} \right\} \tag{6.34}$$

Notice that Pe>0 implies $\lambda_{1,2}>0$. A similar analysis yields identical results for Pe < 0.

Use can now be made of equation (6.32) to obtain

$$A\lambda_1^2 + B\lambda_2^2 = (\,1 + Pe)\,(A\lambda_1 + B\lambda_2)$$

or,

$$A\,[\lambda_1^2 - (1+Pe)\lambda_1] = -B\,[\lambda_2^2 - (1+Pe)\lambda_2]$$

Now equation (6.33) implies

$$\lambda_j^2 - (\,1 + Pe)\lambda_j = Pe\,\left(\frac{\lambda_j - 1}{2}\right) \qquad j = 1,2$$

and from equation (6.34)

$$\frac{Pe}{2}(\lambda_1 - 1) > 0 \quad \text{and} \quad \frac{Pe}{2}(\lambda_2 - 1) < 0$$

Thus, neglecting the degenerate case of A=0 and B=0, AB>0, and hence α_μ is of a uniform sign (bounded).

Regarding the stability of iterative techniques used to solve equation (6.29) it can be shown that such solvers, are well conditioned and converge rapidly with a maximum eigenvalue of the iteration matrix assuming a value of 2/3. Furthermore, a formal Taylor Series Expansion yields the accuracy of the scheme as second order on smoothly varying or uniform grids.

There have been proposed alternative formulations of equation (6.29) due to the extended nature of the molecule implied therein.[71]. One such form is:

$$u\frac{d\phi}{dx} \simeq \frac{3}{2}\frac{u}{\delta x}(\phi_i - \phi_{i-1}) - \frac{1}{2}\frac{u}{\delta x}(\phi_{i-1} - \phi_{i-2}) \qquad u > 0$$

$$\frac{3}{2}\frac{u}{\delta x}(-\phi_i + \phi_{i+1}) + \frac{1}{2}\frac{u}{\delta x}(\phi_{i+1} - \delta_{i+2}) \qquad u < 0 \tag{6.35}$$

The advantage provided by such a rearrangement allows the second terms in these expressions to be treated explicitly as a deferred source term, thus enabling the strict tri-diagonal nature of the discretized equations to be retained in implementation.

It will be seen from the above discussion that SOU solutions in one dimension are bounded, stable and second order accurate. Extension to multi dimensions is straightforward and is based on individual one-dimensional solutions, characteristic of profile schemes, Section (6.1). However, in multi dimensions due to possibility of generating negative coefficients, albeit minor, see equation (6.28), the solutions will not necessarily be bounded. Furthermore, the above one-dimensional analysis carried out for uniform sign of the convecting velocity does not strictly ensure stability for velocity changing sign across a cell, characteristic of recirculation zones. Use of Second Order Upwind differencing by Coakley[72] encountered oscillations in the vicinity of a shock where the Q eigenvalue changes sign across a P-shock.

Finally, characteristic of profile schemes, some smearing of profiles is expected, as the scheme does not explicitly account for the misalignment between the grid and the streamline.

6.2.2 Solution Details

The matrix equation generated by the finite difference molecule implied by (6.28) and its two-dimensional analog is not generally amenable to solution by direct application of the Tri-Diagonal Matrix Algorithm (TDMA) or its Alternating Direction Line Gauss-Sidel (ADI) equivalent; variants of Penta-Diagonal Matrix Solvers formulated in ADI fashion[30] have to be used with attendant computational costs. Alternatively, discretization relations provided by equation (6.35) that retain the strict tri-diagonal nature of the formulation could be used (adopted in this study). However, iterative stability of such solutions incorporating a deferred correction strategy is not assured a priori in multi dimensions and solution costs might be relatively high.

A further point in obtaining solutions using the SOU scheme concerns the application of boundary conditions. Due to the extended nature of the molecule, near the boundaries the scheme must be modified using conventional practices, including the use of Central or lower order Upwind differences. Shyy et al[73] examined in detail the influence on the solution of adopting implicit or explicit treatment of boundary conditions at the outlet boundary. It is also claimed by Gupta and Manohar[29] that the overall accuracy of the scheme is severely affected by the inconsistencies introduced in boundary condition specification. In this study Hybrid differences were used near "flow boundaries" on the grounds of robustness.

6.3 ADVANCED SKEWED UPSTREAM DIFFERENCING SCHEMES (SUDS)

6.3.1 Influence Point Equations

The two SUDS variants considered in this study are primarily designed to reduce the error associated with the evaluation of convective fluxes at the interfaces, C_{ef} in equation (6.5). In both schemes this is accomplished by i) breaking each control volume face into two parts thereby effectively increasing resolution and, ii) improving the evaluation of the influence of nodal values of ϕ for control volume evaluations.

To increase the resolution of the convective flux evaluation, each control volume face is broken up into two parts. For example, the e control volume face is broken up into the parts shown in figure (6.2). As a result, the convective flux evaluation at the e face is given by:

$$J_e^c = \int_{\Delta y} (\rho u \phi)_e dy = J_{ese}^c + J_{ene}^c$$

where (6.36)

$$J_{ese}^c = \int_{\Delta y_s} (\rho u \phi)_e dy \quad ; \quad J_{ene}^c = \int_{\Delta y_n} (\rho u \phi)_e dy$$

Considering, now the evaluation of J_{ese} and introducing the previously used approximations; i.e.,

i) $(\rho u)_e$ is constant along the ese portion of the e face,

ii) ϕ varies at most linearly along the ese face,

then

$$J_{ese}^c \simeq (\rho u)_{ese} \phi_{ese} \qquad \text{(cf. equation (6.5))} \qquad (6.37)$$

where ϕ_{ese} is the value of ϕ midway along the ese face.

It is therefore necessary to evaluate ϕ_{ese} in terms of the surrounding P,E,S and SE nodal values of ϕ. The approach adopted here is to ensure that the evaluation of ϕ_{ese} is based on the physical <u>influence</u> of the nodal values of ϕ on ϕ_{ese}, Stubley.[74] For this reason, ϕ_{ese} is referred to as an influence point value of ϕ.

The next step in the discretization is to define how the influence point value of ϕ is related to nodal point values. However, before proceeding with this, it is necessary to introduce some additional terminology. First, borrowing from the finite element approach, Section (5.1.6), the four nodes surrounding the influence point can, in fact, be seen to define the four corners of a rectangular element, and the element, so defined, is made up from quadrants of four different control volumes. Also, by introducing two influence points along each control volume face in domain, each element contains four influence points. The configuration for the element containing ϕ_{ese} is shown in figure (6.3).

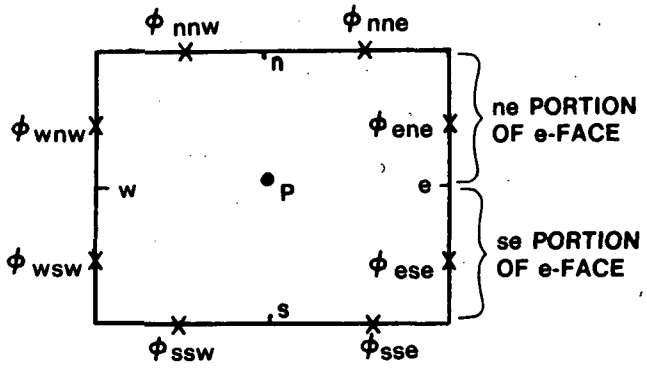

Figure 6.2 Division of Control Volume Faces

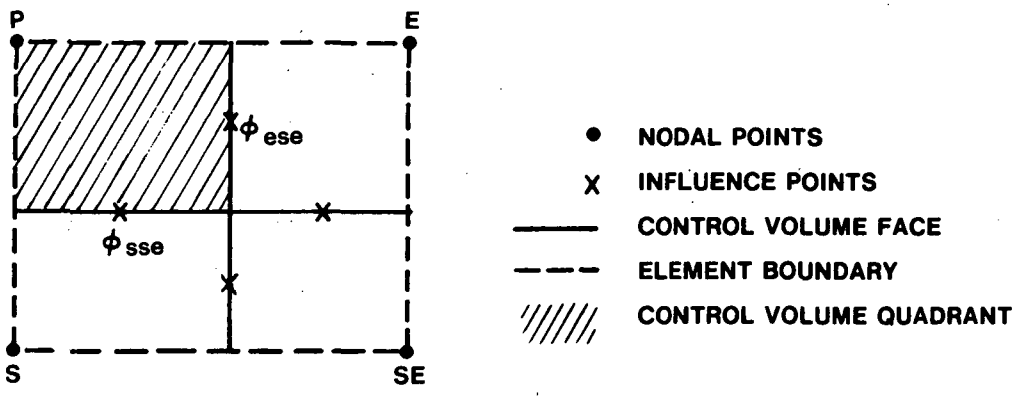

Figure 6.3 Element Surrounding Influence Point Value ϕ_{ese}

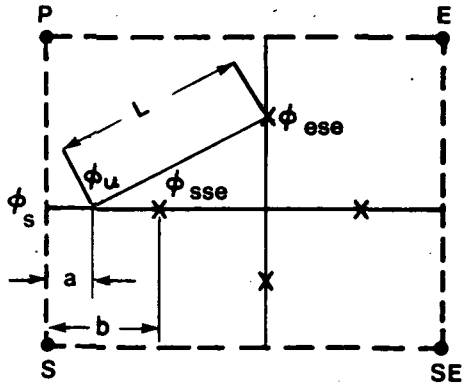

N1679

Figure 6.4 Evaluation of ϕ_u for LP-SUDS

It now remains that ϕ_{ese} must be expressed in terms of nodal values of ϕ and that the influence of the nodal values of ϕ on ϕ_{ese} must reflect the correct physical influence. As suggested by Raw[10] one way of accomplishing this is by way of an approximate algebraic representation of the relevant differential equation. This is discussed next to derive the influence point equations for the linear profile variant of SUDS, (LP-SUDS).

The LP-SUDS influence point equation for face values of ϕ can be arrived at by considering equation (6.1) at each influence point. For instance, at the ese influence point, equation (6.1) can be written as:

$$C_{ese} = D_{ese} + S_{ese} \tag{6.38}$$

where C represents the convective terms, D, the diffusive terms and S the source term. To derive an influence point equation, an approximate representation of each of the terms is required for each influence point.

Consider the convection terms, C, written in non-conservative Cartesian form,

$$C = \rho u \frac{\partial \phi}{\partial x} + \rho v \frac{\partial \phi}{\partial y} = \rho V \frac{\partial \phi}{\partial s}$$

where $V = \sqrt{u^2 + v^2}$ and $ds = u/V\, dx + v/V\, dy$

To approximate the above equation algebraically, original skewed upwinding ideas are upwinding employed such that

$$C_{ese} = \rho V \left(\frac{\partial \phi}{\partial s}\right)_{ese} \simeq \rho V \left(\frac{\phi_{ese} - \phi_u}{L}\right) \tag{6.39}$$

where ϕ_u is an upwind value of ϕ and L is the distance between the upwinded point and the influence point.

To illustrate, consider the case shown in figure (6.4) where the streamline through ϕ_{ese} is such that it intersects the s control volume face to the left of ϕ_{ese}. In this case the value of L is as indicated and the upwind value of ϕ is <u>linearly</u> interpolated between ϕ_{sse} and ϕ_s

$$\phi_u = \frac{a}{b}\,\phi_{sse} + (1 - \frac{a}{b})\,\phi_s \qquad (6.40)$$

where ϕ_{sse} is in turn linearly interpolated between the nodal values of ϕ_P and ϕ_S. The general rule for the calculation of ϕ_u and the length scale L is to take the local streamline, passing through ϕ_{ese}, upwind until it intersects an edge of a control volume quadrant. Then a linear interpolation is used along that edge between appropriate nodal values or influence point values. Therefore, if the upwind portion of the streamline intersects a control volume quadrant edge between two influence points, the value of ϕ_u is determined by linearly interpolating the two influence points. Similarly, if the upwinded streamline intersects the line joining two nodes, the linear interpolation of ϕ between the two nodes is used. Implementations using variants of such practices are discussed later in Section (6.3.3).

As discussed above the value of ϕ_u along quadrant edges is determined by linearly interpolating between nodal or influence point values of ϕ. Equivalently, ϕ_u is determined by assuming a linear profile of ϕ between nodal or influence points. Hence, the resulting scheme is referred to as linear profile SUDS. In a later section a different evaluation of ϕ_u adopted in Mass Weighted SUDS is described.

Considering next the evaluation of diffusion terms in equation (6.1), i.e.,

$$D = \frac{\partial}{\partial x}\left(\Gamma_\phi \frac{\partial \phi}{\partial x}\right) + \frac{\partial}{\partial y}\left(\Gamma_\phi \frac{\partial \phi}{\partial y}\right)$$

means have to be provided to ensure that no non-physical influence results due to their incorporation in the influence point equations. Thus D is usually split into two parts, the component normal to the control volume in question, D^n, and the tangential component, D^t. For ϕ_{ese}, these are:

$$D^n = \frac{\partial}{\partial x}\left(\Gamma_\phi \frac{\partial \phi}{\partial x}\right)$$

$$D^t = \frac{\partial}{\partial y}\left(\Gamma_\phi \frac{\partial \phi}{\partial y}\right)$$

An approximate representation of D^n is given by:

$$D^n \simeq f\,\Gamma_\phi \frac{\left\{\frac{\phi_E - \phi_{ese}}{\Delta^{x+}} - \frac{\phi_{ese} - \phi_P}{\Delta x^-}\right\}}{(\Delta x^+ + \Delta x^-)/2} \tag{6.41}$$

where the distances Δx^+ and Δx^- are indicated in figure (6.5) and f is a correction factor. The correction factor f, is required for two reasons. First, if upwinding is used to represent the convection terms at the influence point and Central differencing is used for D^n, then after combining C and D^n, the most accurate evaluations of ϕ_{ese} require that f range from 0 to 2 depending on the grid Peclet number. Secondly, the correction factor is required to ensure that negative downstream coefficients, which are non-physical and can result in spurious spatial oscillations, do not arise in the control volume equations. It can be shown that for this condition to be met it is sufficient to assign f the value of 0.5. In the interest of simplicity this assignment is adopted in the present study.

For the tangential component of D, the following form is adopted:

$$D^t \simeq \Gamma_\phi \frac{\left\{\frac{\phi_e - \phi_{ese}}{\Delta y^+/2} - \frac{\phi_{ese} - \phi_{SE}}{\Delta y^- + \Delta y^+/2}\right\}}{(\Delta y^+ + \Delta y^-)/2} \tag{6.42}$$

where ϕ_e and ϕ_{ese} and distances Δy^+ and Δy^- are as shown in figure (6.5). To evaluate ϕ_e and ϕ_{SE} in terms of nodal values linear interpolation can be used. However, to ensure that no significant negative downstream coefficients arise, the values of ϕ_e and ϕ_{SE} are determined from the relations:

$$\phi_e = (1 - A)\,\phi_P + A\phi_E \tag{6.43}$$

$$\phi_{SE} = (1 - A)\,\phi_S + A\phi_{SE} \tag{6.44}$$

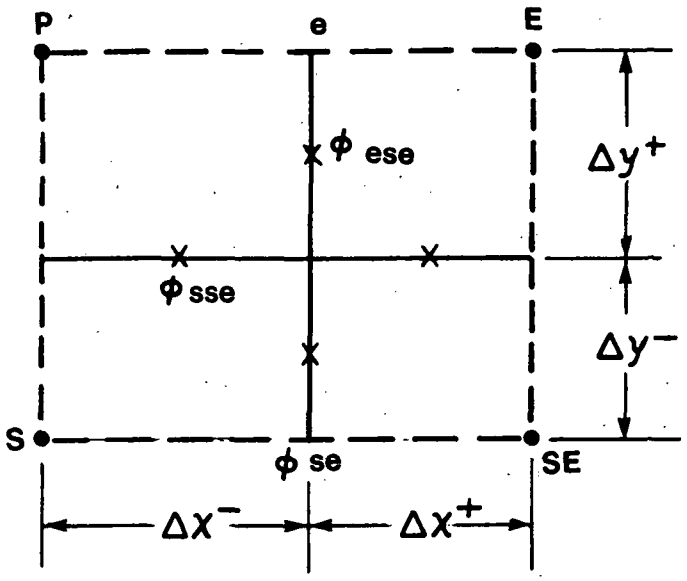

Figure 6.5 Evaluation of Diffusion Influence for SUDS Schemes

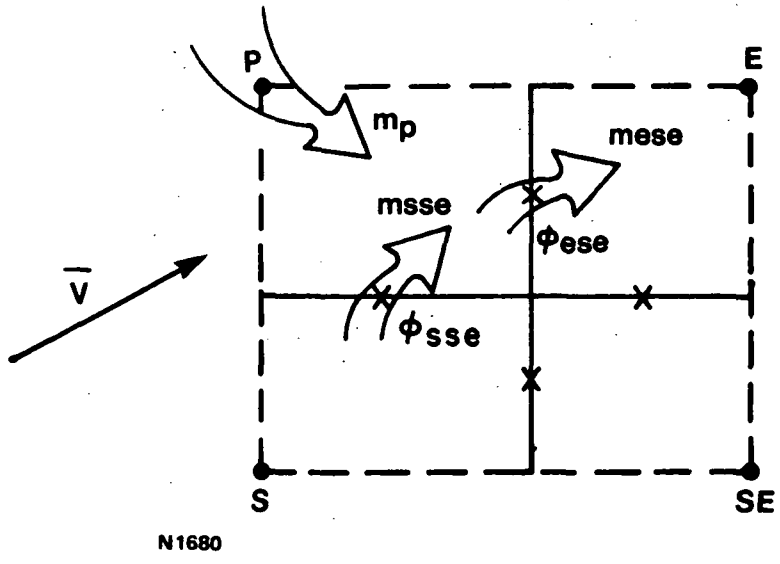

Figure 6.6 Evaluation of ϕ_u for MW-SUDS

where

$$A = (1 - e^{wPe})/(1 - e^{Pe})$$

$$Pe = \rho u_{ese} (\Delta x^{+} + \Delta x^{-})/\Gamma_{\phi}$$

$$w = \Delta x^{-}/(\Delta x^{+} + \Delta x^{-})$$

which can be derived by assuming that transport of ϕ is locally one-dimensional along the x-coordinate direction.

To arrive at the final form of the influence point equation consideration has to be given to approximating the source term, S_{ese}. If no source term influence is desired, then S_{ese}=o. However, to include this source term influence (STI), then, the evaluation of S_{ese} is based on the known values of S in each of the surrounding control volumes. In the present study if the x component of velocity at ϕ_{ese} is positive, then S_{ese} is taken to be the value of S in the P control volume. Otherwise, S_{ese} assumes the value of S in the E control volume.

6.3.2 Assembly of Influences and Discussion of the Finite Difference Equations

Combining together the above approximate representations of each term of the influence point equation, i.e.,

$$C_{ese} = D^{x}_{ese} + D^{y}_{ese} + S_{ese} \qquad (6.45)$$

provides a relationship between ϕ_{ese}, the four nodal values of ϕ as well as the three other influence point values of ϕ contained in the element, figure (6.3). It is important to re-iterate, that, as discussed by Raw,[10] it is essential that equation (6.45) adequately accounts for the appropriate physical influences.

Having described the manner in which the influence point equation for ϕ_{ese} is derived, it is a simple matter of repeating the procedure for each influence point contained in the element. The result is a set of four linear algebraic equations at each influence point involving four nodal values of ϕ and four influence point values of ϕ. It is then a simple matter of inverting a 4x4 matrix to be able to express each of the influence point values of ϕ in terms of the four nodal values of ϕ, Section (6.3.4). Moving from element to element, then the same procedure can be repeated so that each influence point value of ϕ in the computation domain can be related to surrounding nodal values. Finally, substituting these relations for influence points into the evaluations of convective fluxes i.e., equation (6.5), the control volume balance between convective fluxes, diffusion flux and source terms given by:

$$J^C_{ese} + J^C_{ene} - J^C_{wsw} - J^C_{wnw} + J^C_{nne} + J^C_{nnw} - J^C_{sse} - J^C_{ssw} = J^D_e - J^D_w - J^D_n - J^D_s + S_\phi$$

can be expressed in terms of nodal values as:

$$a_P\phi_P = a_E\phi_E + a_W\phi_W + a_N\phi_N + a_S\phi_S + a_{NE}\phi_{NE} + a_{NW}\phi_{NW} + a_{SE}\phi_{SE} + a_{SW}\phi_{SE} + b_p \tag{6.46}$$

Along with the representation of boundary conditions, the result is a set of linear algebraic equations for which a solution for nodal values of ϕ can be found.

As will be seen from an examination of (6.46) nine nodal values of ϕ are involved. The coefficients of equation (6.46), a_P, a_E.....a_{SW} are such that

$$a_P \geq a_E + a_W + a_N + a_S + a_{NE} + a_{SE} + a_{NW} + a_{SW}$$

Also, by the specific choice of algebraic relations used to represent the influence point convection and diffusion terms, the coefficients on the nodal values downstream of ϕ_P are not negative, thereby reducing the occurrence of

non-physical oscillations in the solution. However, a rigorous stability, accuracy and convergence analysis of the kind described in Section (6.2.1) for the SOU scheme is exceedingly difficult to accomplish for equation (6.46) a priori, and hence such characteristics will have to be established by computational experiments, Section (7.3.2).

A close study of equation (6.46) further reveals that, because a linear profile assumption is made to express ϕ_u in the influence point equations in terms of the surrounding values of ϕ, the coefficients of nodal values that are not directly downstream of ϕ_p may be negative. To illustrate, consider uniform flow angled to the grid $\Delta x = 0.1$, $\Delta y = 0.1$ such that $u = 0.5$, $v = 1.0$ and $\Gamma_\phi = 10^{-6}$. For this case the a coefficients normalized by a_p are:

$$\begin{bmatrix} a_{NW} & a_N & a_{NE} \\ a_W & a_P & a_E \\ a_{SW} & a_S & a_{SE} \end{bmatrix} = \begin{bmatrix} 0.0 & 0.0 & 0.0 \\ -0.1153 & 1.0 & -0.1154 \\ 0.5769 & 0.6923 & -0.385 \end{bmatrix}$$

As a result there exists the possibility of spurious oscillations in the solution of ϕ. Although these negative a coefficients do not produce any large oscillations as will be demonstrated in Section (7.3.2), there are some applications such as the k equation of $k - \varepsilon$ turbulence model, where it is essential that the solution be bounded. In this instance the Mass Weighted SUDS which is described next, can be used.

6.3.3 Mass Weighted Skewed Upstream Differencing Scheme (MW-SUDS) for Positive Definite Variables

As discussed by Raw,[75] to prevent negative a coefficients it is necessary to prevent any node external to the control volume from having a net effect of transporting a convected variable out of the control volume. To accomplish this an alternative evaluation of ϕ_u in equation (6.40) is required where now, ϕ_u is determined by logically deducing where the mass crossing the ese face originated. Consider the case shown in figure (6.6) where, m_{ese}, the mass flux through the ese face, is positive and known. The first step is to assume that there are two possible contributions to m_{ese} i) from m_{sse}, the mass flux through the sse face and ii) m_p, the mass flux through the surfaces formed by joining the locations ϕ_s, ϕ_p, and ϕ_e. The second step is to determine m_p from mass conservation, i.e.,

$$m_p = m_{ese} - m_{sse} \tag{6.47}$$

Now, if $m_{sse} > m_{ese}$, then all the mass crossing the ese face originated from the sse face. Therefore,

$$\phi_u = \phi_{sse} \tag{6.48}$$

By similar arguments, if $m_p \geq m_{ese}$ then,

$$\phi_u = \phi_p \tag{6.49}$$

Finally, if $m_{ese} > m_{sse}$ and $m_{ese} > m_p$, then both m_{sse} and m_p contribute to m_{ese} in the proportions

$$\frac{m_{sse}}{m_{ese}} \quad \text{and} \quad \frac{m_p}{m_{ese}} \quad , \quad \text{respectively.}$$

Therefore,

$$\phi_u = \frac{m_{sse}}{m_{sse}} \phi_{sse} + \frac{m_p}{m_{ese}} \phi_p \tag{6.50}$$

Combining all three cases together, the evaluation of ϕ_u in equation (6.49) is replaced by:

$$\phi_u = \alpha \phi_{sse} + (1-\alpha) \phi_p \tag{6.51}$$

where α = MAX (MIN (m_{sse}/m_{ese}, 1.0), 0.0). Considering the evaluation of α given above, the resulting discretization is appropriately referred to as Mass Weighted SUDS (MW-SUDS).

Adopting MW-SUDS, the a coefficients normalized by a_p for the same uniform angled flow case described previously becomes:

$$\begin{bmatrix} a_{NW} & a_N & a_{NE} \\ a_W & a_P & a_E \\ a_{SW} & a_S & a_{SE} \end{bmatrix} = \begin{bmatrix} 0.0 & 0.0 & 0.0 \\ 0.0 & 1.0 & 0.0 \\ 0.5 & 0.5 & 0.0 \end{bmatrix}$$

It is evident that mass weighting has removed the occurrence of negative a coefficients but, although it is not obvious from the coefficients, some false diffusion has been introduced. However, the resulting errors are considerably smaller than those that arise when the Hybrid 5 point discretization schemes are employed. Illustrations of this point are made in Section (7.3.2).

6.3.4 Further Considerations in the Implementation of Advanced SUDS Schemes

The LP-SUDS and MW-SUDS schemes considered above, involve evaluations of the coefficients of influence point equations that require the inversion of a 4x4 matrix in each flux element. These costly inversions are required because each influence point is implicity related to adjacent influence points. In this section an alternate explicit evaluation of the coefficients of the influence point equations is described which does not require the inversion of a 4x4 matrix.

Considering equations (6.38) and (6.39), an explicit formulation for LP-SUDS is accomplished by computing ϕ_u and length scale L in equation (6.39) in a manner compatible with upwinding the local streamline passing through ϕ_{ese} until it intersects an edge of the flux element, figure (6.4). Then, a linear interpolation is used along the flux element edge between appropriate nodal values. Upwinding to flux element edges instead of to control volume quadrant edges as in the implicit approach is necessary to ensure an explicit influence point equation.

To evaluate the diffusive term of equation (6.38) at the ese influence point, D_{ese} is determined from a bilinear interpolation of the approximate values of D available in each of the surrounding control volumes. Note that in the interest of simplicity best estimates of the nodal values of the variables are used to evaluate the control volume D's. Naturally, this deferred correction approach requires iteration which is readily incorporated into the iteration procedures used to solve flow problems.

The evaluation of the source term S_{ese} for the explicit influence point equation is determined in a manner similar to D_{ese}, from a bilinear interpolation of the surrounding nodal values for S.

The explicit influence point equation for MW-SUDS is very similar to the implicit approach. As in the implicit approach, the upwind value of ø is based on a mass weighted average of surrounding nodal and influence point values of ø. In the explicit approach developed by Huget,[30] $ø_u$ is given by a similar but not identical relation to equation (6.51), i.e.,

$$ø_u = \alpha ø'_{sse} + (1-\alpha)\, ø_P \tag{6.52}$$

where $ø'_{sse}$ is not equal to $ø_{sse}$. Instead, $ø'_{sse}$ is given by:

$$ø'_{sse} = \beta ø'_{sese} + (1-\beta) ø_S \tag{6.53}$$

where β = MAX (MIN ($-m_{sese}/m_{sse}$, 1.0), 0.0) and m_{sese} is the mass flow crossing the quadrant face directly south of the ese face. To ensure that no negative a coefficients arise,

$$ø'_{sese} = ø_P \tag{6.54}$$

For the explicit MW-SUDS the diffusion and source terms of the influence point equation are as described for the explicit LP-SUDS.

Finally, the evaluation of $ø_{ese}$ as determined above is appropriate for high grid Peclet numbers. However, for low grid Peclet numbers a bilinear interpolation is more appropriate and for intermediate grid Peclet numbers a combination of the two evaluations can be used, exploiting the flux blending strategy discussed in Section (5.15). Specifically, the Skewed Upstream differencing representation and bilinear representation of $ø_{ese}$, respectively denoted by $ø^s_{ese}$ and $ø^b_{ese}$, can be combined in the following manner:

$$\phi_{ese} = \upsilon\, \phi^{s}_{ese} + (1-\upsilon)\, \phi^{b}_{ese} \qquad (6.55)$$

where

$$\upsilon = \frac{Pe^2}{5+Pe^2}$$

The given evaluation of υ is chosen so that the introduction of a bilinear interpolation for ϕ_{ese} does not introduce any negative a coefficients. Note that the above equation for ϕ_{ese} ensures that for $|Pe| >> 1$, $\phi_{ese} = \phi^{s}_{ese}$, and for $|Pe| << 1$, $\phi^{b}_{ese} = \phi^{b}ese$.

6.3.5 Boundary Conditions

Consistent treatment of the boundary conditions compatible with formulation of LP-SUDS and MW-SUDS described in the previous sections, has been implemented by Raw[10] and Huget[30] for scalar as well as flow equations. However, in this section a specific treatment of boundary conditions appropriate for use in the Pratt and Whitney 2-D TEACH code will be considered.

The default layout of the numerical grid adopted in most production codes based on TEACH structure is such that, for a scalar, the boundary is straddled by nodes. However, the Pratt and Whitney 2-D TEACH code (Appendix A describes a similarly structured 3-D TEACH code) overrides this default by moving all fictitious nodes that are outside the computational domain so that they are coincident with the boundary. In the flux element structure of LP-SUDS and MW-SUDS this shift of fictitious nodes is readily implemented and results in flux element boundaries, quadrant boundaries and the boundary of the domain being coincident, figure (6.7). Note that no adjustment of the flux element is required for u and v velocity nodes which, by virtue of the staggered grid, naturally fall on the boundary. This includes u velocity nodes along east and west boundaries of the domain and v velocity nodes along north and south boundaries of the domain.

In addition to the adjustment of the grid layout in the vicinity of boundaries, the Pratt and Whitney 2-D TEACH code also assumes that for control volumes adjacent to the boundaries, a_{NE}, a_{NW} a_{SE} and a_{SW} are zero. Since this assumption permeates the entire code, any change regarding this assumption would require a complete restructuring of the code. Instead, the

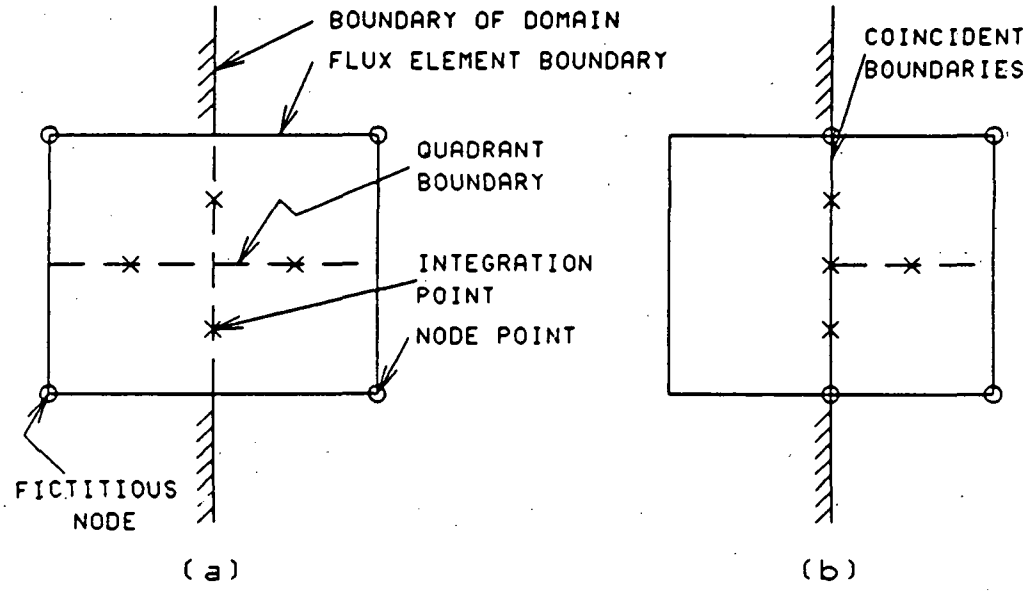

Figure 6.7 Default Flux Element Layout and Adjusted Layout in Vicinity of Boundary

assumption is retained and only MW-SUDS is used in flux elements that are adjacent to boundaries. It can be shown that the use of MW-SUDS will generate coefficients which satisfy this assumption.

Finally, for axisymmetric problems, all length, areas and volumes of a flux element are calculated accordingly, and any additional terms that arise in the differential equations representing momentum conservation are included in the integration point source term.

6.4 COMPACT IMPLICIT DISCRETIZATION SCHEMES

Most of the discussion pertaining to Compact Implicit discretization schemes will be developed in a one-dimensional context for clarity. Extensions to multi-dimensions are given in Section (6.4.1).

6.4.1 Derivative Compact Implicit Scheme (DCI)

Consider the Cartesian, linear convection-diffusion equation of (6.1) with ρ=1,

$$L_x = S(x) \tag{6.56}$$

where

$$L^x = \Gamma_{\phi} \frac{d^2\Phi}{dx^2} + u\frac{d\Phi}{dx}$$

is the spatial differential operator with spatially constant diffusion coefficient ϕ and convective coefficient u and the source term S is a function of the independent variable x.

The DCI approach is most readily described by first considering the discretization of equation (6.56) using standard second order centered difference representations of the derivatives, (uniform grid of spacing h):

$$\frac{d\Phi}{dx} \simeq \frac{\phi_{i+1} - \phi_{i-1}}{2h} + O(h^2) \tag{6.57}$$

$$\frac{d^2\Phi}{dx^2} \simeq \frac{\phi_{i+1} - 2\phi_i + \phi_{i-1}}{h^2} + O(h^2) \tag{6.58}$$

where ϕ_i is a discrete approximate value of ϕ at $x=x_i$ and h is the spacing between discrete points. Using equations (6.57) and (6.58) in (6.56), an explicit relationship can be derived that governs the evolution of ϕ in the form:

$$(1 + \frac{Pe}{2})\,\phi_{i+1} - 2\phi_i + (1 - \frac{Pe}{2})\,\phi_{i-1} = \frac{h^2}{\Gamma_\phi} S_i \qquad (6.59)$$

where Pe is the grid Peclet number.

The DCI procedures depart from the usual explicit form of discretization described above by seeking relations between the derivatives in equation (6.56) and ϕ that implicitly involve evaluations of the derivatives at neighbouring discrete points, Section (6.1.1). DCI schemes were discussed by Collatz,[76] Krause et al[77] who referred to their use as Mehrstellen integration, Adams[78] under the name of Hermetian finite differences and by Kreiss as reported in (31), who coined the Compact Implicit terminology. The standard DCI approximations to the derivatives of equation (6.56), given by:

$$\frac{\phi'_i + 4\phi'_i + \phi'_{i+1}}{6} = \frac{\phi_{i+1} - \phi_{i-1}}{2h} + O(h^4) \qquad (6.60)$$

$$\frac{\phi''_{i-1} + 10\phi''_i + \phi''_{i+1}}{12} = \frac{\phi_{i+1} - 2\phi_i + \phi_{i-1}}{h^2} + O(h^4) \qquad (6.61)$$

where ϕ' and ϕ'' are representations of $d\Phi/dx$ and $d^2\Phi/dx^2$ respectively, at discrete locations, can be derived by simple Taylor series analysis.

Because of the implicit nature of equations (6.60) and (6.61), the simultaneous solution of the following equations is required:

$$\Gamma_\phi \phi''_i + u\phi'_i = S_i \qquad (6.62a)$$

$$\phi'_{i-1} + 4\phi'_i + \phi'_{i+1} = \frac{3}{h}(\phi_{i+1} - \phi_{i-1}) \qquad (6.62b)$$

$$\phi''_{i-1} + 10\phi''_i + \phi''_{i+1} = \frac{12}{h^2}(\phi_{i+1} - 2\phi_i + \phi_{i-1}) \qquad (6.62c)$$

for the values of ϕ, ϕ', and ϕ''. Equations (6.62) are easily solved by the application of a block 3x3 Tri-Diagonal Matrix Algorithm.[79]

Incorporation of boundary conditions in (6.62) is accomplished via either fourth order one-sided representation of the various derivatives using Taylor series or Pade' approximations. Rubin and Graves[80] derived the following fourth order representation of ϕ'.

$$\phi_i - \phi_{i+1} + h\phi'_i - \frac{h^2}{6}(2\phi''_{i+1} + \phi''_i) = 0 + 0(h^4) \qquad (6.63)$$

Alternatively, a fifth order Pade' approximation relating the first and second derivatives is given by:

$$\phi_i - \phi_{i+1} + \frac{h}{2}(\phi'_i + \phi'_{i+1}) + \frac{h^2}{12}(\phi''_i - \phi''_{i+1}) = 0 + 0(h^5) \qquad (6.64)$$

The DCI method discussed above is formally fourth order and can be cast into a block tri-diagonal form. The major shortcomings of DCI are:

i) the inherent grid Peclet number limitation, restricting Pe to be of order 2

ii) the need for closure equations on the derivatives at the boundaries

iii) the need to solve sets of block tri-diagonal equations with particularly large blocks (7x7 for a scalar in three dimensions).

There are several ways to overcome these drawbacks. One approach is given by the subclass of Compact Implicit methods called Operator Compact Implicit (OCI) methods. Several OCI schemes are considered in the following section.

6.4.2 Generalized OCI Schemes

The classical OCI method, first postulated by Swartz[81] and later by Ciment et al,[36] assumes the existence of tri-diagonal relationship between

ϕ and the discrete representations of L^x denoted by $\mathcal{L}^x$, guided by the forms of equations (6.57) and (6.58), i.e.,

$$r^w \phi_{i-1} + r^p \phi_i + r^e \phi_{i+1} = q^w \mathcal{L}^x_{i-1} + q^p \mathcal{L}^x_i + q^e \mathcal{L}^x_{i+1} \qquad (6.65)$$

or

$$R\{\phi\} = Q\{\mathcal{L}^x\}$$

R and Q are tri-diagonal matrix operators. The coefficient of R and Q can be determined in a number of ways including the Taylor series analysis provided in Appendix B.

COCI adopts the following tri-diagonal operators R and Q to discretize equation (6.56) in the form given by (6.56):

$$q^p = 60 + 16\,(u_{i+1} - u_{i-1})z - 4u_{i+1}\,u_{i-1}z^2$$

$$q^e = 6 + (5u_i - 2u_{i-1})z$$

$$q^w = 6 - (5u_i - 2u_{i+1})z \qquad (6.66)$$

$$r^e = \frac{a}{2h^2}\,[q^w(2-zu_{i-1}) + q^p(2+zu_i) + q^e(2+3zu_{i+1})]$$

$$r^w = \frac{a}{2h^2}\,[q^w(2-3zu_{i-1}) + q^p(2-zu_i) + q^e(2+zu_{i+1})]$$

$$r^p = -(r^e + r^w),\quad z = \frac{h}{\Gamma_\phi}$$

An alternative derivation, valid for variable grid spacing is presented by Ciment, et al.[36]

It will be seen from the above discussion (equations (6.65) and (6.66)) that for one-dimensional problems, COCI solutions can be obtained using a single scalar tri-diagonal decomposition when $\mathcal{L}^x$ is known from

$$\mathcal{L}^x \simeq L^x = S(x) \qquad \text{equation (6.56)}$$

Further, COCI does not require boundary closures for higher order derivatives. Instead, evaluations of L^x at boundaries is required, but these are readily determined from equation (6.56) and the supplied conditions of ø. Therefore, by adopting the OCI approach two of the three drawbacks of DCI have been overcome. However, there still remains the problem of a restrictive grid Peclet number limitation. For the COCI scheme derived in Appendix B analysis[82] has shown that solutions remain bounded for $Pe \lesssim \sqrt{12} = 4.208$. However, the behavior of the numerical solution can be very non-physical at a considerably lower value of Pe, Section (7.3.3). In fact, non-physical behavior results when Pe>2. In attempting to remove the restrictive Peclet number criteria, Berger, et al[37] were led to the development of a Generalized OCI (GOCI) family of schemes which suffer from no such restrictions. These will be discussed next.

Berger, et al began by mathematically summarizing the properties of the tri-diagonal matrix operators R and Q of equation (6.65) that are required to ensure a physical (i.e., bounded) solution to

$$L^x = \Gamma_ø \frac{d^2ø}{dx^2} + u \frac{dø}{dx} = S(x)$$

$ø(0) = \alpha_0$; $\alpha(1) = \alpha_1$; $\Gamma_ø \geq 0$; $u \geq 0$ (i.e. advection from x=1 to x=0) and $S(x) \geq 0$.

These properties are postulated to be:

i) $r^w \geq 0$ (downwind influence of ø cannot be negative)

ii) $r^e > 0$ (upwind influence of ø must be positive)

iii) $-r^p \geq (r^e + r^w)$ (diagonal dominance)

iv) $q^e \geq 0$, $q^w \geq 0$, $q^p \geq 0$ (operator influence must be positive)

v) $r^e > r^w$ (upwind influence on ø must be as large as downwind influence on ø)

vi) $q^p u_i \geq q^e u_{i+1} + q^w_{i-1}$ (to ensure invertability of Q)

A review of the coefficients of R and Q of COCI, equations (6.66) reveals that the above requirements cannot be satisfied for all grid Peclet numbers, thus it is necessary to re-examine the structure of truncation error expression given in Appendix C.

The truncation error, τ, associated with equation (6.65), i.e.,

$$\tau = R\,(\Phi_i) - Q\,(L_i^x) \tag{6.67}$$

where Φ_i and L_i^x are defined as the exact values of Φ and L^x respectively, at the i'th discrete location, can be expanded in a Taylor series,

$$\tau = T^0\Phi_i + T^1\Phi_i^1 + T^2\Phi_i^2 + T^3\Phi_i^3 + T^4\Phi_i^4 + \ldots\ldots \tag{6.68}$$

where $\Phi^n = d^n\Phi/dx^n$, see Appendix C for definition of the T terms.

Unlike the COCI method that strictly assumes $T^3 = T^4 = 0$, a family of possible fourth order OCI schemes results by relaxing the constraints on T^3 and T^4 such that, $T^3 = 0$ and $T^4 = O(h^4)$. Unfortunately, as shown by Berger, et al[37], there is still no unique evaluation of the coefficients of R and Q which satisfies the above requirements. However, by further relaxing the constraints such that

$$T^3 = O(h^4)\ ;\ T^4 = O(h^4) \tag{6.69}$$

then, a family of fourth order OCI schemes results that satisfy the above requirements.

By recognizing from equations (6.66) the R can be expressed in terms of Q, the family of OCI schemes resulting from equation (6.69) can equivalently be viewed as a family of coefficients for the Q matrix operator. Furthermore, it is postulated that the coefficients of Q can be expressed as the following polynominal functions of z (cf. equation (6.66)):

$$q^w = q^{w,0} + q^{w,1}z + q^{w,2}z^2 + q^{w,3}z^3 + \ldots + q^{w,\nu}z^\nu \tag{6.70a}$$

$$q^e = q^{e,0} + q^{e,1}z + q^{e,2}z^2 + q^{e,3}z^3 + \ldots + q^{e,\nu}z^\nu \tag{6.70b}$$

$$q^p = q^{p,0} + q^{p,1}z + q^{p,2}z^2 + q^{p,3}z^3 + \ldots + q^{p,\nu}z^\nu \tag{6.70c}$$

where the coefficients of the polynominals are functions of u and are independent of Γ_ϕ. (Note that the Q of COCI belongs to this set).

From equations (6.69), the evaluations of T given in equations (C.4) in Appendix C and a substitution of the polynominal functions for Q gives:

$$T^3 = \Gamma_\phi h \left[t^{3,0} + t^{3,1}z + t^{3,2}z^2 + O(z^3)\right] = O(h^4) \tag{6.71a}$$

$$T^4 = \frac{\Gamma_\phi h^2}{12} \left[t^{4,0} + t^{4,1}z + O(z^2)\right] = O(h^4) \tag{6.71b}$$

where

$$t^{3,0} = q^{w,0} - q^{e,0} = O(h^3),\quad t^{4,0} = q^{p,0} - 5\,(q^{e,0} + q^{w,0}) = O(h^2)$$

$$t^{3,1} = q^{w,1} - q^{e,1} - \frac{1}{6}\,(2q^{e,0}u_{i+1} + 2q^{w,0}u_{i-1} - q^{p,0}u_i) = O(h^2)$$

$$t^{4,1} = q^{p,1} - 5\,(q^{w,1} + q^{e,1}) - (q^{e,0}u_{i+1} - q^{w,0}u_{i-1}) = O(h)$$

$$t^{3,2} = q^{w,2} - q^{e,2} - \frac{1}{6}\,(2q^{e,1}u_{i+1} + 2q^{w,1}u_{i-1} - q^{p,1}u_i) = O(h)$$

Further analysis of equations (6.70) with respect to the requirements (i) to (vi) reveals that the following conditions on the highest order (v=m) polynominal coefficient must be satisfied:

$$q^{e,m} > 0\ ,\ q^{w,m} = 0\ q^{p,m}\ u_i = q^{e,m}u_{i+1} \tag{6.72}$$

and that v=3 in equation (6.70) is the lowest order of the polynominals.

Based on the results of equation (6.72), the coefficients of equations (6.70) can be selected. Begin by choosing $q^{p,0}$=60 consistent with COCI results. Setting $t^{3,0} = t^{4,0} = 0$ it then follows from equation (6.71) that

$$q^{e,0} = q^{w,0} = 6 \tag{6.73}$$

Making use of the fact that,

$$u_{i+1} = u_i + O(h)$$
$$u_{i-1} = u_i + O(h)$$
$$1/2\ (u_{i+1} + u_{i-1}) = u_i + O(h)$$

combined with the t evaluations of equations (6.71) it can be shown that,

$$q^{w,1} = \frac{q^{p,1}}{10} - 3u_i + O(h^2) \tag{6.74a}$$

$$q^{e,1} = \frac{q^{p,1}}{10} + 3u_i + O(h^2) \tag{6.74b}$$

$$q^{e,2} = q^{w,2} + \frac{u_i}{10}\, q^{p,1} + O(h) \tag{6.74c}$$

Finally, from equation (6.72), it is concluded that,

$$q^{w,3} = 0 \tag{6.75a}$$

$$q^{p,3} = \frac{u_{i+1}}{u_i}\, q^{e,3} \tag{6.75b}$$

The remaining unknown coefficients in equations (6.70) are $q^{p,1}$, $q^{p,2}$, $q^{w,2}$ and $q^{e,3}$. Substituting equations (6.73), (6.74) and (6.75) into equations (6.70) and simplifying gives:

$$q^{w} = 6 + (p_1 - 3)Pe + p_2 Pe^2 \tag{6.76a}$$

$$q^{e} = 6 + (p_1 + 3)Pe + (p_1 + p_2)Pe^2 + p_4 Pe^3 \tag{6.76b}$$

$$q^{p} = 60 + 10p_1 Pe + p_3 Pe^2 + \frac{u_{i+1}\, p_4}{u_i} Pe^3 \tag{6.76c}$$

where the yet unknown constants are:

$$p_1 = q^{p,1}/10u_i \quad ; \; p_2 = q^{w,2}/u_i^2 \; , \; p_3 = q^{p,2}/u_i^2 \; ; \; p_4 = q^{e,3}/u_i^3$$

The choice of any one of p_1 to p_4 is arbitrary with the remaining p's to be evaluated from requirements (i) to (vi). One choice is to set $p_1=3$. For uniform u ($u_i=u_{i+1}=u_{i-1}$) and $p_1=3$ it can then be shown that,

$$p_2 = 0 \tag{6.77a}$$

$$p_3 = 9 \tag{6.77b}$$

$$p_4 = 1.5 \tag{6.77c}$$

Substitution of equations (6.77) into equations (6.76) leads to a specific GOCI scheme valid for generating bounded solutions for all values of Pe with u constant, which numerical results have tended to suggest is optimal

$$q^W = 6 \tag{6.78a}$$

$$q^e = 6 + 6Pe + 3Pe^2 + 1.5Pe^3 \tag{6.78b}$$

$$q^p = 60 + 30Pe + 9Pe^2 + 1.5Pe^3 \tag{6.78c}$$

and from equations (6.66)

$$r^W = 72 \tag{6.78d}$$

$$r^e = 72 + 72Pe + 36Pe^2 + 12Pe^3 + 3Pe^4 \tag{6.78e}$$

$$r^p = -(r^W + r^e) \tag{6.78f}$$

It is important to note that the r coefficients given in equations (6.78) are such that $r^e/r^W = e^{Pe} + O(h^4)$ and it is this exponential character which is, in part, responsible for ensuring that the resulting solution is bounded.

Error analysis by Berger, et al[37] demonstrates that GOCI schemes such as the one given in equations (6.78) are formally fourth order (i.e, in the low Pe limit) but automatically change their order of grid convergence as the grid Peclet number increases. In fact, in the high Peclet number limit, GOCI method is only second order accurate and at intermediate values of Pe the order may drop to zero.

In summary GOCI scheme is, for one-dimensional problems, bounded for all values of Pe. In addition, GOCI does not require additional boundary equations for the operator, and solutions to the algebraic equations are readily obtained using TDMA for a single scalar. Variations on the above GOCI approach which sacrifice formal fourth order convergence for uniform second order convergence exist. One such approach will be used as the basis for a new control volume based OCI scheme presented next.

6.4.3 Control Volume Based Operator Compact Implicit Method of Exponential Type (CVOCI)

In this Section is developed a particular scheme for the family of exponential OCI schemes that ensures conservation ø over discrete control volumes. Most, if not all, existing Compact Implicit schemes reported in the literature are of a "point finite difference" nature and hence do not strictly satisfy some of the desired attributes of a discretization scheme discussed in Section (4.2).

Considering equation (6.56) with spatially varying diffusion and convection coefficients, i.e.,

$$L^x = \frac{d}{dx}\left(\Gamma_\phi \frac{d\Phi}{dx}\right) + \frac{d}{dx}(u\Phi) = S(x) \qquad \text{equation (6.56)}$$

a finite volume integration can be performed over the length of control volume ,h, to yield

$$\int_0^h L^x dx = \int_0^h \left[\frac{d}{dx}\left(\Gamma_\phi \frac{d\Phi}{dx}\right) + \frac{d}{dx}(u\Phi)\right] dx = J_{ef} - J_{wf} = \int S(x)dx$$

equation (6.13)

where J_{ef} and J_{wf} denote the interface fluxes of ø given by

$$J_{ef} = \left[\Gamma_\phi \frac{d\Phi}{dx} + u\Phi\right]_e \; ; \; J_{wf} = \left[\Gamma_\phi \frac{d\Phi}{dx} + u\Phi\right]_w$$

To obtain a discrete algebraic representation of equation (6.12) in terms of ø and $\mathcal{L}^x$, the discrete approximations of Φ and L^x are required within the control volumes; it is assumed that both L^x and S(x) vary at most linearly over the control volume, thus,

$$\int_0^h L^x \, dx \simeq h\mathcal{L}_i^x \qquad (6.79a)$$

$$\int_0^h S(x)\,dx \simeq hS_i \tag{6.79b}$$

Also

$$\mathcal{L}_i^x = S_i \tag{6.79c}$$

In equations (6.79) $\mathcal{L}_i^x$ and S_i are approximations of L^x and $S(x)$ at the midpoint of the control volume. The approximate representation of the flux expressions in equation (6.13) is not so simple and requires evaluations of $d\Phi/dx$ and Φ in terms of ϕ and $\mathcal{L}^x$ at both control volume boundaries. In the present exponential scheme, these evaluations are determined from the analytic solution of equation (6.56), i.e.,

$$\Gamma_\phi \frac{d^2\Phi}{dx^2} + \frac{ud\Phi}{dx} = L^x$$

where $0 \le x \le h$, $\Phi(x=0) = \phi_0$, $\Phi(x=h) = \phi_1$ and Γ_ϕ and u are assumed to be constant over the range of x and L^x is an arbitrary function of x. The solution of the above equation, with no further approximation is given by:

$$\Phi(x) = \phi_0 + (\phi_1 - \phi_0)\left[\frac{e^Z - 1}{e^P - 1}\right] + \left(F(x) - F(h)\left[\frac{e^Z - 1}{e^P - 1}\right]\right) \tag{6.80}$$

where

$$F(x) = \frac{1}{u}\left[\int_0^x L^x\,dx - e^Z \int_0^x e^{-Z} L^x dx\right]$$

$$P = -P_e = -\frac{uh}{\Gamma_\phi};\quad Z = -Pe\,\frac{x}{h} = \frac{ux}{\Gamma_\phi}$$

The gradient of ϕ is easily shown to be:

$$\frac{d\Phi}{dx}(x) = -(\phi_1 - \phi_0)\,\frac{ue^Z}{\Gamma_\phi(e^P - 1)} + \left(G(x) + F(h)\,\frac{ue^Z}{\Gamma_\phi(e^P - 1)}\right) \tag{6.81}$$

where

$$G(x) = \frac{e^Z}{\Gamma_\phi} \int_0^x e^{-Z} L^x dx$$

Equations (6.80) and (6.81) require the integrals of L^x in the evaluation of F and G. Unfortunately L^x is not known. Therefore, profiles of L^x have to be assumed. A particular choice that sets L^x to zero yields the well-known Exponential Differencing Scheme, (EDS).[83] With this in mind, for any non-zero L^x profile assumption, equations (6.80) and (6.81) can be seen to provide the corrections to EDS necessary to account for the influence of $L^x = S(x)$ on the solution for ø. Since in this OCI approach the operator is implicit, alternative profiles of L^x can be considered.

Assuming that L^x varies linearly with x, equations (6.80) and (6.81) become:

$$\Phi(x) = \phi_0 + (\phi_1-\phi_0)\left[\frac{e^Z-1}{e^P-1}\right] + \frac{\mathcal{L}_0^x}{u}\left(x-h\left[\frac{e^Z-1}{e^P-1}\right]\right)$$

$$+ \frac{\mathcal{L}_1^x-\mathcal{L}_0^x}{h}\left(\frac{x^2}{2} - \frac{\Gamma_\phi x}{u} - \left(\frac{h^2}{2} - \frac{\Gamma_\phi h}{u}\right)\left[\frac{e^Z-1}{e^P-1}\right]\right) \qquad (6.82a)$$

$$\frac{d\Phi}{dx} = (\phi_0-\phi_1)\frac{ue^Z}{\Gamma_\phi(e^P-1)} + \frac{\mathcal{L}_0^x}{\Gamma_\phi}\left(\frac{\Gamma_\phi}{u} + h\frac{e^Z}{e^P-1}\right)$$

$$+ \frac{\mathcal{L}_1^x-\mathcal{L}_0^x}{h\Gamma_\phi}\left(\frac{\Gamma_\phi x}{u} - \frac{\Gamma_\phi^2}{u^2} + \left(\frac{h^2}{2} - \frac{\Gamma_\phi h}{u}\right)\frac{e^Z}{(e^P-1)}\right) \qquad (6.82b)$$

Substituting equations (6.82) into the flux expression of equation (6.13), the e face flux becomes

$$J_{ef} = \bar{r}^w\phi_0 + \bar{r}^e\phi_1 + \bar{q}^w\mathcal{L}_0^x + \bar{q}^e\mathcal{L}_1^x \qquad (6.83a)$$

where

$$\bar{r}^w = \frac{\Gamma_\phi}{h}\frac{Pe^P}{e^P-1} \tag{6.83b}$$

$$\bar{r}^e = \frac{\Gamma_\phi}{h}\frac{P}{e^P-1} \tag{6.83c}$$

$$\bar{q}^w = h\left(\frac{x}{h} - \frac{x^2}{2h^2} - \frac{1}{P} + \frac{1}{P^2} + \frac{1}{2(e^P-1)} - \frac{1}{P(e^P-1)}\right) \tag{6.83d}$$

$$\bar{q}^e = h\left(\frac{x^2}{2h^2} - \frac{1}{P^2} + \frac{1}{2(e^P-1)} - \frac{1}{P(e^P-1)}\right) \tag{6.83e}$$

Noting that $\phi_0=\phi_i$, $\phi_1=\phi_{i+1}$, $\mathcal{L}^x_0 = \mathcal{L}^x_i$ and $\mathcal{L}^x_1 = \mathcal{L}^x_{i+1}$, equation (6.83a) can equivalently be written as:

$$J_{ef} = \bar{r}^w\phi_i + \bar{r}^e\phi_{i+1} + \bar{q}^w\mathcal{L}^x_i + \bar{q}^e\mathcal{L}^x_{i+1} \tag{6.83f}$$

Similarly, the flux through the w face is given by:

$$J_{wf} = \bar{r}^w\phi_{i-1} + \bar{r}^e\phi_i + \bar{q}^w\mathcal{L}^x_{i-1} + \bar{q}^e\mathcal{L}^x_i \tag{6.84}$$

Combining equations (6.79), (6.83) and (6.84), equation (6.13), the control volume flux balance equation is represented by:

$$r^w\phi_{i-1} + r^p\phi_i + r^e\phi_{i+1} = q^w\mathcal{L}^x_{i-1} + q^p\mathcal{L}^x_i + q^e\mathcal{L}^x_{i+1} \tag{6.85}$$

where

$$r^w = -\bar{r}^w$$
$$r^e = \bar{r}^e$$
$$r^p = -(r^w+r^e)$$
$$q^w = \bar{q}^w$$
$$q^e = -\bar{q}^e$$
$$q^p = h-q^e-q^w$$

Finally using (6.79c) to evaluate $\mathcal{L}^x$ the resulting profiles for ϕ can be determined from the solution of equation (6.85).

At this point it is useful to review some of the characteristics of this discretization scheme. The scheme is an OCI variant of exponential type and is conservative. Further examination of the coefficients of equation (6.85) also reveals that conditions (i), (ii), (iii), (v) and (vi), Section (6.4.2), required to ensure bounded one-dimensional solutions are satisfied. However, it can be shown that condition (iv) is not always satisfied. Consider, for example, the limiting case $P = \infty$ where $q^e = -\bar{q}^e = -x^2/(2h) < 0$ which is in violation of condition (iv). Physically, a negative value of q^e implies that if the value of $\mathcal{L}^x_{i+1}$ which equals the value S_{i+1}, is increased, the value of ϕ_i decreases when in fact the value of ϕ_i should increase. The result is a one-dimensional solution for ϕ which is not necessarily bounded. To remedy this situation, the evaluation of $\bar{q}^e$ must be modified so that it remains negative. Fortunately, positive $\bar{q}^e$ values arise only for large P values. One way to obtain $\hat{q}^e$, a corrected $\bar{q}^e$ value, is from

$$\hat{q}^e = \bar{q}^e - \text{MAX}\,(\bar{q}^e,\ 0.0) \tag{6.86a}$$

Then to ensure that condition (vi) remains satisfied, it is necessary to also modify $\bar{q}^w$.

$$\hat{q}^w = \bar{q}^w - \text{MAX}(\bar{q}^e,\ 0.0) \tag{6.86b}$$

By similar arguments, it can be shown that when P is large in magnitude but negative, $\bar{q}^w$ can also become negative. In this instance $\hat{q}^e$ and $\hat{q}^w$ are given by:

$$\hat{q}^w = \bar{q}^w - \text{MIN}\,(\bar{q}^w,\ 0.0) \tag{6.87a}$$

$$\hat{q}^e = \bar{q}^e - \text{MIN}\,(\bar{q}^w,\ 0.0) \tag{6.87b}$$

Finally, in terms of $\hat{q}^w$ and $\hat{q}^e$, the q evaluations of equation (6.85) which satisfy all conditions for a bounded one-dimensional solution are given by:

$$q^w = \hat{q}^w$$
$$q^e = -\hat{q}^e$$
$$q^p = h - \hat{q}^e \hat{q}^w$$

Adopting the correction strategy outlined above, it is observed that corrections to q are required only when the downstream value of q value becomes negative. The effect of applying the correction, when required, is to make the downstream of q value equal to zero and increase the upstream q value. The resulting q values are then equivalent to those which would have arisen from assuming a constant value of L(x) in equations (6.80) and (6.81) with the upstream value of L(x) prevailing over the range $0 \leq x \leq h$.

6.4.5 Multi-Dimensional Extension of OCI Schemes

Various OCI schemes discussed above have been developed in a one-dimensional context. In this Section will be considered extensions of the most promising variants of OCI schemes, namely GOCI and CVOCI to two dimensions. Also issues related to boundary condition implementation and appropriate solution strategies will be examined in detail, as these now assume great practical significance. GOCI will be discussed first.

i) Two-Dimensional Extension of GOCI

The particular extension of GOCI adopted in this study is straightforward and is largely based on the work of Lecointe and Piquet.[84] Considering the two dimensional form of the transport equation (6.56), i.e.,

$$\Gamma_\phi \left(\frac{\partial^2 \Phi}{\partial x^2} + \frac{\partial \Phi}{\partial y^2}\right) + u \frac{\partial \Phi}{\partial x} + v \frac{\partial \Phi}{\partial y} = S \qquad (6.88)$$

where the exchange coefficient Γ_ϕ, and the components of velocity, u and v are presumed constant over the domain of interest for simplicity of derivation, an OCI scheme can be developed that uses the spatial operators L(x) and L(y) defined as:

$$L^x \equiv \bar{\Gamma}_{\phi} \frac{\partial^2 \Phi}{\partial x^2} + u \frac{\partial \Phi}{\partial x} \tag{6.89a}$$

$$L^y \equiv \bar{\Gamma}_{\phi} \frac{\partial^2 \Phi}{\partial y^2} + v \frac{\partial \Phi}{\partial y} \tag{6.89b}$$

Equation (6.88) can then be expressed as:

$$L^x + L^y = S$$

Using GOCI as developed in Section (6.4.2), the discrete representations of L^x and L^y, given by $\mathcal{L}^x$ and $\mathcal{L}^y$, can be related to the discrete representations of Φ, given by ϕ, as follows, equation (6.65):

$$r^w \phi_{i-1,j} + r^{p,x} \phi_{i,j} + r^e \phi_{i+1,j} = q^w \mathcal{L}^x_{i-1,j} + q^{p,x} \mathcal{L}^x_{i,j} + q^e \mathcal{L}^x_{i+1,j} \tag{6.91a}$$

or equivalently,

$$R^x \left\{ \phi \right\} = Q^x \left\{ \mathcal{L}^x \right\} \tag{6.91b}$$

and

$$r^s \phi_{i,j-1} + r^{p,y} \phi_{i,j} + r^n \phi_{i,j+1} = q^s \mathcal{L}^y_{i,j-1} + q^{p,y} \mathcal{L}^y_{i,j} + q^n \mathcal{L}^y_{i,j+1} \tag{6.92a}$$

or, equivalently

$$R^y \left\{ \phi \right\} = Q^y \left\{ \mathcal{L}^y \right\} \tag{6.92b}$$

The discrete representation of equation (6.90) is then given by:

$$\mathcal{L}^x_{i,j} + \mathcal{L}^y_{i,j} = S_{i,j} \tag{6.93}$$

or, equivalently

$$\left\{ \mathcal{L}^x \right\} + \left\{ \mathcal{L}^y \right\} = S \tag{6.94a}$$

where

$$Q^x \left\{ \mathcal{L}^x \right\} = R^y \left\{ \phi \right\} \tag{6.94b}$$

$$Q^y \left\{ \mathcal{L}^y \right\} = R^y \left\{ \phi \right\} \tag{6.94c}$$

It is important here to note several aspects of equations (6.94). First, the solution of equations (6.94) requires boundary conditions on ϕ, as well as boundary equations for $\mathcal{L}^x$ and $\mathcal{L}^y$. Unfortunately, for multi-dimensional problems it is not always possible to determine the boundary

equations for $\mathcal{L}^x$ and $\mathcal{L}^y$ directly from equation (6.88) and the boundary conditions on ϕ as was the case in one-dimensional problems. In these instances, some appropriately high order representation of L^x and L^y along the boundaries should be provided.

Secondly, equations (6.94) along with appropriate boundary equations form a coupled set of equations for ϕ, $\mathcal{L}^x$ and $\mathcal{L}^y$. (Compare this to the one-dimensional case where $\mathcal{L}^x$ could be determined explicitly). Therefore, it would appear that a coupled 3x3 block solution procedure would be required to solve these equations. One possible alternative is to eliminate $\mathcal{L}^x$ and $\mathcal{L}^y$ from equation (6.93). This can be accomplished by first multiplying both sides of equation (6.94b) by $[Q^x]^{-1}$ and equation (6.94c) by $[Q^y]^{-1}$ so that

$$\left\{\mathcal{L}^x\right\} = [Q^x]^{-1} R^x \left\{\phi\right\} \tag{6.95a}$$

$$\left\{\mathcal{L}^y\right\} = [Q^y]^{-1} R^y \left\{\phi\right\} \tag{6.95b}$$

Thus, substituting for $\left\{\mathcal{L}^x\right\}$ and $\left\{\mathcal{L}^y\right\}$ from equations (6.95) into equation (6.94a) yields the following equation for ϕ.

$$[[Q^x]^{-1} R^x + [Q^y]^{-1} R^y] \left\{\phi\right\} = \left\{S\right\} \tag{6.96a}$$

or simply,

$$A \left\{\phi\right\} = \left\{S\right\} \tag{6.96b}$$

Note that $[Q]^{-1}$ is, in general, a full NxN matrix where there are N discrete unknown values of ϕ. This leads to a relatively sparse A matrix which, unfortunately, has a full band width. Also, the inversions of Q^x, Q^y and A are expensive. As a result, the solution of equation (6.94) by such a procedure requires an excessive amount of computational resources. Nevertheless, the procedure is useful in that the convectivity of $\phi_{i,j}$ to its neighbours can be found in the coefficients of the A matrix. This is discussed next.

To determine the connectivity of a node or computational molecule of the GOCI scheme, it is necessary to consider only the coefficients of matrix A in the row corresponding to the node in question. Examples of the connectivity

of $\phi_{4,4}$ node in a domain with 7x7 nodes for: $Pe = uh_x/\Gamma_\phi = vh_y/\Gamma_\phi =$ 0,1,2,10,100 and ∞ are shown in figures (6.8). The most striking feature of GOCI is that the connectivity, in general, spans from boundary to boundary in both coordinate directions. In the low Peclet number limit, figure (6.8a), the coefficients alternate in sign, are symmetric and diminish rapidly in magnitude with distance form $\phi_{4,4}$. In the high Peclet number limit, the downstream connectivity is zero, and the upstream connectivity is alternating in sign but constant in magnitude except at the boundaries. At the intermediate Peclet numbers, figures (6.8b) and (6.8c), the connectivity is seen to become progressively asymmetric, weighing more heavily on the upstream coefficients and rapidly diminishing on the downstream coefficients as Peclet number increases. Finally, it is noted that for each Peclet number, it can be shown that the central coefficient of $\phi_{4,4}$ is equal to the sum of the neighbouring coefficients, although the Scarborough criterion is far from being satisfied for any Peclet number, i.e., diagonal dominance is violated.

During the course of this study, several <u>iterative</u> methods of solution were developed that treat the coupling between $\mathcal{L}^x$ and $\mathcal{L}^y$ with various degrees of implicitness. Generally, solvers which incorporate minimum implicitness in their formulation performed poorly or even diverged for high Peclet number problems, even when heavy under-relaxation was introduced. Thus the following solver, developed specifically for equation (6.94), was found to display "optimum" characteristics concerning stability and implicitness (hence computational cost).

If $\mathcal{L}^x$ is eliminated from equation (6.91a) using equation (6.93), there results a 2x2 block penta-diagonal equation for ϕ and $\mathcal{L}^y$ of the form:

$$\begin{bmatrix} r^w & q^w \\ 0 & 0 \end{bmatrix} \begin{Bmatrix} \phi \\ \mathcal{L}^y \end{Bmatrix}_{i-1,j} + \begin{bmatrix} r^e & q^e \\ 0 & 0 \end{bmatrix} \begin{Bmatrix} \phi \\ \mathcal{L}^y \end{Bmatrix}_{i+1,j} + \begin{bmatrix} 0 & 0 \\ r^s & -q^s \end{bmatrix} \begin{Bmatrix} \phi \\ \mathcal{L}^y \end{Bmatrix}_{i,j-1}$$

$$+ \begin{bmatrix} 0 & 0 \\ r^n & -q^n \end{bmatrix} \begin{Bmatrix} \phi \\ \mathcal{L}^y \end{Bmatrix}_{i,j+1} + \begin{bmatrix} r^{p,x} & q^{p,x} \\ r^{p,y} & q^{p,y} \end{bmatrix} \begin{Bmatrix} \phi \\ \mathcal{L}^y \end{Bmatrix}_{i,j} = \begin{Bmatrix} d \\ 0 \end{Bmatrix}_{i,j} \qquad (6.97)$$

$$\text{where } d_{i,j} = q^w S_{i-1,j} + q^{p,x} S_{i,j} + q^e S_{i+1,j}$$

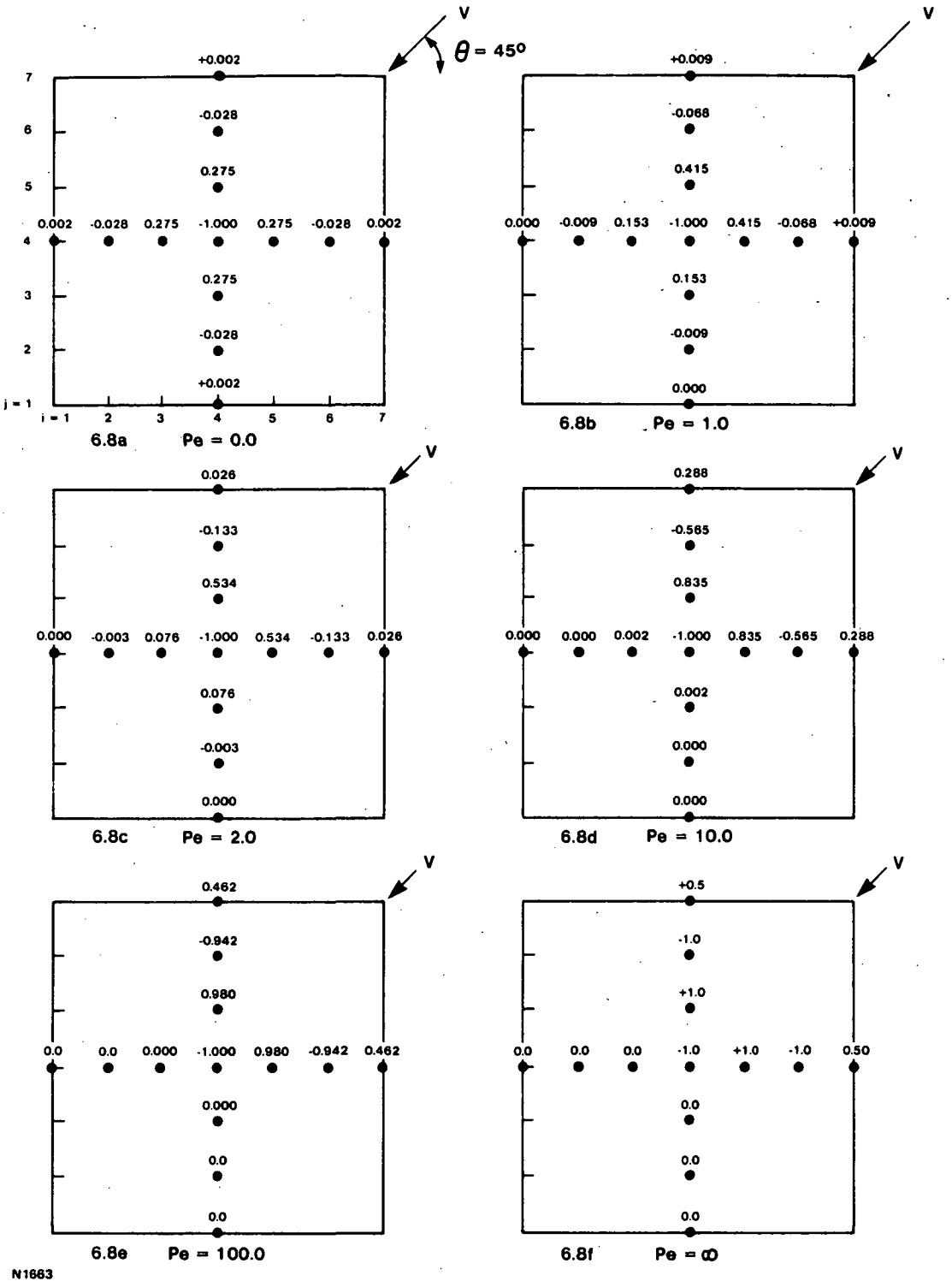

Figure 6.8 Coefficients Connecting $\phi_{4,4}$ with all its Neighbours, Resulting From GOCI Scheme Applied to Convected Step Problem with V at an Angle ϕ = 45° to the Horizontal

Equation (6.97) can be easily solved by a block 2x2 Alternating Direction Line Gauss-Seidel procedure using a block 2x2 TDMA along lines of constant i and constant j. Solution in this manner yields extremely rapid convergence. In fact for a uniform problem convergence is achieved in one iteration as Pe → ∞. In the diffusion limit, the number of iterations required increases but the rate of convergence is usually quite acceptable.

ii) Two Dimensional Extension of CVOCI

Two-Dimensional extension of CVOCI is readily obtained by integrating equation (6.90) over the control volume of dimension h by ℓ , in the following manner:

$$\int_0^h \int_0^\ell L^x dydx + \int_0^h \int_0^\ell L^y dydx = \int_0^h \int_0^\ell S dydx \qquad (6.98)$$

Assuming that over the control volume L^x, L^y and S can be approximated by $\mathcal{L}^x_{i,j}$, $\mathcal{L}^y_{i,j}$ and $S_{i,j}$ the integrals in equation (6.98) can be approximated by such that

$$\int_0^h \int_0^\ell L^x dydx = h\ell\, \mathcal{L}^x_{i,j} \qquad (6.99a)$$

$$\int_0^h \int_0^\ell L^y dydx = h\ell\, \mathcal{L}^y_{i,j} \qquad (6.99b)$$

$$\int_0^h \int_0^\ell S dydx = h\ell\, S_{i,j} \qquad (6.99c)$$

such that

$$\mathcal{L}^x_{i,j} + \mathcal{L}^y_{i,j} = S_{i,j} \qquad \text{equation (6.93)}$$

Using equation (6.89a), the integral of equation (6.99a) can also be written as the difference of fluxes between the e and w faces, as in the one-dimensional formulation.

$$\int_0^h \int_0^\ell L^x dy dx = \int_0^h \int_0^\ell \left[\frac{\partial}{\partial x}\left(\Gamma_\phi \frac{\partial \Phi}{\partial x}\right) + \frac{\partial}{\partial x}(u\Phi)\right] dx dy = J_{ef} - J_{wf} \tag{6.100}$$

where

$$J_{ef} = \int_0^\ell \left[\Gamma_\phi \frac{\partial \Phi}{\partial x} + u\Phi\right]_e dy \tag{6.101a}$$

$$J_{wf} = \int_0^\ell \left[\Gamma_\phi \frac{\partial \Phi}{\partial x} + u\Phi\right]_w dy \tag{6.101b}$$

(cf. equation 6.13)

Introducing the approximation that $\partial\Phi/\partial x$ and Φ along the e face and w face are constants, the fluxes are approximated by:

$$J_{ef} \simeq \ell\left[\Gamma_\phi \frac{\partial \Phi}{\partial x} + u\Phi\right]_e \tag{6.102a}$$

$$J_{wf} \simeq \ell\left[\Gamma_\phi \frac{\partial \Phi}{\partial x} + u\Phi\right]_w \tag{6.102b}$$

Using the <u>one-dimensional</u> analytic solution with an appropriate L profile, Section (6.4.3), expressions can be obtained for $\partial\Phi/\partial x$ and Φ in terms of ϕ and $\mathcal{L}$, thus enabling J_{ef} and J_{wf} to be approximated by:

$$J_{ef} \simeq \ell\left[\bar{r}^w \phi_0 + \bar{r}^e \phi_1 + \hat{q}^w \mathcal{L}_0^x + \hat{q}^e \mathcal{L}_1^x\right]_e \tag{6.103a}$$

$$J_{wf} \simeq \ell\left[\bar{r}^w \phi_0 + \bar{r}^e \phi_1 + \hat{q}^w \mathcal{L}_0^x + \hat{q}^e \mathcal{L}_1^x\right]_w \tag{6.103b}$$

where the evaluations or $\bar{r}$ and $\hat{q}$ are provided in equations (6.83), (6.86) and (6.87). Combining equations (6.99a), (6.100b) and (6.103), the following relation between ϕ and $\mathcal{L}^x$ results:

$$r^{w}_{i,j}\phi_{i-1,j} + r^{p,x}_{i,j}\phi_{i,j} + r^{e}_{i,j}\phi_{i+1,j} = q^{w}_{i,j}\mathcal{L}^{x}_{i-1,j} + q^{p,x}_{i,j}\mathcal{L}^{x}_{i,j} + q^{e}_{i,j}\mathcal{L}^{x}_{i+1,j} \tag{6.104}$$

where

$$r^{w}_{i,j} = -\ell\,\bar{r}^{w}_{w}$$

$$r^{e}_{i,j} = \ell\,\bar{r}^{e}_{e}$$

$$r^{p,x}_{i,j} = \ell\,(\bar{r}^{w}_{e} - \bar{r}^{e}_{w})$$

$$q^{w}_{i,j} = \ell\,\hat{q}^{w}_{w}$$

$$q^{e}_{i,j} = \ell\,\hat{q}^{e}_{e}$$

$$q^{p,x}_{i,j} = \ell\,(h + \hat{q}^{e}_{w} - \hat{q}^{w}_{e})$$

In a similar fashion, the integral in equation (6.99b) can be related to a difference of fluxes through the n face and s face of the control volume. Then using the solution of (6.89b) to obtain expressions for $\partial\Phi/\partial y$, Φ and, subsequently, the fluxes in terms of ϕ and $\mathcal{L}^{y}$, equation (6.99b) can be approximated by an equation of the following form:

$$r^{s}_{i,j}\phi_{i,j-1} + r^{p,y}_{i,j}\phi_{i,j} + r^{n}_{i,j}\phi_{i,j+1} = q^{s}_{i,j}\mathcal{L}^{y}_{i,j-1} + q^{p,y}_{i,j}\mathcal{L}^{y}_{i,j} + q^{n}_{i,j}\mathcal{L}^{y}_{i,j+1} \tag{6.105}$$

where r and q are determined from equations similar to those for r and q in equation (6.104).

Now equations (6.93), (6.104) and (6.105) represent a set of coupled algebraic equations which can be solved in the manner described previously for GOCI. It is important to note, however, that for two-dimensional problems, due primarily to the use of one-dimensional semi-analytic solutions without any explicit regard for streamline orientation to the grid, (like SUDS, Section (6.3)) the solution for ϕ is not necessarily bounded. Nevertheless, the conservative nature of the discretization may reduce the occurrence and size of the overshoots and undershoots.

6.5 IMPROVED SOLVERS FOR A GENERAL SEGREGATED SOLUTION ALGORITHM

Various iterative solvers considered in the following sections are primarily for use with equation (6.11). Equation (6.11) is symmetric, positive definite with only five diagonals, and has coefficients similar to those that would arise from an algebraic representation of a typical Poisson equation. This is in contrast to momentum equations involving both convection and diffusion, i.e., differential transport equations containing both first and second derivative terms, where the coefficient matrix arising from the usual five point finite differencing is generally neither symmetric nor positive definite. Discussion will initially consider base solvers with acceleration techniques to follow.

6.5.1 Implicit Base Solvers for Pressure/Correction Equation of SIMPLE Derivative Algorithms

Equation (6.11) can be expressed as a matrix equation

$$Ap = b \tag{6.106}$$

where A is the sparse symmetric matrix of coefficients. The direct solution of equation (6.106) is accomplished via the explicit Choleski Decomposition method, i.e., the transformation,

$$A = LL^T \tag{6.107}$$

where L is the lower triangular matrix and T denotes transpose. The solution vector is then obtained from:

$$p = (L^T)^{-1}(L^{-1}b) \tag{6.108}$$

However, solving equation (6.107) by simple recursive relations to determine columns of L introduces entries in L that were zero in the original matrix A, thus the sparse nature of the equations is lost.

In general, the various iterative means of solving equation (6.106) can be expressed as:

$$Me_{n+1} = Ap_n - b = -r_n \tag{6.109}$$

where n is the iteration counter, r_n is the residue and $e_{n+1} = p_{n+1} - p_n$ the relative error vector. A is a positive definite matrix. The matrix M depends on the choice of the relaxation procedure. The basic requirement on M is that its inverse be easily obtainable and can be related to the matrix A. The various iterative solution procedures for equation (6.106) utilizing approximate factorization techniques are derived by constructing M in a manner such that:

i) its diagonal entries are those of A (point Jacobi method),

ii) the elements of M correspond to the element of A along a line (line relaxation), etc.

The iterative solution procedures for equation (6.106), as opposed to the direct solution schemes where M=A, suffer as the inherent implicitness expressed by equation (6.106) for the variable field is degraded severely. However, Stone[26] in a widely quoted paper devised the iterative Strongly Implicit Procedure (SIP) which partially overcomes such deficiencies associated with classical iterative methods. In his method, the finite difference coefficient A is decomposed to comprise the product of an upper and lower triangular matrix (cf. equation (6.107)). The product of these two arrays is not exactly the same as the original coefficient array, but means are introduced to partially cancel the effect of spurious non zero entries resulting from the direct decomposition. A parameter, α, is introduced to control the degree of partial cancellation. The set of equations generated by the triangular arrays are easily solved and Stone has shown that the method gives rapid convergence for two-dimensional heat conduction problems involving large anisotropy.

Incomplete Choleski (IC) decomposition algorithm proceeds essentially in a similar manner; in fact, it can be shown that when the value of α is set to zero, i.e. no cancellation, SIP and IC become algebraically equivalent. The coefficient matrix is expressed as:

$$A \simeq M = LDL^T + E \quad \text{(equivalent to } LL^T+E\text{)} \qquad (6.110)$$

where D denotes a diagonal matrix and L is forced to have the same sparsity pattern as A. In equation (6.110) E is a small error matrix. Criteria associated with the stability of the decomposition is provided by Meijerink and Van Der Vorst.[85]

Since M^{-1} can easily be evaluated, equation (6.109) can be written as:

$$M^{-1}Ap_n - M^{-1}b = e_{n+1} \qquad (6.111)$$

In this form equation (6.111) can be viewed as the solution of:

$$(M^{-1}A)p_n = Cp_n = M^{-1}b \qquad (6.112)$$

with e_{n+1} as the residue vector. The accelerators described in the following sections can now be applied to the solution of equation (6.112). Base solvers considered in this study can also be heuristically viewed as providing the preconditioning necessary for efficient solution as for instance, the conjugate gradient method considered next, would converge in one iteration if $M^{-1}A=I$, where I denotes the identity matrix.

6.5.2 Conjugate Gradient Acceleration (CG)

Conjugate Gradient methods are, in essence, based on variational principles with each iterative step designed to minimize, subject to certain restraints, a certain non negative quadratic function of the unknowns e.g., (the Euclidean error norm $\hat{e}^T e$ in equation (6.111)) that vanishes at the solution. The particular form of the quadratic function to be minimized distinguishes whether a symmetric or a non-symmetric variant of the algorithm is to be employed. Even though in this study both variants have been considered, and there exists in the literature recent attempts to develop the algorithm in a manner appropriate for the general non-symmetric equation, notably that of Dongarra et al,[86] the following discussion will emphasize symmetric equations.

The quadratic form for equation (6.106) is defined as[87]

$$Q(p) = -b^T p + \frac{1}{2} p^T A p \qquad (6.113)$$

The minimization problem is given by:

$$\left| \frac{\partial}{\partial \alpha} Q(p + \alpha t) \right|_{\alpha=0} = 0 \qquad (6.114a)$$

or, equivalently

$$-b^T t + \frac{1}{2} [t^T Ap + p^T At] \qquad (6.114b)$$

where t_n denotes a specific search direction for the solution, borrowing terminology from the closely associated descent methods and α is a numerical parameter. Invoking the symmetry of A and the fact that

$$b^T t = t^T b$$

equation (6.114b) is simplified to:

$$t^T[-b + Ap] = 0 \tag{6.115}$$

or Ap=b provided t is not a null vector.

This minimization procedure suggests a solution update of the form

$$p_{i+1} = p_i + \alpha t_i \tag{6.116}$$

where the search direction t_i is said to be A orthogonal if,

$$t_i^T A\, t_j = 0 \qquad \text{if } i \neq j \tag{6.117}$$

In equation (6.117) the mutually conjugate vectors t_i are obtained from a set of arbitrary linearly independent vectors r_i by a Gram-Schmidt process. If,

$$t_1 = r_1 \tag{6.118a}$$

then,

$$t_{i+1} = r_{i+1} + \sum_{j=1}^{i} b_{i+1,j} t_j \tag{6.118b}$$

Utilizing the orthogonal property given by equation (6.117), definition of p_{i+1} is given by:

$$t_{i+1} = r_{i+1} + \beta\, t_i \tag{6.119a}$$

where

$$b_{i+1,j} = \frac{(r_{i+1}^T,\ At_j)}{(t_j^T,\ At_j)}\ \delta_{ij} \tag{6.119b}$$

or

$$\beta = b_{i+1,i} = \frac{(r_{i+1}^T,\ At_j)}{(r_i^T,\ At_i)} \tag{6.119c}$$

δ_{ij} above denotes the Kronecker delta.
The vectors r_i are evaluated using (6.116)

$$r_{i+1} = -Ap_{i+1} + b = r_i - \alpha At_i \tag{6.120a}$$

where, utilizing the orthogonal property leads to:

$$\alpha = \frac{(t_i^T,\ r_i)}{(t_i^T,\ At_i)} \tag{6.120b}$$

In the above, expressions like $(t^T,\ At_i)$ denote the usual inner product of vectors t^T and At_i. β and $b_{i+1,j}$ are scalars, t_i and r_i represent respectively, the current conjugate vector and the residual vector.

Equations (6.116), (6.119) and (6.120) constitute the working equations of CG methods for symmetric positive definite equations which after N steps provide the minimum of Q (p). A specific application of the above algorithm for use with equation (6.112) without requiring explicit evaluation of the matrix C is given in the following algorithm form:

$$p_{i+1} = p_i + \alpha t_i,$$

$$e_{i+1} = e_i - \alpha B_i,$$

$$t_{i+1} = e_{i+1} + \beta t_i,$$

$$B_{i+1} = Ce_{i+1} + \beta B_i$$

where α and β are given by either

$$\alpha = \frac{(t_i^T,\ e_i)}{(t_i^T,\ B_i)} \text{ and } \beta = -\frac{(e_{i+1}^T,\ B_i)}{(t_i^T,\ B_i)}$$

or

$$\alpha = \frac{(B_i^T,\ e_i)}{(B_i^T,\ B_i)} \text{ and } \beta = -\frac{(B_i^T\ Ce_{i+1})}{(B_i^T,\ B_i)}$$

and

$$e_{i+1} = p_{i+1} - p_i \ ;\ B_i = At_i$$

with suitable starting values for p_o, t_o and e_o.

In the above algorithm the preconditioning of A with M^{-1} in equation (6.112) has many desirable features. In particular, the eigenvalues are distributed favorably for the application of the CG method. It is this preconditioning that is responsible for the significant increase in the rate of convergence.

For non-symmetric systems including momentum equations, a quadratic form based on the Eucledian norm can be minimized resulting in a similar algorithm structure.

6.5.3 Block (Additive) Correction Acceleration (BC)

Block correction and the associated Additive Correction Multigrid discussed in the next section are somewhat different in philosophy and structure from the previous CG methods and operate on the premise, as shown by Hutchinson and Raithby,[62] that the solver convergence is enhanced considerably if the correct global solution level is maintained.

Rewriting equation (6.11) in the following equivalent form:

$$a^P_{i,j}\ p_{i,j} = a^E_{i,j}\ p_{i+1,j} + a^W_{i,j}\ p_{i-1,j} + a^N_{i,j}\ p_{i,j+1} + a^S_{i,j} p_{i,j-1} + b_{i,j}$$

the equation for the change δ_i in level of p along the line i, figure (6.9), to ensure that $\overline{p}_i$ (radially averaged value of $p_{i,j}$) is correct relative to its neighbours $\overline{p}_{i+1}$ and $\overline{p}_{i-1}$ is developed following the procedure of Settari and Aziz.[61] It is assumed that the calculation domain is rectangular with m and n nodes in the x and y directions respectively.

The first step is to select blocks containing an integral number of contiguous control volumes, and to sum the above equation for each control volume

within the block. Choosing the block to consist of all control volumes in the i-column results in:

$$\sum_j a^P_{i,j} p_{i,j} - a^N_{i,j} p_{i,j+1} - a^S_{i,j} p_{i,j-1}) = \sum_j a^E_{i,j} p_{i+1,j} + \sum_j a^W_{i,j} p_{i-1,j} + \sum_j b_{i,j} \tag{6.121}$$

The boundary conditions are assumed to be absorbed into the interior equations, so that $a^S_{i,1} = a^N_{i,n} = 0$. Introducing $D_{i,j} = a^P_{i,j} - a^N_{i,j-1} - a^S_{i,j+1}$, the left hand side of equation (6.121) reduces to $\sum_j D_{i,j} p_{i,j}$. If $\tilde{p}_{i,j}$ is the current best estimate of the solution, the improved value of $p_{i,j}$ after the level shift is $p_{i,j} = \tilde{p}_{i,j} + \delta_i$. Substitution of this into equation (6.121) yields:

$$\bar{a}^P_i \delta_i = \bar{a}^E_i \delta_{i+1} + \bar{a}^W_i \delta_{i-1} + \bar{b}_i \tag{6.122a}$$

where

$$\bar{a}^P_i = \sum_j D_{i,j}; \quad \bar{a}^E_i = \sum_j a^E_{i,j}; \quad \bar{a}^W_i = \sum_j a^W_{i,j} \tag{6.122b}$$

$$\bar{b}_i = \sum_j \left(b_{i,j} + a^E_{i,j} \tilde{p}_{i+1,j} + a^W_{i,j} \tilde{p}_{i-1,j} - D_{i,j} \tilde{p}_{i,j} \right) \tag{6.122c}$$

The addition of the equation over the i column block is equivalent to enforcing the integral equation for p conservation over the column. Solution of equation (6.122a) for δ_i using TDMA, and the subsequent adjustment of $\tilde{p}_{i,j}$ to obtain $p_{i,j}$, results in exact satisfaction of the integral balance. It is noteworthy that $\bar{b}_i$, the source term which "drives" the δ_i correction, is the sum of the residuals $\tilde{r}_{i,j}$ of the $\tilde{p}_{i,j}$ equation over the column. After the level correction, the integral balance is satisfied exactly (i.e., the sum of the residuals along the line has been forced to zero) and the task of a point or line iterative solver is to ensure local conservation.

A similar equation can be derived for the correction of the level of $p_{i,j}$ along rows through δ_j additive corrections.

It is worth remarking here that BC formulation as presented above, assumes no restrictive structure of the parent differential or finite volume equation and is thus applicable equally to symmetric and non-symmetric form of

the equations. Equations (6.122), derived for two-dimensional applications, is referred to as 1D Additive Corrections (1DAC) by Hutchinson and Raithby.[62] For completeness and ease of reference, Section (6.5.4), particular extension of the above formulation will be considered next for three-dimensional applications.

The three-dimensional algebraic equation for the control volume centered at ijk is of the form:

$$a^P_{i,j,k}p_{i,j,k} = a^E_{i,j,k}p_{i+1,j,k} + a^W_{i,j,k}p_{i-1,j,k} + a^N_{i,j,k}p_{i,j+1,k} + a^S_{i,j,k}p_{i,j-1,k} + a^U_{i,j,k}p_{i,j,k+1} + a^D_{i,j,k-1}p_{i,j,k-1} + b_{i,j,k} \qquad (6.123)$$

Boundary conditions are again assumed to be absorbed into the interior equations. Block correction is implemented by forming blocks of contiguous control volumes and by summing the equations for the control volumes within each block. The blocks may be selected in any of a number of ways.

1DAC: One-dimensional additive correction (1DAC) for the level 1 grid in figure (6.10a) results when blocks are formed from all the control volumes in the x-z planes (for example). With

$$D_{i,j,k} = a^P_{i,j,k} - a^E_{i-1,j,k} - a^W_{i+1,j,k} - a^U_{i,j,k-1} - a^D_{i,j,k+1},$$

equations like (6.123) are summed over the plane for a j to obtain:

$$\sum_i\sum_k D_{i,j,k}p_{i,j,k} = \sum_i\sum_k a^N_{i,j,k}p_{i,j+1,k} + \sum_i\sum_k a^S_{i,j,k}p_{i,j-1,k} + \sum_i\sum_k b_{i,j,k} \qquad (6.124)$$

The additive correction is similarly introduced into equation (6.124) in the manner $p_{i,j,k}=\tilde{p}_{i,j,k}+\delta_j$, where $\tilde{p}_{i,j,k}$ is the current best estimate of the solution that is to be improved by adding δ_j. A tri-diagonal equation for δ_j results for the Level 2 grid in figure (6.10a).

2DAC: A two-dimensional additive correction (2ADC) results when blocks are formed from all the control volumes in columns that span the calculation

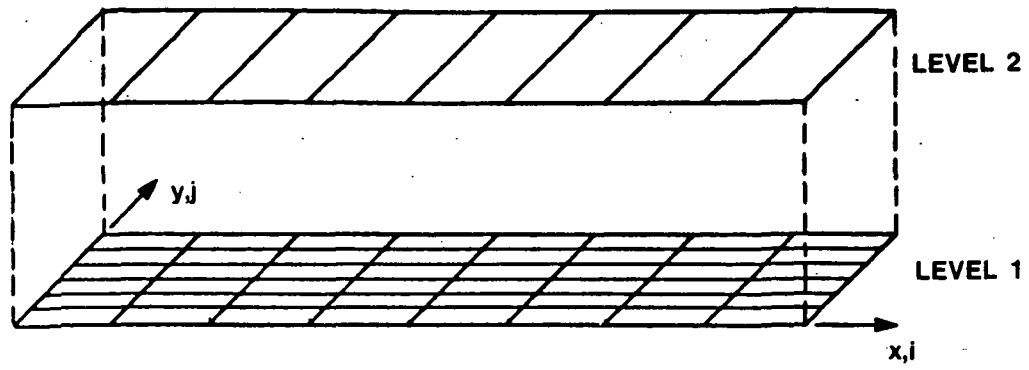

Figure 6.9 Grid Layout for 1D Block Correction

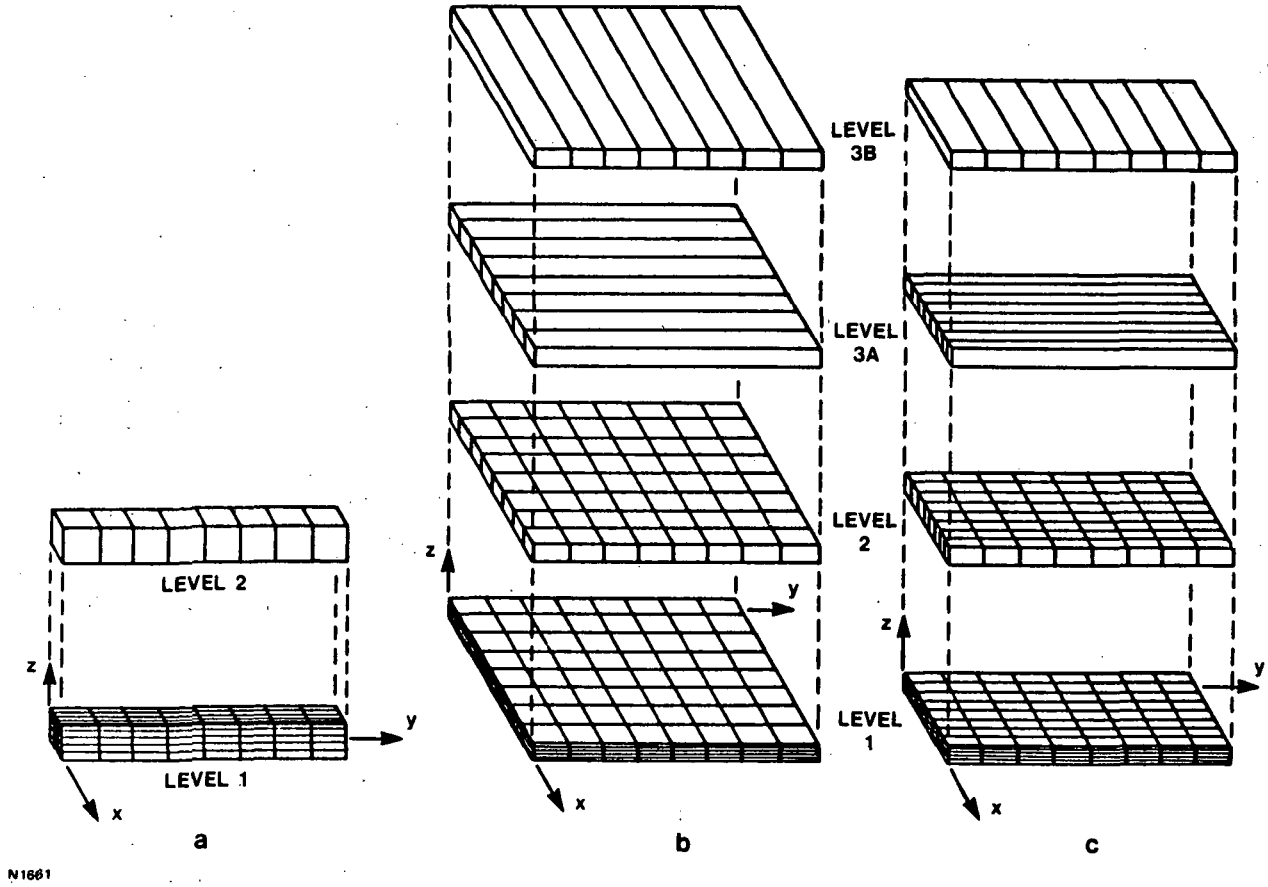

Figure 6.10 Grid Layout for 3D Block Correction. Level 1 is the Fine Grid

domain in the z direction. In this case $D_{i,j,k} = a^{P}_{i,j,k} - a^{U}_{i,j,k-1} - a^{D}_{i,j,k+1}$ is introduced into the summation of equations like (6.123), and the additive correction equation $p_{i,j,k} = \tilde{p}_{i,j,k} + \delta_{i,j}$ is substituted. After rearrangement, the equation for $\delta_{i,j}$ is:

$$\bar{a}^{P}_{i,j}\delta_{i,j} = \bar{a}^{E}_{i,j}\delta_{i+1,j} + \bar{a}^{W}_{i,j}\delta_{i-1,j} + \bar{a}^{N}_{i,j}\delta_{i,j+1} + \bar{a}^{S}_{i,j}\delta_{i,j-1} + \bar{b}_{i,j} \quad (6.125a)$$

where

$$\bar{a}^{P}_{i,j} = \sum_{k} D_{i,j,k}; \quad \bar{a}^{E}_{i,j} = \sum_{k} a^{E}_{i,j,k} \ldots \quad (6.125b)$$

$$\bar{b}_{i,j} = \sum_{k} b_{i,j,k} + \sum_{k} a^{E}_{i,j,k}\,\tilde{p}_{i+1,j,k} + \sum_{k} a^{W}_{i,j,k}\tilde{p}_{i-1,j,k} + \sum_{k} a^{N}_{i,j,k}\tilde{p}_{i,j+1,k} + \sum_{k} a^{S}_{i,j,k}\,\tilde{p}_{i,j-1,k} - \sum_{k} D_{i,j,k}\,\tilde{p}_{i,j,k} \quad (6.125c)$$

This equation for $\delta_{i,j}$ is valid for the level 2 grids in figures (6.10b) and 6.10b.

Equation (6.125a) is a two-dimensional equation that can be solved by iteration. But Hutchinson and Raithby[62] showed that additive corrections can significantly enhance convergence for two-dimensional problems. Thus, if blocks are again chosen to reduce the dimensionality of the additive corrections, solutions are performed on the Level 3A grids to obtain δ_i and this correction is added to $\delta_{i,j}$. This could be followed by a similar solution on the Level 3B grid to obtain a δ_j correction. The use of the three grid levels in this manner is referred to as 1D2DAC.

6.5.4 Additive Correction Multigrid (ACM)

The block (additive) corrections employed in the previous section have much in common with the classical multigrid methods of Brandt[63] and others.[88] Both methods are designed to accelerate convergence by solving a sequence of problems on increasingly coarser grids. Brandt forms the coarse grid equations by discretizing the governing equations on each grid and interpolating the fine grid residuals to the coarser grid equations, while the BC procedure forms the coarse grid equations by asserting integral conservation

over blocks of control volumes. Brandt interpolates coarse grid corrections to the fine grid, while BC simply adds the correction in order to preserve the integral balances. Brandt recommends formation of the coarser grid to include 2x2 nodes of the finer grid (in 2D), while the BC procedure forms the coarse grid in such a way that the dimensionality of the problem is reduced by at least one on each higher level (coarser) grid.

The development of the ACM method is now considered in detail, using the previously established additive correction ideas. It should be noted here that once the ACM method is adopted, there are no further decisions to be made regarding the treatment of boundary conditions, the transfer of residuals, or the interpolation of the dependent variable. The requirement that the sum of the equations for all fine grid control volumes, that lie within the same block of a coarser grid, be correct constrains these choices. As previously discussed, this is equivalent to demanding integral conservation over each coarse grid control volume.

A Cartesian 7x5 grid is shown in figure (6.11). Rather than form BC blocks that span the entire domain in one direction, let the blocks be formed from a number of contiguous control volumes, such as denoted in figure (6.11) by the heavy lines. To form the BC equation for the k,l block, equations like (6.121), one for each control volume in the block, are summed. To facilitate this equation (6.121) is rewritten as:

$$\begin{aligned} a^{P}_{i,j}p_{i,j} - a^{*E}_{i,j}p_{i+1,j} - a^{*W}_{i,j}p_{i-1,j} - a^{*N}_{i,j}p_{i,j+1} - a^{*S}_{i,j}p_{i,j-1} \\ = a^{E}_{i,j}p_{i+1,j} + a^{W}_{i,j}p_{i-1,j} + a^{N}_{i,j}p_{i,j+1} + a^{S}_{i,j}p_{i,j-1} + b_{i,j} \end{aligned} \tag{6.126}$$

where $a^{E}_{i,j} = a^{*E}_{i,j} + \hat{a}^{E}_{i,j}$ and $\hat{a}^{E}_{i,j} = 0$ if $p_{i+1,j}$ is in the k,l block and $a^{*E}_{i,j} = 0$ if $p_{i+1,j}$ is not in the k,l block. Summing the N equations for the N control volumes within the block yields:

$$\sum_{N} D_{i,j}p_{i,j} = \sum_{N}\left(\hat{a}^{E}_{i,j}p_{i+1,j} + \hat{a}^{W}_{i,j}p_{i-1,j} + \hat{a}^{N}_{i,j}p_{i,j+1} + \hat{a}^{S}_{i,j}p_{i,j-1} + b_{i,j}\right) \tag{6.127a}$$

where

$$D_{i,j} = a^{P}_{i,j} - a^{*E}_{i-1,j} - a^{*W}_{i+1,j} - a^{*N}_{i,j-1} - a^{*S}_{i,j+1} \tag{6.127b}$$

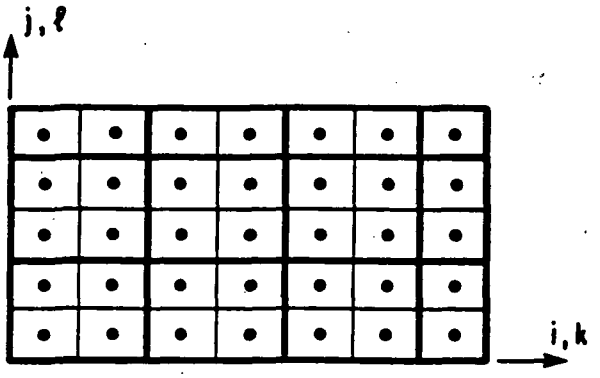

Figure 6.11 The Assembly of Control Volumes on the Fine Grid into Blocks (denoted by heavy lines) that Define the Coarse Grid for ACM

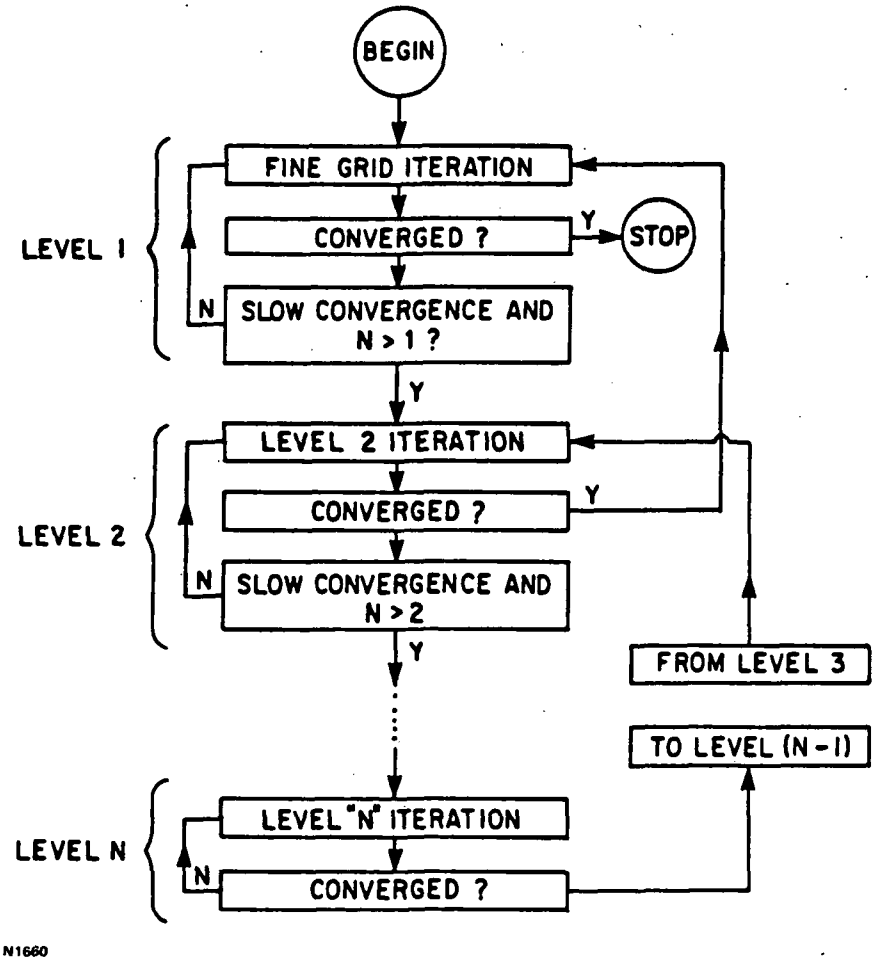

Figure 6.12 Flexible Cycle of Brandt

if $\tilde{p}_{i,j}$ is the best estimate of $p_{i,j}$ on the fine grid, the correction $\delta_{k,l}$ obtained on the coarser grid, is added to $\tilde{p}_{i,j}$ to obtain an improved value of $p_{i,j}$. Inserting $p_{i,j} = \tilde{p}_{i,j} + \delta_{k,l}$ into equation (6.127a) yields:

$$\bar{a}^{P}_{k,l}\delta_{k,l} = \bar{a}^{E}_{k,l}\delta_{k+1,l} + \bar{a}^{W}_{k,l}\delta_{k-1,l} + \bar{a}^{N}_{k,l}\delta_{k,l+1} + \bar{a}^{S}_{k,l}\delta_{k,l-1} + b_k \quad (6.128a)$$

$$a^{P}_{k,l} = \sum_{N} D_{i,j}; \quad \bar{a}^{E}_{k,l} = \sum_{N} \hat{a}^{E}_{i,j} \; ; \quad \bar{a}^{W}_{k,l} = \sum_{N} \hat{a}^{W}_{i,j} \quad (6.128b)$$

$$\bar{b}_{k,l} = \sum_{N} (b_{i,j} + \hat{a}^{E}_{i,j}\tilde{p}_{i+1,j} + \hat{a}^{W}_{i,j}\tilde{p}_{i-1,j} + \hat{a}^{N}_{i,j}\tilde{p}_{i,j+1} + \hat{a}^{S}_{i,j}\tilde{p}_{i,j-1} - D_{i,j}\tilde{p}_{i,j}) \quad (6.128c)$$

The solution of equation (6.128a) yields the value of $\delta_{k,l}$ that is added to each $\tilde{p}_{i,j}$ value that lies within the k,l block to obtain the improved estimate, $p_{i,j}$.

The blocks may be found in any convenient way. If the grid contains 2^P control volumes in the x and y directions, where P is an integer, it is convenient to form all blocks from the 2x2 sets of control volumes (2D) shown in figure (6.11). For other grids it is necessary to use unequal block sizes as also shown in figure (6.11). If, on the other hand, the blocks are formed from the control volumes along columns or rows that span the domain, the 1DAC described previously is recovered.

The general BC equation, equation (6.128a), can be solved by iteration, but convergence can again be enhanced by using BC on a still coarser grid employing exactly the same method used in the formulation of equation (6.128). The use of a sequence of coarser grids is identical to the procedure recommended in conventional multigrid methods. Equations on 2x2 grids or smaller are solved by a direct method.

In the present study the "flexible cycle" algorithm of Brandt[63] is adopted. The flowchart is shown in figure (6.12).

Any iterative base solver can be used with the above acceleration technique, however use of implicit methods including the various approximate factorization techniques considered previously is common.

6.6 ASSESSMENT OF IMPROVED SOLVER CHARACTERISTICS

There are several aspects to be considered when evaluating the performance of the above solvers. These include stability, computational storage requirements and computational efficiency. Computational efficiency will be discussed in detail in Section 7, while the former two items are considered next.

i) Stability

Of the methods considered, only the IC technique with and without CG acceleration have been rigorously proven to be stable for the solution of the symmetric, positive definite pressure/correction equation. For the remaining methods, SIP with some partial cancellation or any method employing BC or ACM acceleration, no mathematical proof of stability has yet been provided. Nevertheless, the experience gained from testing and using these methods indicates that they are in general, stable for the solution of the positive definite, symmetric set of linear equations for pressure/correction.

ii) Storage Requirements

The computer storage requirements of each of the methods is somewhat dependent on the manner in which the methods are implemented. For the implementations adopted in the present study, the Storage Unit (SU) requirements for each of the methods are listed in the table below. A storage unit is defined as the storage required to store only the dependent variable. The storage unit requirements listed in the table below indicate the storage required to store the pressure, as well as the coefficients of the pressure equation.

TABLE 6.1 STORAGE UNIT REQUIREMENTS FOR VARIOUS SOLVERS

Storage Unit Requirements		
Base Solver	IC	SIP
Acceleration		
	10	14
CG	11	N/A
BC	12	16
ACM	20	28

The various entries in the above table comprise the following SU's:

a) 1 SU for dependent variable

b) 6 SU for pressure/correction equation coefficients

c) 3 SU for IC

d) 7 SU for SIP

e) 1 SU for CG

f) 2 SU for BC

g) SU for ACM 2 $\{$(a) + (b) + [(c) or (d)]$\}$

Storage allocations in the above table do not include constants and vectors (as opposed to arrays).

6.7 CLOSURE

This Section has presented detailed deviations of the previously selected techniques for further quantitative evaluation, emphasizing issues of accuracy, stability and convergence, together with implementational details including required computational resources. Various relevant attributes of discretization techniques were discussed in a unified framework along with the associated questions of boundary conditions, solver suitability for the particular computational molecules generated by these schemes. Wherever appropriate, references from the literature were provided to assess a priori the specific issues of interest. Such information will be readily used in the next Section to provide a comparative basis to quantitatively evaluate these schemes in completing selected test cases.

7.0 DISCUSSION OF ONE AND TWO-DIMENSIONAL TEST CASES

7.1 EVALUATION OF IMPROVED SOLVER PERFORMANCE FOR A GENERAL SCALAR (PRESSURE) EQUATION

To evaluate the relative computational efficiencies of each of the solvers presented in Section 6, it would be most desirable to be able to determine in some formal mathematical fashion estimates of the asymptotic rate of convergence of each method. Unfortunately, this is, at present, not feasible. Instead, the relative computational efficiencies of the methods can only be determined through extensive testing and experimentation.

Assessment of individual solver performance in the absence of nonlinearity and variable coupling that generally dominates the behavior of general flow equations is valuable, as it provides quantitative understanding of the solver structure. Also, such exercises establish useful guidelines for the anticipated convergence behavior in the solution of complex coupled equation sets. Thus, the following sections will critically examine the solver performance in isolation for a variety of linear, scalar (pressure) equations, while issues related to coupling and nonlinerity are discussed in in Section (7.2).

7.1.1 Test Problems and Details of Implementation

The following flow problems were adopted to evaluate the solver performance associated with the corresponding pressure/correction solution, Section (6.1).

i) Shear driven flow in a square cavity, Re_h=1000, uniform grid with 48x48 control volumes, figure (7.1).

ii) Flow over a rearward facing step with uniform inlet velocity profile and fully developed outlet conditions, Re_h=250, uniform grid with 48 x 48 control volumes, figure (7.2).

iii) Angled axisymmetric flow through a cannister, Re_r=450, uniform grid with 78x42 control volumes, figure (7.3).

The first test problem was chosen because it is generally accepted as a benchmark, the second because it has a relatively high geometric aspect ratio

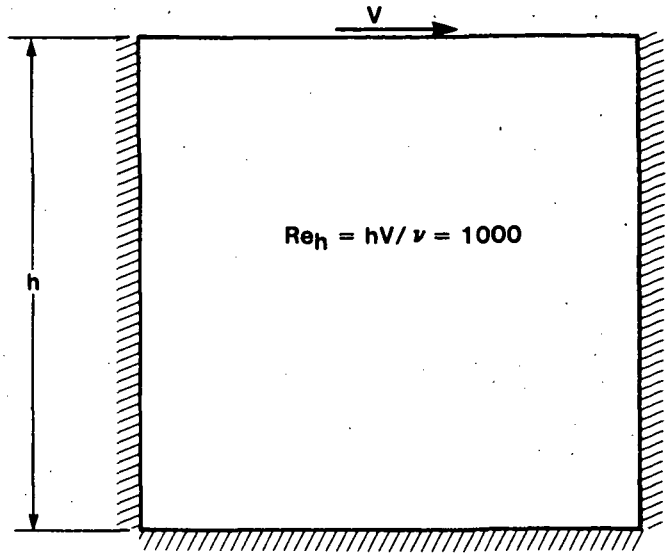

Figure 7.1 Shear Driven Flow in a Square Cavity

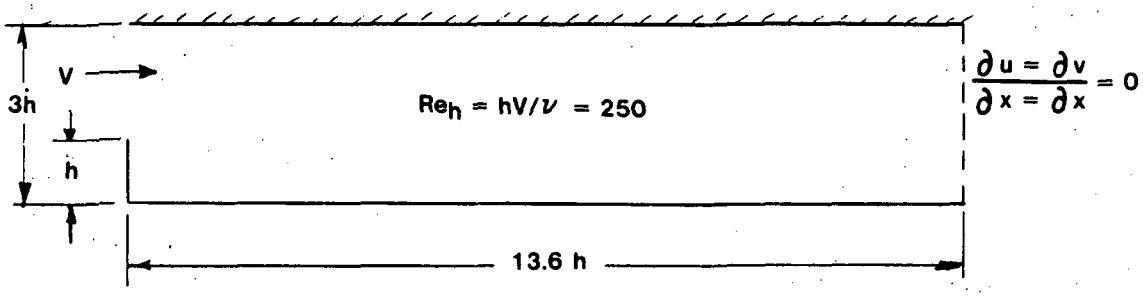

Figure 7.2 Flow Over a Rearward Facing Step

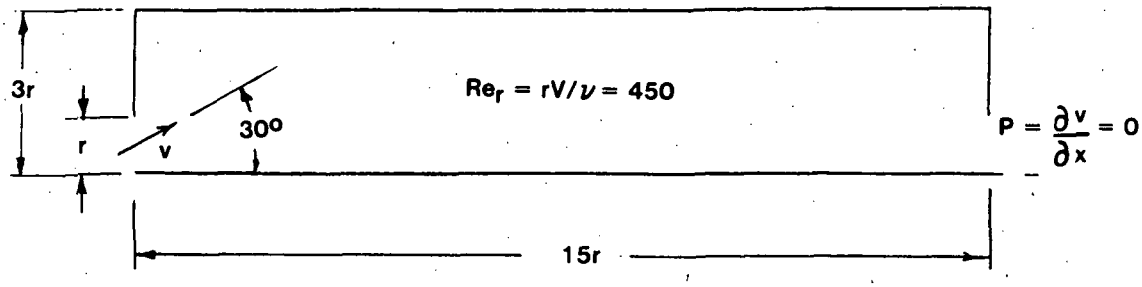

Figure 7.3 Angled Axisymmetric Flow Through A Cannister

for the control volume, typical of those often encountered in practice, and the third problem was chosen because of its geometric similarity to combustion configurations.

To evaluate the solver performance in isolation, the linear pressure equations appropriate for the above flow cases were generated and solved in the following manner:

i) For each test problem, a converged solution was obtained on a staggered grid using the upstream weighted discretization scheme of Raithby and Torrance[8] in a finite volume framework. Relaxation was introduced via the time step multiple, E.[15]

ii) Using the converged solution of the test problem and E=5.0 (corresponding to usual under-relaxation factor of 0.83), the coefficients of the equation for pressure estimation of SIMPLER[1] were determined.

iii) Starting from a zero solution field for each of the methods considered and for each test problem, the solution convergence history (computing effort vs. residual) was monitored and recorded.

In the case of SIP, numerical experiments were performed using values of α, the partial cancellation parameter, which ranged from 0.0 to 0.9 in increments of 0.1. Results for IC were obtained using SIP with α=0.0.

For the shear driven square cavity flow, the closed set of algebraic pressure equations thus generated requires that a pressure be specified at some point in the field. However, for most iterative methods, the iterative behavior is enhanced if the pressure is not specified.[15] A prescribed pressure can then be obtained by adjusting the entire pressure field by an additive constant. This approach was adopted for all methods tested on the pressure equation of the cavity problem, except for the methods employing BC acceleration. Because the BC equations cannot be solved if pressure is unspecified, the pressure was set equal to zero in the upper right corner of the domain.

7.1.2 Results of Numerical Experiments

The convergence history (l_2-norm of pressure equation residuals vs CPU effort) of each method considered for each of the three test problems is shown in figures (7.4) to (7.6). In each figure, the norm of the residuals is

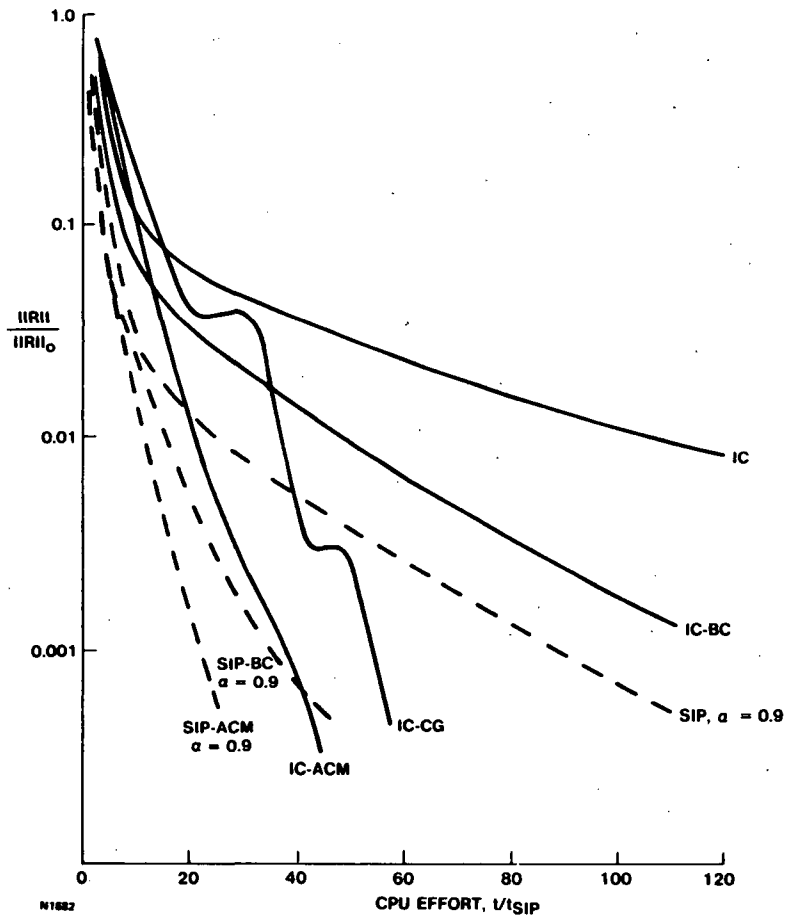

Figure 7.4 Convergence History for Shear Driven Flow in a Square Cavity, 48 x 48 Control Volumes

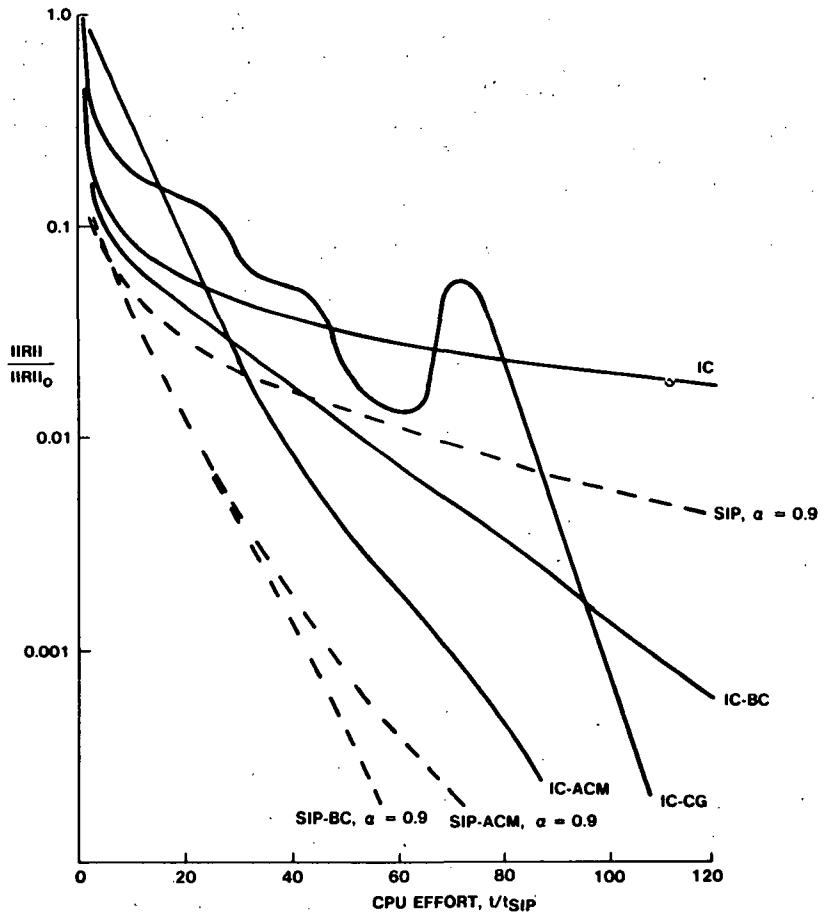

Figure 7.5 Convergence History for Rearward Facing Step Problem, 48 x 48 Control Volumes

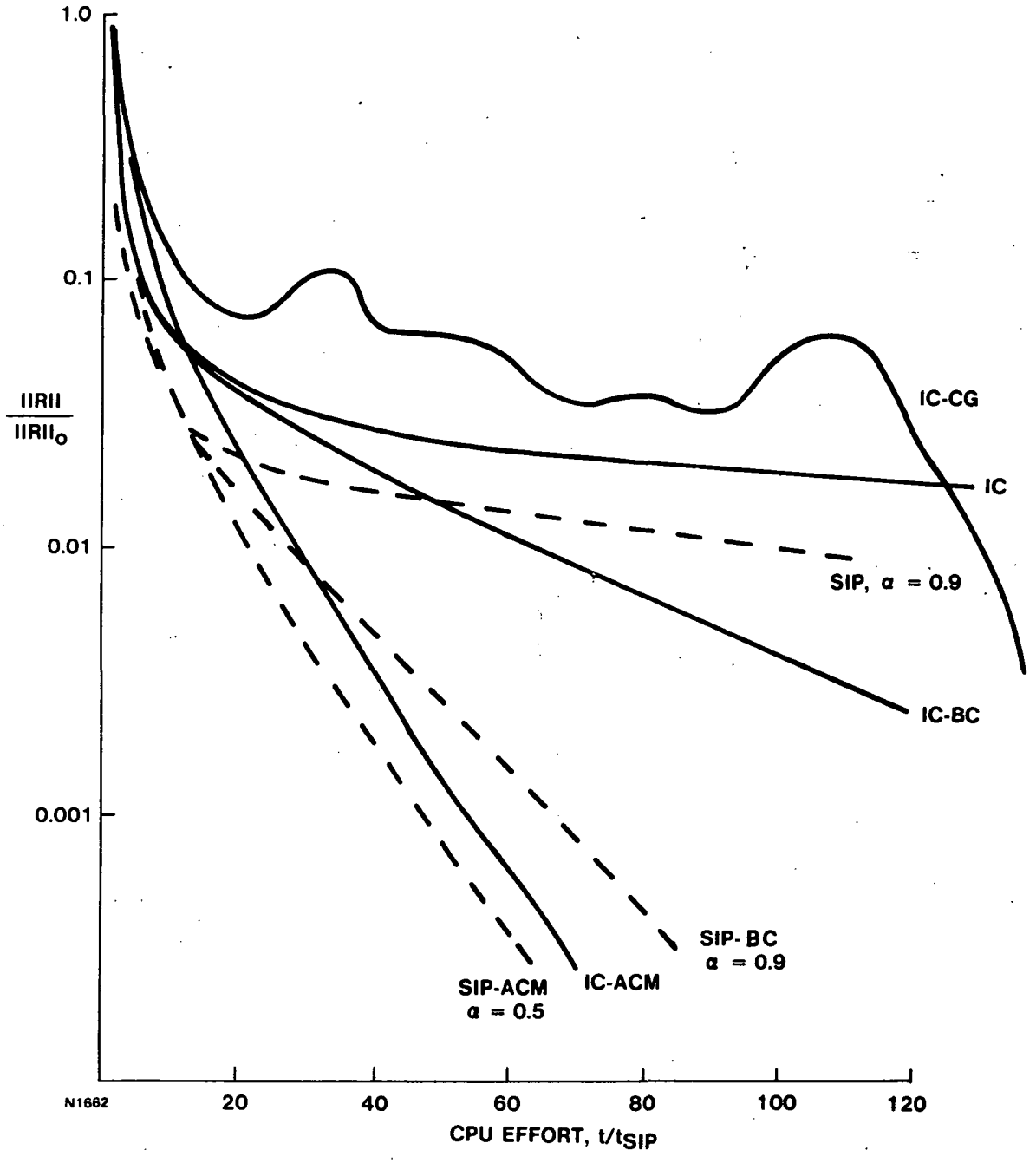

Figure 7.6 Convergence History for Axisymmetric Flow Through a Cannister Problem, 78 x 42 Control Volumes

normalized by $\|R_o\|$, the initial norm of the residuals and CPU effort is normalized by t_{SIP}, the time required to perform one SIP iteration with no acceleration. In cases using SIP with partial cancellation, only the convergence histories for the optimal values of α (to within $\pm$ 0.05) are presented.

Considering first the results for the shear driven square cavity flow problem, shown in figure (7.4), it is observed that the initial rate of convergence of IC is particularly good. However, after reducing the residual by an order of magnitude the rate of convergence of IC slows dramatically. Combining IC with CG acceleration significantly improves the asymptotic rate of convergence but the overall performance of the combination is compromised somewhat by the non-monotonic reduction in residual. The BC acceleration also improves the convergence of IC but not to the same extent as CG. However, the best acceleration of IC is provided by the ACM acceleration where the relatively fast initial rate of convergence is maintained throughout.

The results in figure (7.4) also indicate that the introduction of an appropriate amount of partial cancellation to IC, resulting in the SIP method, can also increase the rate of convergence, but only to a limited degree. However when SIP and BC are combined, the resulting rate of convergence exceeds that of IC with ACM, but does not exceed the rate of convergence experienced by the combination of SIP with ACM.

The results for the rearward facing step, shown in figure (7.5), are only moderately different (qualitatively) from the results for the square cavity problem. The differences lie mainly in the relatively poorer behavior of IC with CG acceleration, which suffers even more from a non-monotonic decrease in residuals, and SIP with BC acceleration is superior to all other methods considered.

For the flow through a cannister the results, shown in figure (7.6), again indicate only minor qualitative differences from the results of the square cavity problem. The most notable difference which arises is again the poor performance of IC with CG acceleration which experiences poor convergence for a considerable portion of its history.

7.1.3 Discussion of Results

From the results shown in figures (7.4) to (7.6) it is observed that the initial rate of convergence of all methods is good. This favorable behavior

is likely due to the manner in which IC and SIP remove the high frequency component of the error.[23] However, once this high frequency component of the error is removed, the convergence, without some form of acceleration, slows dramatically. This decrease in the rate of convergence is then due to the poor manner in which lower frequency components of the error are removed. Although, it seems that the introduction of an optimal amount of partial cancellation is effective in removing more of the error, the introduction of acceleration techniques appears to have a more dramatic effect.

The effectiveness of BC acceleration is particularly evident for the rearward facing step problem, where the solution for pressure has a single, dominant one-dimensional low frequency mode for which BC is ideally suited. Similarly, ACM acceleration which is designed to address all frequency components of the solution error, improves the convergence rate of both IC and SIP for all test problems. It is also worth noting that for the relatively fine grids used, the optimal degree of partial cancellation is obtained by using α=0.9, except with ACM acceleration on the flow through a cannister problem. In this instance it is postulated that the value of α=0.9, used on all of the grids, is not appropriate for the coarse grids (for coarse grids, there is evidence to suggest that the value of α should be decreased).

Finally, the convergence behavior of CG is disappointing. While CG acceleration has been designed to provide a monotonic decrease in error and to provide a solution after all the orthogonal base vectors of the solution have been obtained, there is no guarantee that the intermediate residuals will decrease monotonically and that the rate of convergence at any point will be fast. In fact, the present results suggest that the rate of convergence of CG acceleration is high only after a number of iterations are performed which set up most of the principal (or dominant) orthogonal base vectors.

Based on the above discussion, the following tentative conclusions emerge regarding isolated solver performance for single linear equation sets:

i) Provided the computer storage is available, Section (6.6), ACM acceleration with SIP employing an optimal amount of relaxation is generally the most efficient method, but only moderately more efficient than IC with ACM.

ii) If it is known, a priori, that the solution for pressure varies primarily in a single direction, then BC acceleration should be most effective.

iii) If the computer storage requirements of ACM are excessive for the particular problem, BC acceleration of SIP with an optimal partial cancellation appears to be an appropriate choice.

iv) Because the CG acceleration exhibits at times poor convergence behavior, the method should be used with some caution.

These conclusions are now used in understanding how the choice of the method used to solve the pressure equation would influence the performance of a particular segregated method for incompressible flows. Such information might then also prove useful in comparing the segregated approach to alternative methods, including the coupled approach for incompressible flow problems.

7.2 EVALUATION OF IMPROVED PRESSURE ~ VELOCITY COUPLING ALGORITHMS AND SOLVER PERFORMANCE IN THE TEACH CODE

The following sections adopt a baseline code to quantitatively study the implications of employing various convergence enhancement practices for computing isothermal, turbulent, recirculating flows. The code selected was a variant of the Pratt and Whitney 2-D TEACH Code,[5] supplied as part of this contract, incorporating:

i) Hybrid differencing

ii) An alternating direction line Gauss-Seidel to solve equations for pressure, components of velocity and other scalars with a two-dimensional five-point operator

iii) The PISO variant[6] of SIMPLER[1] algorithm to deal with the coupling between pressure and components of velocity

iv) k-ε turbulence model.

Whereas the previous sections examined the solver performance in isolation for single linear pressure equations, the relevant details of the overall segregated solution algorithm for incompressible flows is considered next.

7.2.1 Details of Implementation

The convergence and efficiency of a typical segregated incompressible solver is primarily dictated by, Sections (3.4.3) and (4.3):

i) The nature of the approximations introduced to deal with the crucial pressure ~ velocity coupling.

ii) Effective solution of the resulting pressure/correction equation.

These issues will be discussed in detail with reference to the particular means of incorporating the associated convergence enhancement algorithms in the TEACH code.

To improve the coupling between pressure and velocity components, the SIMPLEC[15] algorithm was employed. The SIMPLEC algorithm is a more consistent implementation of the original SIMPLE method resulting in considerably improved convergence behavior. Along with the implementation of SIMPLEC, the baseline code was modified so that mass conserving velocity components are always used when discretizing all transport equations. In the baseline code, coefficients of the discretized v momentum equation were based on u* velocities, which, in general, do not satisfy mass conservation, Section (3.4.3).

The standard implementation of PISO and SIMPLEC, as reported in the literature, are such that under-relaxation of momentum equations controlled by α, the under-relaxation parameter, is required. The under-relaxation, in turn, results in a relatively large number of coefficient updates (iterations). To reduce the number of coefficient updates, the SIMPLEC cycle of u*, v* and pressure calculation is applied repeatedly using the same sets of coefficients of the momentum equations. The required under-relaxation of SIMPLEC is accomplished by adding $a_P^u/\alpha_{SIMPLEC}\,(u^{n-1}-u^n)$ to the u momentum equation and $a_P^v/\alpha_{SIMPLEC}\,(v^{n-1}-v^n)$ to the v momentum equation where a_P^p and a_P^v are the central coefficents of the corresponding momentum equations, $\alpha_{SIMPLEC}$ is the SIMPLEC under-relaxation parameter and the superscript n is used to denote the current SIMPLEC iteration. Termination of the SIMPLEC cycle is based on the reduction of the u* and v* mass conservation residuals and is controlled by the value of the residual reduction factor, $\alpha_{SIMPLEC}$. The result is that, after repeated applications of SIMPLEC, pressures and velocities better satisfy mass and momentum conservation and that the under-relaxation of the momentum equations controlled by α, can be substantially reduced, thereby reducing the number of coefficient updates required. This reduction in coefficient updates is particularly important for the more expensive discretization schemes like MW-SUDS and LP-SUDS, where the cost associated with the updating of coefficient is relatively high.

Regarding the convergence enhancements associated with the solution of the pressure/correction equation, SIP with CG, BC or ACM acceleration techniques were implemented in the baseline code. Each of the options was tested, however, guided by the conclusions of the previous section only SIP with BC or ACM accelerations were used in the demonstration problems.

To further enhance convergence, the residual reduction convergence criterion, controlled by the residual reduction parameter, γ^p, Section (4.3), was implemented in the code to establish an efficient termination procedure for the iterative solution of the pressure correction equation. In addition, the approximate factorization of the pressure correction equation is stored, i.e., approximate factorization is performed only when the coefficients of the pressure correction equation are updated. This is particularly useful in PISO where solutions of similar pressure correction equations with differing driving source terms are required in the two stages. The only exception to this artifice arises with SIP-CG where the initialization of CG requires that the decomposition be performed in both stages of PISO.

Finally, as discussed in Section (6.5), SIP with BC or ACM acceleration is equally applicable to symmetric and non-symmetric equations. Therefore, it is possible to use these methods for the solution of momentum equations as well as scalar transport equations. However, as these equations are generally dominated by convection and/or source terms, algebraic solutions are readily obtained without using any acceleration techniques. Therefore, SIP with BC or ACM was not implemented for these equations.

7.2.2 Test Problems and Procedure

To study the impact, the above practices are likely to have on partial computations of flow problems with associated nonlinearity and variable coupling, solutions were obtained to the following demonstration problems:

i) Shear driven flow in a square cavity, Re_h=1000 using a uniform grid with 10x10 control volumes, figure (7.1).

ii) Flow over a rearward facing step, Re_h=250 using the boundary conditions as in Section (7.1.1) and a uniform grid with 10x6 control volumes, figure (7.2).

iii) Coannular, nonswirling, turbulent flow in a sudden expansion geometry. The inlet conditions are presented in Table (7.1). A non-uniform grid with 21x20 control volumes, similar to that described in (5) was used.

TABLE 7.1 INLET CONDITIONS FOR THE COANNULAR TURBULENT FLOW PROBLEM

Variable	Inner Flow	Outer Flow
u (m/s)	0.596	1.74
v (m/s)	0.0	0.0
k (m^2/s^2)	1.776×10^{-3}	1.514×10^{-2}
ϵ (m^2/s^3)	1.52×10^{-2}	3.78×10^{-1}

Computations were performed using the familiar Hybrid differencing to obtain the dicretized algebraic equations. Use of such coarse grids for the above demonstration problems is intentional in that, on finer grids the enhancement of convergence and accuracy provided by the above practices is generally more dramatic. There are several reasons for this including:

i) On coarse grids, the increased computational effort required to set up SIP with acceleration may not be offset by the reduction in the number of iterations required to solve the pressure correction equation.

ii) On coarse grids, the performance of SIMPLER/PISO can be better than the performance of SIMPLEC.

iii) The cost of coefficient updates of the Hybrid discretization scheme is quite low. As a result, the effectiveness of repeated applications of SIMPLEC for fixed momentum coefficients will be diminished.

The various solution parameters adopted for the test problems are summarized in Table (7.2). In all the test problems studied solution was assumed converged when the corresponding normalized maximum residual in the field was reduced to 0.005. The CPU requirements quoted in Tables (7.3) through (7.6) refer to a MASSCOMP Series 500 minicomputer.

TABLE 7.2 PARAMETER SETTINGS FOR CONVERGENCE ENHANCEMENT TESTS

SIP Partial Cancellation Parameter	0.5
Pressure Correction Residual Reduction Factor, γ^p	0.25
SIMPLEC Under-Relaxation of Momentum, $\alpha_{SIMPLEC}$	0.7
SIMPLEC Residual Reduction Factor, $\nu_{SIMPLEC}$	0.4

7.2.3 Results of Numerical Experiments

For the shear driven square cavity problem, the number of coefficient updates and CPU requirements for the baseline code, the baseline code with SIP-BC and the baseline code with repeated SIMPLEC and SIP-BC are presented in Table (7.3).

TABLE 7.3 CONVERGENCE ENHANCEMENT TEST RESULTS FOR SHEAR DRIVEN CAVITY PROBLEM, GRID = 10 X 10

Solver	Under-Relaxation Parameter, α	Coefficient Updates	Total CPU Requirements (Seconds)
Baseline	0.5	86	305
PISO/SIP-BC	0.5	86	182
SIMPLEC/SIP-BC	0.92	20	101

The above results indicate a 40 percent reduction in overall CPU requirements with the introduction of SIP-BC. The introduction of repeated SIMPLEC allows a much higher value of the under-relaxation factor α and results in a 77 percent reduction in the number of coefficient updates, as well as an additional 44 percent reduction in CPU requirements.

For the rearward facing step problem, the number of coefficient updates and CPU requirements for the baseline code, the baseline code with SIP-BC, repeated SIMPLEC, and the baseline code with SIP-ACM and repeated SIMPLEC are given in Table (7.4).

TABLE 7.4 CONVERGENCE ENHANCEMENT TEST RESULTS FOR REARWARD FACING STEP PROBLEM, GRID = 10x6

Solver	Under-Relaxation Parameter, α	Coefficient Updates	Total CPU Requirements (Seconds)
Baseline	0.5	26	37
PISO/SIP-BC	0.5	25	46
SIMPLEC	0.8	13	36
SIMPLEC/SIP-BC	0.8	12	34
SIMPLEC/SIP-ACM	0.8	13	38

As will be seen from the above table, for the coarse grid used for this problem, there is little or no improvement in CPU requirements with the introduction of SIP with acceleration or repeated SIMPLEC. In fact, the introduction of SIP with acceleration is a disadvantage for this coarse grid. However, it is encouraging to note the 50 percent reduction in coefficient updates that result from the introduction of repeated SIMPLEC and a higher value of α. Also note some reduction in CPU requirements with SIP-BC used in conjunction with repeated SIMPLEC.

For the turbulent coannular flow problem, the number of coefficient updates and CPU requirements for the baseline code, the baseline code with SIP-ACM the baseline code with repeated SIMPLEC and the baseline code with SIP-ACM and repeated SIMPLEC are presented in Table (7.5).

TABLE 7.5 CONVERGENCE ENHANCEMENT TEST RESULTS FOR TURBULENT COANNULAR FLOW PROBLEM, GRID = 21x20, TRUE VALUE OF $\Psi_{min} \simeq 0.117$[5]

Solver	Under-Relaxation Parameter, α	Coefficient Updates	Total CPU Requirements (Seconds)
Baseline	0.5	178	40
PISO/SIP-BC	0.5	Unstable	---
SIMPLEC	0.9	110	37
SIMPLEC/SIP-ACM	0.9	109	34

Considering, first, the impact of using SIP-ACM for the solution of the pressure correction equation, it is observed that PISO becomes unstable with the improved method for solving the pressure correction equation. Similar results were obtained using SIP-BC. The reason for this behavior is that for the turbulent coannular flow problem PISO becomes unstable on a 21x20 grid using α=0.5. In the baseline code, use of the recommended 5 iterations of the Alternating Direction Line Gauss-Seidel procedure for the pressure correction equation, which is considerably slower than SIP-ACM, introduces sufficient relaxation to stabilize PISO. It can also be seen from the above table that the use of repeated SIMPLEC results in a 40 percent reduction in the number of coefficient updates. However, with the increased costs of repeated SIMPLEC, total CPU requirements were reduced by only 9 percent. Repeated SIMPLEC together with SIP-ACM results in a 15 percent reduction in CPU requirements.

As indicated previously, dramatic reductions in CPU requirements resulting from the use of repeated SIMPLEC are expected, when CPU intensive schemes, like MW-SUDS or LP-SUDS, are employed for discretization. To illustrate this issue, numerical solutions to the turbulent coannular flow problem employing MW-SUDS on the 21x20 grid were obtained using the baseline code, the baseline code with SIP-ACM, the baseline code with repeated SIMPLEC and repeated SIMPLEC with SIP-ACM. The number of coefficient updates and CPU requirements for each solution are presented in Table (7.6).

TABLE 7.6 CONVERGENCE ENHANCEMENT TEST RESULTS FOR TURBULENT COANNULAR FLOW PROBLEM USING MW-SUDS, GRID = 21x20 TRUE VALUE OF $L_r \approx 6.1$

Solver	Under-Relaxation Parameter, α	Coefficient Updates	Total CPU Requirements (Seconds)
Baseline	0.5	272	160
PISO/SIP-BC	0.5	306	174
SIMPLEC	0.9	160	119
SIMPLEC/SIP-ACM	0.9	137	92

The results indicate that the introduction of repeated SIMPLEC to the baseline code yields a 41 percent reduction in the number of coefficient updates and a corresponding 26 percent reduction in total CPU requirements. Combing SIP-ACM with repeated SIMPLEC results in an additional 14 percent reduction in the number of coefficient updates and an additional 23 percent reduction in total CPU requirements. Compared to the baseline code, SIMPLEC with SIP-ACM results in a 43 percent reduction in total CPU requirements. Finally, it is noted that the introduction of SIP-ACM in PISO results in an increase in both the number of coefficient updates and the total CPU requirements. This behavior again highlights the unstable nature of PISO.

7.2.4 Summary and Conclusions

Convergence enhancement and efficiency for the nonlinear, coupled transport equations of incompressible flow were examined above using an improved pressure ~ velocity coupling algorithm together with a variety of appropriate solvers for the pressure correction equation. Although more extensive testing and use would be required to arrive at any general conclusions, the results for the test problems considered clearly delineate the complex relationship between the structure of a segregated solution algorithm and the efficient solution of the pressure field to yield zero divergence for mass. The suitability of a pressure solver for use with a specific incompressible flow algorithm cannot be overemphasized, as PISO was shown to be unstable for some

of the test problems examined. The above study also highlighted the efficiency aspects of an improved solution algorithm when used with accurate but more CPU intensive discretization schemes. However, the problem is generally much more involved including issues of boundedness, stability and convergence characteristics.

Based on the results of the above test problems, the following conclusions are stated:

i) The introduction of an accelerated SIP to solve the pressure correction equation can significantly reduce CPU requirements; up to 40 percent reduction for laminar flows and 20 percent reduction for turbulent flows.

ii) The introduction of repeated SIMPLEC significantly enhances convergence, reducing both the number of coefficient updates and CPU requirements. Because of the relatively high cost of coefficient updates for CPU intensive discretization schemes, like MW-SUDS and LP-SUDS, the introduction of repeated SIMPLEC has, generally, the largest impact on the CPU requirements of such schemes.

7.3 EVALUATION OF IMPROVED DISCRETIZATION SCHEMES

The governing transport equations for fluid flow in arbitrary configurations of engineering interest express a delicate balance between the various influences of convection, diffusion and source terms, Section (6.1). Different zones in the flow field emphasize the influence of one or more of these transport mechanisms at the expense of others.

Due to the extreme nonlinearities involved in the above equations, especially at high Reynolds numbers, very few exact (analytical) solutions can be found in the literature. These usually relate to simple, idealized (very often linear) problems, constructed in a manner to examine constituent effects in more comprehensive equations like the Navier Stokes. The boundary and initial conditions associated with the above solutions are generally specified as analytical functions. For purposes of developing numerical solution techniques, these exact solutions provide an invaluable tool for evaluation purposes, however, idealized the physical model problem might be.

Very often in the literature, numerical solutions embodying various constituent physical models are compared with fairly complex experimental configurations. Description of the initial and boundary conditions is far from

adequate for numerical model verification. The significant influence boundary conditions exert on the solution behavior has been amply stressed by several researchers.[2-4] Subsequently, the rather disappointing picture that emerges a result of comparing numerical solutions with experiments is further aggravated, as it now becomes an extremely difficult task to identify and isolate the various sources of discrepancy. Among these are the numerical solution techniques, physical modelling assumptions.

Thus, for purposes of evaluating the previously discussed discretization techniques, this study has adopted the strategy that assessment exercises are confined predominantly to examining the performance of discretization schemes in the light of exact solutions. These also include thoroughly exercised (documented) model numerical solutions. Where appropriate, the performance of a scheme was further studied in more demanding flow problems including non-linearity and variable coupling. A typical scheme's performance is also examined with respect to the particulars of the alternative techniques considered. The assessment criteria, presented in Section (4.4), for such comparison exercises were manipulated to comprise the following attributes with a view towards three-dimensional applications:

i) Best accuracy on coarse grids. Even with advanced computers, many three-dimensional calculations will still be limited to grids which are, at best coarse.

ii) Robustness and stability. For many three-dimensional computations it is important to ensure that numerical solutions can be obtained. Particular reference is made here to k and ε equations.

iii) Efficiency. Improvements in accuracy must be attained without excessive computational requirements.

The performance of the schemes will now be discussed in detail. Unless otherwise stated, due to the extended computational molecule, a nine point Alternating Direction Line Gauss-Seidel procedure was used effectively, even in the presence of mild negative coefficients introduced by SOU or LP-SUDS, to solve the linear algebraic equations.

7.3.1 Second Order Upwind (SOU) Differencing Scheme

To evaluate the SOU discretization scheme, SOU is applied to four scalar transport model problems, as well as several flow problems. The scalar transport problems are all described by equation (6.1) in Cartesian form, i.e.,

$$\frac{\partial}{\partial x}(\rho u\phi) + \frac{\partial}{\partial y}(\rho v\phi) = \frac{\partial}{\partial x}(\Gamma_\phi \frac{\partial \phi}{\partial x}) = \frac{\partial}{\partial y}(\Gamma_\phi \frac{\partial \phi}{\partial y}) + S_\phi(x,y) \quad \text{Equation (6.1)}$$

and include the following specific cases:

i) The uniform, angled flow, convected step problem chosen to examine the behaviour of the scheme with the flow at various angles to the grid, figure (7.7).

ii) The uniform angled flow past a unit source chosen to evaluate the performance of SOU in the presence of a source, figure (7.8).

iii) The problem of curved flow through a rectangular domain (the so-called Smith-Hutton[90] problem), adopted to examine the behavior of SOU in the presence of flow curvature, figure (7.9).

iv) Problem (ii) with a distributed source give by:

$$S(x,y) = \rho u(6x-6x^2)(3y^2-2y^3) + \rho v(3x^2-2x^3)(6y-6y^2) - \Gamma_\phi[(6-12x)(3y^2-2y^3) + (3x^2-2x^3)(6-12y)] \quad (7.1)$$

with ρ=1, u=2, v=1.

The solution for ϕ in this case is given by:

$$\phi = (3x^2-2y^3)(3y^2-2y^3) \quad (7.2)$$

For each problem, SOU was applied only to cases where the flow was at an angle to the grid where the performance of SOU is expected to be the worst.

For the problem of scalar transport of a step, three cases were considered: Case I, Pe_L = 250, θ=45° on a uniform 5x5 grid; Case II, Pe_L=250, θ=30.9° on a uniform 5x5 grid; and Case III, Pe_L=250, θ=30.9° on a uniform 25x25 grid.

For Case I, the results shown in figure (7.10a) indicate that for θ=45° the SOU results exhibit an excessive smearing of the step profile as compared to the 'exact' solution obtained by Huget.[30] In fact, comparing the results to previously obtained solutions, the smearing of SOU is comparable to

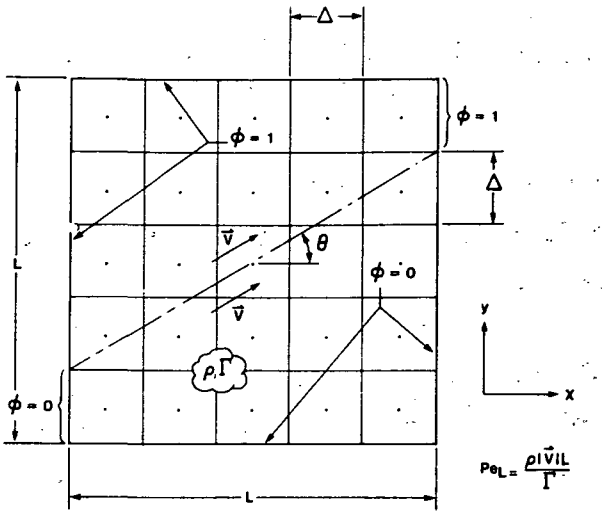

Figure 7.7 Convected Step Profile Problem

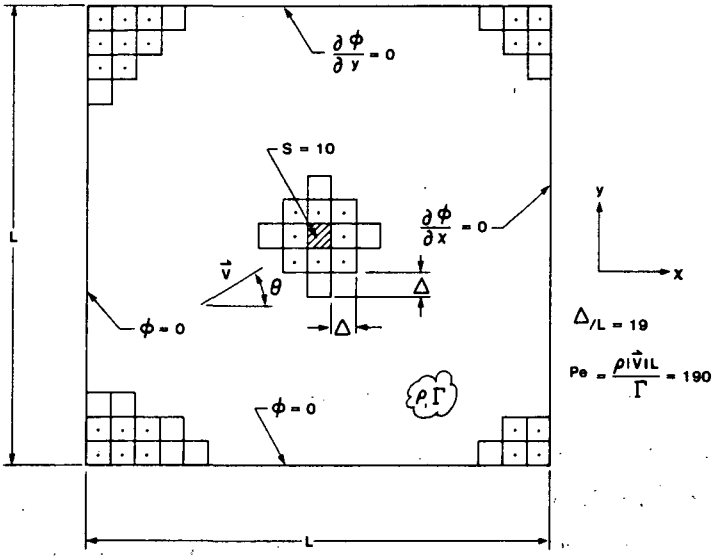

Figure 7.8 Uniform Flow Past a Single Volume Source

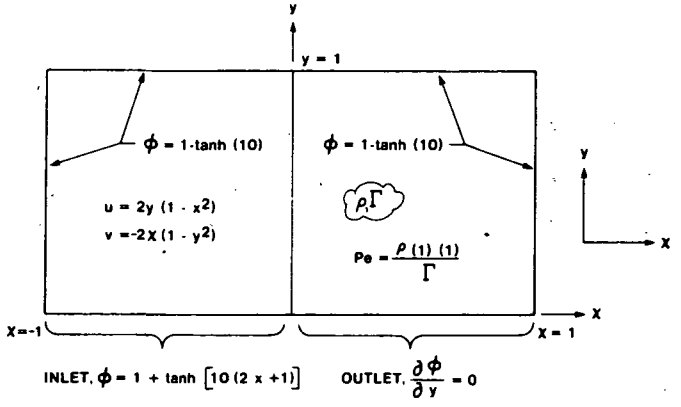

N1690

Figure 7.9 Smith - Hutton Problem

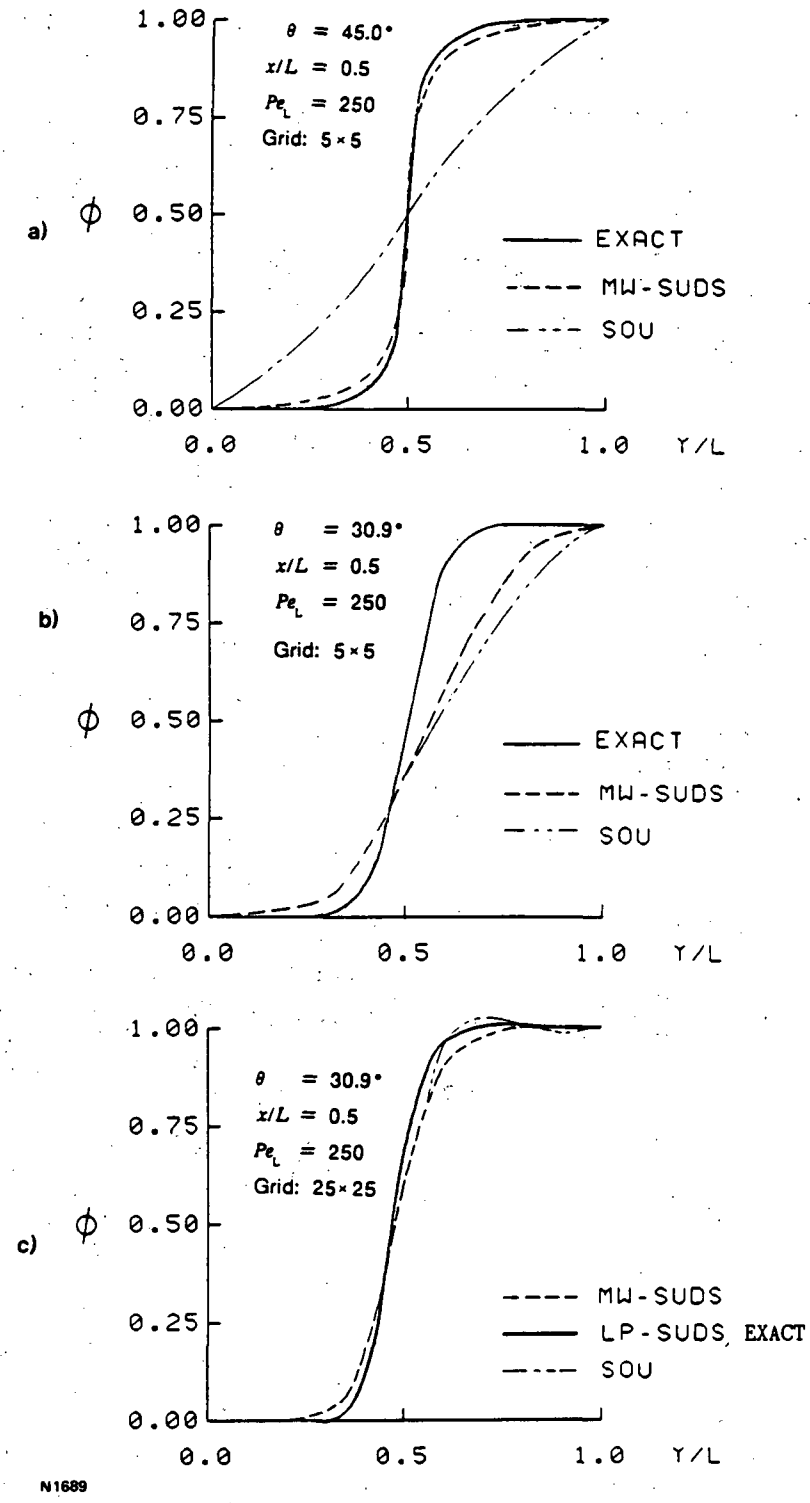

Figure 7.10 Centre-line Profiles of ø for Convected Step Problem

the smearing of the Upwind Differing Scheme (UDS). Also shown in figure (7.10a) are the results of Mass Weighted Skewed Upstream Differencing (MW-SUDS), which exhibit considerably less smearing of the step profile. Case II provides a comparison of SOU and MW-SUDS for θ=30.9 where MW-SUDS exhibits more smearing than for θ=45°. The results shown in Figure (7.10b) indicate that for the coarse 5x5 grid SOU smears the step profile more than MW-SUDS. To determine the behavior of SOU on moderate grids, a grid of 25x25 was used in Case III. The results shown in figure (7.10c) indicate that SOU does not smear the step profile as much as MW-SUDS. However, the SOU result exhibits one percent overshoot, while the results of the Linear Profile Skewed Upstream Scheme (LP-SUDS) exhibited no overshoots, Section (7.3).

For the problem of scalar transport with a unit source, the only case considered was that of θ=45°. The results shown in figure (7.11) indicate that SOU smears or spreads on the influence of the unit source, as compared to the "exact" solution obtained by Stubley.[91]

For the problem of scalar transport of a prescribed inlet profile in a prescribed flow with curvature the case $Pe=10^6$ was considered. The results shown in figure (7.12) indicate that, at the outlet, SOU exhibits smearing of the profile comparable to that of MW-SUDS as well as overshoots and undershoots as large as LP-SUDS.

To evaluate the rate of convergence of SOU with grid refinement, four uniform grids 4x4, 8x8, 16x16 and 32x32 were used to obtain SOU solutions for the scalar transport problem with a distributed source term. The resulting RMS error and the rate of convergence are given in Table (7.7). The results indicate that the rate of convergence of SOU approaches 2 only as the mesh becomes very fine.

TABLE 7.7 RATE OF CONVERGENCE OF SOU

Grid (N)	RMS Error	Rate
4x4	3.194×10^{-2}	
8x8	1.2216×10^{-2}	1.39
16x16	3.665×10^{-3}	1.74
32x32	9.859×10^{-4}	1.89

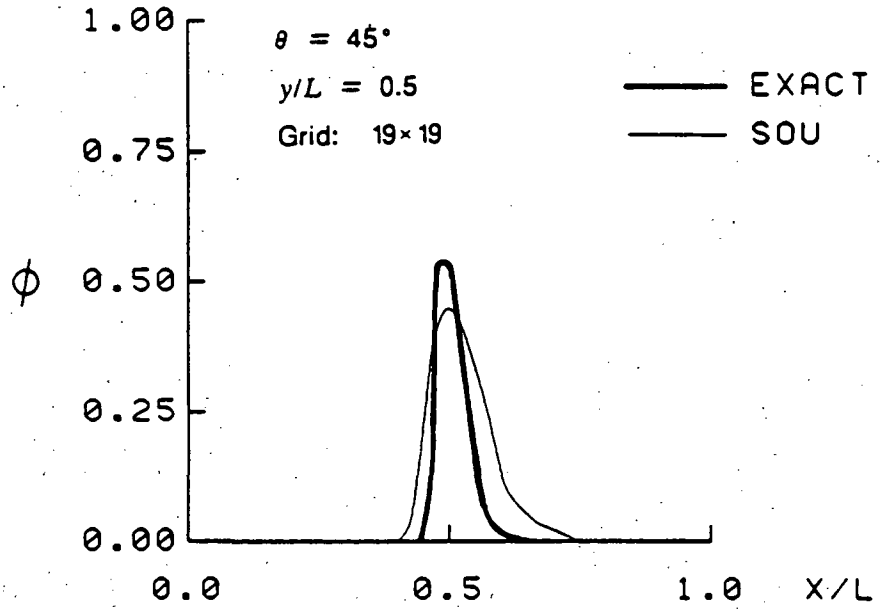

Figure 7.11 Centre-line Profile of ø for Unit Source Problem

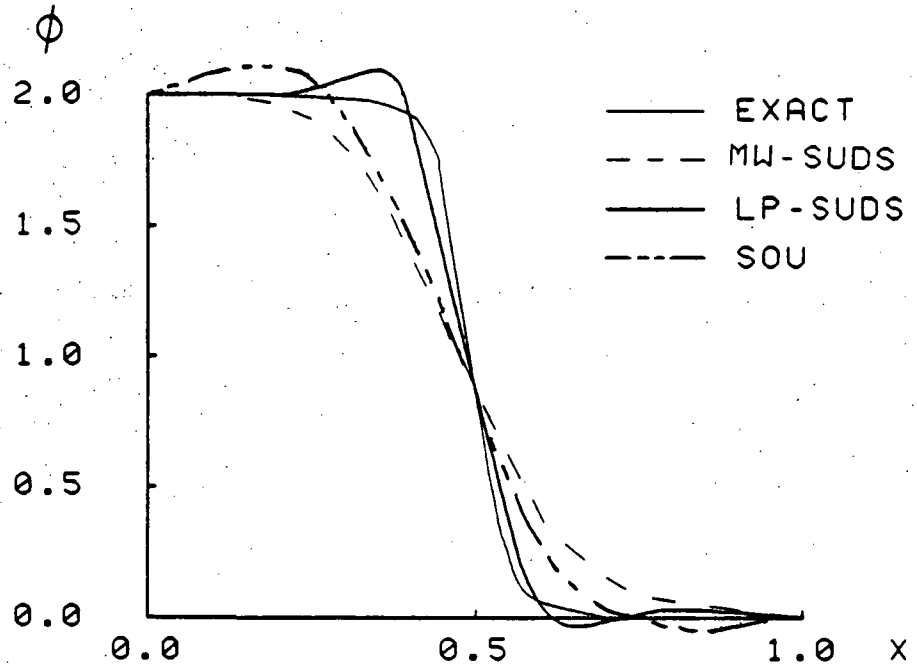

Figure 7.12 Outlet Profiles of ø in Flow with Curvature

In the above table, the convergence rate is defined as:

$$\text{Rate} = \frac{\log \dfrac{[\text{RMS Error}]_{coarse}}{[\text{RMS}_N\text{Error}]_{fine}}}{\log \left(\dfrac{N_{fine}}{N_{coarse}}\right)} \qquad (7.3)$$

In addition to the above scalar transport cases three laminar flow test cases, namely the shear driven flow in a square cavity, flow over a rearward facing step and angled flow into a suddenly expanding pipe were executed. The incompressible flow algorithm used was the PISO variant of SIMPLER algorithm and an Alternating Direction Line Gauss-Seidel scheme was used to solve equations for pressure[19] and components of velocity.

For the shear driven cavity problems, figure (7.1), four global Reynolds numbers, Re_h, of 100, 400, 600 and 1000 were investigated using a uniform grid of 40x40 to examine the changing flow structure in the cavity due to increasing influences of convection. In the case of Re_h=100 both SOU and hybrid differencing are in agreement with the "exact" numerical solution of Burgraff[92] for the axial velocity profile at the vertical centre-plane, as displayed in figure (7.13). However, as the Reynolds number increases and convective influences begin to dominate, the additional accuracy afforded by a higher order scheme like SOU, as compared to first order schemes, becomes apparent. Nevertheless, there is still a considerable smearing of the centre-line axial velocity profile as is apparent from figure (7.14) for Re_h=600. None of the above solutions suffered from the severe solution difficulties reported by Vanka[93] for high Reynolds number cases, but displayed minor overshoots and undershoots (up to 4 percent) for Re_h=1000, Section (6.2.1).

Application of SOU to predict the flow details over a rearward facing step, figure (7.2), yielded the global recirculation zone length to be 5.67 step height employing a non-uniform grid distribution of 62x38 and a tophat (constant) inlet velocity profile. The Reynolds number based on step height was 250, for which the experimentally measured reattachment length is given by Durst[94] as 6.3 step heights. Table (7.8) compares the reattachment length $L_R=x_R/h$, for various alternative differencing schemes and grids.

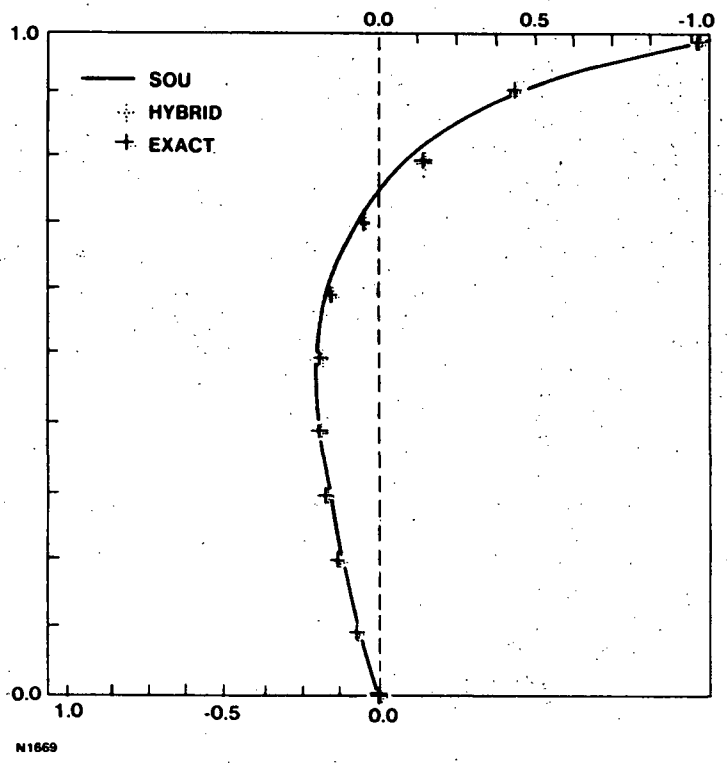

Figure 7.13 Centre-line Profiles of u Velocity for Shear Driven Flow, Re = 100, 40x40 Control Volumes

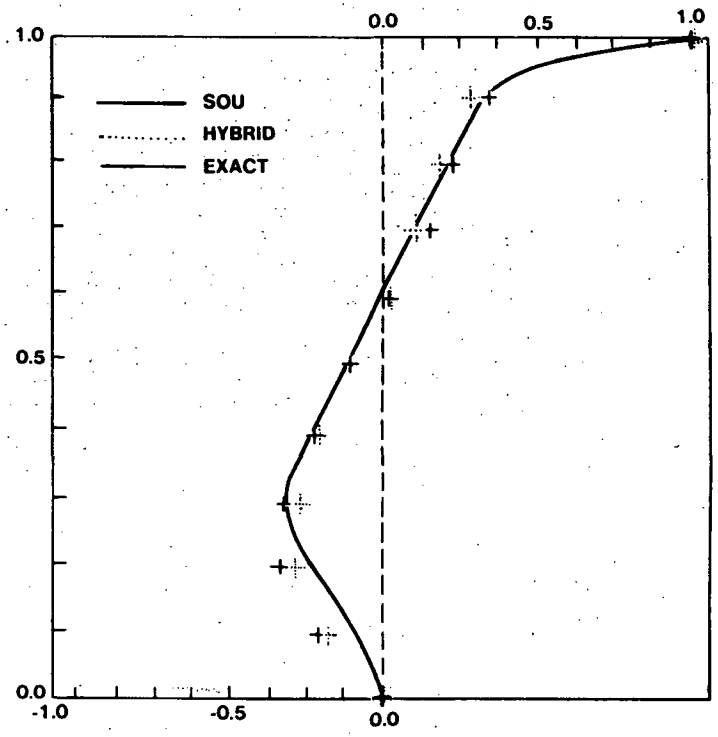

Figure 7.14 Centre-line Profiles of u Velocity for Shear Driven Fow, Re = 600, 40x40 Control Volumes

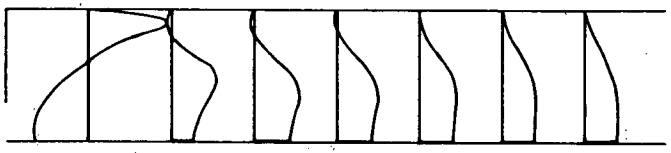

Figure 7.15 SOU Generated Profiles of u Velocity for Angled Flow in a Sudden Expansion, Re = 450, 78x44 Control Volumes

TABLE 7.8 COMPUTED REATTACHMENT LENGTH L_R FOR VARIOUS ALTERNATIVE DIFFERENCING SCHEME FOR THE REARWARD FACING STEP (Re_h=250)

Inlet Profile	Grid	Hybrid	QUDS[69]	BSUDS2[5]	SOU
Tophat 1	10x6	2.5	5.32	2.2	
Tophat 2	20x12	3.14	5.25	3.95	
Tophat 3	40x24	4.52	5.35	5.78	
Tophat 4	62x38				5.67
Tophat 5	78x48	5.53	5.75	5.98	

It will be seen from above table that the performance of SOU indicates a behaviour very similar to that of QUICK differencing of Leonard[69] (better bounded solutions, however) and far superior as compared to Hybrid differencing.

Concerning the problem of angled inflow into a sudden expansion type geometry, the predicted flow field by SOU (non-uniform grid 78x44, Re_h=450, inlet angle=30°) displays qualitatively the expected correct behavior, i.e., the multiplicity of recirculation zones and the complex interaction between the various zones, figure (7.15). In this case, however, there is neither any experimental data nor carefully performed "exact" numerical predictions available for comparison.

7.3.2 Variants of Skewed Upwind Differencing Schems (SUDS)

To demonstrate the applicability of the Linear Profile and Mass Weighted SUDS (LP-SUDS, MW-SUDS) and examine their performance, a number of two-dimensional scalar transport and flow problems have been considered. These will be considered in detail now.

Scalar Transport Problems

Three scalar transport problems, similar to SOU, were chosen to evaluate the variants of SUDS schemes incorporating an implicit determination of the interface values of variables using a simple LU decomposition. These are:

i) The uniform, angled flow convected step problem

ii) The uniform angled flow past a unit source

iii) The problem of curved flow through a rectangular domain, the Smith-Hutton problem.

For problem (i) the relevant problem parameters examined include Pe_L=250, four flow angles, θ=0°, θ=11.3° ($\tan^{-1}(0.2)$), θ=30.9 ($\tan^{-1}(0.6)$) and θ=45° and a variety of uniform grids including 5x5, 15x15 and 35x35 control volumes.

Figure (7.16) displays the results at the domain centreline, x/L=0.5 obtained using LP-SUDS and MW-SUDS and compared to the "exact" results obtained by Huget[30] for problem (i). Also shown on the figure are the coarse grid Exponential Differencing Scheme (EDS) and SUDS results obtained by Huget.[30]

In general, the results indicate that, as the angle of the flow to the grid is increased, MW-SUDS exhibits some false diffusion, but to a much lesser degree than EDS and LP-SUDS exhibits some spurious spatial oscillations, but usually much less than those observed for SUDS.

For problem (ii) three flow angles were considered, θ=0°, 22.5° and 45°. Centre-line (y/L=0.5) profiles obtained using 19x19 uniform control volumes are shown in figure (7.17). Also shown are the exact results obtained by Stubley.[91] In general, the results indicate that:

a) Both LP-SUDS and MW-SUDS benefit from source term influence. In particular, accounting for the influence of the source term reduces the overestimation of maximum ϕ and shifts the location of maximum ϕ downstream and closer to the true location.

b) Due to the false diffusion introduced by MW-SUDS the overestimation of maximum ϕ by MW-SUDS is less than that of LP-SUDS. However, at the downstream boundary, the false diffusion of MW-SUDS results in overestimation of ϕ.

For problem (iii) illustrated in figure (7.9), the flow transports a slightly diffused step profile of ϕ into the computation domain through the left side of the bottom boundary and it leaves the domain through the right side of the bottom boundary with the ϕ profile determined by the Peclet number, Pe. Using a 20x10 uniform mesh, numerical solutions are obtained for five Peclet numbers, Pe=10, 100, 500, 1000 and 10^6. The profiles along the outlet portion of the bottom $0 < x < 1$ are shown in figures (7.18). In general, the results for this problem with flow curvature indicate that:

a) for low values of Pe, LP-SUDS and MW-SUDS results are in close agreement.

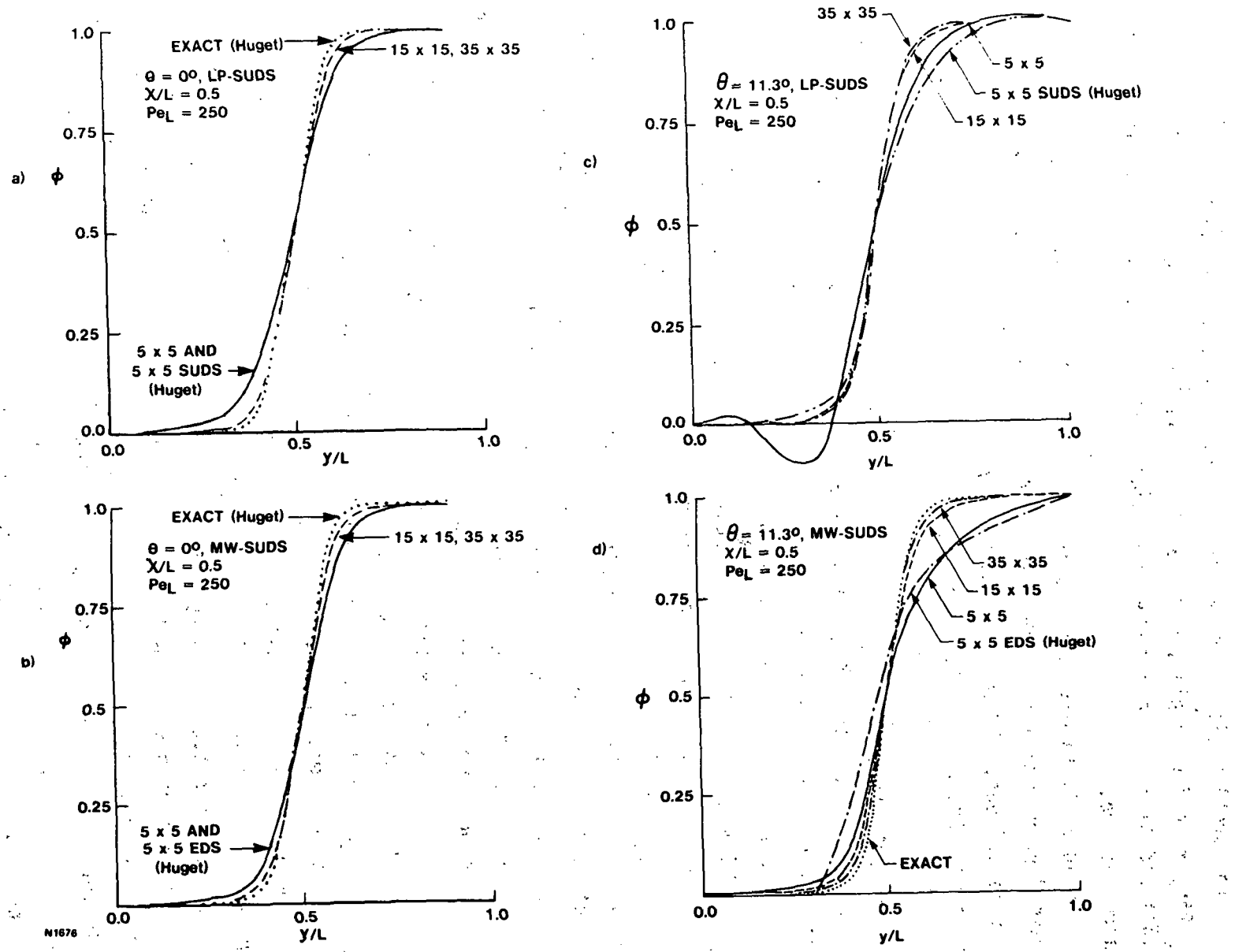

Figure 7.16 Centre-line Profiles of ø for Convected Step Problem SUDS Schemes

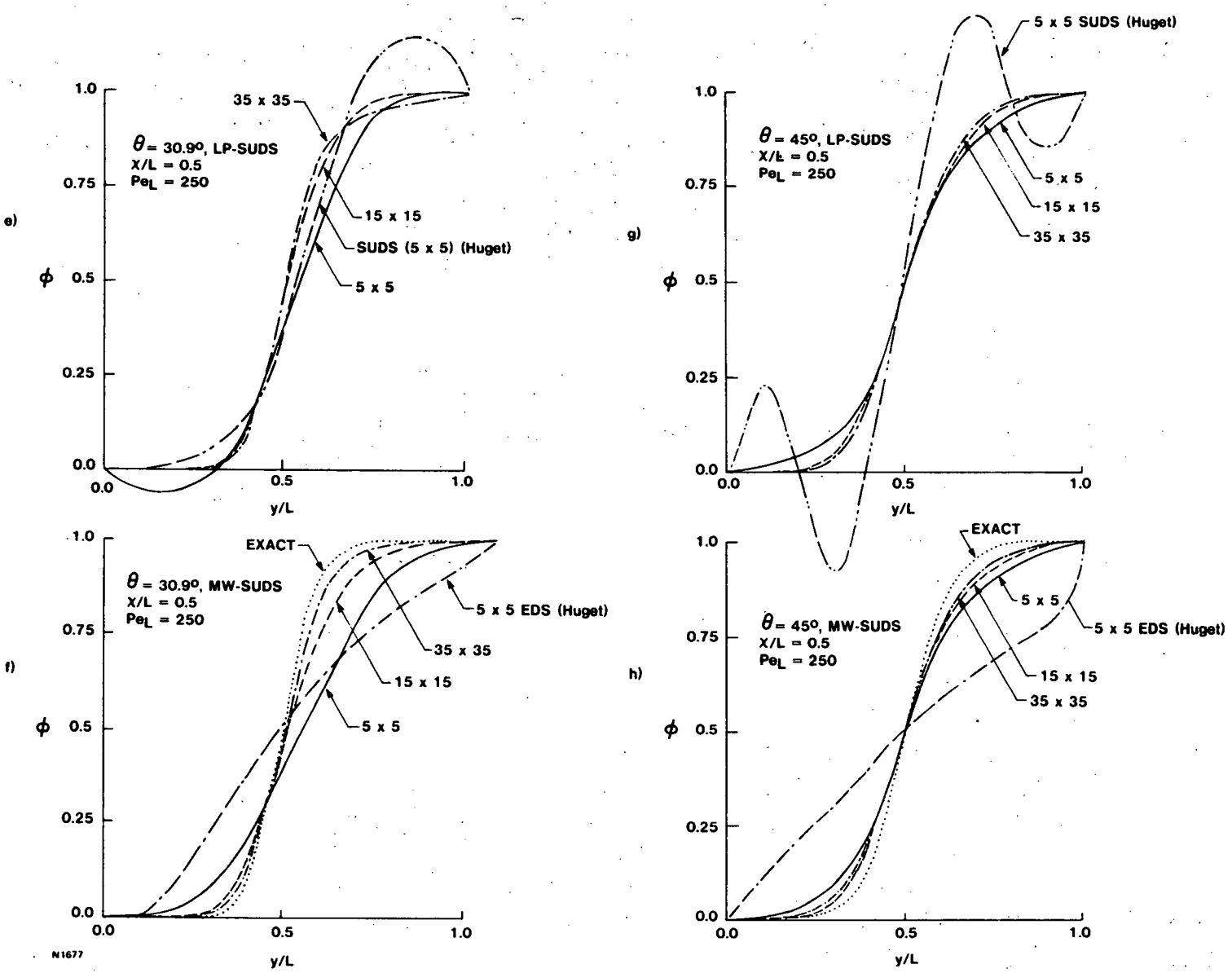

Figure 7.16 (cont.) Centre-line Profiles of ø for Convected Step Problem SUDS Schemes

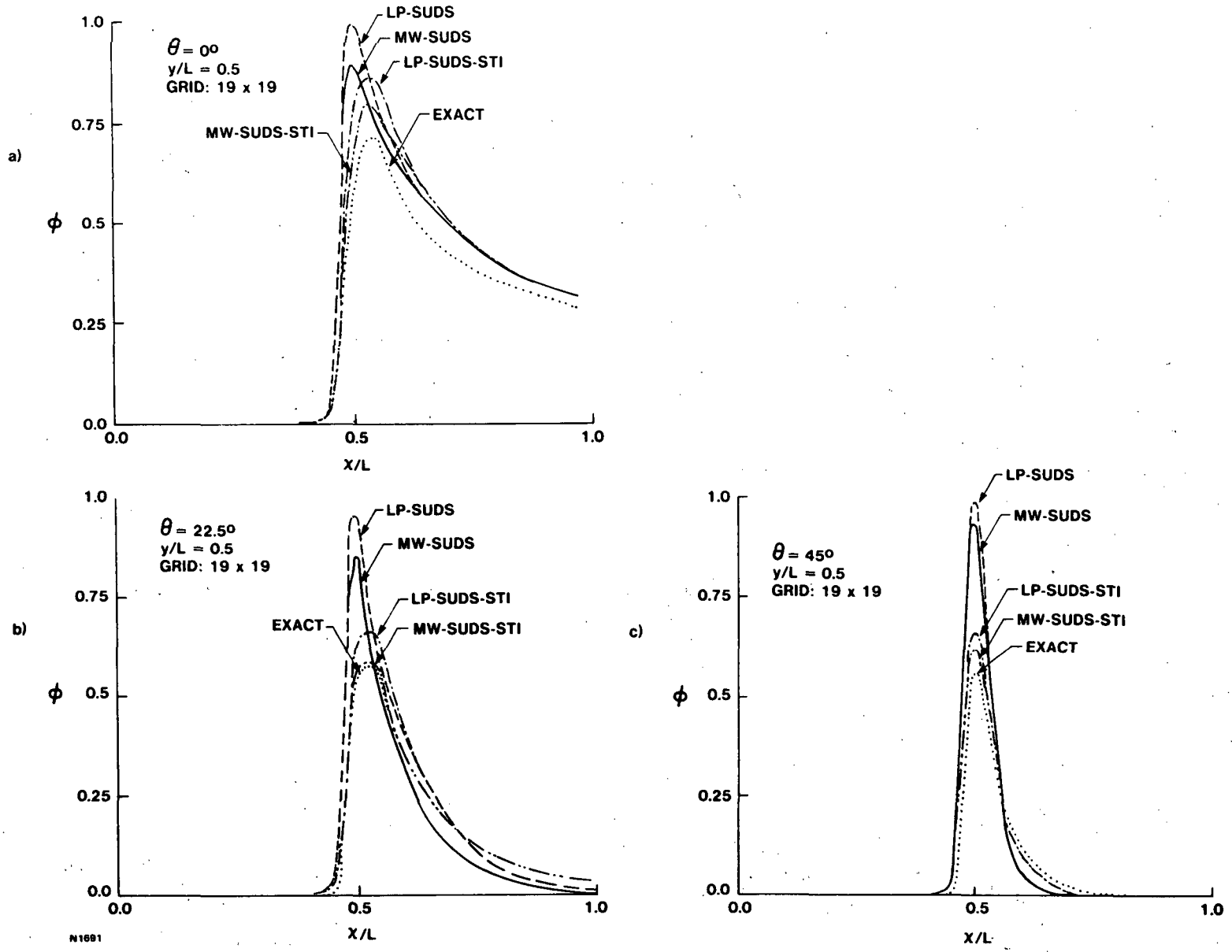

Figure 7.17 Centre-line Profiles of ø for Unit Source Problem SUDS Schemes

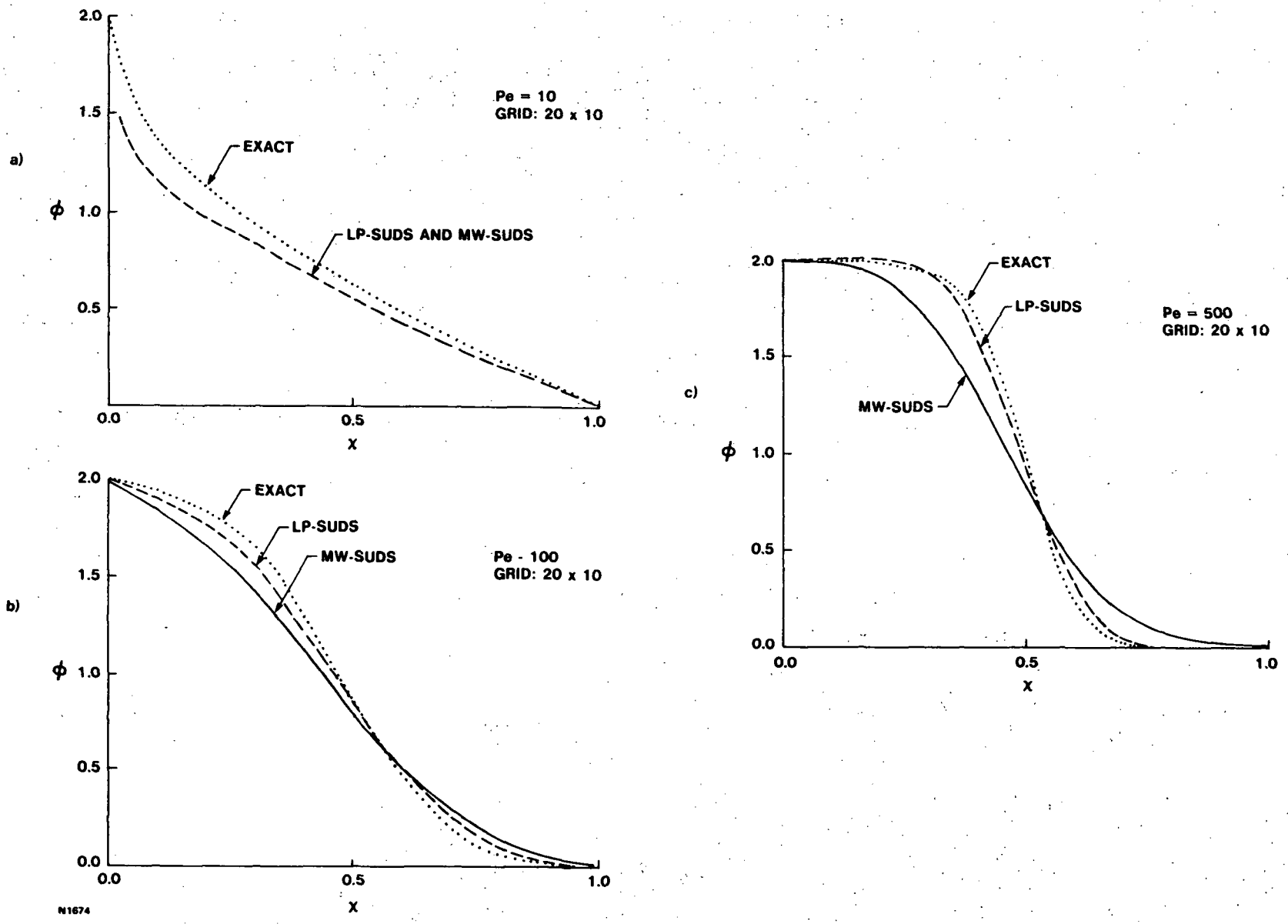

Figure 7.18 Outlet Profiles of ø for Smith-Hutton Problem, SUDS Schemes

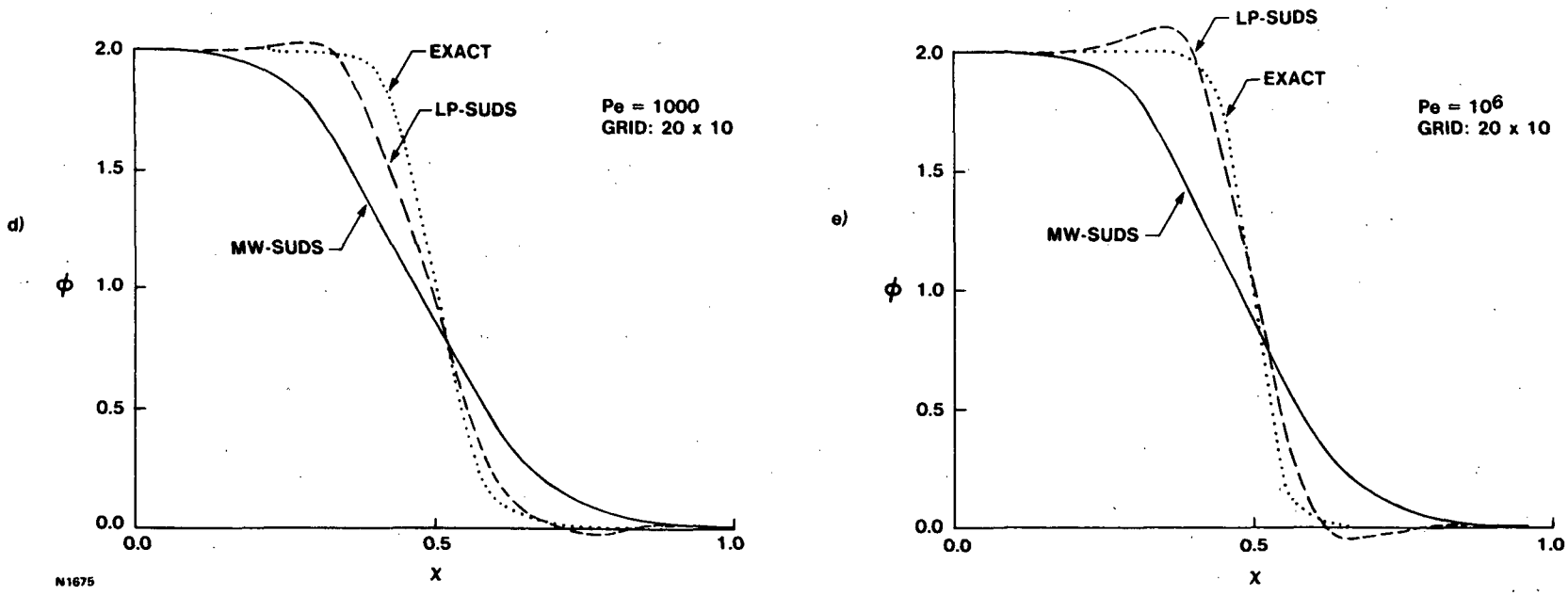

Figure 7.18 (cont.) Outlet Profiles of ø for Smith-Hutton Problem, SUDS Schemes

b) as Pe is increased, the false diffusive nature of MW-SUDS becomes evident. It is also worthy to note that for Pe = 10^6 and 1000, MW-SUDS results do not differ significantly from the results for Pe = 500.

c) as Pe is increased, LP-SUDS exhibits no false diffusion but overshoots become apparent for Pe > 10^3 with a maximum overshoot of 6.25 percent occuring for Pe = 10^6.

All the above scalar transport problems employed an implicit formulation for the determination of interface variable values. To illustrate the applicability of explicit linear profile and mass weighted SUDS, Section (6.3.4), numerical solutions to the same problems were used to demonstrate the performance of explicit skew schemes. For the convected step, unit source and Smith-Hutton problems, the explicit skew results are almost identical to the implicit skew results. However, the explicit skew results required less than 50 percent of the computational effort required by the implicit skew schemes. Using the current implementation, coefficient assembly costs for LP and MW-SUDS are estimated to be four times the assembly cost for the baseline Hybrid differencing.

For the problem of scalar transport with distributed sources in a uniform velocity flow (not discussed above), the explicit skew results are again similar to the implicit skew results. The exception, however, is the performance of the LP-SUDS with source term influence. As shown in Table (7.9), the rate of convergence of LP-SUDS-STI, where suffix STI denotes source term influence, is now 2. This second order rate of convergence is not a result of the explicit skew approach. Instead, it is a result of using a first order approximation to the source term influence in the vicinity of boundaries. In the implicit skew implementations, a zero-order approximation to the source term was used in the vicinity of the boundaries.

TABLE 7.9 RATE OF CONVERGENCE OF LP-SUDS-STI

Grid (N)	RMS Error	Rate
4	2.022×10^{2}	
8	5.0779×10^{-3}	1.99
16	1.2657×10^{-3}	2.00
32	3.0889×10^{-4}	2.03

In summary, explicit LP-SUDS and MW-SUDS require less computational effort and yield numerical results that are almost identical to the corresponding implicit schemes. Also, by ensuring that a first order approximation to the source term influence is used throughout the domain including near boundaries, LP-SUDS-STI has been shown to be a scheme with a second order rate of convergence.

Fluid Flow Problems

The previous laminar flow demonstration problems, i.e., shear driven flow in a square cavity and flow over a rearward facing step, as well as a turbulent coannular flow were chosen to flow evaluate the variants of SUDS for flow problems. The emphasis here is on the discretization of the momentum conservation equations with and without accounting for the pressure gradient source term influence. The solutions discussed below were all obtained using repeated SIMPLEC with SIP-BC or SIP-ACM and an implicit/explicit formulation for the interface value of the relevant variable.

For the driven cavity flow, Re_h=1000, two grids were used to obtain numerical solutions, a uniform 10x10 mesh and a uniform 20x20 mesh. From these numerical results, obtained using an implicit interface value formulation and SIP with BC, values of minimum normalized stream function, ψ_{min} were determined and tabulated in Table (7.10). Also tabulated are the EDS and SUDS results obtained by Huget.[30]

TABLE 7.10 VALUES OF ψ_{min} FOR DRIVEN CAVITY PROBLEM, EXACT VALUE OF $\psi_{min} \sim -0.117$[95]

Scheme \ Grid	10x10	20x20
EDS	-0.0494	-0.0677
SUDS	-0.0370	-0.0577
MW-SUDS	-0.0457	-0.0643
LP-SUDS	-0.0401	-0.0599
MW-SUDS-STI	-0.0610	-0.0786
LP-SUDS-STI	-0.0551	-0.733

From the results tabulated, it is seen that even the best solution obtained by using MW-SUDS-STI differs considerably from the computations of Ghia et. al.[95] In noting similar discrepancies, Huget[30] suggests that they are due to the poor treatment of shear in the vicinity of the moving lid. There are at least two ways to overcome this difficulty; one is to introduce higher order representations for boundary conditions,[30] and another is to introduce influence points to evaluate the mass fluxes in the representation of mass conservation. This latter approach has been demonstrated by Raw[10] to result in more accurate results for the driven cavity problem. In this and other flow problems in this section, the source term influence of pressure in momentum conservation, when it was accounted for, was implemented using a deferred correction approach.

In spite of the errors, the trends shown in Table (7.10) dramatically display the influence of accounting for source term effects in evaluating the interface variable values on the accuracy of resulting solutions. The same problem was repeated using the explicit formulation for flux evaluation and repeated SIMPLEC with SIP-BC or SIP-ACM to examine accuracy issues and CPU requirements in comparison with the baseline code that incorporates Hybrid differencing. The results for ψ_{min} and CPU requirements are displayed in Table 7.11.

TABLE 7.11 VALUES OF ψ_{min} AND CPU REQUIREMENTS FOR DRIVEN CAVITY PROBLEM

Grid \ Scheme	Hybrid		MW-SUDS-STI		LPU-SUDS-STI	
	$-\psi_{min}$	CPU	$-\psi_{min}$	CPU	$-\psi_{min}$	CPU
10x10	-0.0496	101	0.0672	306	0.0734	285
20x20	-0.0655	760	0.0879	1704	0.0954	1813

In the above and remaining tables to follow, CPU's are measured in seconds and refer to a MASSCOMP Series 500 minicomputer.

Review of the above table again demonstrates clearly that LP-SUDS-STI solutions are more accurate than MW-SUDS-STI results which are in turn, more accurate than Hybrid results. Associated with the increased accuracy of MW-SUDS-STI or LP-SUDS-STI is a corresponding increase in total CPU requirements. A significant portion of this increase, apart from the CPU cost associated with coefficient generation, (50 to 100 percent) is most likely due to the use of the particular deferred correction procedure to account for the source term influence, primarily pressure for the momentum conservation equations. Naturally, such CPU requirements could be reduced substantially, if a more implicit treatment of source term influences were used. However, such an implicit treatment of pressure source for interface flux evaluation may give rise to practical solution difficulties within the framework of the segregated solution approach adopted, i.e., decoupling of the pressure field, treatment of boundary conditions for the additional terms in the continuity/pressure equation, etc. Raw[10] using a similar approach formulated a co-located solution procedure that overcomes most of the above problems. Use of the deferred correction approach in the manner outlined above yielded converged solutions without severe solution difficulties, albeit increased CPU requirements.

The increased costs associated with the use of the above SUDS schemes raises the issue of cost effectiveness of such schemes. One way to evaluate cost effectiveness is to determine the relative costs of each scheme to achieve a prescribed accuracy. For instance, the ψ_{min} value of -0.0734 is obtained using LP-SUDS-STI on a 10x10 grid and requires approximately 300 CPU seconds. On the same grid using a similar amount of CPU, the MW-SUDS-STI result is -0.0672. It is estimated that MW-SUDS-STI would require a 15x15 grid and 700 CPU seconds to obtain a solution of similar accuracy as LP-SUDS-STI on a 10x10 grid. Similarly, it is estimated that the Hybrid scheme would require a 27x27 grid and 1800 seconds of CPU to obtain the accuracy of the coarse grid LP-SUDS-STI result. With respect to the coarse grid LP-SUDS-STI results, the storage and CPU requirements of the discretization schemes to obtain similar accuracy as presented in Table (7.12).

TABLE 7.12 STORAGE AND CPU RATIOS FOR EQUIVALENT ACCURACY (DRIVEN CAVITY PROBLEM)

Scheme	Storage Ratio	CPU Ratio
Hybrid	7.3	6.0
MW-SUDS-STI	2.3	2.3
LP-SUDS-STI	1.0	1.0

For the flow over a rearward facing step, Re_h=250 as shown in figure (7.2), three uniform grids were used, 10x6, 20x12 and 40x24. From these numerical results, values of the normalized recirculation zone length $L_R = x_R/h$ were determined to assess discretization accuracy. Table (7.13) displays the L_R values obtained using an implicit interface variable determination with and without source term influences, and SIMPLEC with SIP-BC. Also tabulated are the Hybrid, QUDS and BSUDS2 reported by Syed, et al[5] and the experimental results of Durst.[94]

TABLE 7.13 VALUES OF L_R FOR REARWARD FACING STEP PROBLEM EXPERIMENTAL VALUE OF L_R = 6.3

Grid / Scheme	10x6	20x12	40x24
HYBRID	2.5	3.14	4.52
QUDS	5.32	5.25	5.35
BSUDS2	2.2	3.95	5.78
MW-SUDS	3.94	4.43	4.84
LP-SUDS	4.82	5.24	5.82
LP-SUDS-STI	3.92	4.53	4.92
LP-SUDS-STL	4.94	5.32	5.92

From the tabulated results it is noted that:

i) MW-SUDS results are superior to Hybrid results.

ii) LP-SUDS results are always superior to BSUDS2 results and comparable or better than QUDS results on finer meshes.

iii) In general, accounting for source term influence improves the accuracy of MW-SUDS and LP-SUDS.

As in the previous test problem, application of the explicit interface variable formulation together with repeated SIMPLEC and SIP-ACM in the baseline code, enables a comparative basis to be established for cost effectiveness of each scheme. These are summarized in Table (7.14).

TABLE 7.14 VALUES OF L_R AND CPU REQUIREMENTS FOR REARWARD FACING STEP PROBLEM

Grid \ Scheme	Hybrid		MW-SUDS-STI		LP-SUDS-STI	
	L_R	CPU	L_R	CPU	L_R	CPU
10x6	2.37	34	3.55	63	6.30	69
20x12	2.95	191	4.59	427	5.88	396
40x24	3.68	1265	5.33	2573	5.93	2495

A comparison of storage and CPU requirements for equivalent accuracy based on the medium 20x12 grid LP-SUDS-STI results are also shown in Table (7.15). The tabulated ratios are based on estimates that Hybrid would require at least a 160x96 grid and 8.3 hrs of CPU, and MW-SUDS-STI an 80x48 grid and 4.3 hrs of CPU to approach the accuracy of the medium grid LP-SUDS-STI result.

TABLE 7.15 STORAGE AND CPU RATIOS FOR EQUIVALENT ACCURACY REARWARD FACING STEP PROBLEM)

Scheme	Storage Ratio	CPU Ratio
Hybrid	64	75
MW-SUDS-STI	16	39
LP-SUDS-STI	1.0	1.0

The final flow problem examined was that of turbulent coannular flow as described in (5). For this case only the explicit interface variable formulation with repeated SIMPLEC and SIP-ACM was adopted to study accuracy issues and cost effectiveness.

Regarding the application of SUDS schemes to predict the complex details of a turbulent flow, the initial implementation of both MW-SUDS and LP-SUDS included diffusion and source term influences in the equations for momentum, turbulent kinetic energy, k, and turbulent kinetic energy dissipation, ε, conservation. Although with appropriate treatment of k and ε source term linearizations converged numerical solutions could be obtained, these solutions contained regions where k and/or ε were negative. Stability was maintained only because negative k and ε values were reset to zero. By the very nature of equations for k and ε, negative values for k and ε can only arise through the introduction of negative influences in the discretization schemes. After a careful analysis of the discretization schemes it can be shown that negative influences can arise in the following ways:

i) As a result of the linear profile assumption made to relate ϕ_u to adjacent nodal values of ϕ, Section (6.3.1). Since this assumption is inherent in LP-SUDS, this scheme is not appropriate for the discretization of equations for k or ε. By design MW-SUDS does not suffer from this problem.

ii) As a result of including the influence of diffusion in the integration point equations. At present, the only solution to this problem is not to include the diffusion term influence in the integration point equation for k and ε.

iii) As a result of including the influences of sources as currently implemented. An alternative approach to including source term influences may overcome this difficulty.

Guided by the results of the analysis given above, the baseline code was modified so that only MW-SUDS without diffusion and source term influences was used for k and ε equations. Both LP-SUDS and MW-SUDS with diffusion and source term influences were retained for the momentum equations. The modified code was then used to obtain numerical solutions to the turbulent coannular flow problem using Hybrid, MW-SUDS and LP-SUDS.

A comparison of the calculated centre-line axial velocity distribution is shown in figure (7.19) for the coarse 21x20 grid. As indicated, the

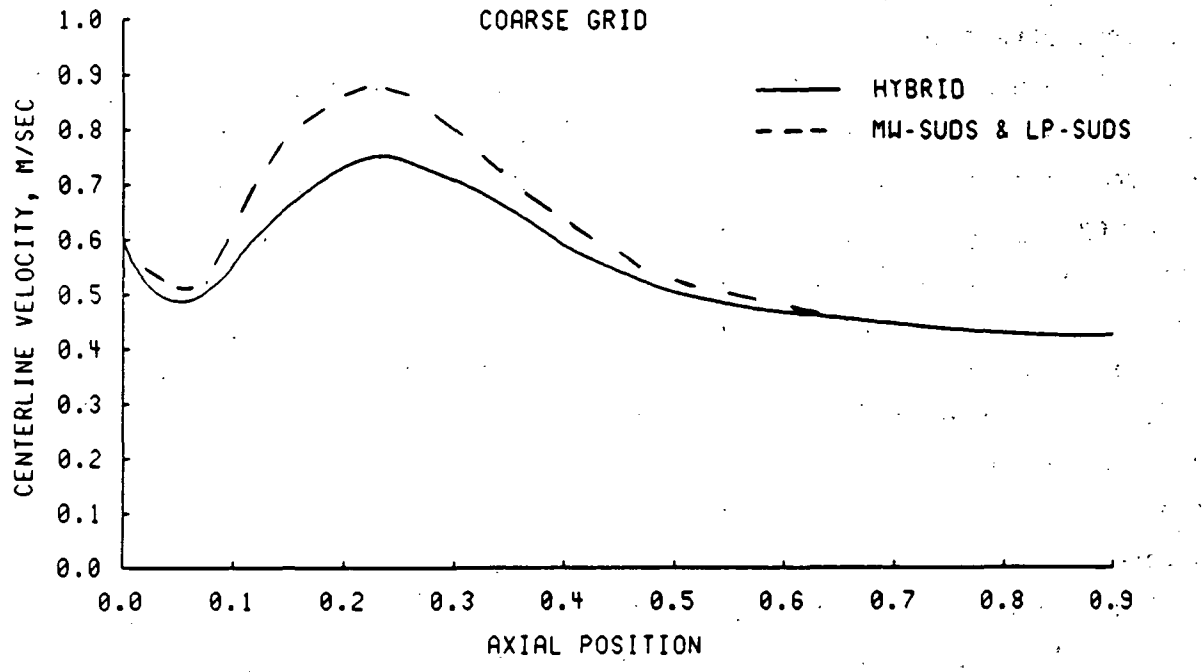

Figure 7.19 Centre-line Axial Velocity Distribution, Turbulent Coannular Flow Problem, SUDS Schemes Using Coarse Grid

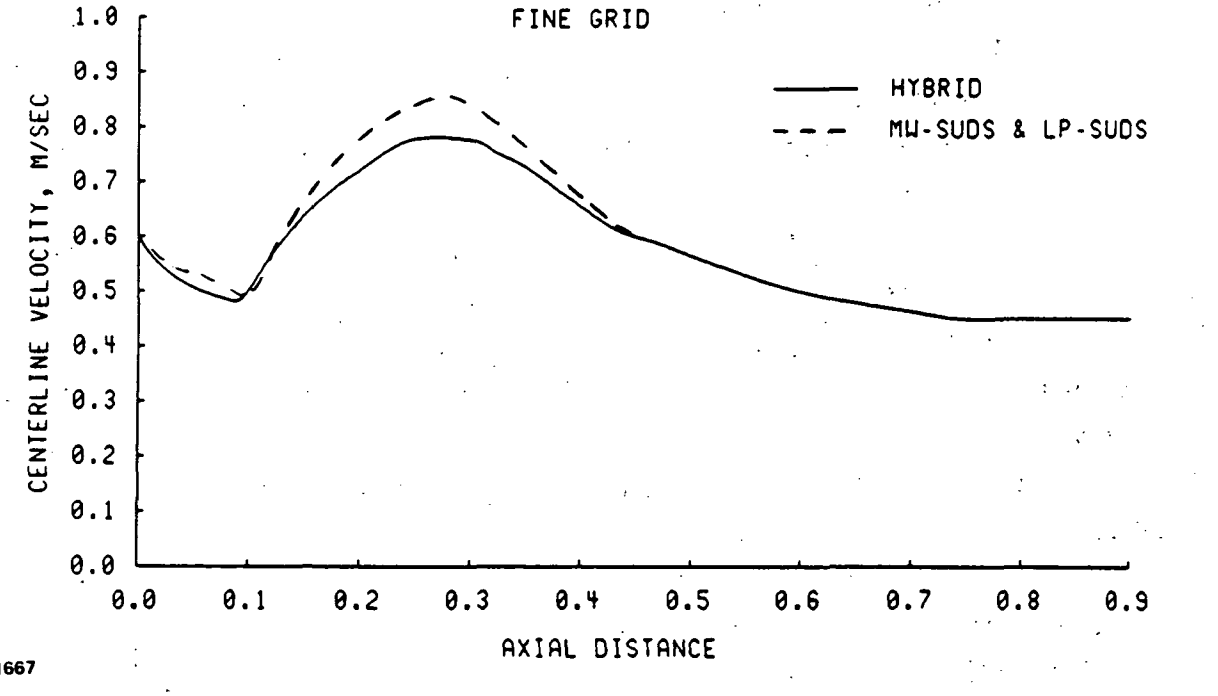

Figure 7.20 Centre-line Axial Velocity Distribution, Turbulent Coannular Flow Problem, SUDS Schemes Using Fine Grid

centre-line axial velocity distributions using MW-SUDS and LP-SUDS are identical. However, the Hybrid and SUDS results do not agree well in the initial region. This discrepancy most likely arises because of the excessive smearing of the Hybrid scheme.

Figure (7.20) shows the comparison of centre-line axial velocity distribution for the fine 38x38 grid. Again, there is no difference between MW-SUDS and LP-SUDS results, and the Hybrid results are in closer agreement with the SUDS results.

For completeness, information about coefficient updates and CPU requirements are summarized in Table (7.16).

TABLE 7.16 COEFFICIENT UPDATE AND CPU REQUIREMENTS FOR TURBULENT COANNULAR FLOW PROBLEM

Grid	Scheme	Coefficient Updates	Total CPU Requirements (hours)
21x20	Hybrid	109	0.5
21x20	MW-SUDS-STI	137	1.5
21x20	LP-SUDS-STI	182	2.0
38x38	Hybrid	421	8.87
38x38	MW-SUDS-STI	457	20.6
38x38	LP-SUDS-STI	451	20.7

7.3.3 Compact Implicit Discretization Schemes (CI)

The performance of several variants of CI schemes will be discussed using the notation and terminology of Section (6.4), primarily in one or two-dimensional scalar transport applications.

Derivative Compact Implicit Scheme (DCI)

DCI was applied to compute the following one-dimensional scalar transport problem including convection and diffusion:

$$\Gamma_\phi \frac{d^2\phi}{dx^2} + u \frac{d\phi}{dx} = 0 \qquad 0 \leq x \leq L$$

$$\phi\ (x=0) = 0.0$$

$$\phi\ (x=L) = 1.0$$

$$u > 0$$

with the solution given by:

$$\phi = \frac{e^{-Pe\ x/L} - 1}{e^{-Pe} - 1} \tag{7.4}$$

where $Pe = uL/\Gamma_\phi$ = Peclet number

Employing 31 uniformly spaced nodes and 5th order Pade' approximations for ϕ' and ϕ'', DCI results for a range of grid Peclet numbers were obtained and are displayed in figure (7.21). A close study reveals that for Pe = 1 the solutions for ϕ are bounded and physically correct. However, as the value of Pe increases, the solution of ϕ is no longer bounded with overshoots and undershoots arising in the vicinity of the large gradient at x/L=1. In fact, Ciment et al [82] have shown that the DCI scheme will give stable and physically reasonable results for $Pe < 4 / 15 \simeq 2.1438$.

Classical Operator Compact Implicit Scheme (COCI)

COCI scheme was also used to obtain solutions of the above one-dimensional equation. The results show in figure (7.22) for various values of Pe indicate for $Pe \leq 2$ the correct behavior is obtained. However, as Pe is increased beyond a value of 2 (corresponding to a decrease in diffusion) the solution for ϕ behaves as though more diffusion were introduced. In fact for $Pe = \sqrt{12}$, the solution is identical to that for pure diffusion Pe = 0.0. Increasing the value of Pe further results in even larger deviations from the correct behavior. Finally, for Pe = 4.208, the COCI scheme generates an entirely non-physical but bounded result, namely that all the values of ϕ in the domain equals the value at the downstream boundary.

Generalized Operator Compact Implicit Schemes (GOCI)

Using the above one-dimensional scalar transport equation GOCI results were generated for a range of Peclet numbers and are displayed in figure (7.23). Review of figure (7.23) clearly demonstrates the boundedness of

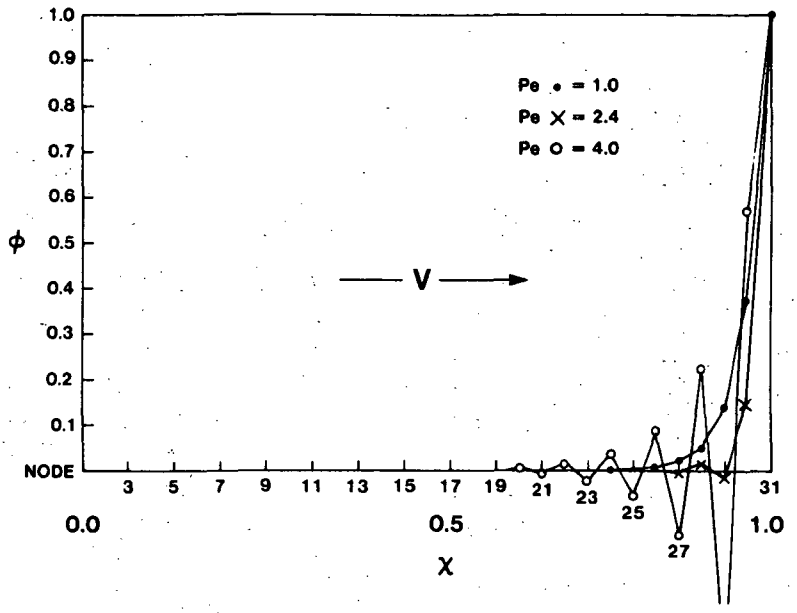

Figure 7.21 Compact Implicit, Block 3 x 3, 5th Order Pade' BC.'s
1D Convection - Diffusion Problem, 31 Nodes

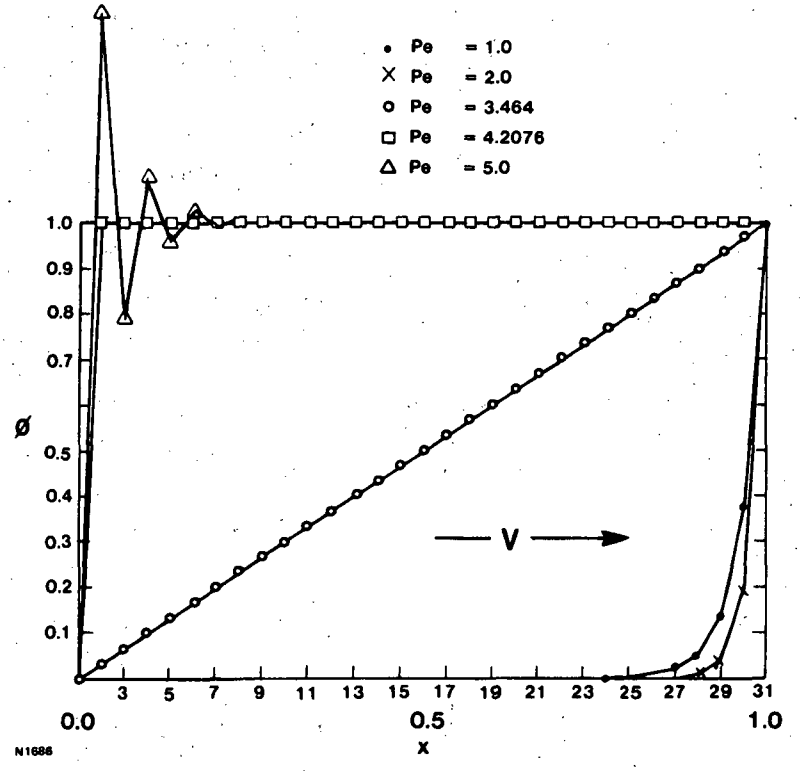

Figure 7.22 Standard OCI
1D Convection - Diffusion Problem, 31 Nodes

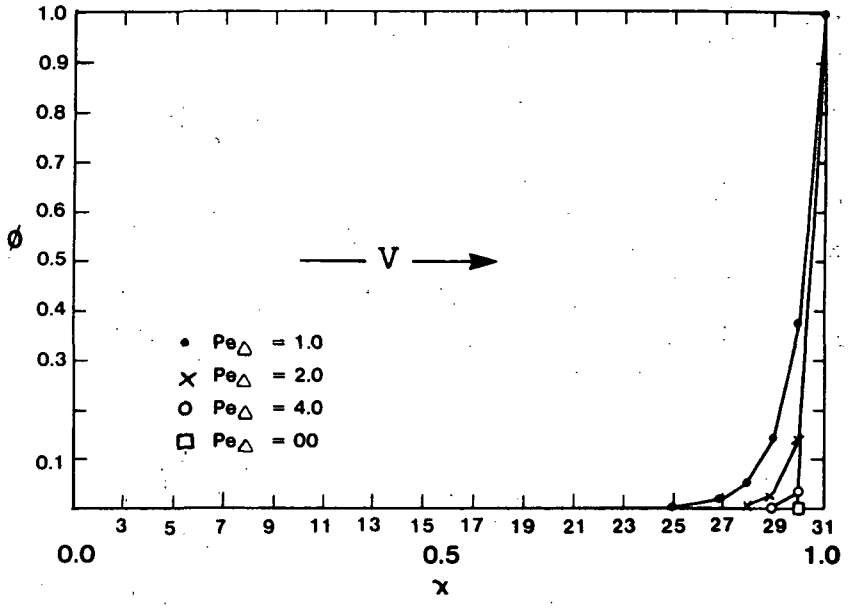

Figure 7.23 Generalized OCI
1D Convection - Diffusion Problem, 31 Nodes

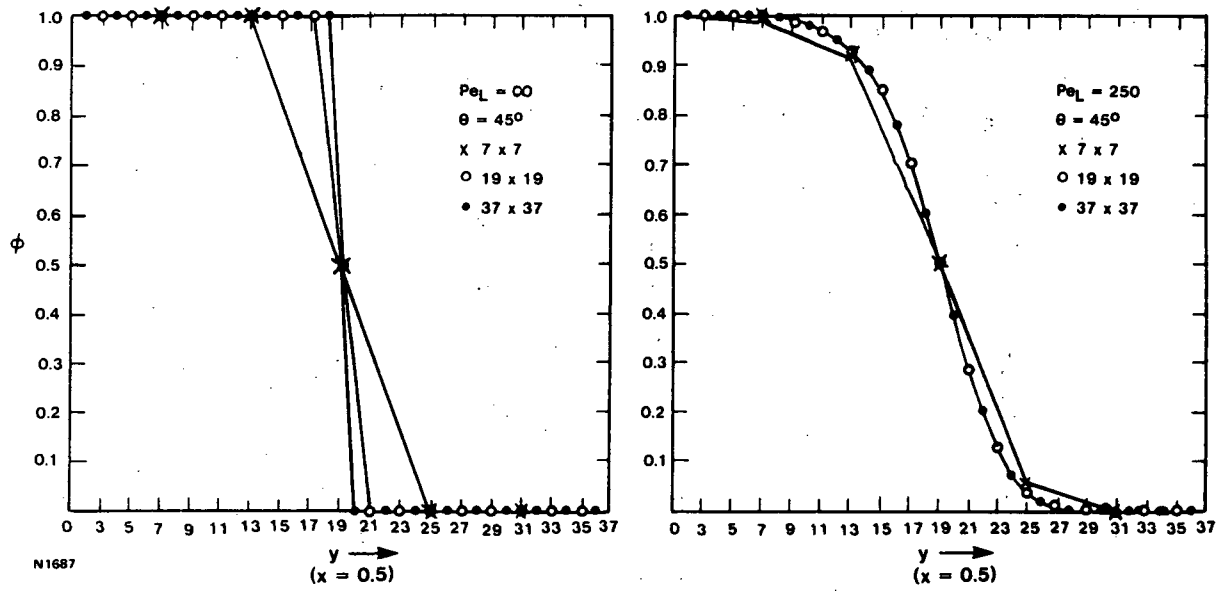

Figure 7.24 Convected Step Problem, GOCI, ø = 45°

solutions for all Pe. Also, as expected from the inherent exponential character of finite difference coefficients and the analytical solution, GOCI solution is in excellent agreement with the latter.

Encouraged by the above results and notwithstanding the reservations discussed in Section (6.4.5), GOCI Scheme was applied to predict the details of two-dimensional angled transport of a boundary specified step profile of ϕ for various Pe's. The results shown in figures (7.24) to (7.26) for θ = 45°, 33.7° and 18.4° respectively, all examine Peclet numbers of 250 and ∞ with grids of 7x7, 19x19 and 37x37 nodes. Each figure displays the predicted profile for ϕ along the centreline x/L = 0.5. The analytical solution for $Pe_L = \infty$ is a step change in ϕ from ϕ=0 to ϕ=1 at y/L = 0.5. The approximate analytical solution for Pe_L=250 case, valid for $Pe_L \geq 50$, is not plotted because it is graphically indistinguishable from the 37x37 node solutions for all flow angles considered.

At θ=45°, figure (7.24) the $Pe_L = \infty$ results for all grids are exact, resolving the profile at y/L=0.5 to within the resolution of the grid. For Pe_L=250, only the 7x7 grid prediction exhibits any distinguishable errors, and even those are relatively small.

At θ=33.7°, figure (7.25), the situation is somewhat different. For Pe= ∞, the predictions on all three grids exhibit significant overshoots and undershoots at the outflow boundary where ϕ=1 is enforced. The magnitude of the maximum overshoot ($\simeq$ 16 percent) does not reduce with grid refinement, since the local grid Peclet Number remains infinite. The oscillatory behavior tends to localize as the grid is refined, concentrating the overshoots and undershoots close to the steep gradient. At Pe_L=250, the GOCI Scheme is very well-behaved with only a small ($\simeq$ 2 percent) overshoot arising on the 7x7 grid near the inflow boundary. For the 19x19 and 37x37 grids, the predictions are comparable.

At θ=18.4°, figure (7.26), the results are similar to these described for θ=33.7°. The maximum overshoot on the downstream boundary for Pe=∞ remains at approximately 16 percent with behavior similar to that of θ=33.7°, as the grid is refined. For Pe_L=250, the 7x7 grid prediction has a maximum overshoot of 4 percent. As the grid is refined to 19x19, the overshoots disappear and the prediction is very close to that obtained using a 37x37 grid.

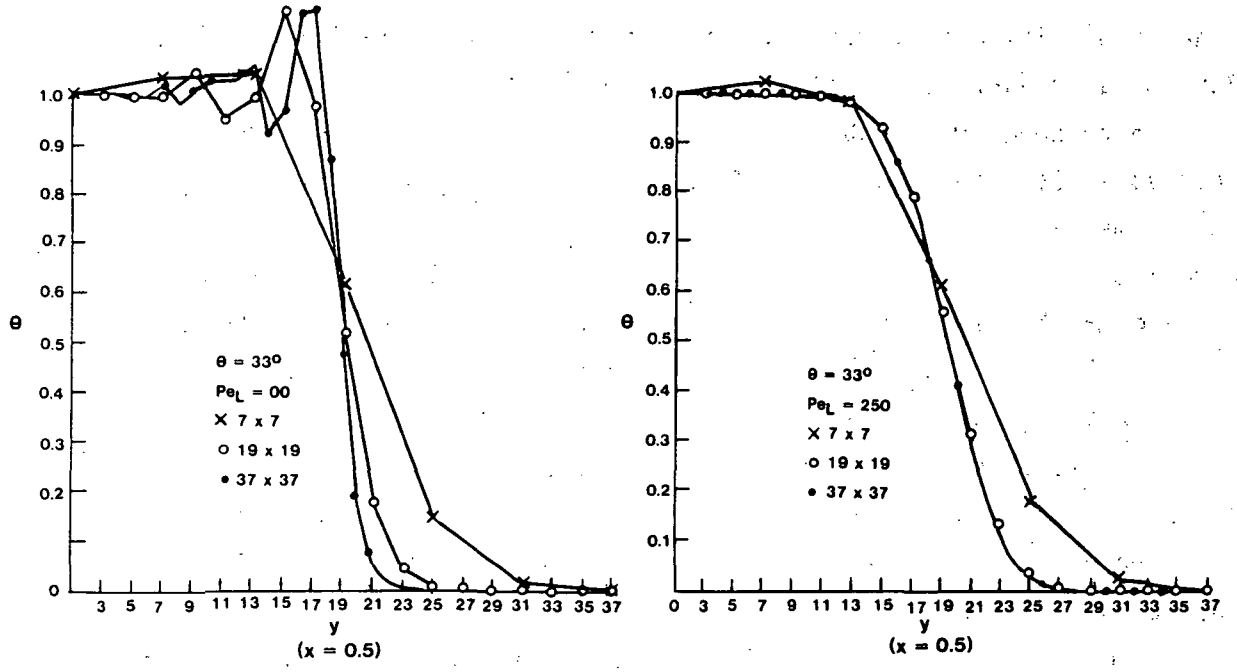

Figure 7.25 Convected Step Problem, GOCI, ø = 33.7°

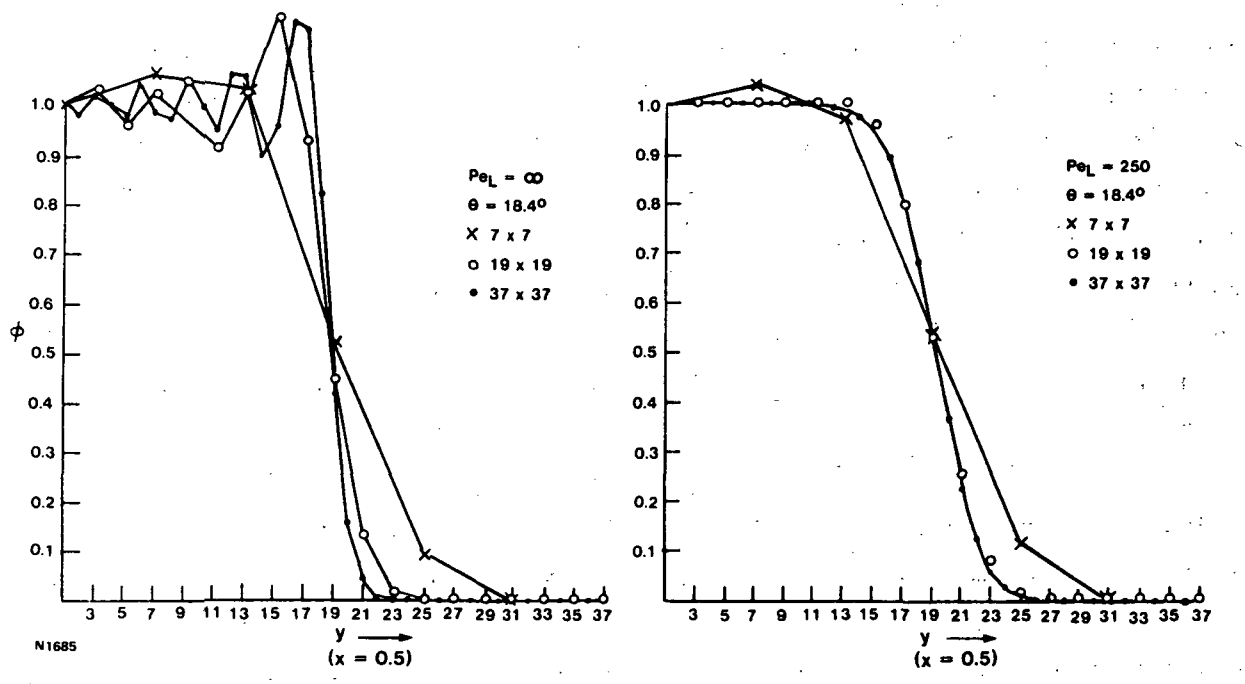

Figure 7.26 Convected Step Problem, GOCI, ø = 18.4°

Control Volume Based Operator Compact Implicit Method of Exponential Type CVOCI

To demonstrate the applicability and determine the characteristics of the CVOCI discussed in Section (6.4.3), the three scalar transport problems chosen to assess the performance of SOU and SUDS schemes were adopted to provide a uniform comparison basis for all the schemes considered in this study.

For the uniform, angled flow convected step problem, the results of CVOCI at the domain centre-line, x/L=0.5 are shown in figures (7.27). In general, the results indicate that:

i) for θ=o°, CVOCI generates no significant overshoots, even on the coarse 5x5 grid;

ii) for θ=11.3° and 30.9°, CVOCI generates a 10 percent undershoot on the coarse 5x5 grid with the magnitude of the undershoot diminishing with grid refinement;

iii) for θ=45°, CVOCI generates only a mild 1 percent overshoot.

For the uniform angled flow past a unit source problem, the CVOCI profiles along the centre-line (y/L=0.5) and the exact results of Stubley[91] are shown in figures (7.28). The results for the 19x19 grid indicate that:

i) no overshoots or undershoots were observed with overall good agreement between the CVOCI and exact results;

ii) for θ=0, the centre-line profile of ϕ is overestimated by CVOCI;

iii) for θ=22.5°, the centre-line profile of ϕ is in excellent agreement with the exact solution;

iv) for θ=45°, the centre-line profile of ϕ is underestimated by CVOCI.

For the Smith-Hutton[90] problem of curved flow of a diffused step profile through a rectangular domain, the CVOCI profiles along the outlet boundary are shown in figure (7.29). The results for this problem indicate that

i) for Pe = 10 and 100, the coarse 20x10 grid CVOCI results are in good agreement with the fine grid results presented by Smith and Hutton;

ii) for Pe = 500 and 1000, the CVOCI results display a 10 percent overshoot and a small 1 percent undershoot;

iii) for $Pe=10^6$, the CVOCI results exhibit oscillatory behavior on both sides of the steep gradient with errors as large as 17 percent arising.

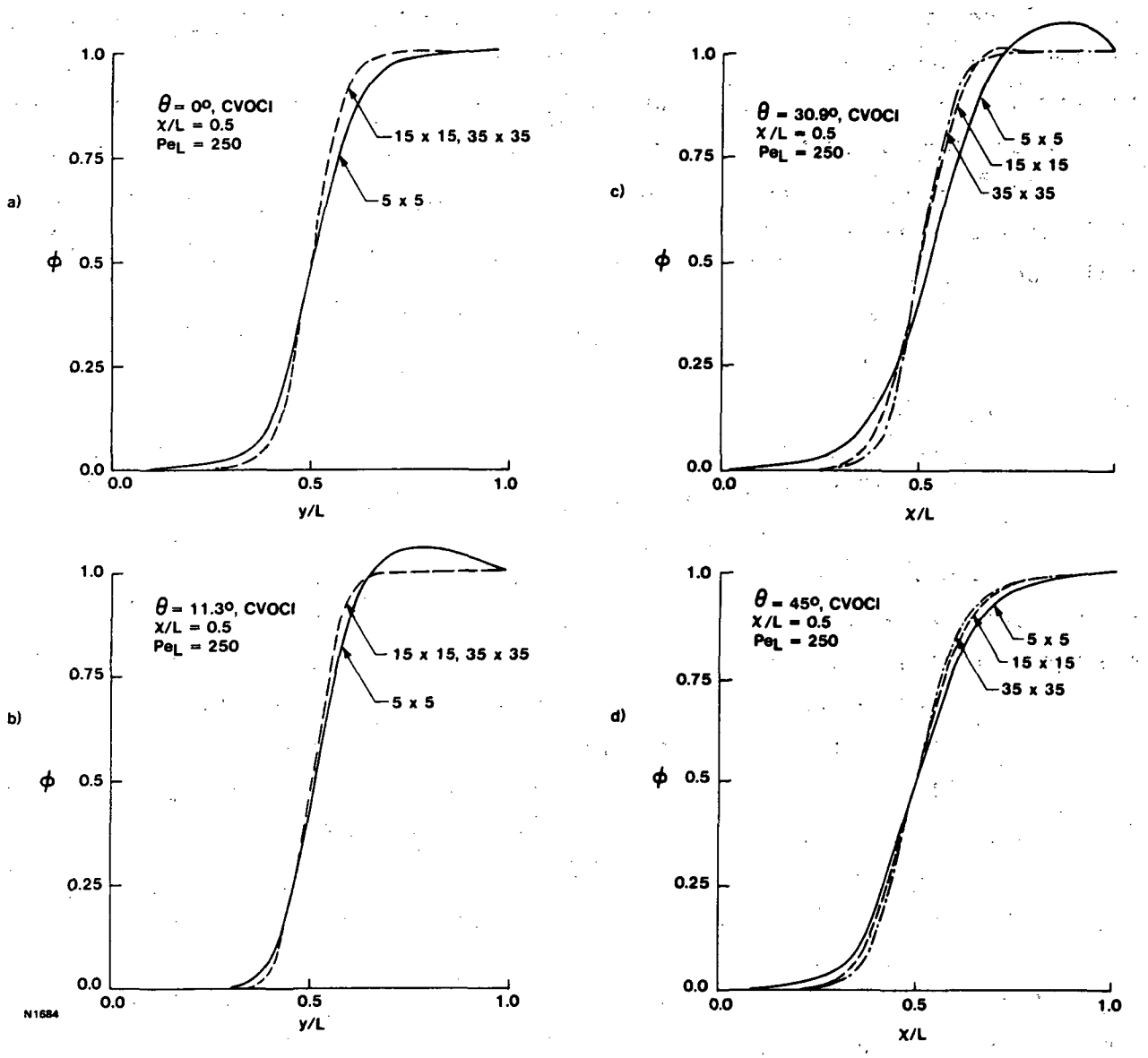

Figure 7.27 Centre-line Profiles of ø for Convected Step Problem, CVOCI

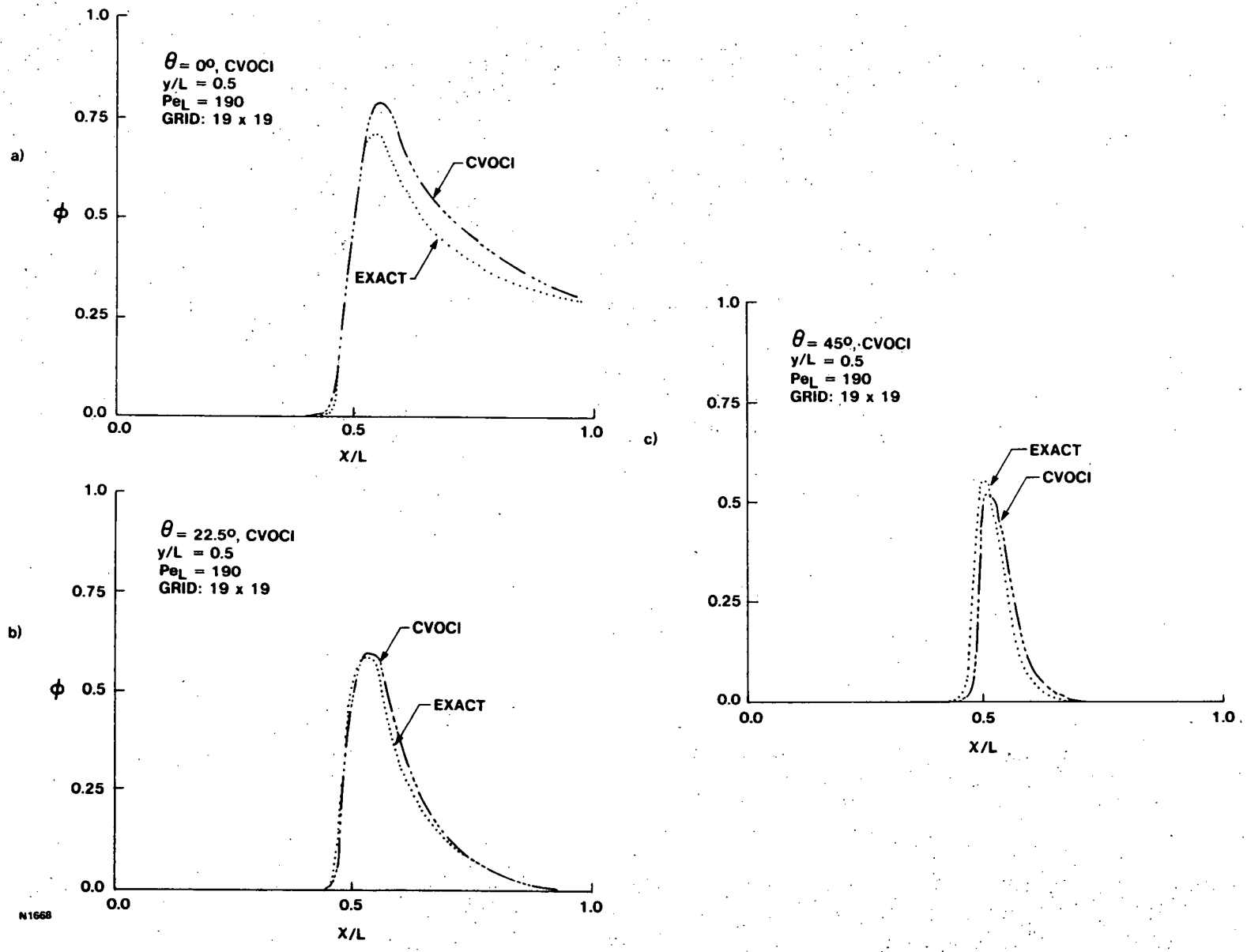

Figure 7.28 Centre-line Profiles of ø for Unit Source Problem, CVOCI

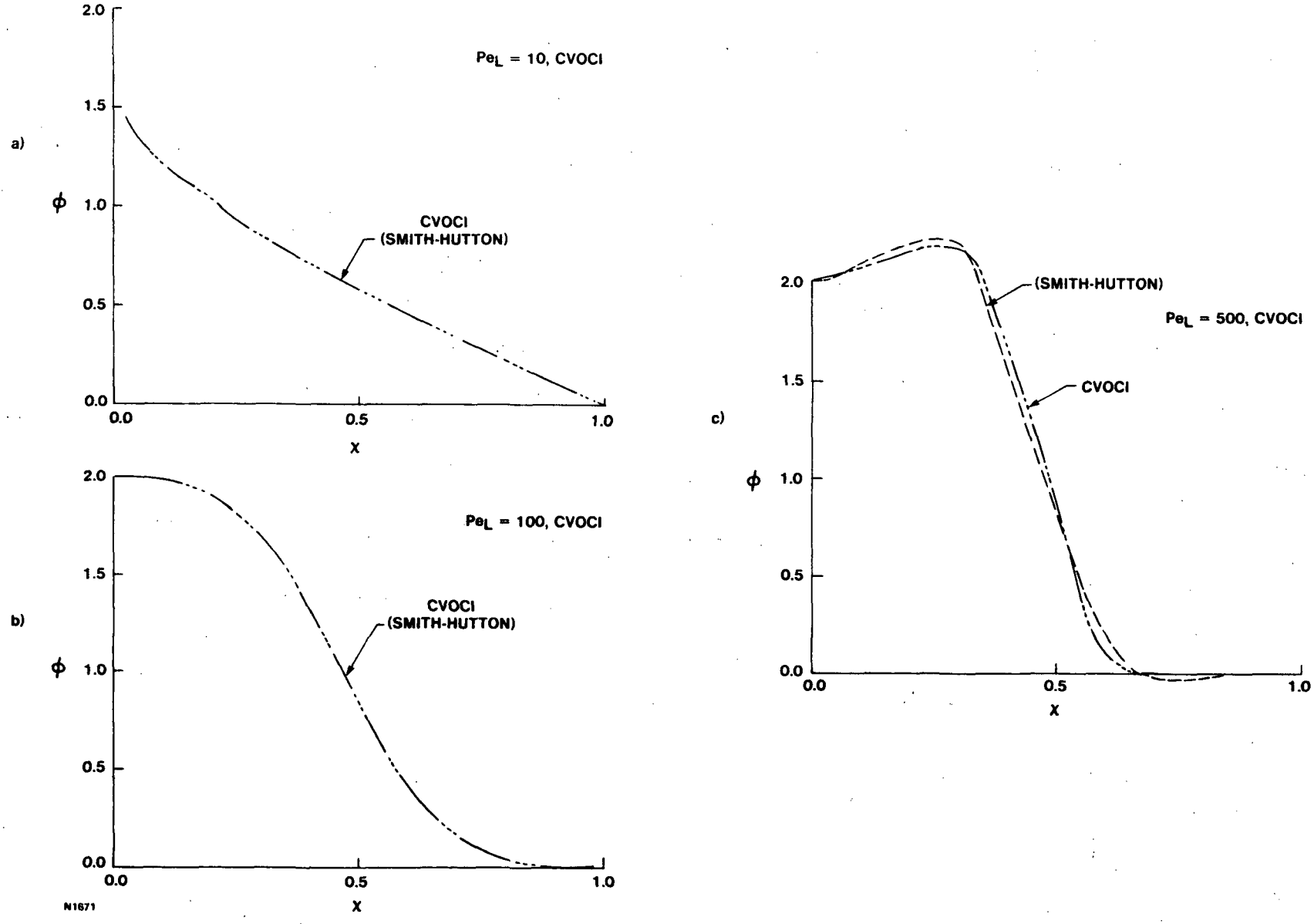

Figure 7.29 Outlet Profiles of ø for Smith-Hutton Problem, CVOCI

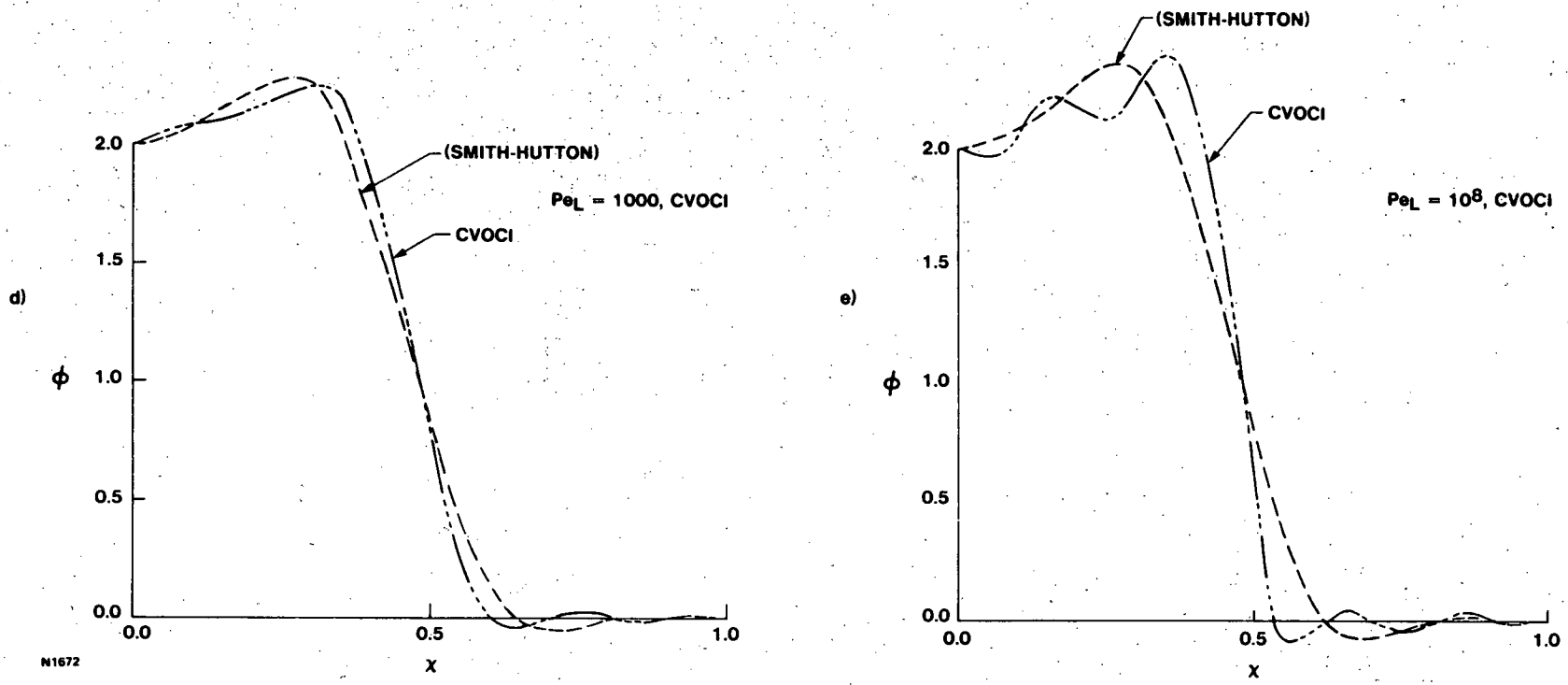

Figure 7.29 (cont.) Outlet Profiles of ø for Smith-Hutton Problem, CVOCI

7.4 CLOSURE AND SELECTION OF SCHEMES FOR THREE-DIMENSIONAL EVALUATION

This Section has presented the results of applying the previously selected techniques to test problems in order to evaluate their performance in enhancing convergence and efficiency as well as discretization accuracy. A summary is now provided outlining the conclusions along with recommendations for choices selected for three-dimensional evaluation. Convergence and efficiency enhancement aspects are discussed first.

Efficient numerical techniques for incompressible, viscous, recirculating flows should incorporate appropriate practices in the solution procedure to deal with the following issues of concern:

i) techniques used to treat nonlinearities

ii) techniques used to treat coupling between variables, e.g., pressure and velocity, swirl, etc.

iii) techniques used to solve equations for single scalars, specifically, the equation for pressure correction that arises in general segregated solution procedures.

In the present study attention was directed primarily towards improved techniques to effectively couple pressure and velocity and to solve efficiently the resulting pressure correction equation. Based on the results of suitable numerical experiments designed to evaluate the performance of repeated SIMPLEC together with SIP accelerated by CG, BC or ACM, the following conclusions are reached:

i) The introduction of repeated SIMPLEC significantly enhances convergence, reducing both the number of coefficient updates and CPU requirements. This is especially valuable for use with coefficient updates of CPU intensive discretization schemes like MW-SUDS and LP-SUDS.

ii) The introduction of an accelerated SIP to solve the pressure correction equation can significantly reduce CPU requirements; up to 40 percent for laminar flows and 20 percent for turbulent flows. Concerning the choices for the acceleration technique the following points are noted:

iii) Provided the computer storage is available, ACM provides the most effective acceleration of SIP.

iv) If it is known, a priori, that the solution for pressure varies principally in one coordinate direction, then BC acceleration is effective.

v) Conjugate Gradient acceleration exhibits poor convergence behavior on fine grids.

Based on these conclusions it is recommended that to enhance the efficiency of numerical solution of three-dimensional viscous, recirculating flows, SIP with ACM be used. Also, the improvement in efficiency provided by ACM in two-dimensional flows is expected to be even more dramatic in three-dimensional flows, where even on coarse grids, the number of unknowns is large. Finally, for three-dimensional applications, the incremental storage penalties associated with ACM are considerably smaller than they are in two-dimensional applications.

Further consideration of repeated SIMPLEC algorithm, despite its impressive performance in two dimensions, is outside the scope of the current effort. Thus, PISO was adopted as the improved pressure ~ velocity coupling algorithm in three dimensions.

Concerning improvements in discretization accuracy, the following points are noted based on the results of numerical experiments presented above:

i) Second Order Upwind differencing solutions are more accurate than solutions yielded by UDS, but can exhibit overshoots and undershoots as well as smearing of gradients on coarse grids, when the flow is at an angle to the grid. It is only on fine meshes where the second order rate of convergence is approached that the smearing and overshoots and undershoots diminish.

ii) Variants of Compact Implicit Schemes, specifically Control Volume based Operator Compact Implicit Schemes, produce solutions that are substantially more accurate than UDS solutions, but can exhibit relatively large overshoots and undershoots for multi-dimensional flows when the flow is at an angle to the grid. A probable cause for such non-physical solution features is identified as due to errors that arise from an inadequate treatment of flow curvature in the present implementation.

iii) Linear profile Skewed Upstream Differencing solutions have been demonstrated to be more accurate than the above SOU or CVOCI solutions with smaller overshoots and undershoots. Also for

laminar flow problems LP-SUDS has been shown to be at least 5 times more cost effective than UDS or its variants such as Hybrid.

iv) Mass Weighted Skewed Upstream Differencing solutions have been demonstrated to be free of overshoots and undershoots but not free of numerical diffusion. However, the numerical diffusion of MW-SUDS is considerably less than that of UDS. Consequently, MW-SUDS solutions are, in general, more accurate than UDS solutions, and, for laminar flows, MW-SUDS has been shown to be at least 2 times more cost effective than UDS.

v) The most accurate SUDS solutions are obtained when the Skewed Upstream differencing is modified to account for the effects of diffusion and sources. However, for positive definite variables like k and ε, incorporating diffusion and source term influences using the present implementation, together with the linear profile assumption is inappropriate. Thus, Mass Weighted skew without diffusion and source term influences is adopted for these equations with a corresponding degradation in performance, Section (7.3.2).

Based on the above conclusions, the recommendations for improved accuracy in three-dimensional applications are now stated, guided by the following criteria:

1) Best accuracy on coarse grids: even with advanced computers, many three-dimensional computations will still be limited to grids which are, at best, coarse.

ii) Robustness and stability: for three-dimensional applications it is important to ensure that numerical solutions are obtained. Particular reference is made here to k and ε equations.

iii) Efficiency: improvements in accuracy must be attained without excessive additional computational requirements.

Three-dimensional computations that use UDS or its variants such as Hybrid should instead adopt LP/MW-SUDS for improved discretizaton accuracy. The use of LP/MW-SUDS will: i) ensure robustness provided MW-SUDS is used whenever the potential of minor overshoots and undershoots of LP-SUDS cannot be tolerated; ii) significantly reduce or eliminate numerical diffusion, thereby providing a considerable improvement in accuracy; and iii) provide significant improvements in cost effectiveness. Naturally, modification of

skewed upstream differencing to include effects of diffusion and source terms should be included in LP/MW-SUDS whenever possible. Future efforts should be directed towards suitable incorporation of these effects in the k and ε equations. Finally, if only one scheme is to be considered for prediction of three-dimensional flows, the use of MW-SUDS is recommended.

8.0 DISCUSSION OF THREE-DIMENSIONAL TEST CASE

In Section 7, various techniques for improving the computational efficiency of numerical methods for two-dimensional, viscous, recirculating flows were tested and evaluated to assess convergence and accuracy issues. Based on these results it was recommended that, for three-dimensional applications the Strongly Implicit Procedure (SIP) with Additive Correction Multigrid (ACM), and Linear Profile or Mass Weighted Skewed Upstream Differencing (MW-SUDS and LP-SUDS) with corrections for diffusion and source term influences, when appropriate, be used. Upon implementing these recommendations and testing the resulting software, it was determined that several alternatives regarding solver performance and additional considerations in the implementation SUDS schemes were worthy of further study. These will now be discussed in detail.

8.1 EVALUATION OF TECHNIQUES FOR IMPROVING COMPUTATIONAL EFFICIENCY

The alternatives concerning the previously recommended solver choices included the following:

i) using Incomplete Choleski (IC) instead of SIP to save computer storage

ii) using 3x3x3 blocks for ACM instead of 2x2x2 blocks, again, to save storage, Section (6.5.4)

iii) using Block Correction (BC) in conjunction with ACM to further improve computational efficiency.

The merits and shortcomings of these alternatives are now assessed using the following test problem in Cartesian coordinates

$$\nabla^2 \phi + S = 0 \quad \begin{matrix} 0 \le x \le 32 \\ 0 \le y \le 10 \\ 0 \le z \le 8 \end{matrix} \qquad (8.1)$$

where

$$\frac{\partial \phi}{\partial h} = 0 \quad \text{at all boundaries and}$$

$S(x,y,z) = 0$ except $S(0,5,z) = -1.0$ and $S(32,5,z) = 1.0$. In equation (8.1) ∇^2 is the usual Laplacian and h is normal to the boundary. This problem

was chosen because the resulting discrete algebraic equations are similar to the pressure correction equations of Section (6.1).

Using a Central Differencing Scheme (CDS) on a 32x10x8 grid, solutions to the resulting algebraic equations were obtained using the various solution techniques. Figures (8.1), (8.2) and (8.3) present the sum of the squares of residuals versus computational effort for the various solution techniques. A more detailed discussion of the results presented in each figure follows:

8.1.1 SIP vs IC

The recommendation to use SIP in conjunction with ACM is based on two-dimensional results, where the storage requirements of iterative solvers such as SIP are not a primary concern. However, in three-dimensional applications computational storage requirements can very often exceed the resources available. One approach to reducing the storage requirements is to use SIP with no partial cancellation, which is algebraically equivalent to IC. Storage requirements for various solution techniques are summarized in Table (8.1).

TABLE (8.1) STORAGE REQUIREMENTS OF ALTERNATIVE SOLUTION TECHNIQUES

Technique	Storage Words/Node
SIP	9.0
IC	3.0
SIP-ACM(2)	11.6
IC-ACM(2)	4.7
IC-ACM(3)	3.5
IC-BC-ACM(2)	4.7
IC-BC-ACM(3)	3.5

As illustrated in figure (8.1), it is clear that the rate of convergence of SIP with a near optimal partial cancellation is superior to the rate of convergence of IC. Even with the storage penalty it may be more advantageous to use SIP over IC. However, when ACM(2) (the (2) notation denotes blocks of 2x2x2 fine grid control volumes used) is used to accelerate SIP or IC there is little or no advantage to using SIP-ACM(2), especially if the cost of determining the optimal partial cancellation is taken into account. Also, the

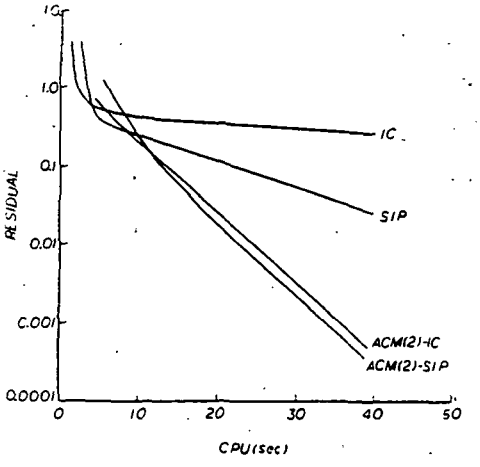

Figure 8.1 **Residual versus CPU for IC, SIP, ACM(2)-IC and ACM(2)-SIP**

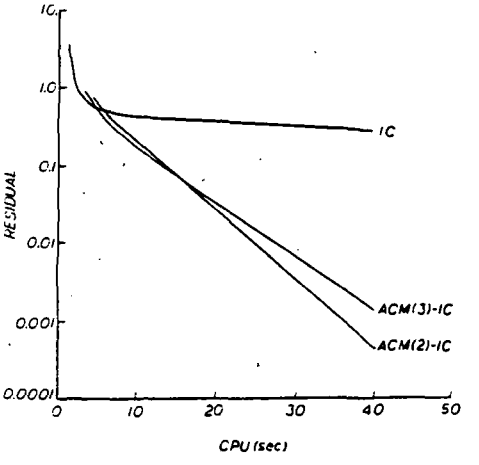

Figure 8.2 **Residual versus CPU for IC, ACM(2)-IC and ACM(3)-IC**

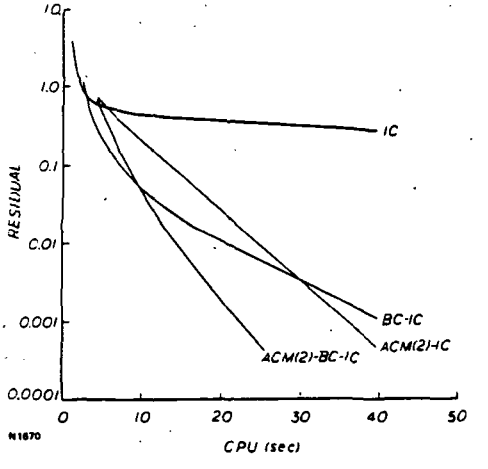

Figure 8.3 **Residual versus CPU for IC, BC-IC, ACM(2)-BC-IC and ACM(2)-BC-IC**

results in figure and Table (8.1) indicate that it is more cost effective, in terms of both computational storage and effort to use IC-ACM(2) instead of SIP-ACM(2).

8.1.2 ACM(2) vs ACM(3)

Another approach to reducing the storage requirements of the solution techniques is to apply the Additive Correction Strategy to blocks consisting of 3x3x3 fine grid control volumes, denoted by ACM(3), instead of blocks of 2x2x2 fine grid control volumes. As listed in Table (8.1) the storage requirements of ACM are reduced by 1.2 words/control volume by using blocks of 3x3x3 instead of blocks of 2x2x2. The results show in figure (8.2) indicate that the reduced storage requirements of ACM(3) are offset by a lower rate of convergence. Considering the minimal reduction in storage requirements and lower rate of convergence of ACM(3), it is recommended that ACM(3) be used only if the reduction in storage is necessary.

8.1.3 Block Correction (BC)

The results shown in figures (8.1) and (8.2) illustrate the dramatic acceleration of convergence that results from using ACM. However, based on two-dimensional results, an even more dramatic acceleration was expected. This is especially true of problems, like the test problem in rectangular domains and a solution having a significant (but not necessarily dominant) one-dimensional component (in this case the x-direction). A more appropriate acceleration technique for problems with a dominant one-dimensional component is BC, Section (6.5.3). As illustrated in figure (8.3), BC provides an acceleration of IC which is comparable to that of ACM(2) indicating that there is a strong but not dominant one-dimensional component to the solution of the test problem (if the one-dimensional component were dominant, IC-BC would converge considerably faster than IC-ACM(2)). As shown in figure (8.3), combining both ACM and BC to accelerate IC, denoted by IC-BC-ACM(2), results in convergence acceleration which is superior to either ACM or BC used alone. Note also that there is no significant storage penalty associated with the use of BC, Table (8.1).

These results indicate that for three-dimensional problems, the IC base solver does not always provide a sufficient amount of smoothing or relaxation of the solution for ACM to be most effective. Combining BC with IC provides

C-3

the necessary smoothing, particularly if there is a strong, but not necessarily dominant, one-dimensional component to the solution.

8.1.4 Conclusions

These results, as well as others, indicate that IC-BC-ACM(2) is a solution procedure with a high rate of convergence over a wide range of problems with a minimal storage penalty, and should significantly improve the computational efficiency of numerical methods used to predict three-dimensional viscous, recirculating flows.

8.2 CONSIDERATIONS IN EXTENDING MW-SUDS AND LP-SUDS FORMULATION IN THREE-DIMENSIONS

The variants of SUDS Schemes, MW-SUDS and LP-SUDS, are designed to provide an accurate representation of the convective component of a general transport problem within the framework of a finite volume discretization approach. Using extensions of the two-dimensional ideas discussed in Section (6.3), an approximation is required for the interface convective flux, upon suitably integrating the parent transport equation over the finite volume, i.e.,

$$C = \int_A \rho \vec{v} \phi \, dA \qquad \text{Equation (6.4)}$$

where ϕ is the dependent variable, ρ is the density, $\vec{v}$ is the component of velocity normal to the control volume face and A is the area of the control volume face. In three-dimensions the above integral is evaluated using four integration points on each control volume force, figure (8.4).

To express the variable values at the integration point in terms of neighbouring nodal values, a discrete representation is required for the following non-conservative differential transport equation in streamline coordinates,

$$\rho V \frac{\partial \phi}{\partial s} = Q \qquad \text{Equation (6.39)}$$

where V is the magnitude of the velocity, s is the streamwise coordinate and Q represents all diffusive and source term influences. The different approaches to obtaining representations of equation (6.39), as discussed in Section (6.3), distinguish LP-SUDS from MW-SUDS.

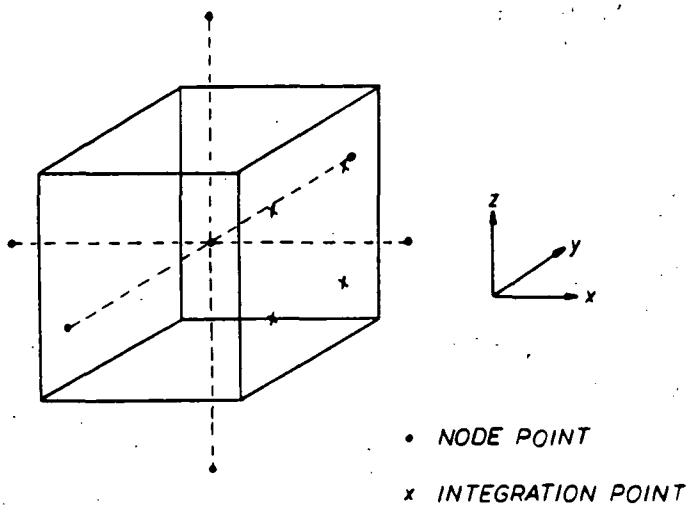

Figure 8.4 Three-Dimensional Node Layout

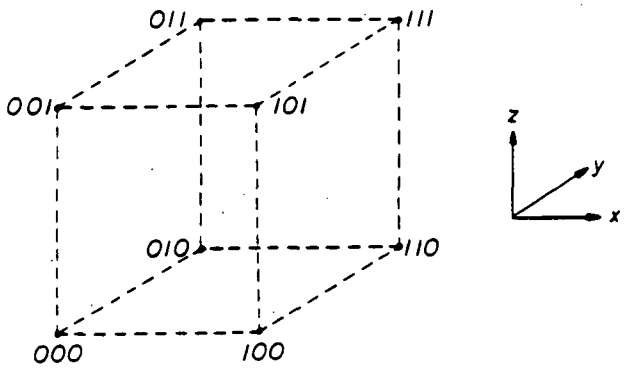

Figure 8.5 Three-Dimensional Flux Element

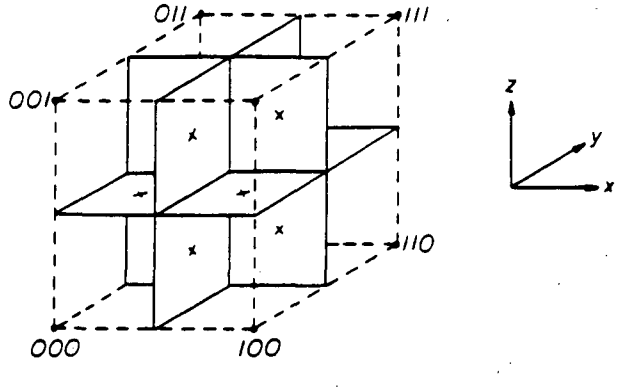

N1692

Figure 8.6 Flux Element with Control Volume Faces and Integration Points

To describe the manner in which the discrete representations of equation (6.39) are arrived at in three dimensions, a systematic basis is required in the following formulation, to describe the indexing associated with nodes, integration points, flux elements, etc. This is introduced in figures (8.5) and (8.6). It will be seen from figure (8.5) that the eight nodes surrounding any integration point define the eight corners of a flux element, and the element so defined contain octants of eight different control volumes, figure (8.6). Also each element contains twelve integration points with four integration points lying on each of the three planes that are coincident with control volume faces and intersect the flux element, figures (8.7), (8.8) and (8.9).

In the interest of clarity, the triplet of binary indices illustrated in figure (8.5) will be used to refer to a node or quantities associated with a node. When reference is made to integration points or quantities associated with the integration point, the symbols X, Y and Z along with the corresponding triplet of binary indices, shown in figures (8.6), (8.7), (8.8) and (8.9) will be used.

8.2.1 Explicit LP-SUDS Integration Point Equation

To formulate a discrete representation of equation (6.39) for the integration point O11 lying on the control volume faces coincident with the X plane, figure (8.7), the streamline is upwinded from the integration point until it intersects a flux element side. The convective component of equation (6.39) is then discretized, in a similar manner to the two-dimensional case, as:

$$\rho V \frac{\partial \phi}{\partial s} = \rho \frac{V}{L} (\phi_{X011} - \phi_u) \qquad (8.2)$$

where ϕ_u is the value of ϕ at the point of intersection and L is the distance from the integration point to the intersection. In LP-SUDS, as discussed in Section (6.3), the value of ϕ_u is determined from a bilinear interpolation of the node values of ϕ lying on the intersected flux element side. The discrete representation of the right-hand side of equation (6.39), Physical Advection Correction (PAC), is obtained from a trilinear interpolation of the discrete nodal values of Q.

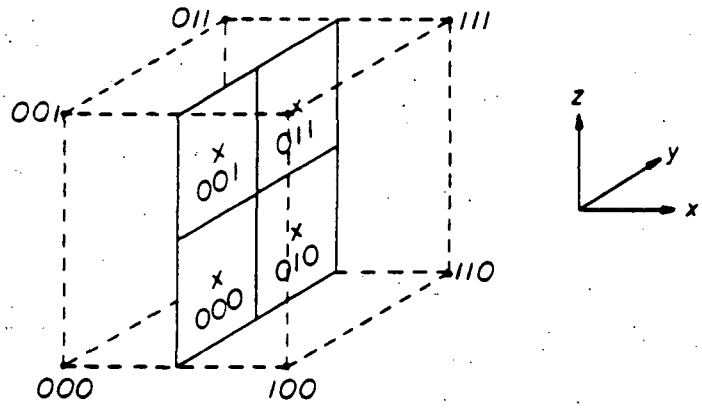

Figure 8.7 Integration Points on Control Volumes Faces Coincident with X-Planes

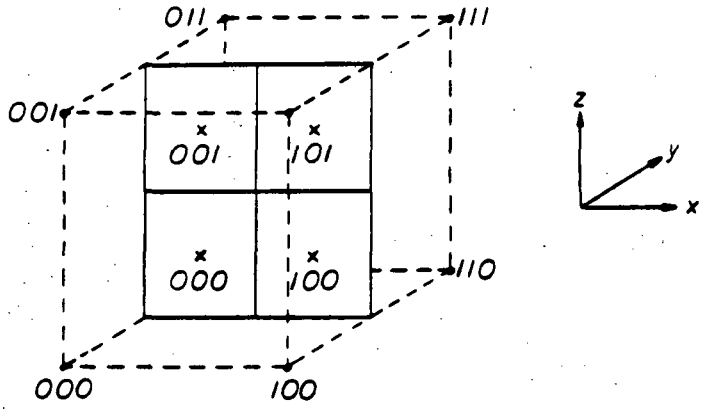

Figure 8.8 Integration Points on Control Volume Faces Coincident with Y-Planes

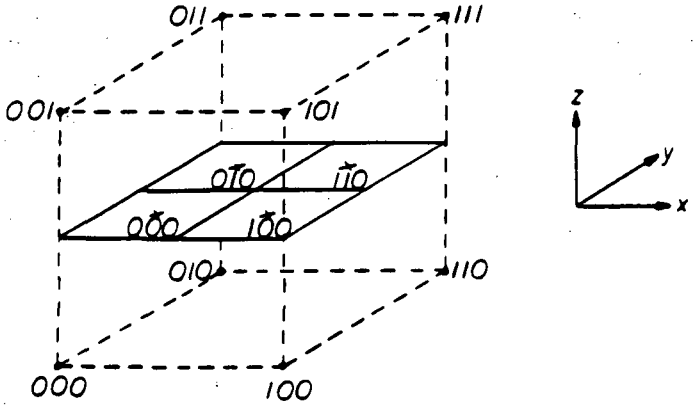

N1681

Figure 8.9 Integration Points on Control Volume Faces Coincident with Z-Planes

Rearranging, the discrete representation of equation (6.39) is expressed as:

$$\phi_{XO11} = \phi_u + \frac{L}{\rho V} Q \qquad (8.3)$$

Examining the last term of equation (8.3), it is evident that some difficulties may arise when evaluating this term as V approaches zero. Fortunately, as V approaches zero the grid Peclet number also becomes small (i.e., the Peclet number is much less than 2). Thus, the integration points representation of ϕ given in equation (8.3) can instead be evaluated using a trilinear interpolation of node values (cf. flux blending approaches),

$$\phi_{XO11} = \sum_{NP} N_{NP} \phi_{NP} \qquad (8.4)$$

where the N are the shape functions, borrowing from the finite element approach, and the summation is made over the eight nodes of the flux element. Since the Peclet number is low, the resulting CDS-like scheme will not generate negative downstream a coefficients as would occur for high Peclet numbers. To ensure that equation (8.4) is used instead of equation (8.3) for low Peclet number applications, the integration point value is determined from a weighted average of equations (8.3) and (8.4)

$$\phi_{XO11} = (1-B) \sum_{NP} N_{NP} \phi_{NP} + B \left(\phi_u + \frac{L}{\rho V} Q\right) \qquad (8.5)$$

where $B = Pe^2 / (5 + Pe^2)$ and is derived using the approximate exponential weighting scheme of Raithby and Torrance[80] ensuring that no downwind negative a coefficients result.

It is seen from the above discussion that the explicit LP-SUDS formulation in three-dimensions follows readily from two dimensions, once an appropriate set of indices is introduced.

8.2.2 Explicit MW-SUDS Integration Point Equations

In the process of extending the two-dimensional explicit MW-SUDS integration point equations to three dimensions, it became evident that the

extensions to three dimensions was not uniquely determined by analogy with the two-dimensional algorithm. To overcome this, additional constraints had to be imposed on the mass weighting logic. As a result, the following description of explicit MW-SUDS is not a direct extension of the two-dimensional scheme. However, in the two-dimensional limit the three-dimensional MW-SUDS presented below is algebraically equivalent to two-dimensional MW-SUDS.

The primary difference between LP-SUDS and MW-SUDS lies in the evaluation of ϕ_u. In MW-SUDS the evaluation of ϕ_u is chosen to ensure that the resulting a coefficients are everywhere non-negative. To accomplish this the evaluation of ϕ_u is determined by logically deducing where the mass flows crossing a control volume face originated. For instance, consider the case where the mass flow crossing the X011 integration point control volume face is leaving the 011 octant. The possible contributions to this mass flow are from the mass flows through the two integration point faces, Y001 and Z010, as well as the mass flows through the three octant faces intersecting at node 011. To ensure positive a coefficients it is assumed that any integration or node mass flows leaving the octant cannot contribute to the X011 mass flow. Taking a positive mass flow weighted average, ϕ_u is approximated by:

$$\phi_u = \frac{F_{Y001}\,\phi'_{Y001} + F_{Z010}\,\phi'_{Z010} + F_{011}\,\phi_{011}}{F_{Y001} + F_{Z010} + F_{011}} \tag{8.6}$$

where F represents the mass flow through the corresponding face of the octant and the value of F is nonzero only if the mass flow is into the octant, and where ϕ'_{Y001} and ϕ'_{Z010} are estimates of the corresponding integration points. By similar positive mass weighting augments, the estimates of the integration points are given by:

$$\phi'_{Y001} = \frac{F_{X001}\,\phi_{011} + F_{Z000}\,\phi'_{Z000} + F_{001}\,\phi_{001}}{F_{X001} + F_{Z000} + F_{001}} \tag{8.7}$$

$$\phi'_{Z010} = \frac{F_{X010}\,\phi_{011} + F_{Y000}\,\phi'_{Y000} + F_{010}\,\phi_{010}}{F_{X010} + F_{Y000} + F_{010}} \tag{8.8}$$

where ϕ'_{Y000} and ϕ'_{Z000} are, again, estimates of integration point values. Also note that in equation (8.7) the node value, ϕ_{011}, is used to approximate the value of the integration point, ϕ_{X011}. This approximation is used to ensure that an explicit relation for ϕ_{X001} results and that the resulting a coefficients are not negative.[30] Similarly, ϕ_{011} is used to approximate the value of ϕ_{X010}. Finally, positive mass weighting arguments and approximations are used to obtain:

$$\phi'_{Y000} = \frac{F_{000}\,\phi_{000} + F_{X000}\,\phi_{011} + F_{Z000}\,\phi_{011}}{F_{000} + F_{X000} + F_{Z000}} \tag{8.9}$$

$$\phi'_{Z000} = \frac{F_{000}\,\phi_{000} + F_{X000}\,\phi_{011} + F_{Y000}\,\phi_{011}}{F_{000} + F_{X000} + F_{Y000}} \tag{8.10}$$

Combining equation (8.3) and equations (8.6) through (8.10), ϕ_{X011} can be expressed in terms of the nodal values ϕ_{011}, ϕ_{010}, ϕ_{001} and ϕ_{000}.

The evaluation of the PAC term of equation (8.3) is identical to that described for LP-SUDS except that the application of the PAC term may have to be omitted if bounded solutions are to be guaranteed, Section (7.3.2). Therefore, for the solution of turbulent kinetic energy and dissipation PAC is not incorporated in the formulation.

In the low Peclet number limit, MW-SUDS scheme outlined above is combined with a linear interpolation of nodes 011 and 111, with the same weighting given in equation (8.5). For instance, for ϕ_{X011}

$$\phi_{X011} = (1-B)\,[N_{011}\,\phi_{011} + N_{111}\,\phi_{111}] + B\,(\phi_u + \frac{L}{\rho V}\,Q) \tag{8.11}$$

Note that when PAC terms are omitted in MW-SUDS, the linear interpolation of nodes in equation (8.11) is not required and B can be set to unity.

8.2.3 Flux Element Assembly

Using either the LP-SUDS or MW-SUDS approach, expressions explicitly relating integration points to node points can be obtained for each integration point in the flux element. The influences of each integration point are then assembled into the appropriate control volume flux balance equation by substituting each integration point expression into the appropriate control volume face convective evaluation. The result is a control volume flux balance equation which is expressed in terms of nodal points.

8.3 THREE-DIMENSIONAL TEST CASE

To illustrate the potential quantitative impact of incorporating the above techniques to enhance discretization accuracy and solution convergence in the baseline TEACH code, Section (7.2), a number of numerical predictions were obtained. The test problem considered here refers to the flowfield characteristics of a typical three-dimensional turbulent flow in which a row of jets are injected normal to the incoming flow in a duct with a rectangular cross section. The problem details adopted (configurations, inlet velocity and turbulence description, etc.) are similar to those examined in (5) with the exception that the initial computations employed square cross-section jets rather than circular. The case of circular jets along with comparison with experimental data, provided by Khan[96], are also presented for rigorous quantitative evaluation.

To illustrate the improvements in computational efficiency, the CPU requirements of a Masscomp MSC Series 500 were measured to obtain predictions using the baseline code and the modified code with ACM (2x2x2 blocks) in conjunction with IC-BC for the pressure correction updates of PISO. To achieve a convergence of 0.005 using Hybrid differencing, the baseline code, on a 18x8x4 grid, required 80 iterations and 62 minutes of CPU. To achieve the same convergence with the same differencing and on the same grid, the use of IC-BC-ACM reduced the iterations required to 39 and the CPU requirements to 29 minutes. The results of this exercise indicate that, for the problem selected, the convergence of the baseline code is limited by the poor convergence characteristics of the TDMA used to solve the pressure correction equations and that the IC-BC-ACM technique can dramatically improve overall convergence and computational efficiency.

To illustrate the impact of the improvements in accuracy, numerical predictions of the test problem were obtained using the baseline Hybrid differencing, MW-SUDS and LP-SUDS on 18x8x4 and 18x14x8 grids.

All of the calculations were performed using PISO with IC-BC-ACM used to solve the pressure correction equations. The number of iterations required to achieve a convergence level of 0.005 are presented in Table (8.2).

TABLE 8.2 NO. OF ITERATIONS FOR JET IN A CROSS FLOW PROBLEM

SCHEME	GRID	NO. OF ITERATIONS
Hybrid	18x8x4	39
MW-SUDS	18x8x4	46
LP-SUDS	18x8x4	53
Hybrid	18x14x8	61
MW-SUDS	18x14x8	74
LP-SUDS	18x14x8	82

The computational effort per iteration for the SUDS schemes is approximately 7 times that required by the Hybrid Scheme. This large increase is not surprising considering that the SUDS schemes use four integration points per control volume face compared to the one for Hybrid and that the calculations required at each integration point are more complex for the SUDS schemes. This increase in computational effort could be reduced significantly with more efficient coding techniques. Unfortunately, this would require a complete overhaul of the existing TEACH Code.

Comparisons of calculated results for the axial velocity components at a location 4 jet widths downstream of the jet centre-line are shown in figure (8.10). As expected, the Hybrid results exhibit what appears to be a considerable amount of smearing with only minor improvements on the finer grid. Using the modified code, the SUDS results exhibit considerably less smearing with LP-SUDS producing results with the least amount of smearing. These results indicate that the accuracy of turbulent flows can be improved using the modified SUDS schemes and, considering the excessive smearing exhibited by Hybrid, even on finer grids, the additional cost per iteration of the modified SUDS schemes may very well be offset by the improved accuracy of the results.

Considering the performance of LP-SUDS in the light of experimental data, figures (8.11), (8.12) and (8.13) display axial velocity profiles at locations 4 and 6 jet widths downstream of the jet centre-line using grids of 34x10x15 and 40x20x17 respectively. The grids used in these predictions approximate the circular cross-section of the jets as well as the axial domain

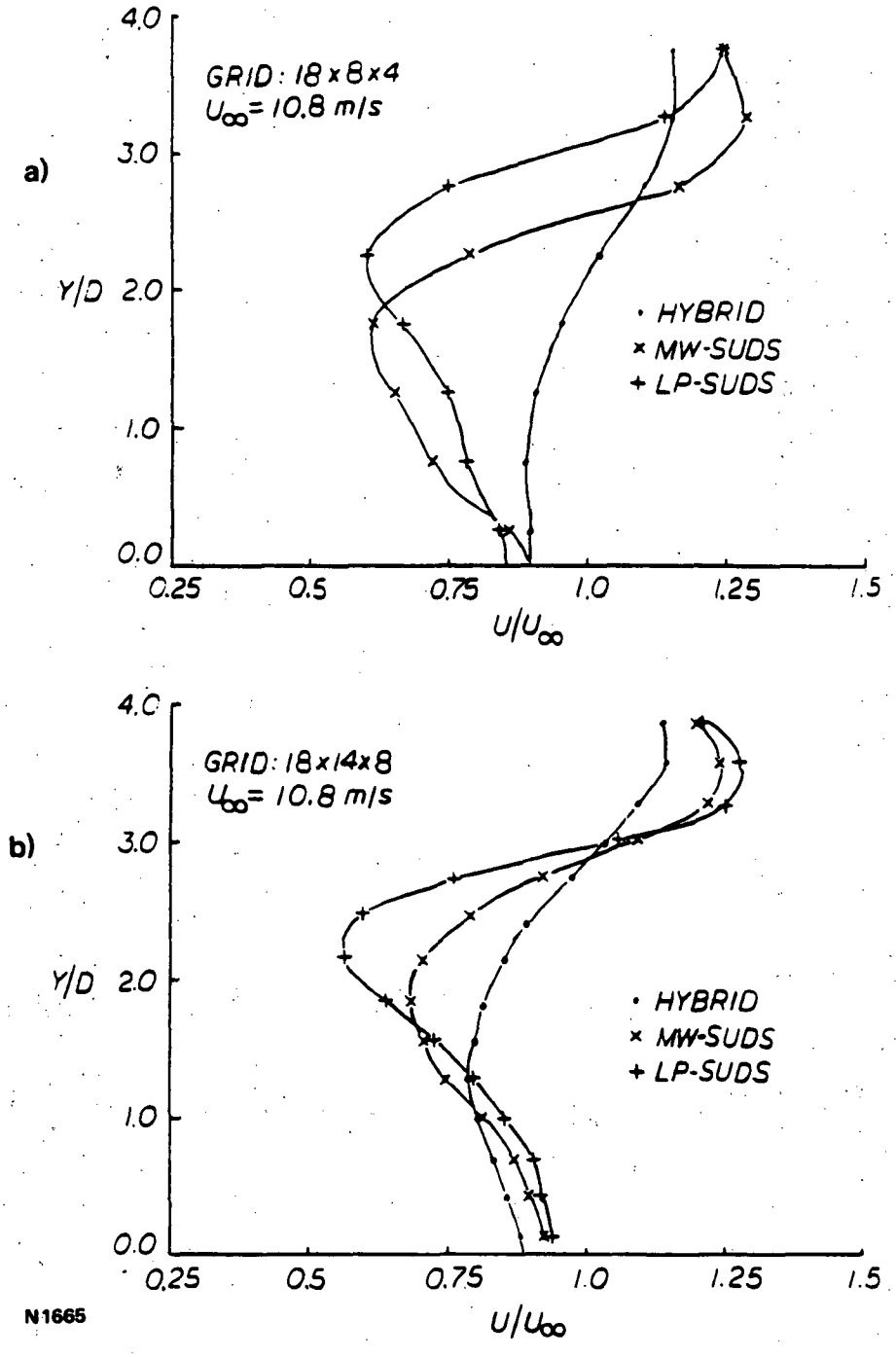

Figure 8.10 Axial Velocity Profiles 4 Jet Widths Downstream of the Jet Centre-line

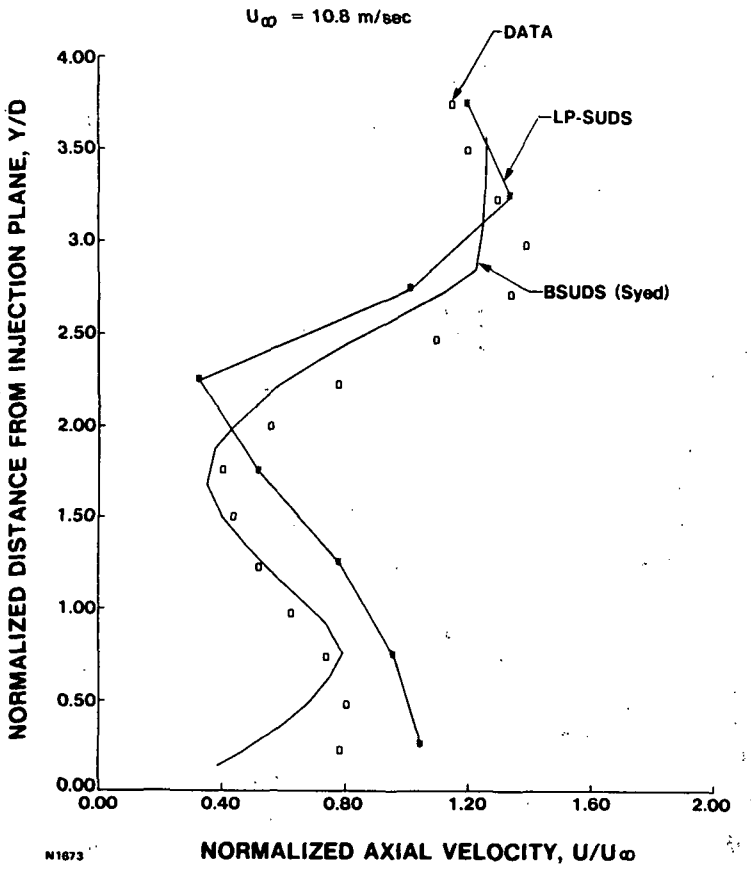

Figure 8.11 Comparison of Calculated and Measured Axial Velocity Profiles at x/D = 4 From Jet Centre-line and z/D = 0 using a Grid of 34 x 10 x 15

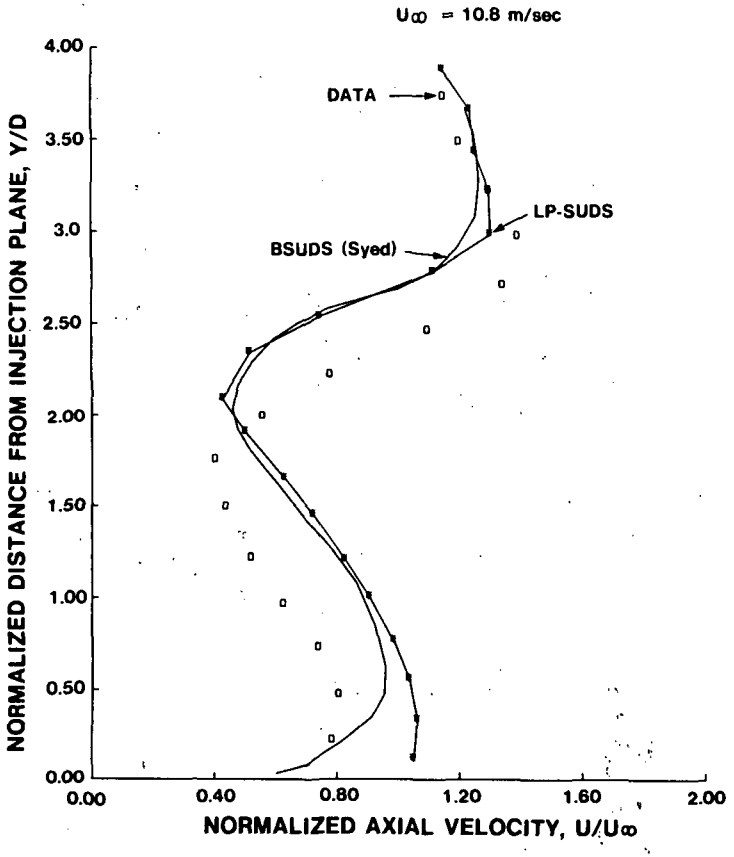

Figure 8.12 Comparison of Calculated and Measured Axial Velocity Profiles at x/D = 4 From Jet Centre-line and z/D = 0 Using a Grid of 40 x 20 x 17

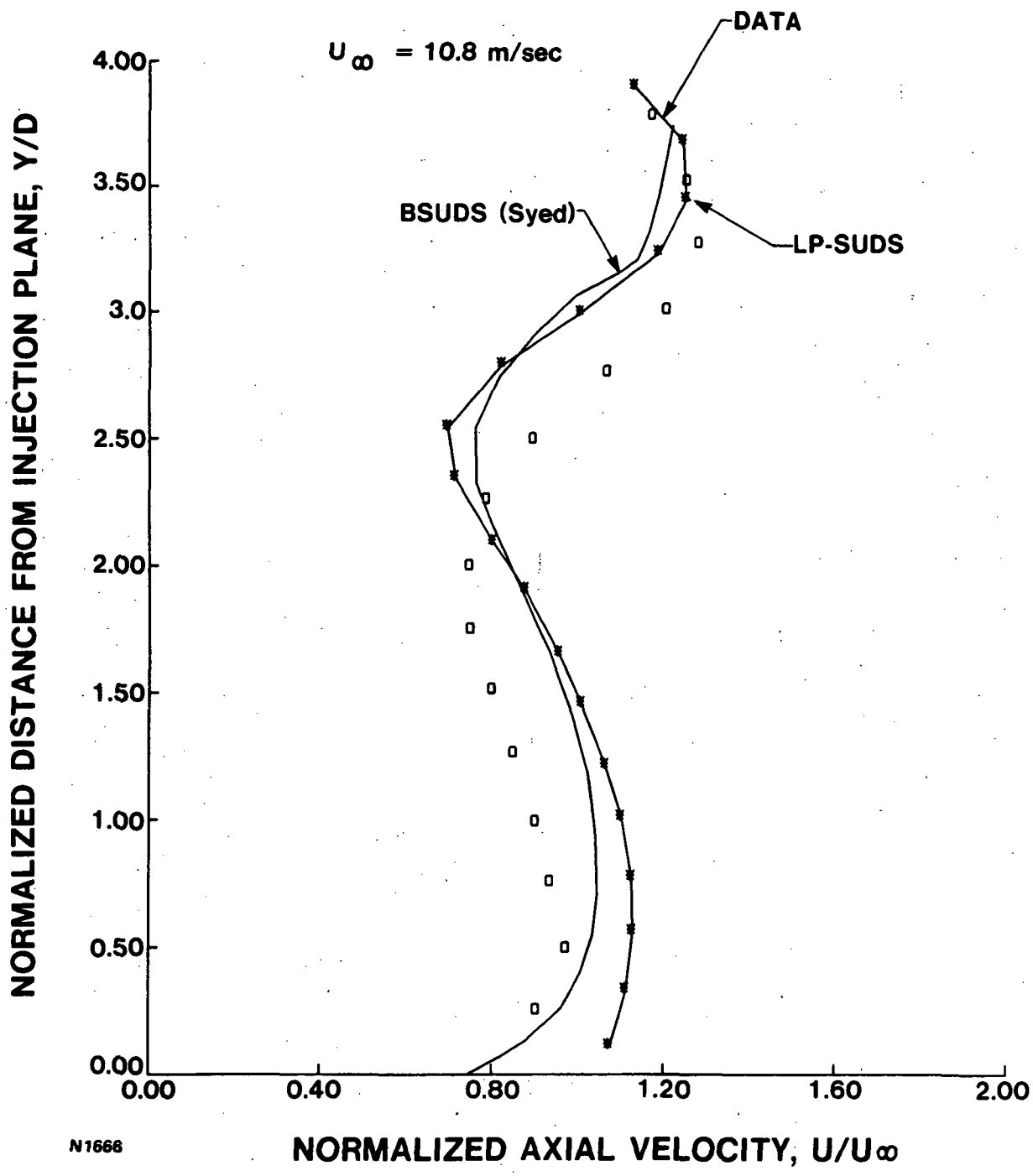

Figure 8.13 Comparison of Calculated and Measured Axial Velocity Profiles at x/D = 6 From Jet Centre-line and z/D = 0 Using a Grid of 40 x 20 x 17

width in a manner identical to that reported in (5), but otherwise employ a uniform grid distribution in the radial direction. Also, plotted on the above figures are the corresponding experimental data provided by Khan[96] and the predictions obtained by Syed, et al[5] using bounded skewed differencing.

The initial jet velocity profile used for the predictions incorporate the experimentally measured centre-line profile,[5] but otherwise use a mass conserving similarity criteria to provide the variation in the tangential and axial width of the jet. The inlet profile for the approach flow assumed a top hat profile due to unavailability of experimental data. Use of such an idealized profile, considering the proximity of the jets to the inlet, along with the assumed turbulence intensity levels (1 percent for both flows) are serious issues of concern for rigorous quantitative evaluation. However, figure (8.11) revelas that the basic profile shape is predicted well with some radial displacement in the peak minimum velocity location. This latter feature is characteristic of profiles generated by both grids and would tend to suggest need for a closer examination of the various inlet profiles used. Also, the coarseness of the grid in the vicinity of the jets, as well as the inappropriateness of the k-ϵ model to model severely anisotropic turbulence fields, Crabb,[97] might have contributed to the observed behavior. Even though the bounded skewed differencing profiles agree with the experimentally measured values better at certain locations, both near the jet inlet and the roof, significant discrepancies are apparent due to the coarseness of the grid employed. In general, LP-SUDS profiles are less corrupt by numerical diffusion but tend to overpredict experimental values, possibly due to poor modelling of turbulence and inlet profiles.

Figures (8.12) and (8.13) display the axial velocity profiles obtained at 4 and 6 jet widths of the jet centre-line using a grid of 40x27x17. The solution difficulties reported by Syed, et al[5] in determining an appropriate local blending factor for use with bounded skewed differencing (corresponding results are also displayed) were absent from LP-SUDS predictions. It is seen from the above figures that LP-SUDS produces improved profiles that agree well with the experimental values in basic shape, albeit radially shifted, with the numerical values of the peak minimum velocities in much closer agreement with experiments than bounded skew predictions. However, the two schemes in this case yield profiles that agree closely over a larger portion of the flow field (hence significant improvements over Hybrid differencing) in spite of the large discrepancies observed in the vicinity of the jet

inlet. The reservations expressed in relation to figure (8.11) are also valid for these figures in quantitatively evaluating the performance of LP-SUDS with experimental data.

Although significant improvements are observed in LP-SUDS prediction with grid refinement from a study of figures (8.11) and (8.12), it is not assured that the solution yielded by a grid of 40x27x17 (still coarse for a problem of this kind) is grid independent. Local grid refinement near the jet inlet might be required to capture the relevant flow details. However, the computational cost associated with obtaining grid independent solutions during the present effort was prohibitive.

8.4 CLOSURE

This Section has developed and assessed the previously selected SUDS schemes, as well as various accelerated schemes appropriate for pressure correction equation of segregated solution algorithms for three-dimensional applications. For modelling the jet in a cross flow problem, adopted as the relevant test case, significant improvements in overall convergence and computational efficiency were provided by the use of IC-BC-ACM, while the variants of SUDS yielded solutions that exhibit considerably less smearing than those of Hybrid differencing. A number of questions pertaining to inlet profile specification, along with the previously reported shortcomings of $k-\varepsilon$ to model the details of the anisotopic turbulence field generated by a jet in a cross flow, were raised for a quantitative assessment. It was also concluded that, in spite of the significant additional cost associated with the use of improved SUDS schemes in three-dimensional applications, their cost effective use is still recommended on grounds of improved accuracy, as Hybrid solutions are plagued with excessive smearing.

9.0 CLOSURE

9.1 SUMMARY AND DISCUSSION

Numerical techniques to predict incompressible, turbulent, viscous, recirculating flows frequently encountered in gas turbine engine components have undergone rapid development within the last decade. However, some fundamental problems still exist that limit the performance of such methods in routine engineering computations. Such issues refer to discretization inaccuracies introduced when the parent differential transport equations are replaced by discrete algebraic equations and the computer resources required to solve these discrete equations. This study was motivated by the need to address both of these problems in a comprehensive manner.

The effort was initiated by identifying the desirable attributes that optimum discretization schemes and cost effective solution methodologies should possess to provide a unified assessment criteria for subsequent quantitative/qualitative evaluations. As adopted in the present study, these criteria comprise guidelines to define critical issues of accuracy, stability (robustness), efficiency, storage requirements and ease of implementation in a three-dimensional code structured in TEACH methodology. The initial evaluation of more than ten potential techniques considered was primarily based on examination of accuracy and linear stability of the resulting difference equations via evaluation of the properties of the coefficient matrix, Taylor series analysis and existing heuristic stability analyses for iterative solvers commonly used in segregated solution procedures.

Upon completion of this initial evaluation four of the most promising techniques were incorporated in a variant of 2D-TEACH code for further quantitative evaluation using carefully selected test problems. The particular schemes selected address issues of both discretization accuracy and convergence enhancement. The latter concern in this study specifically refers to the solution techniques adopted for the pressure/correction equation(s) generated by general segregated solution algorithms for incompressible flows, although similar practices could be equally employed in solving for momentum and other scalars. However, the pressure/correction equation which displays a symmetric

structure with properties similar to those for a diffusion process, accounts for a major portion of the solution cost associated with segregated solution procedures.

Effective solution of the pressure/correction equation in this study was accomplished by adopting approximate factorization techniques, including the Incomplete Choleski (IC) and Stone's Strongly Implicit Procedure (SIP), in place of the Alternating Direction Line Gauss-Seidel (ALGS) commonly used. However, the high initial convergence rate displayed by IC and SIP in test problems due to removal of high frequency error components was severed, as the asymptotic convergence rate is usually dictated by removal of low frequency error components which are not diminished effectively by such base solvers. To overcome this difficulty and to simultaneously address the complete error spectrum, a series of accelerators including Conjugate Gradient (CG), Block Correction (BC) and Additive Correction Multigrid (ACM) were considered for use with IC and SIP.

The performance of these accelerated solvers were evaluated in a variety of test problems where the behavior of IC-CG, as measured by residual reduction, was shown to be erratic for many iterations. For fine grid performances of interest here, the number of iterations required by IC-CG to reach the point of precipitous residual reduction were found to be prohibitive, as each iteration establishes an orthogonal base vector of the solution in a manner that minimizes a prescribed norm of the error. For the same single scalar problems, accelerations of both SIP and IC by ACM resulted in exceptionally improved (comparable) convergence rates, while BC acceleration of these respective solvers yielded improvements in performance that range from dramatic to moderate. The cost reduction factor associated with the introduction of ACM accelerated SIP for pressure/correction solution in a segregated solution procedure was found to be up to 40 percent for laminar flows and 20 percent for turbulent flows.

For incompressible flow computations using segregated solution methodologies there also exists substantial additional cost associated with the appropriate coupling of pressure and velocity fields to yield the required zero divergence for mass. In this study (for two-dimensional applications) repeated SIMPLEC was adopted to enhance convergence by reducing both the number of coefficient updates and CPU requirements. The introduction of repeated SIMPLEC was shown to have the largest impact on the high cost of coefficient updates of CPU intensive schemes like MW-SUDS and LP-SUDS.

Concering the discretization schemes selected for quantitative evaluation using a finite volume method, a unified framework was devised to delineate the nature of the approximations introduced by the various treatment of convective fluxes at the cell interfaces. This involved a study of the separate components of the discretization error (profile and operator errors) in a manner indicated by Stubley[74] and concluded that a low truncation error profile used for convective fluxes might not necessarily result in small solution error, because the finite difference operator does not embody the correct physical influence. Furthermore, poor physical influence schemes, that fail to correctly incorporate the influences of convection, diffusion and source terms in the discretization procedure, were shown to invariably result in algebraic equations that are difficult to solve using iterative methods and possibilities for physically unbounded solutions exist.

Viewed in this light, the schemes selected, notably Second Order Upwind (SOU) differencing and appropriate variants of Compact Implicit schemes (CI), are seen to incorporate increasing physical corrections in their respective grid upstream formulations, over the conventional Upwind differencing (UDS). However, due to the possibility of generating negative coefficients and the inappropriateness of the strictly one-dimensional boundedness in criteria in multi dimensions, the solutions generated by these schemes suffered from overshoots and undershoots for some test problems, especially when the flow was at an angle to the grid. Specifically, SOU solutions were found to be more accurate than UDS solutions with accompanying overshoots and undershoots as well as smearing of gradients on coarse grids, when appreciable streamline inclination to the grid was present. In fact, only on fine meshes where the second order rate of convergence for SOU was approached that the smearing and overshoots and undershoots diminished. Variants of CI schemes, particularly CVOCI, that implicitly relate the nodal values of the variable and the operator yielded significantly more accurate solutions than UDS. However, using the current implementation, probabilities of generating relatively large overshoots and undershoots for multi-dimensional flows still exist in the presence of streamline skewness to the grid for high Peclet numbers.

Skewed Upstream Differencing Schemes (SUDS) eliminate the need for the convective component of the PAC term by a suitable transformation ignored in Grid Upstream Schemes, but otherwise incorporate the correct physical

influences of diffusion and source terms in their formulation. The two variants examined in this study are distinguished merely by the definition of the upstream value of the variable which, in turn, determines whether the unbounded, but accurate LP-SUDS or physically bounded, but less accurate MW-SUDS results. Both LP-SUDS and MW-SUDS using implicit and explicit integration point values were evaluated in a variety of test problems in which different balances were dominant to examine their respective accuracy, stability and cost effectiveness characteristics. It was concluded that the Physical Advection Correction (PAC) to LP-SUDS leads to a full second order scheme that was shown to be robust, although the solution cannot be guaranteed a priori to be physically bounded. MW-SUDS, in turn, provided the best alternative, among the schemes examined, for problems where physical bounding is mandatory.

The above quantitative two-dimensional evaluations also identified LP/MW-SUDS coupled with SIP accelerated by ACM as deserving further evaluation on three-dimensions, based on the practical criteria of best accuracy on coarse grids, robustness and stability and efficiency. Subsequently, these schemes, with appropriate modifications, were incorporated in a variant of 3D-TEACH code and were further evaluated regarding issues of accuracy and convergence enhancement characteristics in modelling of a jet in cross flow. Dramatic improvements in overall convergence and computational efficiency were realized for this problem regarding the solution of the pressure correction equations using IC-BC-ACM, while use of SUDS schemes yielded considerably reduced smearing of the solution, hence justifying the additional cost per iteration associated with their use.

It can be said in conclusion that for the problems examined, this study has clearly demonstrated that appropriate solution techniques for incompressible, turbulent, viscous recirculating flows in current use benefit substantially from the introduction of the convergence enhancement techniques adopted here (up to 40 percent). Furthermore, the various improved discretization schemes considered, specifically improved SUDS with PAC, usually provide a significant improvement in accuracy and hence cost effectiveness relative to most of the schemes currently used.

This study has also identified various areas where further research might prove beneficial. These will now be discussed briefly.

9.2 RECOMMENDATIONS FOR FUTURE RESEARCH

i) As the results of this study are based on a limited and carefully selected set of problems, the performance of the techniques considered should be evaluated on a broader scope of test problems that emphasize relevant numerical aspects, before more general conclusions can be reached regarding their utility.

ii) The current treatment of source terms in the integration point equations of SUDS is explicit. For the discretized momentum equations that incorporate pressure gradients as additional sources in the determination of integration point variable, such a practice when employed in a segregated solution procedure yields the usual pressure/correction equation. While this deferred correction approach eventually provides the required solution at convergence, it significantly increases the number of coefficient updates. What is required is an implicit treatment of pressure gradient sources for momentum especially, coupled with the appropriate numerical techniques to deal with the potentially troublesome pressure/correction equation.

iii) The current discretization for the positive definite variables like k and ε, adopts MW-SUDS without considering the influences of source and diffusion in the integration point equations. Such a numerical treatment for primarily source and diffusion dominated k and ε (in most regions of the flow) may not be appropriate for flows driven by the details of the turbulence field (aside from the physical modelling issues of turbulence). Thus, alternative formulations that properly incorporate the predominant source term influences have to be evaluated. A related concern pertains to the current implementation of MW-SUDS which has been shown to be frequently prone to excessive numerical diffusion. The implications of adopting a MW-SUDS formulation, suggested by Huget,[30] that simultaneously attenuates the inherent numerical diffusion and eliminates the possibility of unbounded solutions should be examined.

iv) This study has adopted the use of a nine point Alternating Direction Line Gauss-Seidel procedure to solve the linear algebraic equations generated by LP-SUDS (and SOU), even in the presence of mildly negative coefficients, without any serious solution difficulties. However, solution stability and convergence via such solvers is not strictly assured. To circumvent potential problems associated with these and alternative discretization schemes, that introduce computational molecules incompatible with ADI,

development and use of appropriate matrix solvers should be seriously considered.

v) Current solution algorithms for incompressible flows invariably employ a staggered grid arrangement for variables to prevent the decoupling of the pressure field. The PAC approach used here for improved accuracy, specifically the correction of momentum fluxes via pressure gradient source correction, however, does provide naturally the coupling between the pressure and velocity fields to eliminate the need for such cumbersome and unwieldy practices. Raw [10] has recently incorporated similar ideas in his co-located finite element algorithm. Furthermore, using such a co-located solution procedure, implementation and use of adaptive gridding via moving or stationary adaptive grids to resolve fronts better, becomes manageable and should be examined.

vi) The particular formulations of SOU and variants of CI examined in this study incorporate various Grid Upstream practices resulting in inaccuracies and solution difficulties in the presence of appreciable streamline skewness to the grid for high Peclet numbers. Considering the high accuracy provided by GOCI schemes (CVOCI in particular), albeit accompanied by non-physical oscillations, a natural multi-dimensional extension for such schemes that does not violate the one-dimensional boundedness criteria should consider a "skewed" formulation. In this manner it is possible to retain strict implicitness between the nodal values of the variable and the operator to yield improved accuracy, while eliminating the non-physical solution wiggles.

vii) The above formulation for GOCI will also require development and use of appropriate cost effective solvers in multi dimensions for the scheme to be routinely used in engineering computations. Such solvers must recognize the implications inherent in the equations, while using practices to substantially reduce the solution cost associated with block coupled systems.

viii) The significant reduction in cost provided by the introduction of repeated SIMPLEC in the current segregated solution procedure was demonstrated for two-dimensional problems using CPU intensive schemes like LP/MW-SUDS. In practical three-dimensional applications, where the coefficient update costs associated with such schemes become almost prohibitive for routine use, repeated SIMPLEC should be incorporated in the solution algorithm. Furthermore, most current segregated solution algorithms including SIMPLEC degrade

severely in performance with grid refinement.[22] Thus, development and use of "grid-insensitive" segregated solution procedures in the same philosophy as SIMPLEX[22] should provide substantial savings for appropriate problems.

ix) While this study emphasized the relevant details of the predominant pressure-velocity coupling, appropriate for "simple" incompressible flows, by a careful study of the various approximations employed, additional and/or alternative couplings might significantly influence the solution characteristics for some problems. For instance, the nature of the couplings provided by swirl (not considered in this study) as well as turbulence variables should be examined and appropriate practices be developed.

x) The turbulent test cases examined in this study introduce additional considerations in quantitatively evaluating the performance of discretization schemes. Appropriateness of the physical modelling assumptions implied by the particular turbulence model and availability of benchmark data for initial and boundary condition specification, as well as quantitative assessment, significantly influence the nature of the solutions. For such problems improved predictions are generally obtained by solution procedures that incorporate appropriate physical and computational models, in addition to improved discretization techniques.

xi) Finally, a deeper understanding and appreciation of accurate discretization techniques and solution algorithms should be developed. This study has only presented a phase of progress in a complex but steadily evolving subject. For example, future numerical techniques for the problems considered here might adopt spectral iteration techniques in conjunction with a lower order scheme (like SUDS) to achieve higher accuracy via a deferred corrector approach.[53] Also fully coupled numerical schemes/solution algorithms[20] might be appropriately formulated to yield practical solutions for engineering problems.

10.0 REFERENCES

1. Patankar, S.V., Numerical Heat Transfer, Hemisphere, Washington, D.C., 1980.

2. Kenworthy, M.J., Correa, S.M. and Burrus, D.L., "Aerothermal Modelling Program, Phase I-Final Report", NASA CR-168296, 1983.

3. Sturgess, G.J. "Aerothermal Modelling Program, Phase I-Final Report", NASA CR-168202, 1983.

4. Srinivasan, R., Reynolds, R., Ball, I., Berry, R., Johnson, K. and Mongia, H., "Aerothermal Modelling Program, Phase I-Final Report", NASA-CR-168243, 1983.

5. Syed, S.A., Chiappetta, L.M. and Gosman, A.D. "Error Reduction Progran, Final Report", NASA-CR 174776, 1985.

6 Issa, R.I., "Solution of Implicitly Discretized Fluid Flow Equations by Operator Splitting", Rept. FS/82/15, Imperial College, London, 1982.

7. Launder, B.E. and Spalding, D.B., Mathematical Models of Turbulence, Academic Press, London, 1972.

8. Launder, B.E. and Spalding D.B., "The Numerical Computation of Turbulent Flows", Comp. Meth. in Appl. Mech. and Eng. 3, 269, 1974.

9. Harlow, F.H. and Welch, J.E., "Numerical Calculation of Time-Dependent Viscous Incompressible Flow of Fluid with Free Surface", Phys. Fluids, 8, 12, 2182, 1965.

10. Raw, M.J., "A New Control Volume Based Finite Element Procedure for the Numerical Solution of the Fluid Flow and Scalar Transport Equaitons", Ph.D. Thesis, University of Waterloo, 1985.

11. Spalding, D.B., "A Novel Finite Difference Formulation for Differential Expressions Involving Both First and Second Derivatives", Int. J. Num. Meth. Eng., 4, 551, 1972.

12. Raithby, G.D., "Skew Upstream Differencing Schemes for Problems Involving Fluid Flow", Comp. Meth. Appl. Mech. Eng., 9, 153, 1976.

13. Zedan, M. and Schneider, G.E., "Investigation into the Simultaneous Variable Solution of Velocity and Pressure in Incompressible Fluid Flow Problems", AIAA Paper No. 83-1519, presented at the AIAA 18th Thermophysics Conference, Montreal, Quebec, Canada, 1983.

14. Van Doormaal, J.P., "Numerical Methods for the Solution of Incompressible and Compressible Fluid Flows", Ph.D. Thesis, University of Waterloo, 1985.

15. Van Doormaal, J.P. and Raithby, G.D., "Enhancements of the SIMPLE Method for Predicting Incompressible Fluid Flows", Numer. Heat Transfer, 7, 147, 1984.

16. Gosman, A.D. and Lai, K.Y., "Finite Difference and Other Approximations for the Transport and Navier Stokes Equations", FS/82/18, Imperial College, London, 1982.

17. Forsyhte, G.E. and Wason, W., Finite Difference Methods for Partial Differential Equations, Wiley, New York, 1960.

18. Roache, P.J., Computational Fluid Dynamics, Hermosa, Albuquerque, N.M., 1972.

19. Van Doormaal, J.P., Turan, A. and Raithby, G.D., "Evaluation of New Techniques for the Calculation of Internal Recirculating Flows", AIAA Paper No. 87-0059, presented at the AIAA 25th Aerospace Sciences Meeting, Reno, NV, 1987.

20. Vanka, S.P. and Leaf, G.K. "Fully Coupled Solution of Pressure-Linked Fluid Flow Equations", ANL-83-73, Argonne National Laboratory, Argonne, IL, 1983.

21. Patankar, S.V., "Efficient Numerical Techniques for Complex Fluid Flows", NASA CP-2444, 141, 1986.

22. Van Doormaal, J.P. and Raithby, G.D., "An Evaluation of the Segregated Approach for Predicting Incompressible Fluid Flows", ASME Paper 85-HT-9, presented at the National Heat Transfer Conference, Denver, CO., 1985.

23. Van Doormaal, J.P., Hutchinson, B.R. and Turan, A., "An Evaluation of Techniques Used to Accelerate Segregated Methods for Predicting Viscous Fluid Flow", AIAA paper No. 86-1653, presented at the AIAA/ASME/SAE/ASEE 22nd Joint Propulsion Conference, Huntsville, AL, 1986.

24. Schumann, U. and Sweet, R.A., "A Direct Method for the solution of Poisson's Equation with Neumann Boundary Conditions on a Staggered Grid of Arbitrary Size", J. Comp. Phys., 20, 171, 1976.

25. Hageman, L.A., and Young, D.M., Applied Iterative Methods, Academic Press, New York, 1981.

26. Stone, H.L., "Iterative Solution of Implicit Approximations of Multi-Dimensional Partial Differential Equations", SIAM J. Numerical Analysis, 5, 530, 1968.

27. Schneider, G.E. and Zedan, M., "A Coupled Modified Strongly Implicit Procedure for the Numerical Solution of Coupled Continuum Problems", AIAA Paper No. 84-1743, presented at the AIAA 19'th Thermophysics Conference, Snowmass, CO, 1984.

28. Atias, M., Wolfshtein, M. and Israeli, M., "Efficiency of Navier Stokes Solvers", AIAA J., 15, 263, 1977.

29. Gupta, M.M. and Manohar, R.P., "A Critique of a Second-Order Upwind Scheme for Viscous Flow Problems", AIAA J., 16, 759, 1978.

30. Huget, R.G., "The Evaluation and Development of Approximation Schemes for the Finite Volume Method", Ph.D. Thesis, University of Waterloo, 1985.

31. Orszag, S.A. and Israeli, M., "Numerical Simulation of Viscous Incompressible Flows", Annual Review of Fluid Mechanics, 6, 281, 1974.

32. Orszag, S.A., "Numerical Simulation of Incompressible Flows Within Simple Boundaries: Accuracy", J. Fluid Mech., 49, 1, 75, 1971.

33. Arakawa, A., "Numerical Simulation of Large Scale Atmospheric Motions", Numerical Solution of Field Problems in Continuum Physics, Proc. SIAM-AMS, Vol. 2, 24-40, Providence AMS, 1970.

34. Phillips, N.A., "An Example of Non-Linear Computational Instability", The Atmosphere and the Sea in Motion, 501, New York, Rockefeller Institute Press, 1959.

35. Rubin, S.G. and Khosla, P.K., "Higher Order Numerical Methods Derived from Three Point Polynominal Interpolation", General Applied Science Labs. Inc., NASA CR-2735, 1976.

36. Ciment, M., Leventhal, S.H. and Weinberg, B.C., "The Operator Compact Implicit Method for Parabolic Equations", Naval Surface Weapons Centre, NSWC/WOL/TR-77-29, 1977.

37. Berger, A.E., Solomon, J.M., Ciment, M., Leventhal, S.H. and Weinberg, B.C., "Generalized OCI Schemes for Boundary Layer Problems", Math. Comp. 35, 151, 695, 1980.

38. Von Neumann, J. and Richtmeyer, R.D., "A Method for Numerical Calculation of Hydrodynamic Shocks", J of Applied Physics, 21, 232, 1950.

39. MacCormack, R.W., "A Numerical Method for Solving the Equations of Compressible Viscous Flow", AIAA Paper No. 81-0110, 19'th Aerospace Sciences Meeting, Reno, NV, 1981.

40. Jameson, A., Schmidt, W. and Turkel, E., "Numerical Solutions of the Euler Equations by Finite Volume Methods Using Runge-Kutta Time Stepping Schemes", AIAA Paper NO. 81-1259, 14'th Fluid and Plasma Dynamics Conference, Palo Alto, CA, 1981.

41. Beam, R.M. and Warming, R.F., "An Implicit Finite Difference Algorithm for Hyperbolic Systems in Conservation-Law Form", J. Comp. Phys. 22, 87, 1976.

42. MacCormack, R.W. and Baldwin, B.S., "A Numerical Method for Solving the Navier-Stokes Equations with Application to Shock-Boundary Layer Interactions", AIAA Paper No. 75-1, Pasadena, CA, 1975.

43. Pulliam, T.H., "Artificial Dissipation Models for the Euler Equations", AIAA paper No. 85-0438, 23'rd Aerospace Sciences Meeting, Reno, NV, 1985.

44. Kwak, D. and Chang, J., "An Incompressible Navier-Stokes Flow Solver in Three-Dimensional Curvilinear Coordinate System Using Primitive Variables", AIAA Paper No. 84-0253, 22'nd Aerospace Sciences Meeting Reno, NV, 1984.

45. Chorin, A.J., "A Numerical Method for Solving Incompressible Viscous Flow Problems", J. Comp. Phys. 2, 12, 1967.

46. Boris, J.P. and Book, D.L., "Flux-Corrected Transport, I A Fluid Transport Algorithm That Works", J. Comp. Phys. 11, 38, 1973.

47. Zalesak, S.T., "Fully Multi-Dimensional Flux-Corrected Transport Algorithms for Fluids", J. Comp. Phys. 11, 38, 1973.

48. Steger, J.L. and Warming, R.F., "Flux Vector Splitting of the Inviscid Gas Dynamic Equations with Application to Finite Difference Methods" J., Comp. Phys. 40, 263, 1981.

49. Gresho, P.M. and Lee, R.L., "Don't Supress the Wiggles - They're Telling You Something!", in Hughes, T.J.R. (ed.) Proc. of a Symp. on Finite Element Meth. for Convection Dominated Flows, ASME Winter Annu. Meet., New York, 37, 1979.

50. Heinrich, J.C., Huyakorn, P.S., Zienkiewicz, O.C. and Mitchell, A.R., "An 'Upwind' Finite Element Scheme for Two-Dimensional Convective Transport Equation", Int. J. Num. Meth. Eng., 11, 131, 1977.

51. Gottlieb, D. and Orszag, S.A., "Numerical Analysis of Spectral Methods", NSF-CBMS Monograph, No. 26, Soc. Ind. and Appl. Math., Philadelphia, PA, 1977.

52. Gottlieb, D., Hussaini, A.K. and Orszag, S.A., Paper Drafted for Publication (private communication).

53. Orszag, S.A., "Spectral Methods for Problems in Complex Geometries", Numerical Methods for PDE's, Academic Press, 273, 1979.

54. Hirt, C.W., Amsden, A.A. and Cook, J.L., "An Arbitrary Lagrangian-Eulerian Computing Method for All Flow Speeds", J. Comp. Phys. 14, 227, 1974.

55. Thompson, J.F., Warsi, Z.U.A. and Mastin, C.W., "Boundary-Fitted Coordinate Systems for Numerical Solution of Partial Differential Equations- A Review", J. Comp. Phys. 47, 1, 1982.

56. Dwyer, H.A., Kee, R.J. and Sanders, B.R., "An Adaptive Grid Method for Problems in Fluid Mechanics and Heat Transfer", AIAA Computational Fluid Dynamics Conference, Williamsburg, VA, 1979.

57. Brackbill, J.V. and Saltzman, J.S., "Adaptive Zoning for Singular Problems in Two Dimensions", J. Comp. Phys. 46, 342, 1982.

58. Klopfer, G.H. and McRae, D.S., "The Non-Linear Modified Equation Approach to Analyzing Finite Difference Schemes", AIAA Computational Fluid Dynamics Conference, Palo Alto, CA, 1981.

59. Chandra, R., "Conjugate Gradient Methods for Partial Differential Equations", Ph.D. Thesis, Yale University, Dept. of Computer Science, 1978.

60. Concus, P., Golub, G.H. and O'Leary, D.P., "A Generalized Conjugate Gradient Method for the Numerical Solution of Partial Differential Equations", Stanford University, STAN-CS-76-5333, 1976.

61. Settari, A. and Aziz, K., "A Generalization of the Additive Correction Methods for the Iterative Solution of Matrix Equations", SIAM J. Numerical Analysis, 10, 506, 1973.

62. Hutchinson, B.R. and Raithby, G.D., "A Multigrid Method Based on the Additive Correction Strategy", Numerical Heat Transfer, 9, 511, 1986.

63. Brandt, A., "Multi-Level Adaptive Solutions to Boundary-Value Problems", Math. Computation, 31, 333, 1977.

64. Neely, G.M. and Claus, R.W., "Accelerated Convergence for Incompressible Flow Calculations", NASA TM-86863, 1985.

65. Caretto, L.S., Gosman, A.D., Patankar, S.V. and Spalding, D.B., "Two Calculation Procedures for Steady Three-Dimensional Flows with Recirculation", Proc. of Third Int. conf. on Numerical Methods in Fluid Dynamics, 60, 1972.

66. Srivastava, B.N., Werle, M.J. and Davis, R.T., "Viscous Shock Layer Solutions for Hypersonic Sphere Cones", AIAA J. 16, 2, 136, 1978.

67. Srivastava B.N., Werle, M.J. and Davis, R.T., "Numerical Solution of Hypersonic Viscous Shock Layer Equations", AIAA J. 17, 1, 107, 1979.

68. Keller, H.B. and Cebeci, T., "Accurate Numerical Methods for Boundary Layer Flows- I. Two-Dimensional Laminar Flows", in Holt, M. (ed) Proc of 2'nd Inter. Conf. on Numerical Methods in Fluid Dynamics, New York, 1971.

69. Leonard, B.P., "A Stable and Accurate Convective Modelling Procedure Based on Quadratic Upstream Interpolation", Comp. Math. Appl. Mech. Eng., 19, 59, 1979.

70. Raw, M.J., Personal Communication, ASC, 1986.

71. Wilkes, N.S. and Thompson, C.P., "An Evaluation of Higher Order Upwind Differencing for Elliptic Flow Problems", Rept. CSS-137, AERG Harwell, 1983.

72. Coakley, T.J., "Numerical Method for Gas Dynamics Combining Characteristic and Conservation Concepts", AIAA Paper No. 81-1257, 14th Fluid and Plasma Dynamics Conference, Palo Alto, CA, 1981,

73. Shyy, W., "Numerical Outflow Boundary Condition for Navier Stokes Flow Calculations by a Line Iterative Method," AIAA J. 23, 12, 1847, 1985.

74. Stubley, G.D., Raithby, G.D., Strong, A.B. and Woolner, A.K., "Simulation of Convection and Diffusion Processes by Standard Finite Difference Schemes and by Influence Schemes", Comp. Methods Eng. Appl. Mech., 35, 153, 1982.

75. Schneider, G.E. and Raw, M.J., "A Skewed Positive Influence Coefficient Upwinding Procedure for Control Volume Based Finite Element Convection-Diffusion Computation", Numer. Heat Transfer, 8, 1, 1986.

76. Collatz, L., The Numerical Treatment of Differential Equations, Springer Verlag, Berlin, 1960.

77. Krause, E., Hirschel, E.H. and Kordulla, W., "Fourth Order 'Mehrstellen'- Integration for Three-Dimensional Turbulent Boundary Layers", Comp. Fluids 4, 77, 1976.

78. Adams, Y., "A Hermitian Finite Difference Method for the Solution of Parabolic Equations", Comp. Maths. Appls., 8, 393, 1975.

79. Anderson, D.A., Tannehill, J.C. and Pletcher, R.H., Computational Fluid Mechanics and Heat Transfer, Series in Computational Methods in Mechanics and Thermal Sciences, Hemisphere, 1984.

80. Rubin, S.G. and Graves, R.A., "A Cubic Spline Approximation for Problems in Fluid Mechanics", Tech. Report 74-T1, Old Dominion Univ., Norfolk, VA, 1974.

81. Swartz, B.K., "The Construction and Comparison of Finite Difference Analogs of Some Finite Element Schemes," in Mathematical Aspects of Finite Elements in Partial Differential Equations," (C.de Boor, ed.), Academic Press, NY, 279, 1974.

82. Ciment, M., Leventhal, S.H. and Weinberg, B.C., "The Operator Compact Implicit Method for Parabolic Equations", J. Comp. Phys. 28, 125, 1978.

83. Wong, H.H. and Raithby, G.D., "Improved Finite Difference Methods Based on a Critical Evaluation of Approximation Errors", Numer. Heat Transfer, 2, 139, 1979.

84. Lecointe, Y. and Piquet, J., "On the Use of Several Compact Methods for the Study of Unsteady Incompressible Viscous Flow Round a Circular Cylinder", Computers and Fluids, 12, 4, 225, 1980.

85. Meijerink, J.A. and Van Der Vorst, H.A., "An Iterative Solution Method for Linear Systems of which the Coefficient Matrix is a Symmetric M-Matrix", Math. Comp. 1977.

86. Dongarra J.J., Leaf, G.K. and Minkoff, M., "A Pre-conditioned Conjugate Gradient Method for Solving a Class of Non-Symmetric Linear Systems", ANL-81-71, Argonne National Laboratory, Argonne, IL 1981.

87. Hestenes, M. and Steifel, E., "Methods of Conjugate Gradients for Solving Linear Systems", J. Res. Nat. Bur. Standards 49, 409, 1952.

88. Phillips, R.E. and Schmidt, F.W., "Multigrid Techniques for Numerical Solution of the Diffusion Equation", Numer. Heat Transfer, 7, 251, 1984.

89. Raithby, G.D. and Torrance, K.E., "Upstream-Weighted Differencing Schemes and Their Application to Elliptic Problems Involving Fluid Flow", Comp. Fluids, 8, 12, 191, 1974.

90. Smith, R.M. and Hutton, A.G., "The Numerical Treatment of Advection: A Performance Comparison of Current Methods", Numer. Heat Transfer, 5, 439, 1982.

91. Stubley, G.D., "A New Discrete Method for Convection Dominated Flows Based on a Clear Understanding of Solution Errors", Ph.D. Thesis, Unviersity of Waterloo, 1981.

92. Burgraff, O.R., "Analytical and Numerical Studies of Structure of Steady Separated Flow", J. Fluid Mech. 24, 2, 113, 1966.

93. Vanka, S.P., Personal Communication, Argonne National Labs, 1986.

94. Armaly, B.F. and Durst, F., "Reattachment Length and Recirculation Regions Downstream of a Two-Dimensional Single Backward Facing Step", Symp. on Momentum and Heat Transfer Processes in Recirculating Flows, HTD, 13, ASME 101'st Winter Annual Meeting, Chicago, 1, 1980.

95. Ghia, U., Ghia, K.N. and Shin, C.T., "High-Re Solutions for Incompressible Flow Using the Navier Stokes Equations and a Multi-Grid Method", J. Comp. Phys. 48, 387, 1982.

96. Khan, Z.A., McGuirk, J.J. and Whitelaw, J.H., "A Row of Jets in Crossflow", Fluid Dynamics of Jets with Applications to V/STOL, AGARD CP-308, Paper 14, 1982.

97. Crabb, D., Durao, D.F.G. and Whitelaw, J.H., "A Round Jet Normal to a Crossflow", J. Fluids Eng. 103, 1, 142, 1981.

APPENDIX A
IMPLEMENTATION OF MODIFICATIONS IN THE PRATT AND WHITNEY 3-D TEACH CODE TO IMPROVE ACCURACY AND EFFICIENCY

INTRODUCTION

The following notes briefly outline the modifications of the Pratt and Whitney 3-D TEACH code to incorporate various numerical techniques for improving accuracy and computational efficiency. Relevant modifications for the 2-D TEACH code follow a similar implementation structure and corresponding details can be appreciated fully by a careful study of the material presented here.

The outline presented includes descriptions of new routines and modifications to the supplied TEACH code. These notes assume that the reader is familiar with the supplied TEACH code and all relevant documentation,[5] as well as the appropriate discussion presented Section 8 regarding formulation and extension of schemes.

MODIFICATIONS FOR IMPROVING EFFICIENCY

To improve the computational efficiency of TEACH, the following numerical techniques were implemented:

i) Residual reduction convergence criterion for solution of the pressure correction equation.

ii) Stone's Strongly Implicit Procedure (SIP) for the solution of the pressure correction equation.

iii) Incomplete Choleski (IC) for the solution of the pressure correction equation.

iv) Additive Correction Multigrid (ACM) to accelerate the convergence of SIP and IC. ACM was implemented for both 2x2x2 and 3x3x3 blocks.

v) Block Correction (BC) to accelerate the convergence of IC with the option of further accelerating convergence by ACM.

Originally, there was no intention to include BC in the modifications of the 3-D TEACH code, Section (8.1), however, for some 3-D applications, particularly involving geometries with high cell aspect ratios, the convergence acceleration provided by ACM was limited. For these applications

BC provides considerably greater acceleration to convergence. To take advantage of the features of both acceleration schemes, the two acceleration schemes have been implemented so that they can be used together. As demonstrated in Section (8.1), the combination of the two techniques results in convergence acceleration which exceeds the acceleration provided by either technique alone.

Residual Reduction Convergence Criterion

To implement the residual reduction convergence criterion for the solution of the pressure correction equations, Section (4.3), modifications to the subroutines CALCP and PISO were required. These changes include the introduction of the following variables:

RES (I,J,K) = array of residuals for pressure correction equation

RESNOW = variable containing the square root of the sum of the squares of values of entries in RES of current p' iteration.

RESMAX = maximum value of resnow

RDCP = required reduction factor of residual, iteration terminated when RSDNOW < RSDMAX*RDCP. Note: RDCP is an input parameter passed into CALCP and PISO via the labelled COMMON/PXLR8/.

The residual reduction convergence criterion is implemented in both pressure correction stages of PISO (including the single correction stage of SIMPLE) and is in effect only when SIP or IC with or without acceleration is being used.

Strongly Implicit Procedure

To implement Stone's SIP,[26] the following new subroutines were provided:

i) ITRSOS with entry ITRSIS to set up the pointers into the real workspace for subsequent calls to SIPO and SIPI. This data structure arrangement, requiring the set up of pointers, was adopted to facilitate a modular code structure.

ii) SIPO with entry SIPI to perform one SIP iteration. The SIPO portion of the routine performs the approximate factorization of SIP required only before the first SIP iteration and the SIPI portion performs the forward and backward substitution required for each SIP iteration.

iii) RESIDL to determine residuals of the equations.

iv) NOTENF to generate an error message when there is not enough available work space.

v) OUTTLE to generate a message indicating which routine is being used.

The argument list of these subroutines and entries include the following:

T = dependent variable array
V = correction array to current values of T
RES = residual array
AP, AE, AW, AN, AS, AU, AD } coefficients of algebraic equations
BP = source term of equation
RLX = relaxation = 1. + partial cancellation of Stone
1.0 < RLX < 2.0; for RLX set to unity, equivalent to IC
(recommended use of IC subroutines described below)
IOFLE = unit number for output
IB, IE, JB, JE, KB, KE = limits on index triplet (i,j,k)
ID, JD, KD = dimensions of arrays
WRK = work space containing NAVAIL elements
NAVAIL = number of available elements or words available in WRK
NREQ = number of elements WRK required by SIP.

Incomplete Choleski

The implementation of SIP with RLX=1 as described above is algebraically equivalent to IC.[59] However, the use of SIP routines for IC results in an unneccessary and considerable storage penalty. To overcome this, IC was implemented separately with the following new subroutines provided:

i) ITRSOI with entry ITRSII to set up the pointers into the real workspace for subsequent calls to ICO and ICI. Again, this data structure arrangement requiring the set up of pointers was adopted to facilitate a modular code structure.

ii) ICO with entry ICI to perform one IC iteration. The ICO portion of the routine performs the approximate factorization of IC required only before the first IC iteration, and the ICI portion performs the forward and backward substitution required for each IC iteration. The argument list of these subroutines and entries are identical to those for the implementation of SIP.

Routines Providing No Acceleration of Base Solvers

Identifying SIP and IC as the base solvers used to solve for pressure corrections, routines designed to provide the desired convergence of the base solvers are required. To provide no acceleration of the base solvers, the following new subroutines are provided:

i) NOACO with entry NOACI to call the appropriate base solver routines for approximate factorization and forward and backward substitution. The base solver routines called depend on the value of RLX:
If RLX < 1.001, then IC is used
IF RLX > 1.001, then SIP is used
The argument list of these subroutines and entries are identical to those for the implementation of SIP.

Routines Providing BC Acceleration

To provide BC acceleration of the IC base solver, the following new subroutines are provided:

i) ITRBCO to set up pointers into workspace for subsequent call to BCO,

ii) ITRBCI to set up pointers into workspace for subsequent call to BCI,

iii) BCO to call COFBC to determine the coefficients of the block correction equations for each of the three (E-W, N-S, and U-D) index directions and to call ITRSOI to perform the approximate factorization for IC,

iv) BCI to call SORBC to determine source term of block correction equations for each of the three index directions, to call FACTR1 and SWEEP1 to solve the block correction fields, to call TMODBC to apply the appropriate block correction and to call ITRSII to perform the forward and backward substitution of IC,

v) COFBC to determine the coefficients of the block correction equations for each of the three index directions,

vi) SORBC to determine the source terms of the block correction equations for each of the three index directions,

vii) TMODBC to apply the block correction (note that only the block correction that has the largest sum of the squares of corrections is applied),

viii) FACTR1 and entry SWEEP1 to perform Tri-Diagonal Matrix Algorithm for solving the three block correction fields.

In addition to the arguments described above, the argument lists of the above routines include the following:

VEWB = E-W block correction vector

APEWB, AEB, AWB, BPEWB = coefficients of E-W block correction equations

VNSB = N-S block correction vector

APNSB, ANB, ASB, BPNSB = coefficients of N-S block correction equations

VUDB = U-D block correction vector

APUDB, AUB, ADB, BPUDB = coefficients of U-D block correction equations

Note: To ensure that block correction equations are not singular, one block correction equation for each index direction is adjusted so that the corresponding block correction is zero. Also, BC is currently implemented for IC only. Implementation for SIP is readily accomplished by adding appropriate calls to ITRSOS and IRSIS.

Routines Providing Additive Correction Multigrid Acceleration of Base Solvers

To provide ACM acceleration of the IC and SIP base solvers as well as IC-BC, the following new subroutines are provided:

i) XLR8OM to call ACMPNT to set pointers into workspace, to call NCRMNT to determine the number of fine grid control volumes in each coarse grid block, to call COFGEN to determine coefficients of coarse grid additive correction equations and to call ITRSOI, ITRSOS or ITRBCO to perform the approximate factorization for all grids. The current implementation of ACM required the introduction of a number of variables and vectors including the following:

TC = vector of pointers into real workspace pointing to first element of coarse grid additive correction arrays

RESC= vector of pointers into real workspace pointing to first element of coarse grid residual arrays

VC = vector of pointers into real workspace pointing to first element of coarse grid corrections to additive corrections, required for current implementation of base solvers

WC = vector of pointers into real workspace pointing to first element of base solver workspaces required for each grid.

APC
AEC
AWC
ANC
ASC
AUC
ADC

vector of pointers into real workspace pointing to first elements of coefficients of additive correction equations for each grid

BPC = vector of pointers into real workspace pointing to first element of coarse grid arrays of additive correction equation source term

INC, JNC, KNC = vector of pointers into integer workspace pointing to first elements of vectors of increments for each grid

IBC, IEC, JBC, JEC, KBC, KEC = vectors containing limits on index triplet (i,j,k) for each grid.

IDC, JDC, KDC = vectors containing dimension of arrays for each grid

RESNOW = vector of square root of the sum of the squares of the current residuals for each grid

RESPRV = vector of square root of the sum of the squares of the previous iteration residuals for each grid

RESO = vector of square root of the sum of the squares of the original residuals for each grid

IBLK, JBLK, KBLK = nominal size of blocks

RESRAT = required rate of convergence

RESRDC = required reduction of residuals

WRKMAX = maximum number of allowable total work units

NLVLS = number of coarse grids

LVL = current grid level, finest grid is LVL = 0, coarsest grid is LVL = NLVLS

ii) Entry XLR8IM to call SORGEN to determine source terms of coarse grid additive correction equations, to call ITRSII, ITRSIS, or ITRBCI and TCCOR to perform appropriate forward and backward substitution and

obtain required update of solution for the current grid, to call RESID1, RESCAL and LEVCON to evaluate residuals on current grid, to evaluate sum of squares of residuals and decide whether to remain on current grid or to move to finer or coarser and to call TMODAC to apply additive correction to finer grid solution and adjust finer grid residuals.

iii) ACMPNT to set up pointers into workspace for coefficients of all coarser grid additive correction equations. The number of coarse grids is based on logic used to determine increments, see (iv).

iv) NCRMNT to determine increment of fine grid control volumes which are used to make up a coarse grid block in each of three index directions. Increments in each direction are nominally set to value of IJKBLK, except at boundaries where the number of fine grid control volumes in an index direction is not evenly divisible by IJKBLK. In this case the remaining increment is set to the integer remainder of the division. The logic of NCRMNT is set up so that the number of blocks in any index direction is not less than 2. The number of coarse grid levels assumed in ACMPNT is such that the coarsest grid is 2x2x2.

v) COFGEN to determine coefficients of coarser grid additive correction equations. The coarse grid AP coefficient is determined by first summing fine grid AP values over coarse grid blocks. Then coarse grid AP values are modified by subtracting fine grid AE, AW, AN, AS, AU and AD coefficients where these coefficients are not coincident with coarse grid control volume faces. The coarse grid coefficients AE, AW, AN, AD are determined by summing the fine grid coefficients, where fine grid and coarse grid control volume faces are coincident.

vi) SORGEN to determine the source term of coarse grid additive correction equations. These source terms are simply determined from the sum of fine grid residuals over coarse grid blocks.

vii) RESCAL to calculate the square root of the sum of the squares of the residuals.

viii) LEVCON to set a flag controlling movement of ACM from one grid to another. Note that the current implementation of ACM adopts the flexible cycle multigrid approach. ACM moves to a finer grid if residuals are 20 percent of original value and moves to a coarser grid

if residuals have not been reduced to 10 percent of the previous value. ACM also moves to a finer grid if the number of total work units, summed over all grids but the LVL = 0 grid, exceeds 1.0.

ix) TCCOR to apply corrections from base solver to the current estimate of solution.

x) TMODAC to apply additive correction to finer grid solution and adjust finer grid residuals. Fine grid residual adjustments are made in several steps: the first step is to adjust all fine grid residuals assuming that the additive corrections to neighbouring fine grid control volumes are the same; the second step then adjusts all fine grid residuals where fine grid faces and coarse grid faces are coincident (where neighbouring additive corrections are not necessarily the same).

In addition to the arguments already described, the argument lists of the ACM routines also include the following:

TB = dependent variable array for coarse grid

RESB = residual array for coarse grid

APB, AEB, AWB, ANB, ASB, AUB, ADB = coefficients of coarse grid additive correction equations

BB = source term of coarse grid additive correction equation

LB,LE,MB,ME,NB,NE = limits on index triplet (l,m,n) for coarse grid

LD, MD, ND = dimensions of arrays for coarse grid.

Modifications to Routines to Calculate Pressure Corrections

To invoke the various improved techniques for solving the equation for pressure correction, a number of calls were added to the CALCP and PISO routines. These calls can be broken into two types; calls to routines with names beginning with XLR80 which perform to necesssary initializations and approximate factorization and calls to routines with names beginning with XLR8I to perform one base solver iteration with acceleration. In general, calls to XLR80 routines are required only when the A coefficients of the p' equation change. Therefore a call to XLR80 is not required prior to solving

the second set of p' of PISO. The call to the appropriate XLR8O-XLR8I pair is controlled by the value of IPXLR8:

IPXLR8 = 0 use original Alternating Line Gauss-Seidel
= 1 no acceleration of SIP or IC
= 2 ACM acceleration of SIP or IC (2x2x2 blocks)
= 3 ACM acceleration of SIP or IC (3x3x3 blocks)
= 4 BC acceleration of IC
= 5 ACM acceleration of IC-BC (2x2x2 blocks)
= 6 ACM acceleration of IC-BC (3x3x3 blocks)

For IPXLR8 = 1,2 or 3 the choice of SIP or IC is dependent on the value of RLXP, the parameter controlling the partial cancellation of SIP

RLXP < 0.001 : IC is used
> 0.001 : SIP is used

The variables IPXLR8, RLXP and RDCP are passed into CALCP and PISO via the labelled COMMON/PXLR8/. Recommended values for these variables are:

IPXLR8 = 5 (IC-BC-ACM 2x2x2 blocks)
RLXP = 0.0 (IC, by default if IPXLR8 = 5)
RDCP = 0.1 (terminate p' solution if p' residuals are reduced to within 10 percent of their original value)

Although these values are not necessarily optimal, they should be appropriate for a wide range of problems.

For the solution of the pressure correction equations required in CALCP and PISO, the coefficients and source terms of pressure correction equations must have effects of all boundaries eliminated. This is the default for the TEACH code. As a result no additional modifications are required.

Finally, the modified PISO routine contains changes required to correct the block-off logic when applying pressure corrections to the velocities.

MODIFICATIONS FOR IMPROVING ACCURACY

To improve the accuracy of the TEACH code the Linear Profile (LP) and Mass Weighted (MW) Skewed Upstream Differencing Schemes (SUDS) were implemented. Details of the implementation for these techniques can be found in Section (8.2). To implement MW-SUDS and LP-SUDS, new subroutines were required to determine integration point expressions, to evaluate positive octant mass flows and to assemble integration point influences. Modifications to existing routines to calculate exchange coefficients for various variables are also required.

Integration Point Expression for MW-SUDS and LP-SUDS

To determine the integration point expression, subroutine IPEQ is provided. The routine is written using the notation outlined in Section (8.2) and determines the integration point expression for only one integration point, 011. IPEQ is broken into four sections: i) preliminaries, ii) LP-SUDS, iii), MW-SUDS, and iv) Physical Advection Correction (PAC).

In the preliminary section of IPEQ, the exponential weighting factor and the value of $\rho V/L$ are determined. To determine the value of $\rho V/L$ the first step is to calculate the six different values of $\rho V/L$ corresponding to the cases where the streamline intersects each of the six sides of the flux element. The value of $\rho V/L$ chosen is that which corresponds to the smallest positive value of L (i.e., the side first intersected by following the streamline upstream) or the largest value of $\rho V/L$.

The LP-SUDS section of IPEQ determines the coefficients of the integration point equation from a bilinear interpolation of the nodes on the flux element side intersected by the streamline. For low grid Peclet numbers LP-SUDS is blended with a trilinear interpolation of the eight flux element nodes. The blending is determined from the exponential weighting factor, B.

The MW-SUDS section applies the positive mass weighted algorithm, to determine coefficients of the integration point equation. The mass weighted algorithm is applied to the 000, 010, 001 and 011 set of nodes if the mass flow at the X011 integration point is positive and to the 100, 110, 101, and 111 set of nodes if the mass flow is negative. Note that the notation used for the positive mass flows of octant faces is slightly different in IPEQ than that used in Section (8.2). In the IPEQ routine mass flows through integration point faces and faces adjacent to nodes are required on an octant basis. See description of OCTMAS below. For low grid Peclet numbers MW-SUDS is blended with a linear interpolation of the flux element nodes 011 and 111.

The physical advection correction is determined from a trilinear interpolation of nodal estimates of the correction.

The argument list of IPEQ includes the following:

AIP
BIP
ANP000
ANP100
•
•
•
ANP111

} = coefficients of integration point equations

DX0,DX1 =	distances in X direction from integration point to flux element sides
DY0,DY1 =	distances in Y direction from integration point to flux element sides
DZ0, DZ1 =	distances in Z direction from integration point to flux element sides
RVX000, RVX010,...	= mass flux at integration point on faces coincident with X plane
RVY000, RVY100,...	= mass flux at integration point on faces coincident with Y plane
RVZ000, RVZ100,...	= mass flux at integration point on faces coincident with Z plane
FNP000, FNP100,...	= positive (into octant) mass flows through faces adjacent to flux element node
FXI000, FXI100,...	= positive mass flows through octant integration point faces coincident with X plane
FYI000, FYI100,...	= positive mass flows through octant integration point faces coincident with Y plane
FZI000, FZI100,...	= positive mass flows through octant integration point faces coincident with Z plane
QNP000, QNP100,...	= estimates of PAC at flux element nodes
DIFIP	= diffusion coefficient at X011 integration point
ACC	= parameter controlling formulation of integration point equation
	= 0 then MW-SUDS without PAC
	= 1 then MW-SUDS with PAC
	= 2 then LP-SUDS with PAC

Positive Octant Mass Flow

MW-SUDS for three-dimensional applications requires the evaluation of positive mass flows through octant faces. The routine OCTMAS performs this function. Mass flows are defined to be positive, if they are into the octant. For flows leaving the octant, the value of the positive mass flow values are required for four sets of faces: i) flows through the X integration point face of the octant, ii) flow through the Y integration point face of the octant, iii) flow through the Z integration point face of the octant, and iv) net flow through octant faces intersecting at octant node.

In addition the the variables described above, the argument list of OCTMAS includes the following:

AX000, AX010,... = area of X integration point faces of octant
AY000, AY100,... = area of Y integration point faces of octant
AZ000, AZ100,... = area of Z integration point faces of octant

Flux Element Assembly

To assemble the influences of integration point equations of a flux element into the appropriate control volume flux balance equation, the routine FEASM is provided. There are four major sections to FEASM: i) data statements initializing maps, ii) determination of positive mass flows, iii) determination of integration point equation coefficients for each integration point of the flux element, and iv) assembly of influences.

As described above, the routine IPEQ, provided to determine the coefficients of the integration point equations, is written for only the X011 integration point. To make use of one routine for all twelve integration points of a flux element it is necessary to use transformations. In FEASM these transformations are made through the use of maps. To use these maps it is first necessary to introduce a change in notation. Instead of the indexed triplet notation described in Section (8.2) and used in IPEQ and OCTMAS, node points and integration points are assigned the integer numbers listed below:

Index Triplet Node Notation	Numbered
000	1
100	2
010	3
110	4
001	5
101	6
011	7
111	8

Integration Point Notation	
X000	1
X010	2
X001	3
X011	4
Y000	5
Y100	6
Y001	7
Y101	8
Z000	9
Z100	10
Z010	11
Z110	12

Using the numbered notation, transformations are readily created and implemented. For instance, if the coefficients of the integration point for integration point 1 (or integration point X001) are required, then IPEQ can be called with integration point 1 arguments used in place of integration point 4 arguments, integration point 2 arguments in place of integration point 3 arguments, etc. The transformation of integration points is given in FEASM in the map IM. Note that a map is required for each integration point with 12 entries in each map, hence IM is dimensioned 12x12. In addition to the integration point maps, node point maps are required. For each of the twelve integration points, the eight entries required to map nodes are given by NM. Maps are also provided for three dimensions of the flux element and the sense of the coordinates under each of the twelve transformations. The map for the flux element dimensions assumes that dimensions have been assigned numbers in the following order:

Index Notation	Numbered Notation
DX0	1
DX1	2
DY0	3
DY1	4
DZ0	5
DZ1	6

The assignment of indexed notation variables to numbered notation variables follows the call to OCTMAS. This is followed by twelve calls to IPEQ. After normalizing the coefficients of the integration point equations and multiplying by the appropriate mass flows, the flux element influences are assembled. This assembly is done on a flux element octant basis. Each control volume octant has three flux element integration points with each integration point expressed in terms of the eight flux element nodes.

In addition to the variables described previously, the argument list of FEASM includes the following:

ADSW
ADS
ADSE
•
•
•
•
•
AP
•
•
•
•
•
AUNE

} = exchange coefficient arrays

BT = source term coefficient

I,J,K = integer index triplet of 000 flux element mode

ID,JD,KD = dimensions of all exchange coefficient arrays

Modifications to Routines Calculating Exchange Coefficients

MW-SUDS and LP-SUDS discretizations are implemented for the calculation of the coefficients of equations for u (CALCU), v (CALCV), w (CALCW), turbulent kinetic energy (CALCTE), and dissipation (CALCED). In general, the type of discretization used is controlled by the value of IFESKW passed into the routines through the labelled COMMON/FESKW/:

IFESKW = 0 default to baseline TEACH
= 1 MW-SUDS
= 2 LP-SUDS

As outlined above, the flux element assembly of coefficients using SUDS, invoked by calling FEASM, requires information regarding geometry, mass fluxes and estimates of diffusion and source term influences. Geometric information is readily available in TEACH. The mass flux terms are required on an octant basis and re-derived from the control volume mass fluxes which are stored in RVX, RVY and RVZ and passed as arrays through /FESKW/. To obtain diffusion and source term influences when using SUDS, the TEACH calculations of diffusion

calculations of diffusion coefficients and source terms are retained and assembled in the A and SU coefficients prior to the call to FEASM. Note however, that no convective influences are included until after the call to FEASM. The results is that, before the call to FEASM, the A coefficients contain all the sufficient diffusion information and SU coefficients contain source term information. The estimate of combined diffusion and source term influences, required to estimate the physical advection correction term, is obtained from the residual of the conservation equation (without convective influences) using the best available estimates of the dependent variable. Normalized by the volume of the control volume, these influences are stored in the array QU passed into the subroutine through /FESKW/.

In the vicinity of boundaries, some modification of the procedure outlined above is required. First, in TEACH, fictitious modes are located coincident with the boundary. The implementation of flux element SUDS retains this by appropriately adjusting distances between integration points and flux element boundaries. Second, in the supplied TEACH, any influence of any boundary node which is not E,W,N,S,B or F must be zero. In the flux element implementation of SUDS this assumption remains valid if, in flux elements adjacent to boundaries, only MW-SUDS is used. This assumes that, at specified openings, the components of velocity tangent to the boundary are zero. Finally, at boundary nodes the value of QU cannot be defined in the manner given above. Instead, boundary QU values are set equal to adjacent interior values.

With the necessary geometric, mass and diffusive fluxes and source term information available, coefficients are assembled on a flux element basis by calling FEASM. The evaluation of mass fluxes and source term influences, required by FEASM, are determined in a manner which is appropriate for either Cartesian or cylindrical coordinates.

Finally, for kinetic energy and dissipation equations the value of QU are everywhere set to zero and, if IFESKW > 0, then only MW-SUDS, ACC = 0, is used. This is done to ensure the required boundedness of the kinetic energy and dissipation solutions.

MODIFICATIONS TO INPUT AND OUTPUT ROUTINES

To implement the modifications in TEACH for improving accuracy and efficiency, it was necessary to add several new variables which must be supplied by the user from an input file. This required the modification of the INPUT routine. These changes are summarized below:

i) the labelled COMMONs /PXLR8/ and /FESKW/ are included

ii) following card type 9, a statement to read FESKW (format statement 5491, i5) was introduced

iii) following card type 11, a statement to read IPXLR8, RLXP, RDCP (format statement 5471, i5, 2f5.3) was introduced

iv) the introduction of a statement to overide the use of MW-SUDS or LP-SUDS if BSUDS1 or BSUDS2 were specified, ie., MW-SUDS or LP-SUDS are used only if ISKEW > 0 and FESKEW > 0

v) the introduction of a statement to ensure that RLXP = 0 for IPXLR8 > 3. This ensures that only IC is used with BC.

vi) write and format statements to echo input of changes 2 and 3 were introduced.

The routine XINPUT was also modified so that explanations of the additional options could be provided. Note, all additional input is read from unit 5 and additional output is directed to unit 6.

In addition to the changes listed above, the following modifications to the BLOCK DATA and RESTRT as well as the MAIN were required:

i) in the interest of saving compute resources (disk space and memory) the inclusion of SKW3.INCL and initialization of the variable SMALL were removed from BLOCK DATA. The variable SMALL is initialized in MAIN.

ii) so that the restart feature of TEACH could be used, the variable KMBSTR was removed from the second record read from unit 1 in RESTRT.

APPENDIX B
DERIVATION OF COEFFICIENTS FOR R AND Q MATRICES IN THE COCI SCHEME

It is shown in Appendix C that the truncation error defined by:

$$\tau = [R]\left\{\Phi_i\right\} - [Q]\left\{L^x_i\right\} \tag{B.1}$$

can be expressed as, using Taylor Series Expansion:

$$\tau = T^0\Phi_i + T^1\Phi_i^1 + T^2\Phi_i^2 + T^3\Phi_i^3 + T^4\Phi_i^4 +$$

where $\Phi^n = d^n\Phi/dx^n$ and

$$T^0 = [r^e + r^p + r^w]$$

$$T^1 = h\,[r^e - r^w - \frac{z\Gamma_\phi}{h^2}(q^w u_{i-1} + q^p u_i + q^e u_{i+1})]$$

$$T^2 = \frac{h^2}{2!}[r^e + r^w - \frac{2\Gamma_\phi}{h^2}(q^w + q^e + q^p) - \frac{2z\Gamma_\phi}{h^2}(q^e u_{i+1} - q^w u_{i-1})] \tag{B.2}$$

$$T^3 = \frac{h^3}{3!}[r^e - r^w - \frac{6\Gamma_\phi}{h^2}(q^e - q^w) - \frac{3z\Gamma_\phi}{h^2}(q^e u_{i+1} + q^w u_{i-1})]$$

$$T^4 = \frac{h^4}{4!}[r^e + r^w - \frac{12}{h^2}\phi(q^e + q^w) - \frac{4z\Gamma_\phi}{h^2}(q^e u_{i+1} - q^w u_{i-1})]$$

$$\vdots$$

$$T^v = \frac{h^v}{v!}[r^e + (-1)^v r^w - v(v-1)\frac{\Gamma_\phi}{h^2}(q^e + (-1)^v q^w) - \frac{vz}{h^2}\phi(q^e u_{i+1} + (-1)^{v-1} q^w u_{i-1})]$$

for $v = 3, 4, 5$ and $z = h/\Gamma_\phi$

COCI is said to be formally fourth order if τ in Equation (B.1) = $O(h^4)$ implying that $T^{\upsilon} = O(h^4)$ in equations (B.2). Since $T^5 = O(h^5)$, then to obtain a fourth order scheme consideration need only be given to T^{υ} for $\upsilon = 0,1,2,3$ and 4. Rearrangement of $T^0 = T^1 = T^2 = 0$ defines tri-diagonal matrix operator R in terms of Q in equation (6.65), as:

$$2r^W = \frac{\Pi_\phi}{h^2}\left[q^W(2-3zu_{i-1}) + q^P(2-zu_i) + q^E(2+zu_{i+1})\right] \tag{B.3a}$$

$$2r^E = \frac{\Gamma_\phi}{h^2}\left[q^W(2-zu_{i-1}) + q^P(2+zu_i) + q^E(2+3zu_{i+1})\right] \tag{B.3b}$$

$$r^P = -(r^E + r^W) \tag{B.3c}$$

COCI is uniquely defined by further insisting that $T^3=T^4=0$. The resulting expressions for T^3 and T^4 become:

$$r^E - r^W - \frac{6\Pi_\phi}{h^2}(q^E-q^W) - \frac{3z\Gamma_\phi}{h^2}(q^Eu_{i+1}+q^Wu_{i-1}) = 0 \tag{B.4a}$$

$$r^E - r^W - \frac{12\Pi_\phi}{h^2}(q^E-q^W) - \frac{4z\Pi_\phi}{h^2}(q^Eu_{i+1} - q^Wu_{i-1}) = 0 \tag{B.4b}$$

Normalizing Equations (B.3) and (B.4) by q^P and rearranging,

$$\hat{r}^E - \hat{r}^W = \frac{\Gamma_\phi}{h^2}\left[\hat{q}^W(zu_{i-1}) + zu_i + \hat{q}^E(zu_{i+1})\right] \tag{B.5a}$$

$$\hat{r}^E + \hat{r}^W = \frac{2\Gamma_\phi}{h^2}\left[\hat{q}^W(1-zu_{i-1}) + 1 + \hat{q}^E(1+zu_{i+1})\right] \tag{B.5b}$$

$$\hat{r}^E - \hat{r}^W = \frac{6\Gamma_\phi}{h^2}(\hat{q}^E-\hat{q}^W) - \frac{3z\Pi_\phi}{h^2}(\hat{q}^Eu_{i+1} - \hat{q}^Wu_{i-1}) \tag{B.5c}$$

$$\hat{r}^E + \hat{r}^W = \frac{12\Gamma_\phi}{h^2}(\hat{q}^E+\hat{q}^W) - \frac{4z\Gamma_\phi}{h^2}(\hat{q}^Eu_{i+1} - \hat{q}^Wu_{i-1}) \tag{B.5d}$$

where

$$\hat{q}^i = q^i/q^p,\ \hat{r}^i = r^i/q^p,\ i = e,\ p,\ w$$

Equations (B.5) can now be solved for $\hat{r}^e$, $\hat{r}^w$, $\hat{q}^e$ and $\hat{q}^w$ to yield

$$\hat{q}^w = [6 + (2u_{i+1} - 5u_{i+1})z - u_i u_{i+1}] \,/\, [60 + 16(u_{i+1} - u_{i-1})z - 4u_{i+1}u_{i-1}z^2]$$

$$\hat{q}^e = [6 + (5u_i - 2u_{i-1})z - u_i u_{i-1}] \,/\, [60 + 16(u_{i+1} - u_{i-1})z - 4u_{i+1}u_{i-1}z^2]$$

Based on the common denominators of $\hat{q}^w$ and $\hat{q}^e$, a logical selection for q^p is:

$$q^p = 60 + 16(u_{i+1} - u_{i-1})z - 4u_{i+1}u_{i-1}z^2 \qquad \text{(B.7a)}$$

Hence, the remaining coefficients are:

$$q^e = 6 + (5u_i - 2u_{i-1})z \qquad \text{(B.7b)}$$

$$q^w = 6 - (5u_i - 2\,u_{i-1})^z \qquad \text{(B.7c)}$$

$$r^e = \frac{\Gamma_\phi}{2h^2}\,[q^w(2 - zu_{i-1}) + q^p(2 + zu_i) + q^e(2+3zu_{i+1})] \qquad \text{(B.7d)}$$

$$r^w = \frac{\Gamma_\phi}{2h^2}\,[q^w(2-3zu_{i-1}) + q^p(2-zu_i) + q^e(2 + zu_{i+1})] \qquad \text{(B.7e)}$$

$$r^p = -\,(r^e + r^w) \qquad \text{(B.7f)}$$

The above relationships provide the coefficients in the postulated COCI expression, i.e.,

$$r^w\phi_{i-1} + r^p\phi_i + r^e\phi_{i+1} = q^w\mathcal{L}^x_{i-1} + q^p\mathcal{L}^x_i + q^e\mathcal{L}^x_{i+1}$$

$$\text{or } [R]\left\{\phi\right\} = [Q]\left\{\mathcal{L}^x\right\}$$

APPENDIX C
DETAILS OF TRUNCATION ERROR SERIES FOR COCI DISCRETIZATION

The COCI scheme postulates that a tri-diagonal relation exists between ϕ_i and the spatial operator $\mathcal{L}_i^x = \Gamma_\phi \phi_i'' + u_i \phi_i'$ (assuming Γ_ϕ = constant and u varies in space) of the form:

$$r^w \phi_{i-1} + r^p \phi_i + r^e \phi_{i+1} = q^w \mathcal{L}_{i-1}^x + q^p \mathcal{L}_i^x + q^e \mathcal{L}_{i+1}^x \qquad (C.1)$$

If the truncation error is now defined as:

$$\tau = [R]\{\Phi_i\} - [Q]\{L_i^x\}$$

where Φ_i and L_i^x are the exact solution to equation (C.1). By expanding each neighbouring value of ϕ and $\mathcal{L}^x$ in equation (C.1) about x_i, the following relationship results:

$$\begin{aligned}
&r^w[\phi_i - h\phi_i' + \frac{h^2}{2}\phi_i'' - \frac{h^3}{6}\phi_i''' + \frac{h^4}{24}\phi_i^{iv} + ...] + \\
&r^e[\phi_i + h\phi_i' + \frac{h^2}{2}\phi_i'' + \frac{h^3}{6}\phi_i''' + \frac{h^4}{24}\phi_i^{iv} + ...] + r^p\phi_i - \\
&q^w\left\{\Gamma_\phi\,[\phi_i'' - h\phi_i''' + \frac{h^2}{2}\phi_i^{iv} - \frac{h^3}{6}\phi_i^v + \frac{h^4}{24}\phi_i^{vi} + ...] + \right. \\
&\qquad \left. u_{i-1}\,[\phi_i' - h\phi_i'' + \frac{h^2}{2}\phi_i''' - \frac{h^3}{6}\phi_i^{iv} + \frac{h^4}{24}\phi_i^v + ...]\right\} - \\
&q^e\left\{\Gamma_\phi\,[\phi_i'' + h\,\phi_i''' + \frac{h^2}{2}\phi_i^{iv} + \frac{h^3}{3}\phi_i^v + \frac{h^4}{24}\phi_i^{vi} ....] + \right. \\
&\qquad \left. u_{i+1}\,[\phi_i' + h\phi_i'' + \frac{h^2}{2}\phi_i''' + \frac{h^3}{6}\phi_i^{iv} + \frac{h^4}{24}\phi_i^v ....]\right\} - \\
&q^p\left\{\Gamma_\phi\,\phi_i'' + u_i\phi_i'\right\} = \tau
\end{aligned} \qquad (C.2)$$

Collecting terms common to each derivative of ϕ, τ is expressed as:

$$\tau = T^0\phi_i + T^1\phi_i' + T^2\phi_i'' + T^3\phi_i''' + T^4\phi_i^{iv} \qquad (C.3)$$

where it follows directly from equation (C.2) that

$$T^0 = r^e + r^w + r^p$$

$$T^1 = h[r^e - r^w - \frac{z\Gamma_\phi}{h^2}(q^w u_{i+1} + q^p u_i + q^e u_{i+1})]$$

$$T^2 = \frac{h^2}{2!}[r^e + r^w - \frac{2\Gamma_\phi}{h^2}(q^w + q^e + q^p) - \frac{2z\Gamma_\phi}{h^2}(q^e u_{i+1} - q^w u_{i-1})] \qquad (C.4)$$

$$T^3 = \frac{h^3}{3!}[r^e - r^w - \frac{6\Gamma_\phi}{h^2}(q^e - q^w) - \frac{3z\Gamma_\phi}{h^2}(q^e u_{i+1} + q^w u_{i-1})]$$

$$T^4 = \frac{h^4}{4!}[r^e + r^w - \frac{12\Gamma_\phi}{h^2}(q^e + q^w) - \frac{4z\Gamma_\phi}{h^2}(q^e u_{i+1} - q^w u_{i-1})]$$

$$\vdots$$

$$T^\upsilon = \frac{h^\upsilon}{\upsilon!}[r^e + (-1)^\upsilon r^w - \upsilon(\upsilon-1)\frac{\Gamma_\phi}{h^2}(q^e + (-1)^\upsilon q^w) - \frac{\upsilon z\Gamma_\phi}{h^2}(q^e u_{i+1} + (-1)^{\upsilon-1} q^w u_{i-1})]$$

for $\upsilon = 3, 4, 5$ and $z \equiv h/\Gamma_\phi$

It is important to note that the above deviation is equally valid, allowing for spatial variation of Γ_ϕ and h, which was not accounted for here only for simplicity.

NASA
National Aeronautics and Space Administration

Report Documentation Page

1. Report No.	2. Government Accession No.	3. Recipient's Catalog No.
NASA CR-180852		

4. Title and Subtitle

Improved Numerical Methods for Turbulent Viscous Recirculating Flows

5. Report Date

July 1988

6. Performing Organization Code

7. Author(s)

A. Turan and J.P. VanDoormaal

8. Performing Organization Report No.

None

10. Work Unit No.

533-04-11

9. Performing Organization Name and Address

Avco Research Laboratory, Inc.
2385 Revere Beach Parkway
Everett, Massachusetts 02149

11. Contract or Grant No.

NAS3-24351

13. Type of Report and Period Covered

Contractor Report
Final

12. Sponsoring Agency Name and Address

National Aeronautics and Space Administration
Lewis Research Center
Cleveland, Ohio 44135-3191

14. Sponsoring Agency Code

15. Supplementary Notes

Project Manager, David A. Jacqmin, Internal Fluid Mechanics Division, NASA Lewis Research Center.

16. Abstract

The performance of discrete methods for the prediction of fluid flows can be enhanced by improving the convergence rate of solvers and by increasing the accuracy of the discrete representation of the equations of motion. This report evaluates the gains in solver performance that are available when various acceleration methods are applied. Various discretizations are also examined and two are recommended because of their accuracy and robustness. Insertion of the improved discretization and solver accelerator into a TEACH code, that has been widely applied to combustor flows, illustrates the substantial gains that can be achieved.

17. Key Words (Suggested by Author(s))	18. Distribution Statement
Numerical method; Recirculating flows; High order upwind; Differencing schemes; Multigrid algorithms	Unclassified - Unlimited Subject Category 02

19. Security Classif. (of this report)	20. Security Classif. (of this page)	21. No of pages	22. Price*
Unclassified	Unclassified	244	A11

*For sale by the National Technical Information Service, Springfield, Virginia 22161

National Aeronautics and
Space Administration

Lewis Research Center
Cleveland, Ohio 44135

FOURTH CLASS MAIL

ADDRESS CORRECTION REQUESTED

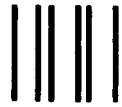

Official Business
Penalty for Private Use $300

Postage and Fees Paid
National Aeronautics and
Space Administration
NASA-451

NASA